Chemical studies of cytotoxic natural products from toxic and edible plant sources

Andrea Estefania Carpinteyro Diaz

Thesis for the degree of Philosophiae Doctor (PhD)
University of Bergen, Norway
2024

UNIVERSITY OF BERGEN

Chemical studies of cytotoxic natural products from toxic and edible plant sources

Andrea Estefania Carpinteyro Diaz

Thesis for the degree of Philosophiae Doctor (PhD)
at the University of Bergen

Date of defense: 19.04.2024

Year: 2024

Title: Chemical studies of cytotoxic natural products from toxic and edible plant sources

Name: Andrea Estefania Carpinteyro Diaz

Print: Skipnes Kommunikasjon / University of Bergen

“La pluma es lengua del alma; cuales fueren los conceptos que en ella se engendraron, tales serán sus escritos”

El Quijote, Miguel de Cervantes

Content

Scientific environment

The Pharmacognosy Group, of the Department of Chemistry at the University of Bergen, thrives in a dynamic and resource-rich scientific environment. This environment fosters the group's commitment to studying natural products and their medicinal properties, driving innovation and excellence. The group enjoys access to modern laboratories equipped with the necessary equipment for the isolation, purification, and structural elucidation of bioactive compounds.

The Faculty of Mathematics and Natural Sciences at the University of Bergen is home to a diverse and accomplished selection of Departments and research groups. The research group benefits from the expertise of its own department members, and also collaborates with professors in related disciplines, enhancing its multidisciplinary approach to research. The group also collaborates with the University Botanical Garden experts, and different research groups situated at Haukeland University Hospital and the Centre of Pharmacy of the University of Bergen.

The research projects of the Pharmacognosy Group are supported by competitive research grants from government agencies such as the Research Council of Norway and the Norwegian Society for Children's Cancer. Regular attendance at national and international conferences, such as the International Congress of Polyphenols and Farmasidagene, fosters intellectual exchange and enables the presentation of research findings in Norway and the rest of the world.

The research conducted by the group strictly adheres to ethical guidelines and regulations, ensuring the responsible and sustainable use of natural resources. Members of the Department of Chemistry and graduate students in the current department are actively engaged in teaching courses, enriching the academic experience of undergraduate and graduate students in the department.

This well-rounded scientific environment provides the Pharmacognosy Group with the resources, mentorship, and collaborative opportunities necessary to advance the

understanding of bioactive natural products and their potential applications in drug discovery.

Acknowledgements

Completing a PhD is a journey that no one undertakes alone. I am deeply grateful to the many individuals and institutions that have supported and guided me throughout this demanding but rewarding endeavour.

First and foremost, I would like to express my heartfelt gratitude to my thesis advisors, Professor Torgils Fossen, Professor Lars Herfindal, and Professor Svein Haavik, for their unwavering support, patience, and expert guidance. Your mentorship has been invaluable, and I am fortunate to have had the opportunity to learn from all of you, especially from you, Torgils: gracias por compartir tus conocimientos y experiencias como investigador, significa mucho para mi.

I sincerely thank the University of Bergen, the Department of Chemistry, and the Centre of Pharmacy, which provided a stimulating academic environment and access to their research facilities. The resources, both material and intellectual, made this research possible. I extend my gratitude to all co-authors of the papers incorporated into this thesis and all the people involved in the KJEM110 lecture during my PhD period for their collaboration and invaluable contribution.

I am grateful to my fellow colleagues, Solmaz Ghoreishi, Milan Chhaganlal, Stian Hersvik Hegdahl and Lina Angeliki Barouti, who provided a supportive network for sharing ideas and experiences. Your friendship has been an essential part of this journey. To the master students in the Pharmacognosy group: Tone Råket Ås, Bjørn Tobiassen Heieren, Vilde Sigrid Skar Bulling, Malgorzata Dominika Szymczak, Vebjørn Bjerg-Mikkelsen, Markus Jespersen Waage to be there in the lab days and the unparallel support through the madness of isolation.

My friend Nivedita, and my family (Andrea, Ray Ruben, Fernando, and Sofia, especialmente tu mi corazón) thank you for your unwavering encouragement and understanding. Your belief in me has strengthened me throughout this dark process.

"All that we see or seem is but a dream within a dream" Edgar Alan Poe

Preface

This thesis is submitted for the degree of Philosophia Doctor (PhD) in the field of Pharmacognosy and Natural Products Chemistry at the University of Bergen. Experimental and writing work on this thesis has been performed from August 2018 to December 2023 at the Department of Chemistry and the Department of Clinical Science at the University of Bergen.

A collection of five papers makes up the content of this thesis, which are mentioned in the list of publications with Roman numerals. This list of articles reflects the experimental work performed during my PhD period (with four first-author manuscripts) and one collaboration that has enriched my development as a researcher.

The following pages are presented within two parts. **Part I** comprises five chapters. Chapter 1 briefly introduces the four different plants used during this project, *Narthecium ossifragum*, *Osmunda Regalis*, *Cryptogramma crispa,* and *Anthriscus cerefolium,* as well their different isolated and characterised compounds. Chapter 2 contains the scope and aims of this work. Chapter 3 describes the methodology used during the project, which was performed at Department of Chemistry and Department of Clinical Science. Chapter 4 presents the results of papers **I-V,** which were published in different open-access scientific journals, and Chapter 5 is a summary of the conclusions obtained. **Part II** contains an expanded appendix with a list of compounds isolated from these plants. In addition, NMR tables for the undescribed compounds are provided. The last section of the thesis comprises the papers on which the thesis is based.

Abstract

This PhD thesis focuses on the isolation and identification of natural compounds from four selected plant materials, where the cytotoxic activity in novel and interesting natural products was tested towards cancer and normal cell lines.

During this work, it was possible to isolate saponins from *Narthecium ossifragum*, a plant associated with poisoning of domesticated animals. Three saponins were identified, as well as their sapogenin core structure sarsasapogenin. The cytotoxic activities of these compounds were tested against normal cells and leukaemia cell lines. Moreover, the five previously undescribed di-*C*-glycosylflavones chrysoeriol 6-*C*-*β*-arabinofuranoside-8-*C*-*β*-glucopyranoside, chrysoeriol 6-*C*-*β*-arabinopyranosyl-8-*C*-*β*-glucopyranoside, chrysoeriol 6-*C*-*β*-xylopyranosyl-8-*C*-*β*-galactopyranoside, chrysoeriol 6-*C*-*β*-galactopyranosyl-8-*C*-*β*-glucopyranoside and chrysoeriol 6-*C*-*β*-glucopyranosyl-8-*C*-*β*-galactopyranoside were isolated and characterised from the methanolic extract from flowers of *N. ossifragum*.

The significant cytotoxicity of the main saponin sarsasapogenin-3-*O*-(2′-*O*-*β*-glucopyranosyl-3′-*O*-*α*-arabinopyranosyl-β-galactopyranoside) against kidney cells strongly indicate that this saponin is the primary cause of the observed lethal kidney damage in cattle that ingest *N. ossifragum*. The research also explores the effect of these compounds on biological membranes, revealing a concentration-dependent mechanism, as well an increasing toxicity with the increasing of the sugar moieties that leads to cell death.

In addition, the study examines the phytochemical composition of the medicinal plant *Osmunda regalis*, identifying 17 natural products, 15 of which were found in this species for the first time, which include 6 undescribed compounds. The new natural products identified were the flavonoids kaempferol 3-*O*-(2’’-*O*-(2’’’-α-rhamnopyranosyl)-*β*-glucopyranosyl)-*β*-glucopyranoside, quercetin 3-*O*-(2’’-*O*-(2’’’-α-rhamnopyranosyl)-*β*-glucopyranosyl)-*β*-glucopyranoside, and kaempferol 3-*O*-(2’’-*O*-(2’’’-*α*-rhamnopyranosyl-6’’’-*O*-(*E*)-caffeoyl-)-*β*-glucopyranosyl)-*β*-glucopyranoside, and the three lactones 3-methoxy-5-hydroxy-4-olide, 4-hydroxy-3-

(3'-hydroxy-4'-(hydroxyethyl)-oxotetrafuranone-5-methyl tetrahydropyranone, 4-*O*-(5-hydroxy-4-oxohexanoyl) osmundalactone. Two of the isolated lactones (the known 5-hydroxy-2-hexen-4-olide, and the novel compound 4-*O*-(5-hydroxy-4-oxohexanoyl) osmundalactone) showed significant cytotoxic activity against MOLM13 cells, as well as normal cell lines.

This work also investigated the natural products of *Cryptogramma crispa*, also known as Parsley fern. The study reports the characterisation of 15 natural products isolated from the aerial parts of *C. crispa*, including a previously undescribed compound, 3-malonyl pteroside D. The pteroside derivatives isolated from this plant material showed selective moderate cytotoxic activity against the acute myeloid leukaemia MOLM13 cell line, but no cytotoxicity against normal heart and kidney cell lines.

Furthermore, the study Garden chervil, scientifically known as *Anthriscus cerefolium*, is an herb frequently used in large-scale Norwegian commercial kitchens. It was possible to isolated four new compounds from this plant source in which the previously undescribed compound 1,3-dicaffeoyl-5-malonyl-δ-quinide was isolated. This plant is a potent good source of phenolics, and the novel compounds have a mild cytotoxic activity towards normal and cancer cell lines.

A combination of advanced NMR spectroscopic techniques, CD spectroscopic and high-resolution mass spectrometry were used for the structure determination of the 43 compounds presented in this thesis. Results from the cytotoxic activity studies from these natural products motivate further and more extensive studies of their cytotoxic activity and the mechanisms of their cytotoxicity at the cellular and molecular levels. However, contrary to the conclusions that exist in the scientific literature, results presented in this work demonstrate that sarsasapogenin derivatives from *N. ossifragum* should not be used as anticancer agents because of their significant non-selective cytotoxicity towards cancer and normal cell lines.

Sammendrag

Denne doktorgradsavhandlingen fokuserer på isolering og identifikasjon av naturstoffer fra fire utvalgte planter, hvor den cytotoksiske aktiviteten til nyoppdagede og interessante naturstoffer ble testet på blodkreftceller og normale cellelinjer. I løpet av dette arbeidet var det mulig å isolere saponinene i *Narthecium ossifragum*, en plante assosiert med omfattende tilfeller av forgiftninger av gårdsdyr. Tre saponiner ble identifisert, i tillegg til deres sapogeninkjernestruktur sarsasapogenin aglykon. Cytotoksisiteten til disse forbindelsene ble testet mot normale celler og leukemiceller. Videre ble de fem nye naturstoffene di-*C*-glykosylflavonene chrysoeriol 6-*C*-*β*-arabinofuranoside-8-*C*-*β*-glukopyranoside, chrysoeriol 6-*C*-*β*-arabinopyranosyl-8-*C*-*β*-glukopyranoside, chrysoeriol 6-*C*-*β*-xylopyranosyl-8-*C*-*β*-galaktopyranoside, chrysoeriol 6-*C*-*β*-galaktopyranosyl-8-*C*-*β*-glukopyranoside og chrysoeriol 6-*C*-*β*-glukopyranosyl-8-*C*-*β*-galaktopyranoside isolert og karakterisert fra det metanoliske ekstraktet fra blomstene til *N. ossifragum*.

Den betydelige cytotoksiske aktiviteten til hovedsaponinet sarsasapogenin-3-*O*-(2'-*O*-β-glukopyranosyl-3'-*O*-α-arabinopyranosyl-β-galaktopyranoside) overfor nyreceller indikerer sterkt at dette saponinet er hovedårsaken til de observerte dødelige nyreskadene hos storfe som beiter på *N. ossifragum*. Studier av effekten av disse forbindelsene på biologiske membraner avdekket konsentrasjonsavhengig toksisitet, samt økt giftighet med økende antall sukkersubstituenter overfor både kreftceller og normale cellelinjer.

I tillegg ble den fytokjemiske sammensetningen av medisinplanten *Osmunda regalis* undersøkt, noe som førte til identifikasjon av 17 naturstoffer, hvorav 15 ble funnet for første gang i denne planten, inkludert 6 nye naturstoffer. De nye naturstoffene ble identifisert som flavonoidene kaempferol 3-*O*-(2"-*O*-(2"'-α-rhamnopyranosyl)-*β*-glukopyranosyl)-*β*-glukopyranoside, quercetin 3-*O*-(2"-*O*-(2"'-α-rhamnopyranosyl)-*β*-glukopyranosyl)-*β*-glukopyranoside, og kaempferol 3-*O*-(2"-*O*-(2"'-*α*-rhamnopyranosyl-6"'-*O*-(*E*)-caffeoyl-)-*β*-glukopyranosyl)-*β*-glukopyranoside, og de

tre laktonene 3-metoksy-5-hydroxy-4-olid, 4-hydroxy-3-(3'-hydroxy-4'-(hydroksyetyl)-okstetrafuranon-5-metyl tetrahydropyranon, 4-*O*-(5-hydroxy-4-oksohexanoyl) osmundalakton. To av de isolerte laktonene, det kjente naturstoffet 5-hydroxy-2-hexen-4-oliden og det nye naturstoffet 4-*O*-(5-hydroxy-4-oksohexanoyl) osmundalakton) viste betydelig cytotoxisk aktivitet overfor MOLM13-celler, så vel som normale cellelinjer.

Naturproduktene i *Cryptogramma crispa*, også kjent som hestespreng, ble også isolert og strukturbestemt. I alt ble 15 naturstoffer isolert fra bladene til *C. crispa*, inkludert det nye naturstoffet 3-malonyl pteroside D. Pteroside-derivatene isolert fra dette plantematerialet viste selektiv moderat cytotoxisk aktivitet mot akutt myeloide leukemi MOLM13 cellelinjen, men ingen cytotoksisk aktivitet mot normale hjerte- og nyrecellelinjer.

I tillegg ble naturstoffene i kjørvel, vitenskapelig kjent som *Anthriscus cerefolium,* en urt som ofte brukes i norske storkjøkken, isolert og karakterisert. Det var mulig å isolere fire nye forbindelser fra denne plantekilden, deriblant det nye bisykliske laktonet 1,3-dikaffeoyl-5-malonyl-δ-kinidin. Denne planten er en rik kilde til fenoliske forbindelser, og det nye naturstoffet har en mild cytotoxisk aktivitet overfor normale cellelinjer og kreftcellelinjer.

En kombinasjon av avanserte NMR-spektroskopiske teknikker, CD spektroskopi og høyoppløselig massespektrometri ble brukt for strukturbestemmelsen av de 43 forbindelsene presentert i denne avhandlingen. Resultatene fra studiene av cytotoksisk aktivitet av disse naturstoffene motivere for vider og mer omfattende studier av deres cytotoksiske aktivitet og mekanismene for deres cytotoksisitet på cellulært og molekylært nivå. I motsetning til konklusjoner i eksisterende vitenskapelig litteratur viser resultatene i avhandlingen at sarsasapogenin-derivater fra *N. ossifragum* ikke kan brukes som virkestoffer i kreftlegemidler på grunn av signifikant ikke-selektiv cytotoksisitet overfor både kreftceller og normale cellelinjer.

List of Publications

This thesis incorporates the following papers, which will be cited within the text using Roman numerals.

I. Carpinteyro Díaz, A.E., Herfindal, L., Rathe, B.A., Sletta, K.Y., Vedeler, A., Haavik, S., & Fossen, T. (2019). Cytotoxic saponins and other natural products from flowering tops of *Narthecium ossifragum* L. Phytochemistry (Oxford), 164, 67–77. https://doi.org/10.1016/j.phytochem.2019.04.014.

II. Carpinteyro Díaz, A.E., Haavik, S., Lunde, T.H.F., Fossen, T., Herfinal, L. (2023) Cytotoxic Saponins from the livestock-poisoning plant *Narthecium ossifragum* (L) – Death through destruction of biological membranes. Toxins (Manuscript).

III. Carpinteyro Díaz, A.E., Herfindal, L., Holmelid, B., Brede, C., Andersen, H.L., Vedeler, A., Fossen, T. (2023). Cytotoxic Natural Products from the Jurassic Relic *Osmunda regalis L*. Phytochemistry (Oxford). (Submitted and under revision)

IV. Carpinteyro Diaz, A.E., Herfindal, L, Andersen, H.L., & Fossen, T. Cytotoxic Natural Products Isolated from *Cryptogramma crispa* (L.) R. Br. Molecules. 2023; 28(23):7723. https://doi.org/10.3390/molecules28237723

V. Slimestad, R., Rathe, B. A., Aesoy, R., Carpinteyro Diaz, A. E., Herfindal, L., & Fossen, T. (2022). A novel bicyclic lactone and other polyphenols from the commercially important vegetable *Anthriscus cerefolium*. Scientific Reports, 12(1), 7805–7805. https://doi.org/10.1038/s41598-022-11923-0

Abbreviations symbols

$[M^+]$	Positively charged molecular ion
$[M^-]$	Negatively charged molecular ion
1D	One Dimensional
2D	Two Dimensional
AML	Acute Myeloid Leukemia
Bge	Bunge
br	broad
C	Carbon
CAPT	Compensated Attached Proton Test
CD	Circular Dichroism
$CHCl_3$	Chloroform
CMC	Critical Micelle Concentration
COSY	Correlation Spectroscopy
‘d'	semi doublet
d	doublet
dd	double doublet
ddd	double double doublet
DMSO-D_6	Hexadeuterodimethyl sulfoxide
EC_{50}	Half maximal effective concentration
EDTA	Ethylenediaminetetraacetic acid
GCMS	Gas Chromatography-Mass Spectrometry
H	Hydrogen
H2BC	Heteronuclear-2-Bond Correlation
H9c2	Rat cardiomyoblasts
HMBC	Heteronuclear Multiple Bond Correlation
HPLC	High-Performance Liquid Chromatography
HRMS	High-Resolution Mass Spectrometry
HSQC	Heteronuclear Single Quantum Coherence
HSQC-TOCSY	Heteronuclear Single Quantum Coherence-Total Correlation Spectroscopy
Hz	Herz
kg	kilogram
L	Litre
L.	Linnaeus
m	multiplet
min	minute
mL	Millilitre
MS	Mass Spectrometry
Na	Sodium
nm	nanometre
NMR	Nuclear Magnetic Resonance
NRK	Normal Rat Kidney

O	Oxygen
PBS	Phosphate-buffered saline
PC	Phosphatidylcholine
ppm	Parts per million
R. Br.	Robert Brown
ROESY	Rotating Frame Overhauser Effect Spectroscopy
RPM	Revolution Per Minute
s	Singlet
t	triplet
TEM	Transmission Electron Microscope
TFA	Trifluoro acetic acid
TOCSY	Total Correlation Spectroscopy
UV	Ultraviolet
δ	Chemical shift

Part I

Chapter 1: Introduction

1.1. Plant Materials

This research work was conceptualised using three different plant sources. During this project an industry research collaboration allowed addition of an extra plant source to be studied, as described below.

The first plant material used in this work was *Narthecium ossifragum*, commonly known as bog asphodel, or rome in Norwegian, which is a species of flowering plants in the family Nartheciaceae. It is native to North- Western Europe, and it is found on wet, boggy swamps. The flower stems are 5-40 cm long and produce bright yellow flowers that are 10-16 mm wide occurring in clusters with 6-20 flowers. Flowering of this species occurs between July and August (Summerfield, 1974; Mossberg et al., 2018).

This plant has been associated with toxic effects in grazing animals. In several Northern European countries, including Norway, Ireland, and certain regions of the UK, it has been observed that ruminants can develop renal failure and hepatotoxicity after ingestion of *N. ossifragum* (Flåøyen et al., 1995; Uhlig et al., 2007; Malone et al., 1992; Angell & Ross, 2011). Similarly, reports from Japan indicate that cattle can experience nephrotoxicity due to intake of *Narthecium asiaticum*, a plant closely related to *N. ossifragum* (Suzuki et al., 1985; Kobayashi et al., 1993; Inoue et al., 1995).

Fresh flowering plant material of *N. ossifragum* was collected in a bog area located at southwestern part of Ulriken, Bergen (Figure 1), and used during the isolation and characterization of the natural products named in Paper **I-II**. A Voucher specimen has been deposited at the ARBOHA, University of Bergen (accession number BG/S-162115)

Figure 1. Flowering tops from *Nartecium ossifragum* collected around the city mountain of Ulriken, Bergen.

Two fern species were investigated. On of these is the unique species *Osmunda regalis* belonging to the Osmundaceae family, which encompasses three extant genera: Osmunda, Todea, and Leptopteris. These are seen as a foundational group of leptosporangiate ferns, which have remained relatively unchanged in terms of morphology and anatomy since the Mesozoic era. As a result, they are often referred to as "primitive" species by some researchers (Bomfleur et al., 2014; Moore et al., 2009; Bouazzi et al., 2018).

Osmunda regalis (L), also known as the royal fern, has remained unchanged for a period of at least 180 million years (Bomfleur et al., 2014). This plant is found in temperate regions across both Northern and Southern hemispheres, including Europe, Southern Africa, America, and New Zealand. Its fronds are bi-pinnate, meaning each leaf is divided into two or more leaflets, which are further divided into smaller leaflets or pinnules. The royal fern is commonly found in moist environments such as woods, swamps, lakes, or along stream banks (Dehgan, 2022).

The Botanical Garden of University of Bergen, Norway (ARBOHA) provided fresh plant material of *Osmunda regalis* L. (Osmundaceae). The collection took place in the autumn season, more precisely in September 2020 (Figure 2) (accession number

1996.700). Isolated and characterised natural products from this plant source are presented in Paper **III**.

Figure 2. Ferns leaves from *Osmunda regalis* collected in the Botanical Garden of the University of Bergen, in Milde, Bergen

Natural products of a second fern belong to the genus Cryptogramma, which is a type of leptosporangiate fern comprising nine species, were also characterized. Leptosporangiate ferns are often referred to as parsley ferns due to the similarity of their foliage to parsley (Metzgar et al., 2013).

Cryptogramma crispa (L.) R. Br. (Pteridaceae) is widely found in the montane to the subalpine zone of the temperate and boreal regions of Europe. It has two primary distribution centres: a northern one that includes the highest mountains on the British Isles and west Scandinavia, and a southern one that includes Cordillera Cantabria, Pyrene´ es, Massif Central, Corsica, the Alps, and the northern Apennines (Veit et al., 1995; Tomaselli et al., 2005).

Interestingly, a Norwegian tradition suggests horses consuming excessive amounts of parsley fern may suffer from colic, leading to its Norwegian name “hestespreng,”

which translates to “horse bloating.” However, the accuracy of this tradition seems somewhat uncertain (Fægri, 1970).

Fresh plant material of *Cryptogramma crispa* (L.) R.Br. was collected during the summer of 2021 and 2022 in the mountain of Fløyen, in Bergen, Norway (Figure 3). A voucher specimen of *C. crisp* has been deposited at the herbarium BG, University of Bergen (accession number BG/S-168787). This plant material was used for the isolation, characterisation of the natural products described in Paper **IV**.

Figure 3. Aerial parts from *Cryptogramma crispa* collected in the city mountain Fløyen, in Bergen.

The plant material used during the industrial scientific collaboration with PlantChem AS was garden chervil or French parsley (*Anthriscus cerefolium* (L.) Hoffm.). This plant species is an annual umbelliferous plant with delicate 2- to 3-pinnate leaves with dentated to pinnatisect leaflets. The plant has been utilised as a medicinal plant by humankind for millennia. It is mentioned in the Encyclopaedia Historia Naturalis by Plinius the Elder (23–79 AD) as an ingredient in vinegar recommended against hiccups (Plinius Maior, 77). This species is also mentioned by the seventeenth-century Danish pioneer scientist Simon Paulli (1648), who reported on its use against gallstones (Paulli, 1648).

The use of Garden chervil as a food in private households is limited as this species is only to a limited extent made available for customers by retailers and supermarkets.

However, this species is established as one of the major herbs applied within Norwegian large-scale commercial kitchens (Chizzola, 2011, **Paper V**), where garden chervil is used as a cheaper alternative to parsley to give a mild taste of anise, parsley, black pepper, and caraway.

Fresh-cut chervil from Frøvoll Farm, Randaberg, located in Southwestern Norway (59°0′56.3″ North, 5°37′25.8″ East) were used to carried out this study.

1.2. Isolated Compounds

A multitude of natural products were isolated from the above-mentioned unique plant sources during this project. These natural products, including several aromatic compounds, terpenoids, and lactones are described in detail in the sections below.

1.2.1. Aromatic compounds

Shikimic acid derivatives are natural products that have shikimic acid as a common biosynthetic precursor. The shikimate pathway is the common route leading to the production of the aromatic amino acids, phenylalanine, tyrosine, and tryptophan, as well as several important classes of polyphenolic compounds. The shikimate biosynthetic pathway is only found only in plants, bacteria, archaea, and fungi.

Several natural products can be biosynthesized from phenylalanine, including benzoic acid derivatives, phenylpropenes, flavonoids and lignans.

1.2.1.1. Benzoic acid derivatives

Benzoic acid and its natural products derivatives are widely distributed in nature, been one of the simples' aromatic acids derived from shikimic acid pathway (Heinrich et al., 2012; del Olmo et al., 2017). Several benzoic acid derivatives have

been isolated and characterized in this thesis including vanillic acid, *p*-hydroxy benzoic acid, and *p*-hydroxy benzoic acid methyl ester from *O. regalis* (Paper **III**).

1.2.1.2. Phenylpropenes

Phenylpropenes are the simplest natural products in this group, which consist of an aromatic ring with an attached unsaturated C_3 chain (Heinrich et al., 2012). Several phenylpropene derivatives have been isolated and characterised in this thesis including ferulic acid, ferulic acid 4-*O*-*β*-glucopyranoside, *p*-coumaric acid 4-*O*-*β*-glucopyranoside, caffeic acid, methyl chlorogenic acid 4'-*O*-*β*-glucopyranoside, and methyl ester chlorogenic acid from *C. crispa* (Paper **IV**).

1.2.1.3. Flavonoids

Flavonoids, which are the most abundant polyphenols of higher plants, occur in all parts of the plants including roots, bulbs, stamens, leaves, fruits, and seeds. These compounds have multiple roles in plants that have been of attention over the years, for example, controlling cell development, attracting pollinating insects, and defence at molecular level against various pathogens (Dias et al., 2021; Winkel-Shirley, 2001; Panche et al., 2016, Andersen & Markham, 2006). Flavonoids can be classified into major subgroups including anthocyanins, flavones, flavonols, chalcones, dihydroflavonols, flavanones, flavanols, isoflavonoids, aurones and flavandiols (Andersen & Markan, 2006). Most flavonoids hitherto discovered occur as either *O*-glycosides or *C*-glycosides. In *C*-glycosylflavonoids, the glycosyl substituent(s) is directly attached to the flavonoid aglycone with a C-C bond. Flavonoid *O*-glycosides are formed by attaching the glycosyl substituents to the phenolic oxygens of the flavonoid nucleus through an ether bond. The hydroxyl groups of the glycosyl moieties can be further modified by glycosylation with additional glycosyl substituents or by esterification (acylation) with aliphatic or aromatic acids (Andersen & Markham, 2006).

Flavonoids are recognized for their dual health benefits, play a crucial role in mitigating oxidative damage due to their antioxidant effect. These compounds exhibit a range of biological activities, including anticancer, antiviral, and antioxidant properties. They are also known to prevent cardiovascular diseases, a phenomenon referred to as the 'French paradox', and display significant anti-inflammatory activity (Andersen & Markham, 2006). However, biological activity of flavonoids strongly depends on their individual molecular structures.

Five novel di-*C*-glycosylflavones (Figure 4): chrysoeriol 6-C-*β*-arabinofuranoside-8-*C*-*β*-glucopyranoside, chrysoeriol 6-*C*-*β*-arabinopyranosyl-8-*C*-*β*-glucopyranoside, chrysoeriol 6-*C*-*β*-xylopyranosyl-8-*C*-*β*-galactopyranoside, chrysoeriol 6-*C*-*β*-galactopyranosyl-8-*C*-*β*-glucopyranoside, chrysoeriol 6-*C*-*β*-glucopyranosyl-8-*C*-*β*-galactopyranoside were isolated from flowering tops of N. ossifragum, in addition to the known di-*C*-glycosylflavone chrysoeriol 6,8-di-*C*-*β*-glucopyranoside (Paper **I**).

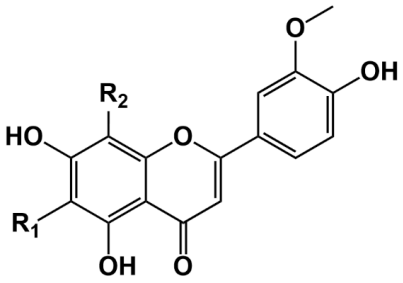

Figure 4. Core structure of the flavone chrysoeriol. Di-*C*-glycosylflavones based on this core structure were the main aromatic compounds isolated from flowering tops of *N. ossifragum*.

Flavonoids isolated and characterised from *O. regalis* included the three novel flavonols kaempferol 3-*O*-(2''-*O*-*β*-glucopyranosyl-2'''-*α*-rhamnopyranosyl-*β*-glucopyranoside), quercetin 3-*O*-(2''-*O*-*β*-glucopyranosyl-2'''-*α*-rhamnopyranosyl-*β*-glucopyranoside), and kaempferol 3-*O*-(2''-*O*-*β*-glucopyranosyl-2'''-*α*-rhamnopyranosyl-*β*-glucopyranoside)-6'''-*O*-(*E*)-caffeoyl.chalcones, in addition to the known compounds chalconaringenin 2'-*O*-*β*-glucopyranoside and apigenin 7-(2''-*O*-*α*-rhamopyranosyl-*β*-glucopyranoside) (rhoifolin) (Paper **III**).

The flavonoids present in *C. crispa* proved to be predominantly flavonols. From this species, the flavonols quercetin, quercetin 3-*O*-*β*-galactopyranoside, quercetin 3-*O*-*β*-glucopyranoside, quercetin 7-*O*-*β*-glucopyranoside, and kaempferol 7-*O*-*β*-glucopyranoside were isolated and characterised (Paper **IV**).

1.2.1.4. Lignans

Lignans constitute a vast group of phytochemicals, widely distributed in terrestrial plant lineages, which have important roles in plant physiology, development, and ecology (Hano et al., 2021). Lignans in plants are a type of polyphenols that are formed from precursors known as coniferyl alcohols (Plaha et al., 2022). In the current thesis, the lignans dihydrodehydrodiconiferyl alcohol 4-*O*-*α*-rhamnopyranoside and epoxyconiferyl alcohol were isolated from *O. regalis* (Paper **III**).

1.2.2. Terpenoids

Terpenoids, also called isoprenoids, are modified terpenes in which the carbon skeleton is modified by oxidation or a rearrangement. They are formed by the mevalonic acid pathway (Brahmkshatriya & Brahmkshatriya, 2013).

Classification of terpenoids is based upon the number of isoprene (or isopentane) units incorporated in the basic molecular skeleton, mainly ranging from the C_5 having hemiterpenes, comprised by one isoprene unit, to C_{40} carotenoids, comprised by eight isoprene units.

1.2.2.1. Steroidal saponins

Sapogenins are derived from isoprenoids (specifically steroid-derived structures derived from triterpenoids) and are biosynthesised from the mevalonate pathway.

Sterols and steroids are important structural components of membranes and play important roles in signalling processes. (Osbourn, et al., 2011; Thimmappa et al., 2014).

Saponins are glycosides containing one or more sugar chains attached to a triterpene or steroid aglycone, called sapogenin. Saponins are classified according to the number of sugar units in their structure as mono, di-, or tridesmosidic (Güçlü-Üstündağ & Mazza, 2007).

The sapogenin sarsasapogenin (Figure 5), in addition to the three saponins sarsasapogenin-3-*O*-*β*-galactopyranoside, sarsasapogenin-3-*O*-(2′-*O*-*β*-glucopyranosyl-*β*-galactopyranoside), sarsasapogenin-3-*O*-(2′-*O*-*β*-glucopyranosyl-3′-*O*-*α*-arabinopyranosyl-*β*-galactopyranoside) were isolated from flowering tops of *N. ossifragum* (Paper **I**). The effects of these compounds on biological membranes were studied in Paper **II.**

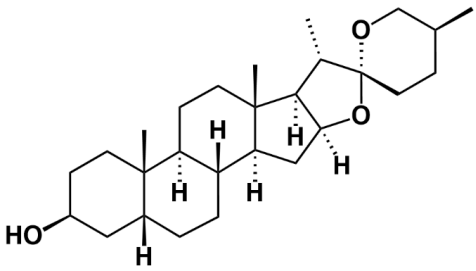

Figure 5. Structure of the steroidal sapogenin Sarsasapogenin. Sarsasapogenin is the sapogenin of all saponins isolated from *N. ossifragum*

1.2.2.2. Lactones

Lactones are cyclic esters formed by intramolecular esterification of hydroxy acids, where the biosynthesis depends on the mutual position of the hydroxyl and carboxyl groups. Five types of lactones are frequently occurring: α-, β-, γ-, δ-, and ε-lactones, which differ in the relative position of the condensed hydroxyl and carboxyl groups, and thus, the size of the lactone ring (Kowalczyk et al., 2021).

Lactones isolated from natural products can be grouped into five main classes based on their biosynthetic origins: Lactones based on (1) amino acids, (2) fatty acids, (3) polyketides, (4) hybrid PKS/NRPS pathways, and (5) terpenoids. Plants and marine sponges are the only known source of terpenoid lactones (Robinson et al., 2019).

The three novel lactones 3-methoxy-5-hydroxy-4-olide, a bi-lactone 4-hydroxy-3(3'-hydroxy-4'(hydroxyethyl)-oxotetrafuranone-5-methyl tetrahydropyranone (Figure 6), and 4-*O*-(5-hydroxy-4-ketohexanoyl) osmundalactone, in addition to the known γ-lactone 5-hydroxy-2-hexen-4-olide were isolated from *O. regalis* (Paper **III**).

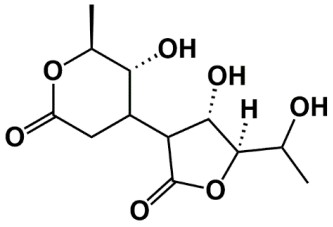

Figure 6. Structure of the bi-lactone 4-hydroxy-3(3'-hydroxy-4'(hydroxyethyl)-oxotetrafuranone-5-methyl tetrahydropyranone isolated from *O. reaglis*.

Quinic acid has a widespread occurrence in nature. Bicyclic lactones based on quinic acid are classified as quinides (Crozier et al., 2006). The novel bicyclic lactone 1,3-dicaffeoyl-5-malonyl-δ-quinide belonging to this group of lactones was characterised from *A. cerefolium* (paper **V**).

1.2.2.3. Sesquiterpenoids

Sesquiterpenoids (C_{15}) are comprised by three isoprene units, occurring with simple to complex mono- and polycyclic ring system which contribute with the chemical defense of the producing organism (Heinrich et al., 2012).

Pterosins are sesquiterpenoids with a 1-indanone core structure; the glucoside version is called pterosides. This name originates from the fern *Pteridium aquilinum* var.

latiusculum (Fukuoka et al., 1978). In this thesis, four 1-indanone derivatives were characterised from *C. crispa*, including the novel compound 3-manolyl-pteroside D, in addition to the known compounds pteroside D, pteroside X and pterosin (paper **IV**).

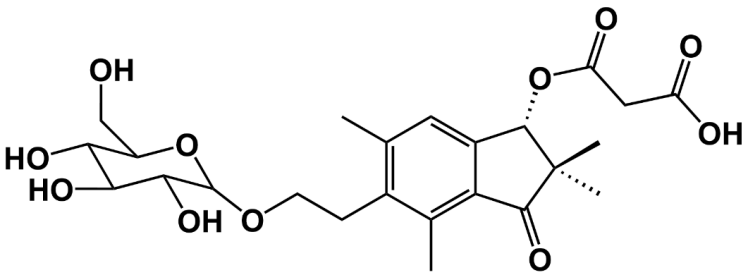

Figure 7. Molecular structure of the novel 1-indanone derivative 3-manolyl-pteroside D isolated from *C. crispa*.

1.2.2.4. Blumenols

Blumenols are C-13 cyclohexenone derivatives produced by the cleavage of C-40 carotenoids (You et al., 2023). In this thesis, Blumenol C glucopyranoside was characterised from *O. regalis* (paper **III**).

1.2.3. Fatty acids

Fatty acids are a widely distributed group of polyketides which are crucial components of cell membranes of living organisms (Heinrich et al., 2012). In this thesis, the short chain fatty acid 2-hexenoic acid, in addition to the glucosyl conjugate hexyl-*β*-glucopyranoside, were characterised from *O. regalis* (paper **III**). The latter compound is a conjugate between glucose and hexanol (hexanol is biosynthesised from hexanoic acid (Kottenhahn et al., 2021).

Chapter 2: Aim and Scope

2.1. Aim

The general aim of this PhD project was to isolate and identify bioactive natural products from unique plant sources, and to perform initial investigations of biological activity of the isolated compounds. The selection of the plant sources, justified in the introduction of this thesis, includes unique plants such as *N. ossifragum*, known for its toxicity towards domesticated animals, and the ancient ferns *O. regalis* and *C. crispi* as well as the edible plant *A. cerefolium*. As part of our ongoing research, we aim to isolate and identify new lead compounds for future anticancer drugs.

2.2. Scope

The scope of this PhD thesis in Pharmacognosy will primarily focus on two key areas: Phytochemical Analysis and Bioactivity Testing.

For the **Phytochemical Analysis**, the research was dedicated to the isolation, identification, and characterisation of bioactive compounds isolated from the unique plant sources *Narthecium ossifragum*, *Osmunda regalis*, *Cryptogramma crispa* and *Anthiscus cerefolium*. This research involved the use of a combination of several isolation techniques such as, solvent extraction, several types of chromatography for isolation of pure compounds. The molecular structures were established by a combination of several advanced NMR spectroscopic techniques, in addition to High resolution mass spectrometry and Circular Dichroism (CD) spectroscopy.

The **Bioactivity Testing** was dedicated to testing of cytotoxic activity of the isolated compounds towards cancer cells and normal cell lines. This encompassed a range of cell culture studies, towards acute monocyte leukaemia cells (MOLM13), rat cardiomyoblasts cells (H9c2), and kidney epithelial cells (NRK) to ascertain the therapeutic potential and safety profile of these compounds for further metabolic

studies. Initial studies of the effects of toxic saponins of *N. ossifragum*, on biological membranes were also conducted.

.

Chapter 3: Methodology

The specific experimental strategy for isolation and characterization of natural products from the three plant sources are described in Papers **I-V**. A concise summary of the primary experimental techniques applied and their roles is provided in the following section.

3.1. Isolation

3.1.1. Extraction

The general solvent methanol is frequently chosen as the extraction solvent of plant material due to its useful properties to extract a wide range of polar and non-polar natural products. Methanol possesses a relatively low boiling point, which allows for easy removal of solvent from the crude extract by concentration on rotavapor. Moreover, many bioactive compounds are soluble in methanol, enhancing its effectiveness in extraction. Furthermore, methanol is practical for use as a central component of the mobile phases in partial purification of the crude extract by the application of specialized chromatographic techniques.

3.1.2. Partitioning

This method serves as a gentle separation technique used for purification and as a "clean-up" step (Heinrich, 2012). It enables the separation of hydrophobic and less polar compounds such as chlorophylls and terpenoids from the more polar ones.

3.1.3. Chromatographic separation

Several chromatographic methods were used during the isolation of the bioactive compounds mentioned below; chromatographic separations were used for isolation of pure compounds. The progress of the isolation process was monitored by analytical HPLC and TLC.

The first column chromatographic technique used during the processes of isolating pure natural products from the three plant sources was absorption chromatography with Amberlite XAD-7 as the stationary phase. Thereafter, fractions from the XAD-7 chromatographic separation were further purified by Sephadex LH-20 gel filtration chromatography. Experimental details about the columns and the gradients applied for separation are provided in Papers **I**, **III**, **IV** and **V**.

For isolation of saponins from *N. ossifragum*, silica gel absorption chromatography was applied as the final isolation step, resulting in isolation of the four sarsasapogenin derivatives presented in paper **I**.

With exception of the saponins, all compounds characterised during this project, were isolated by preparative HPLC separations of fractions obtained from Sephadex LH-20 column chromatography as a final stage of purification, resulting in the 43 compounds presented in papers **I-V**.

3.1.4. Analytical characterisation

Analytical HPLC was used to determine the composition and purity of the extracts and fractions obtained during the isolation process. The method applied was described by Nguyen et al. (2014) and was used through papers **I-V**.

Saponins isolated from *N. ossifragum* are compounds without a UV-absorbing chromophore and with low solubility in aqueous solvent systems, thus, HPLC-DAD was not possible to use for analyses of these compounds. Therefore, a TLC analytical method was created, to analyse these compounds. The TLC method applied is described in detail in paper **I**.

3.2. Structure elucidation

3.2.1. Ultraviolet-Visble absorption spectroscopy

Ultraviolet-visible (UV-vis) spectroscopy is an effective tool for partial structure identification of UV-absorbing organic compounds because it provides information about the presence of conjugated π-bonding systems in a molecule. The UV-Vis absorption spectra of the compounds isolated during this project were recorded online during the analytical HPLC analysis over the wavelength range of 190-600 nm in steps of 2 nm.

3.2.2. Circular Dichroism spectroscopy

Circular Dichroism (CD) spectroscopy was an essential technique used to analyse configuration of isolated chiral compounds, giving the absolute configuration of the novel compounds presented in this thesis. The CD spectra were recorded at 20 °C under nitrogen atmosphere in a JASCO J-810 spectropolarimeter equipped with a Peltier temperature control unit. The spectra were recorded by scanning from 185 to 400 nm using a 1 mm path-length cuvette.

3.2.3. Mass-Spectrometry

Mass Spectrometry (MS) was crucial to identify and verify the molecular structures and atomic compositions of novel compounds by determining their molecular weight with high accuracy. High-Resolution Mass Spectrometry (HRMS) was used to verify the molecular weight and atomic composition of the novel bioactive compounds isolated from the three plant sources. These spectra were recorded using a JEOL AccuTOF™ JMS T100LC instrument fitted with an electrospray ion source operated in positive mode at a resolving power of approximately 6000 FWHM over the mass range of 50-2000 *m/z*.

3.2.4. Nuclear Magnetic Resonance

Nuclear Magnetic Resonance (NMR) spectroscopy provides detailed structural information of molecules in solution at atomic resolution and is the most important technique to determine molecular structures of organic compounds. During this project, several 1D and 2D NMR techniques were performed, including 1D ^{1}H, 1D ^{1}H selective TOCSY, 1D ^{13}CAPT and the 2D ^{1}H-^{13}C HMBC, the 2D ^{1}H-^{13}C HSQC, ^{1}H-^{13}C HSQC-TOCSY, the 2D ^{1}H-^{13}C H2BC, 2D ^{1}H-^{13}C 1,1-ADEQUATE, 2D ^{1}H-^{1}H COSY and 2D ^{1}H-^{1}H ROESY experiments. These experiments were obtained on a Bruker BioSpin AVANCE III HD 850 MHz equipped with a ^{1}H, ^{13}C, ^{15}N triple resonance cryogenic probe at 298 K.

3.3. Cytotoxicity

3.3.1. Cell culture

For the studies of cytotoxic activity, three mammalian cell lines were used; the normal rat kidney epithelial cells (NRK, ATCC no.: CRL-6509) and rat cardiomyoblasts (H9c2, ATCC no.: CRL-1446), and the Acute Myeloid Leukaemia cell line MOLM13 (DSMZ no.: ACC554). The culture medium and diverse growth parameters (Matsuo et al., 1997; Oftedal et al., 2010; Myhren et al., 2014) are described in detail in paper **I**, **III**, **IV** and **V**.

EC_{50} values were determined by a four-parameter regression analysis described by Viktorsson et al. (2017) using the SigmaPlot ver. 14 software (Systat Software Inc.).

3.3.2. Membrane interaction

The significant non-specific cytotoxic activity observed for saponins isolated from *N. ossifragum* towards leukaemia cells and normal cell lines, encouraged us to perform a study of the influence of these compounds on biological cellular membranes to be able to understand how the toxicity of these compounds are affecting the animals that ingests *N. ossifragum* (Paper **II**).

3.3.2.1. Transmission Electron Microscope (TEM)

Acute myeloid leukaemia MOLM13 cells underwent treatment using the four saponins isolated from *N. ossifragum* (referred to as Compounds **1**, **2**, **3**, and **4**) at a concentration of 300 μM for 3 hours. The specification of cell culture of cell fixation is described in paper **II**.

The microscopy procedure was carried out at the Molecular Imaging Center, situated within the Department of Biomedicine at University of Bergen.

3.3.2.2. Determination of membrane permeability

Determination of liposome integrity by observation of calcein leakage was performed as described by Oftedal et al. (2012).

The release of calcein from liposomes was continuously measured for 12 min using a fluorescence spectrophotometer (Varian Cary Eclipse, Agilent, USA) with an excitation wavelength of 495 nm and an emission wavelength of 515 nm. After 30 s of recording to confirm stable liposomes, the saponins were added and after 10 min, a 10% Tween® 20 (Sigma, St. Louis, USA) solution was added to release all remaining calcein.

3.3.2.3. Haemolysis activity

Fresh blood from a healthy human donor was donated voluntarily and collected in tubes with EDTA. One mL of blood was incubated with various concentrations of saponins and solvent for 30 minutes at room temperature. They were next centrifuged for 10 minutes at 1500 RPM. The supernatant containing plasma was collected, and 0.3 mL was analysed for the presence of haemoglobin. These experiments were done in the Laboratory Clinic of Haukeland University Hospital in Bergen.

Chapter 4: Results and Discussions

In this section, the main results of this research project are highlighted. These results are divided into sections based on the papers from which they are retrieved.

4.1. Paper I: Cytotoxic saponins and other natural products from flowering tops of *Narthecium ossifragum* (L).

In numerous publications, the flowering tops of *Narthecium ossifragum* have been reported to contain significant amounts of saponins, which are toxic components of the plant (Uhlig et al., 2007; Flåøyen et al., 1997; Flåøyen et al., 1991). Even though more than thirty publications in the current literature deal with saponins of *N. ossifragum*, none of these compounds has hitherto been characterised in detail from this plant source, and their molecular structures remain unknown.

Stabursvik (1959) identified the aglycone of the saponins of *N. ossifragum* to be a sarsasapogenin core structure. Ceh and Hauge (1981) tentatively identified two saponins from *N. ossifragum* based on sarsasapogenin (spirostan-3-ol) aglycone. Both saponins were indicated to be glycosylated with trisaccharides consisting of galactose-glucose-arabinose (major compound) and galactose-glucose-xylose (minor compound). However, the linkages between the individual sugar units were not determined, and the structures were not confirmed by NMR spectroscopy and HRMS.

Using LC-MS Uhlig et al. (2007) tentatively identified saponins based on smilagenin and sarsasapogenin with two and three sugar units. However, neither the sugar composition nor the individual glycosyl substituents could be identified. Even though the connection between the intake of *N. ossifragum* and the occurrence of alveld in lambs seems to be well documented (Abdelkader et al., 1984; Ceh & Hauge, 1981), the original assumption about a potential connection between saponins of this plant species and the phototoxic disease is controversial and has been challenged (Flåøyen et al., 1991).

In this work, we reported the structure determination and cytotoxicity of individual saponins of *N. ossifragum*. A methodology for large-scale separation and isolation of these compounds in the pure state is provided for the first time. Also, no aromatic compound has hitherto been identified from the plant at the flowering stage, where intake of *N. ossifragum* has been associated with livestock toxicity. As part of our ongoing research concerning the characterisation of aromatic compounds from *N. ossifragum*, several di-*C*-glycosyl flavones from this plant source were isolated for the first time.

Following the methodology presented in full in paper **I**, individual pure saponins were isolated and identified as sarsasapogenin (**1**), sarsasapogenin-3-*O*-*β*-galactopyranoside (**2**), sarsasapogenin-3-*O*-(2'-*O*-*β*-glucopyranosyl-*β*-galactopyranoside) (**3**) and sarsasapogenin-3-*O*-(2'-*O*-*β*-glucopyranosyl-3'-*O*-*α*-arabinopyranosyl-*β*-galactopyranoside) (**4**) by 1D and 2D NMR spectroscopy (which the NMR tables are presented in the second part of this thesis), and HRMS (Figure 8).

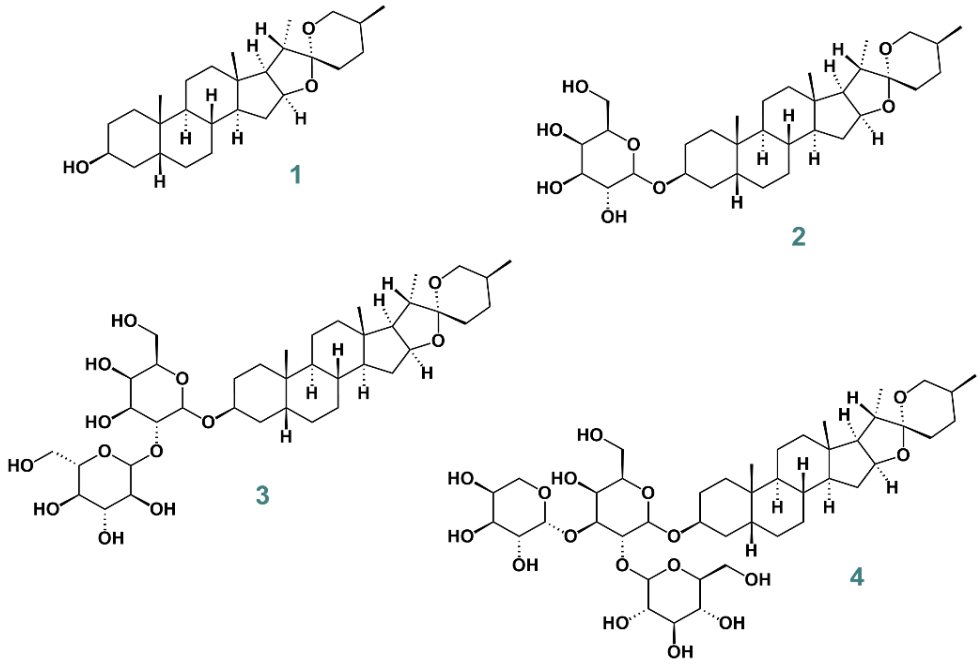

Figure 8. Structures of sarsasapogenin (**1**), sarsasapogenin-3-*O*-*β*-galactopyranoside (**2**), sarsasapogenin-3-*O*-(2'-*O*-*β*-glucopyranosyl-*β*-galactopyranoside) (**3**) and sarsasapogenin-3-*O*-(2'-*O*-*β*-glucopyranosyl-3'-*O*-*α*-arabinopyranosyl-β-galactopyranoside) (**4**) isolated from flowering tops of *N. ossifragum*.

The 1D ^{1}H NMR spectrum of compound **4** showed the presence of sarsasapogenin aglycone and three glycosyl substituents. The glycosyl units were identified to be galactopyranosyl, glucopyranosyl and arabinopyranosyl by the 17 ^{13}C signals observed in the 1D ^{13}C CAPT NMR spectrum of **4**. The ^{13}C signals belonging to these sugar units agreed with reference values of galactopyranosyl, glucopyranosyl and arabinopyranosyl, respectively (Inoue et al., 1995; Fossen & Andersen, 2006). The combined information in the 2D ^{1}H–^{1}H COSY spectrum and the 2D ^{1}H–^{13}C edited HSQC spectrum, the 2D ^{1}H–^{13}C HSQC-TOCSY spectrum and the 2D ^{1}H–^{13}C H2BC spectrum were of paramount importance with respect to complete assignments of all ^{1}H and ^{13}C resonances belonging to the glycosyl substituents. The identities of the glycosyl substituents were further confirmed by the observed coupling constants in the 1D ^{1}H NMR spectrum and the 1D ^{1}H selective TOCSY spectra of **4**. The configurations of C-1′, C-1″ and C-1‴ belonging to the galactopyranosyl, the

glucopyranosyl and the arabinopyranosyl units, respectively, were determined to be in *β*-configuration for the former two units and in *α*-configuration for the latter, by the observed large 3 J_{HH} vicinal coupling constants of 7.7 Hz, 7.9 Hz and 7.2 Hz. The configurations of the anomeric carbons were further confirmed by the $^{1}H–^{13}C$ coupling constants of H-1'/C-1' (163 Hz), H-1''/C-1'' (162 Hz) and H-1‴/C-1‴ (164 Hz), which are like literature values for *β*-galactopyranosyl, *β*-glucopyranosyl and *α*-arabinopyranosyl, respectively (Pedersen et al., 1995). The cross-peaks at δ 4.27/73.0 (H-1'/C-3), δ 3.88/99.8 (H-3/C-1′) observed in the HMBC spectrum and the cross-peaks at δ 4.27/3.88 (H-1'/H-3), δ 4.27/1.67 (H-1'/H-4A), δ 4.27/1.48 (H-1'/H-2A) and δ 4.27/1.39 (H-1'/H–4B) observed in the ROESY spectrum confirmed the linkage between the galactopyranosyl unit and the aglycone to be at the 3-position. The cross-peaks at δ 4.64/75.5 (H-1''/C-2′), δ 3.75/102.2 (H-2'/C-1″) observed in the HMBC spectrum, and the cross-peak at δ 4.64/3.75 (H-1''/H-2′) observed in the ROESY spectrum confirmed the linkage between the glucopyranosyl and the galactopyranosyl units to be at the 2′-position. The cross-peaks at δ 4.41/82.1 (H-1‴/C-3′), δ 3.56/104.7 (H-3'/C-1‴) observed in the HMBC spectrum, and the cross-peak at δ 4.41/3.56 (H-1‴/H-3′) observed in the ROESY spectrum confirmed the linkage between the arabinopyranosyl and the galactopyranosyl units to be at the 3′-position. Thus, 4, which is the main saponin of *N. ossifragum*, was identified as sarsasapogenin-3-*O*-(2′-*O*-*β*-glucopyranosyl-3′-*O*-*α*-arabinopyranosyl-*β*-galactopyranoside). A sodiated molecular ion $[M+Na]^{+}$ at *m/z* 895.46624 (calculated: *m/z* at 895.46681; Δ: −0.53 ppm) observed in HRMS of **4** corresponding to $C_{27}H_{30}O_{15}Na^{+}$ confirmed this identity. Following a similar strategy, compounds **1**, **2** and **3** were identified as sarsasapogenin (**1**), sarsasapogenin-3-*O*-*β*-galactopyranoside (**2**) and sarsasapogenin-3-*O*-(2′-*O*-*β*-glucopyranosyl-*β*-galactopyranoside) (**3**), respectively.

The stereochemistry of the sapogenin aglycones of compounds **1**-**4** was in all instances determined to be (3*β*,5*β*,25*S*)-spirostan-3-ol by 2D 1H ROESY NMR (Figure 9), with the same stereochemistry as the aglycone sarsasapogenin reported in the literature (Inoue et al., 1995).

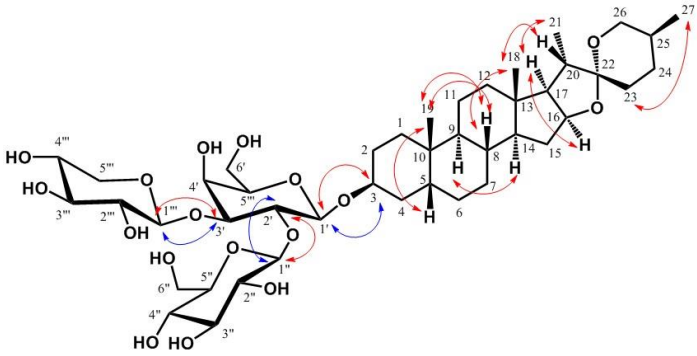

Figure 9. HMBC correlations (blue curved arrows) and ROE correlations (red curved arrows) important for complete structure determination of sarsasapogenin-3-*O*-(2'-*O*-*β*-glucopyranosyl-3'-*O*-*α*-arabinopyranosyl-*β*-galactopyranoside) (**4**) isolated from flowering tops of *N. ossifragum*.

We identified sarsasapogenin-3-*O*-(2′-*O*-*β*-glucopyranosyl-3′-*O*-*α*-arabinopyranosyl-*β*-galactopyranoside) as the main saponin of *N. ossifragum*. This compound, in addition to sarsasapogenin-3-*O*-(2′-*O*-*β*-glucopyranosyl-*β*-galactopyranoside), has previously been identified in the related Asian species *N. asiaticum* (Inoue et al., 1995). Sarsasapogenin-3-*O*-*β*-galactopyranoside is identified for the first time in the genus Narthecium. The compound mentioned before was previously identified in *Anemarrhena asphodeloides* (Bge) (Sy et al., 2016).

The components of the aqueous phase were further separated by gradient XAD-7 adsorption chromatography, Sephadex LH-20 gel filtration chromatography and preparative HPLC; detailed methodology can be found in Paper **I**. The UV spectra of compounds **5**–**10** (Figure 10) recorded online during HPLC analysis showed UV maximum absorptions at 346–347 nm and 269–271 nm, indicating that these compounds have a flavone core structure. These six compounds were identified using 1D and 2D NMR spectroscopic techniques and HRMS, and they are described below.

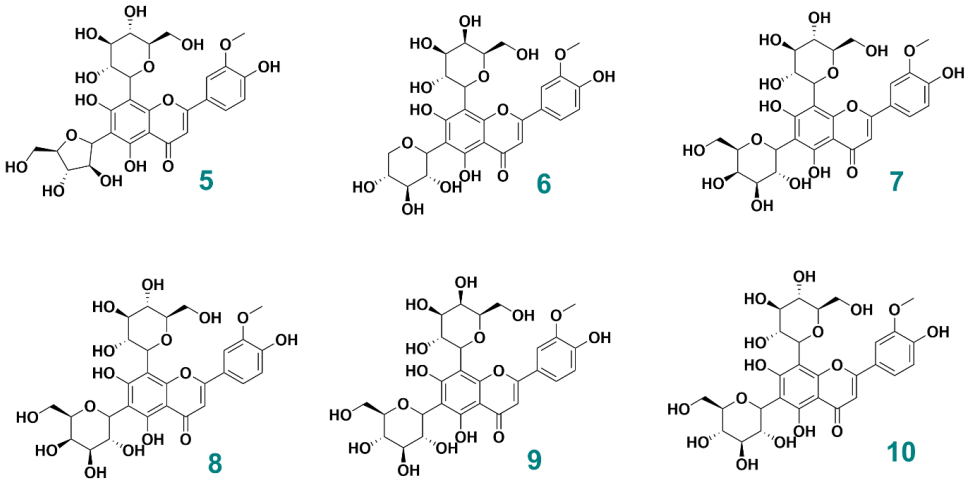

Figure 10. Structures of the aromatic compounds chrysoeriol 6-*C*-*β*-arabinofuranosyl-8-*C*-*β*-glucopyranoside (**5**), chrysoeriol 6-*C*-*β*-arabinopyranosyl-8-*C*-*β*-glucopyranoside (**6**), chrysoeriol 6-*C*-*β*-xylopyranosyl-8-*C*-*β*-galactopyranoside (**7**), chrysoeriol 6-*C*-*β*-galactopyranosyl-8-*C*-*β*-glucopyranoside (**8**), chrysoeriol 6-*C*-*β*-glucopyranosyl-8-*C*-*β*-galactopyranoside (**9**) and chrysoeriol 6,8-di-*C*-*β*-glucopyranoside (**10**) isolated for the first time from flowering tops of *N. ossifragum*.

Compound **10** was identified as the known compound chrysoeriol 6,8-di-*C*-*β*-glucopyranoside (Figure 10). A di-*C*-glycoside of chrysoeriol was first indicated to occur in the moss *Mnium affine* Bland (Melchert & Alston, 1965). Chrysoeriol 6,8-di-*C*-*β*-glucopyranoside was originally identified in *Larrea tridentata* (Sakakibara et al., 1977), but has also been identified in several quite diverse sources such as *Spergularia rubra* (Bouillant et al., 1979), the liverwort *Trichocolea tomentella* (Mues, 1982) and *Tricophorum cespitosum* (Salmenkallio et al., 1982).

The downfield region of the 1D ^{1}H NMR spectrum of compound **5** showed a 3H ABX system at δ 7.55 (d 2.2 Hz; H-2′), δ 7.73 (dd 8.3, 2.2 Hz; H-6′) and δ 6.88 (d 8.3 Hz; H-5′), in addition to a 1H singlet at δ 6.94 (H-3), which is in accord with chrysoeriol aglycone with substituents at C-6 and C-8. A 3H signal corresponding to a methoxy group attached to the 3′-position of the aglycone of **5** was observed at δ 3.88 ppm. The methoxy group was confirmed to be attached to C-3′ of the aglycone by the cross-peak at δ 3.88/148.0 (3′-OCH$_3$/C-3′) observed in the HMBC spectrum of **5** and the cross-peak at δ 3.88/7.55 (3′-OCH$_3$/H-2′) observed in the ROESY spectrum

of **5**. The glycosyl substituent attached to the 6-position of the aglycone was identified as arabinofuranose by the observed $^{1}H–^{1}H$ coupling constants in the 1D ^{1}H NMR spectrum, in addition to the characteristic downfield shifts of C-2″, C-3″ and C-4″ of this glycosyl unit (Fossen & Andersen, 2006). The linkage between the arabinofuranosyl and chrysoeriol aglycone was confirmed to be at the 6-position by the observed cross-peaks at δ 5.44/162.7 (H-1’’/C-7), δ 5.44/157.1 (H-1’’/C-5) and δ 5.44/103.3 (H-1’’/C-6) in the 2D $^{1}H–^{13}C$ HMBC spectrum of **5** and the cross-peak at δ 5.44/13.81 (H-1’’/5-OH) observed in the 2D ^{1}H ROESY spectrum of **5**. The glycosyl unit attached to the 8-position of the aglycone of **5** was identified as glucose by observation of seven proton resonances, where large axial-axial coupling constants between the ring protons of the glycosyl were found, and the characteristic values (Fossen & Andersen, 2006) of the six ^{13}C resonances belonging to this unit. The anomeric coupling constant (9.9 Hz) observed in the 1D ^{1}H NMR spectrum of **5** confirmed the *β*-configuration of H-1‴. The linkage between the glucopyranosyl and chrysoeriol aglycone was confirmed to be at the 8-position by the observed cross-peaks at δ 4.70/162.7 (H-1‴/C-7), δ 4.70/154.9 (H-1‴/C-9) and δ 4.70/104.5 (H-1‴/C-8) in the 2D $^{1}H–^{13}C$ HMBC spectrum of **5**. Thus, **5** was identified as the previously undescribed compound chrysoeriol 6-*C*-*β*-arabinofuranosyl-8-*C*-*β*-glucopyranoside (Figure 10). Tables and the NMR data can be found in the second part of this thesis. A sodiated molecular ion $[M+Na]^{+}$ at *m/z* 617.14848 (calculated: *m/z* at 617.14832; Δ: 0.39 ppm) observed in the HRMS of **5** corresponding to $C_{27}H_{30}O_{15}Na^{+}$ confirmed this identity.

The 1D and 2D NMR spectra of **6** shared many similarities to that of **5**, showing chrysoeriol aglycone glycosylated with an arabinosyl unit at the 6-position and a glucopyranosyl substituent at the 8-position, respectively. The arabinosyl substituent of compound **6** was, however, determined to be in the pyranose form by the characteristic carbon signals at δ 73.9 (C-1″), δ 68.1 (C-2″), δ 73.6 (C-3″), δ 69.3 (C-4″) and δ 69.9 (C-5″) which are accord with an arabinopyranosyl unit (Fossen & Andersen, 2006). Thus, compound **6** was identified as the previously undescribed di-*C*-glycosyl flavone chrysoberyl 6-*C*-*β*-arabinopyranosyl-8-*C*-*β*-glucopyranoside

(Figure 10) chemical shifts values and coupling constants can be found in the second part of this work. The sodiated molecular ion $[M+Na]^+$ at m/z 617.14867 (calculated: *m/z* at 617.14832; Δ: 0.71 ppm) observed in HRMS of **6** corresponding to $C_{27}H_{30}O_{15}Na^+$ confirmed this identity.

The 1D and 2D NMR spectra of **7** shared many similarities to that of **5**, showing chrysoeriol aglycone glycosylated with a pentose at the 6-position and a hexose at the 8-position, respectively. The 6-glycosyl substituent of **7** was identified as *β*-xylopyranose by comparing the five ^1H resonances in the region 4.55–3.05 in the 1D ^1H NMR spectrum of **7** and the corresponding five ^{13}C resonances belonging to this unit. The 8-glycosyl substituent of the 6-position was identified as *β*-galactopyranose by the signals corresponding to seven hydrogens in the region 5.00–3.47 in the 1D ^1H NMR spectrum of **7** and the corresponding six ^{13}C resonances belonging to this unit. The observed characteristic small axial-equatorial coupling constant for the coupling between H-3‴ and H-4‴ (2.8 Hz) verified the identification of the galactopyranose unit of **7**. Thus, compound **7** was identified as the previously undescribed compound chrysoeriol 6-*C*-*β*-xylopyranosyl-8-*C*-*β*-galactopyranoside (Figure 10). A sodiated molecular ion $[M+Na]^+$ at *m/z* of 617.14855 (calculated: *m/z* at 617.14832; Δ: 0.51 ppm) was observed in HRMS of **7** corresponding to $C_{27}H_{30}O_{15}Na^+$. A further sodiated molecular ion $[M+2Na–H]^+$ at *m/z* 639.13064 (calculated: *m/z* at 639.13027; Δ: 0.71 ppm) observed in HRMS of **7** corresponding to $C_{27}H_{29}O_{15}Na_2^+$ confirmed this identification.

The 1D and 2D NMR spectra of **9** shared many similarities to that of **7**, showing chrysoeriol aglycone glycosylated at positions -6 and -8 of the aglycone, with galactopyranose as the 8-glycosyl substituent. The 6-*C*-glycosyl substituent of **9** was, however, identified as glucopyranosyl. Thus, compound **9** was identified as the previously undescribed flavonoid chrysoeriol 6-*C*-*β*-glucopyranosyl-8-*C*-*β*-galactopyranoside) (Figure 10). The sodiated molecular ion $[M+Na]^+$ at *m/z* 647.15899 (calculated: *m/z* at 647.15889; Δ: 0.29 ppm) observed in HRMS corresponding to $C_{28}H_{32}O_{16}Na^+$, and $[M+2Na–H]^+$ at *m/z* 669.14084 (calculated: *m/z*

at 669.14084; Δ: 0.34 ppm) observed in HRMS of **9** corresponding to $C_{28}H_{31}O_{16}Na_2^+$ confirmed this identification.

The 1D and 2D NMR spectra of **8** shared many similarities to that of **9**, showing chrysoeriol aglycone C-glycosylated with glucose and galactose at positions **6** and **8** of the aglycone. However, the positions of the *C*-glycosyl substituents were interchanged as compared to those of **9**. Thus, compound **8** was identified as the previously undescribed flavonoid chrysoeriol 6-*C*-*β*-galactopyranosyl-8-*C*-*β*-glucopyranoside (Figure 10). The sodiated molecular ions $[M+Na]^+$ at *m/z* 647.15868 (calculated: *m/z* at 647.15889; Δ: −0.19 ppm) observed in HRMS of **8** corresponding to $C_{28}H_{32}O_{16}Na^+$, and $[M+2Na–H]^+$ at *m/z* 669.14138 (calculated: *m/z* at 669.14084; Δ: 0.94 ppm) corresponding to $C_{28}H_{31}O_{16}Na_2^+$ confirmed compound **8** to be the previously undescribed compound chrysoeriol 6-*C*-*β*-galactopyranosyl-8-*C*-*β*-glucopyranoside.

Circular Dichroism (CD) spectra of all isolated di-*C*-glycosylflavones were recorded. All these compounds are based on the same chrysoeriol aglycone. According to Gaffield et al. (1978), the CD bands of di-*C*-glycosylflavones are often relatively weak because of the overlapping of oppositely signed adjacent CD bands (Wellman et al., 1965). The similarity of the recorded CD spectra of compounds **6**–**10** indicates that the configurations of C-1 of the glycosyl substituents are similar for these compounds (Gaffield et al., 1978). The fact that the CD spectrum of compound **5**, which exhibited a strong negative band at 275 nm, differed from the CD-spectra recorded of compounds **6**–**10** may not be unexpected since compound **5** is the only di-*C*-glycosylflavone among the isolated compounds which is substituted by an arabinofuranosyl moiety.

Compounds **8**–**10** exhibit most of their ^1H and ^{13}C-NMR signals in double sets. These signals reveal two conformational isomers created by rotational hindrance at the $C(sp^3)$-$C(sp^2)$ glucosyl–flavone linkage in each of these 6,8-di-*C*-substituted flavones (Rayyan et al., 2005). The equilibrium between the rotamers was supported by observations of strong exchange peaks between equivalent protons of each rotameric

pair in their ROESY spectra. The isomerisation of di-*C*-glycosyl flavones by Wessely Moser rearrangement was demonstrated to occur by the fact that during the final isolation of pure compounds by preparative HPLC, compound **5** was isolated at two different retention times from the same mixture. This may not be surprising since we have previously observed similar isomerisation of *C*-glycosyl-3-deoxyanthocyanins occurring under similar mild experimental conditions (Bjorøy et al. 2009a, 2009b).

To investigate if any of the compounds could be responsible for the death of sheep and cattle, their cytotoxic potential was investigated on three cell lines. The rat kidney epithelial cell line NRK, the rat cardiomyoblast H9c2, and the human AML cell line MOML13. The flavonoids (compounds **5**-**10**) exhibited no or very low toxicity towards the cell lines, with either activity above 0.5 mM or no detectable cytotoxic activity at 1 mM (Table 1). The saponins (compounds **1**-**4**) were more potent. Interestingly, the cytotoxic potential increased proportionally with the increasing number of glycosyl substituents, where compound **4** (sarsasapogenin-3-*O*-(2'-*O*-*β*-glucopyranosyl-3'-*O*-*α*-arabinopyranosyl-*β*-galactopyranoside)) showed an EC_{50} between 2-8 μM after 72 hours of incubation (Table 1 and Figure 11).

Table 1. Cytotoxicity of compounds **1**–**10** against three mammalian cell lines. The compounds were diluted in DMSO, and a dilution series was made on each cell line. The cells were tested for metabolic activity after 72 h of incubation. The EC_{50} values were determined by non-linear regression from 3 to 5 independent experiments (NRK and MOLM13) as described in the methods section. The data from H9c2 is from one experiment. "– "denotes that no data is available due to low toxicity.

	NRK		**MOLM 13**		**H9c2**	
	EC_{50} (mM)	**R^2**	**EC_{50} (mM)**	**R^2**	**EC_{50} (mM)**	**R^2**
1	0.5-1.0	-	0.4	0.66	> 0.3	-
2	0.12	0.86	0.22	0.69	0.2-0.6	-
3	0.05	0.77	0.08	0.74	0.02	0.92
4	0.007	0.94	0.002	0.85	0.006	0.96
5	> 1.0	-	0.5-1.0	-	-	-
6	> 1.0	-	0.5-1.0	-	-	-
7	> 1.0	-	> 1.0	-	-	-
8	> 1.0	-	> 1.0	-	-	-
9	> 1.0	-	> 1.0	-	-	-
10	> 1.0	-	0.5-1.0	-	-	-

These results indicate that the saponins, and particularly the main saponin (**4**), are responsible for some of the toxic effects observed in livestock after ingestion of flowering tops of *N. ossifragum*. All cell lines were severely affected by this compound, indicating that the presence of this substance in the vascular system might affect the function of the heart, leukocytes, and kidneys. Furthermore, our data suggests that compounds **3** and **4** induce both sub-acute and protracted toxicity since we found significant cell death at 24 hours, which increased after 72 hours (Figure 11). It has previously been shown that orally administered saponins induced damage in the intestinal mucosa, as well as causing liver and kidney necrosis (Aguilar-Santamaría et al., 2013; Diwan et al., 2000). Moreover, case reports of cattle with suspected *N. ossifragum* poisoning showed hepatic fibrosis and reduced renal function (Flåøyen et al. 1995a Flåøyen et al. 1995b; Angel & Ross, 2011). Interestingly, Angell and Ross (2011) observed that the condition of one of the cattle was exacerbated even after treatment was initiated (Angell & Ross, 2011), indicating

irreparable damage or a protracted toxic effect. The kidney and liver might be particularly vulnerable to compounds like compounds **3** and **4** due to their high perfusion rate and their ability to actively take up (hepatocytes) or concentrate (kidney tubule) xenobiotics.

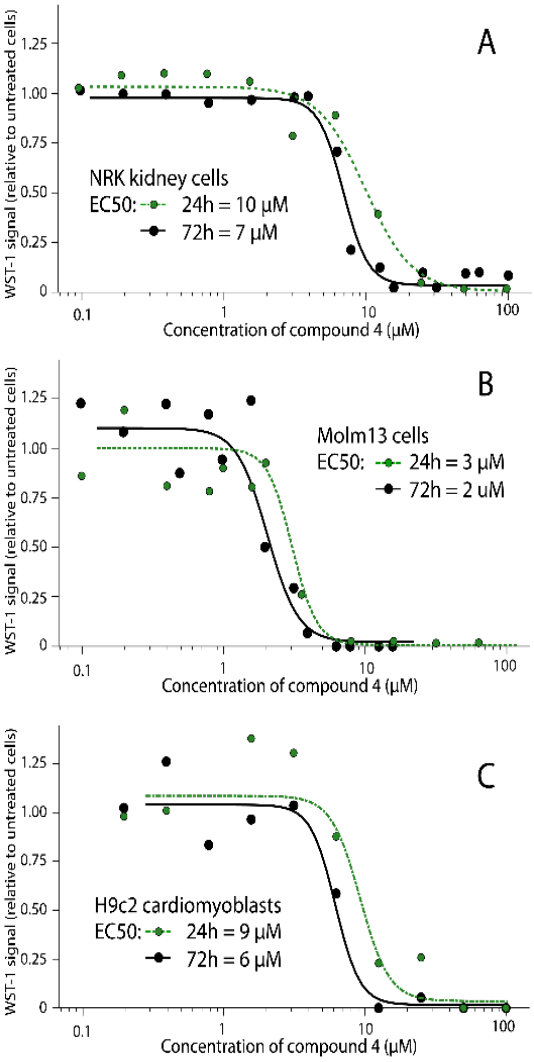

Figure 11. EC_{50} values of the main saponin (**4**) isolated from flowering tops of *N. ossifragum* towards normal rat kidney (NRK) cells, MOLM13 cells and H9c2 cardiomyoblasts.

4.2. Paper II: Cytotoxic saponins from the livestock-poisoning plant *Narthecium ossifragum* (L). – Effect on biological membranes

In the current literature, several papers suggest that sarsasapogenin derivatives may have significant potential as active principals of new anticancer drugs. These studies are about the cell-death mechanism in different cancer cells lines using sarsasapogenin and sarsasapogenin-3-*O*-(2'-*O*-*β*-glucopyranosyl-*β*-galactopyranoside) (Peng et al., 2020; Bao et al., 2007; Trouillas et al., 2004; Shen et al., 2013; Han et al., 2018; Lin et al., 2020; Kim et al., 2016; Song et al., 2019; King et al., 2009; Liu et al., 2023; Wang et al., 2013; Zhang et al., 2021; Chiang et al., 2019; Liu et al., 2020).

However, there is a lack of studies on how the different elements of the cells are affected by these compounds. Consequently, we aimed to reveal how four sarsapogenins derivatives affected the cell membrane of mammalian cells, using electron microscopy followed by mechanistic studies on the membranes. Our findings give indications on the underlying cause of the reported kidney failure of livestock after ingestion of the plant, in addition to providing insight which may be crucial in the further research of these steroidal saponins in cancer therapy.

4.2.1. Microscopic evaluation of cell membrane

Saponins can trigger various mechanisms of cell death involving cell lysis, necrosis, apoptosis, and autophagy (Loret et al., 2014) and this could be dose dependent. It has been demonstrated that the cyanobacterial toxins microcystin and nodularin have opposite effects on liver cells depending on whether they are exposed to large, intermediate, or very low doses of the toxin (Herfindal & Selheim, 2006). However, we have previously reported that saponins isolated from *N. ossifragum* were cytotoxic against three cell lines with no selectivity towards cancer and normal cells lines (Carpinteyro Diaz et al., 2019), and the fact that sarsasapogenin has been reported to

affect endothelial and epithelial cells (Whang et al., 2002; Choi, 2023) encouraged us to study of the sarsasapogenin-induced morphological changes on a subcellular level.

MOLM13 cells were treated with the different sarsasapogenins derivatives for three hours, and TEM images were acquired after fixation and processing (Figure 12). Untreated cells have a distinct bean-shaped nucleus with a visible nucleolus. Furthermore, different organelles can be observed in the cytoplasm, such as mitochondria, ribosomes, and Golgi apparatus (Figure 12A). Cells treated with sarsasapogenin aglycone (compound **1**) had changes in the cell membranes, notably loss of microvilli, and the chromatin appears to be more condensed (Figure 12B). For cells treated with sarsasapogenin-3-*O*-*β*-galactopyranoside (compound **2**), we could observe some cytoplasm vacuolisation, and the mitochondria were more visible compared to the cytosol. Here, there were no microvilli left on the surface membrane (Figure 12C).

MOLM13 cells treated with sarsasapogenin-3-*O*-(2'-*O*-*β*-glucopyranosyl-*β*-galactopyranoside, (compound **3**) or sarsasapogenin-3-*O*-(2'-*O*-*β*-glucopyranosyl-3'-O-*α*-arabinopyranosyl-*β*-galactopyranoside) (compound **4**) were more heavily affected (Figure 12D and 12E), with considerable vacuolisation (Figure 12D) and a change in nuclear morphology to a more spherical, with hypercondensed chromatin. Furthermore, the cell surface is completely without microvilli or invaginations. In Figure 12D it is also possible to observe signs of autophagy (inset). We also found necrotic cells with a disintegrated cell membrane and ruptured nuclear envelope, where most of the cytosolic content, including organelles, was lost (Figure 13). However, some remnants of mitochondria could be found. There were also some cases of cells with fragmented and hypercondensed nuclei, typical for apoptosis (Figure 13B). From these images, it is evident that the alterations in cell morphology were more severe when exposed to sarsasapogenin-3-*O*-(2'-*O*-*β*-glucopyranosyl-*β*-galactopyranoside, (compound **3**) or sarsasapogenin-3-*O*-(2'-*O*-*β*-glucopyranosyl-3'-O-*α*-arabinopyranosyl-*β*-galactopyranoside) (compound **4**). This aligns with our previous results, which showed that the different sarsapogenins have different

cytotoxic potency, with the triglycerides being the most potent and the aglycone the least potent (Carpinteyro Diaz et al., 2019).

Poisoning of cattle leading to kidney failure is caused by ingesting flowering tops of *N. ossifragum*, which contains a mixture of compounds **1**-**4**. We therefore investigated how a 1:1:1:1 mixture of compounds **1**-**4** with a total saponin concentration of 300 µM (75 µM of each), affected MOLM-13 cells. As seen in Figure 12F, the morphology resembles that of the most severely affected cells, such as those treated with compounds **3** or **4**. This suggests that the saponins are able to work in concert to induce cellular damage. This observation is important in relation to the toxic effects seen in cattle after ingesting *N. ossifragum*. It is apparently the total saponin content that determines the toxic effects, where the impact of less toxic variants may be potentiated in the presence of the most toxic.

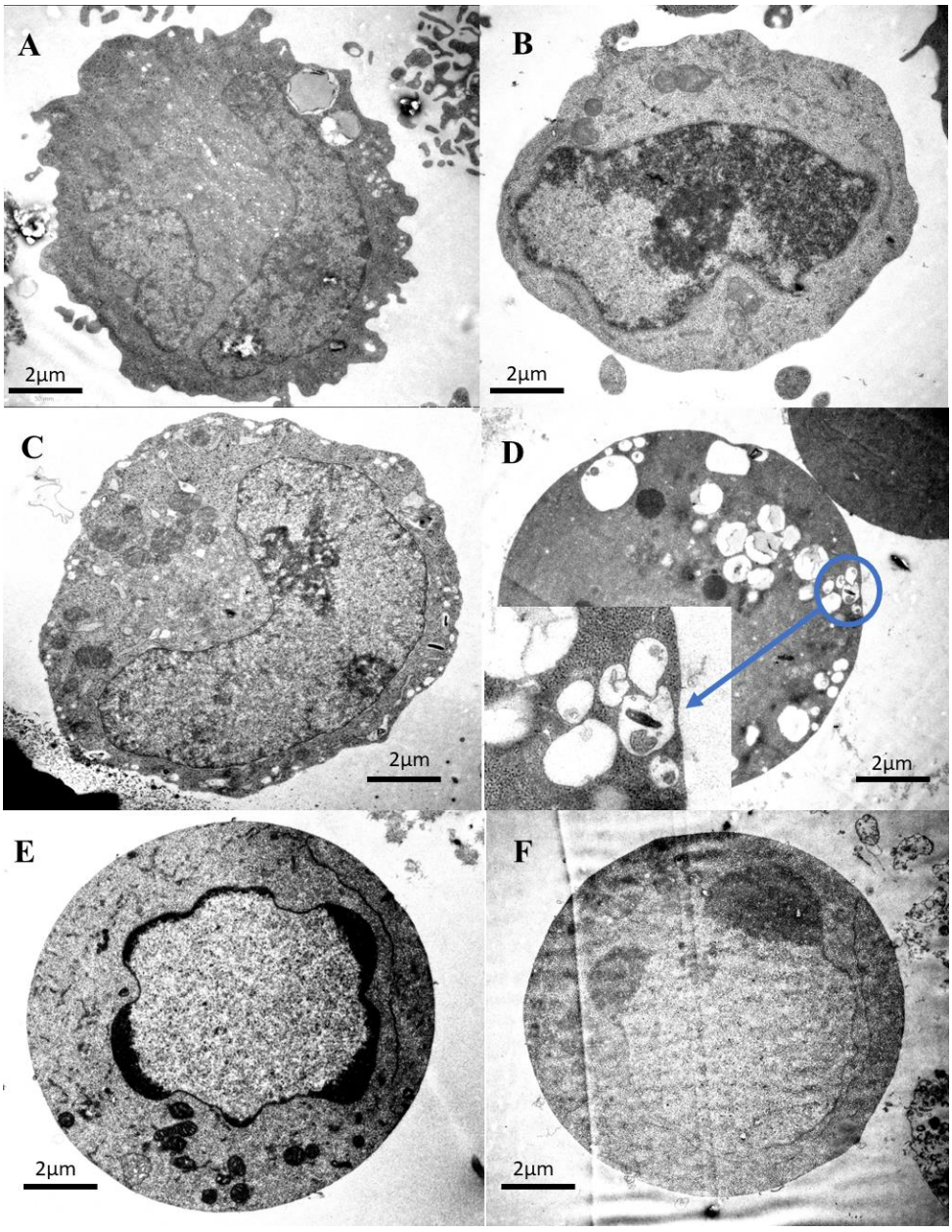

Figure 12. AML MOLM13 cells were treated with sarsasapogenin (**1**), sarsasapogenin-3-*O*-*β*-galactopyranoside (**2**), sarsasapogenin-3-*O*-(2'-*O*-*β*-glucopyranosyl-*β*-galactopyranoside) (**3**), and sarsasapogenin-3-*O*-(2'-*O*-*β*-glucopyranosyl-3'-*O*-*α*-arabinopyranosyl-*β*-galactopyranoside) (**4**) with a final concentration of 300 µM of each compound (B-D) a mixture of compound 1-4 with total saponin concentration of 300 µM (E). An untreated AML MOLM13 cells (A).

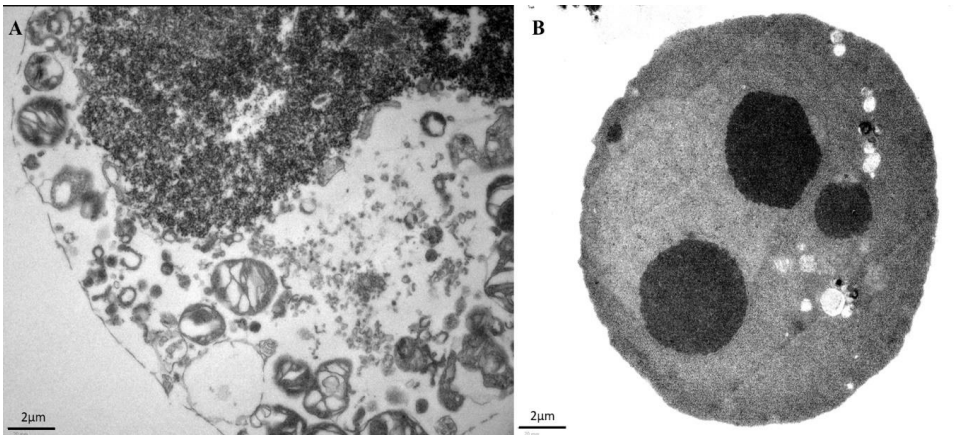

Figure 13. MOLM13 AML cells treated with 300 µM compound 4. A: A necrotic cell with a destroyed membrane and with complete loss of the cell nuclei. B: An apoptotic cell with altered membrane structure.

Another interesting change that was possible to observe was how the cytoplasm of the cell changed in the presence of these compounds. In Figure 14, the differences between the control cell (Figure 14A) and a cell affected by compound 4 are displayed (Figure 14B). In the control cell, it is possible to see how the cytoplasm is intact. The ribosomes of the intact cells are in clusters, whereas in the cells treated with sarsasapogenin derivatives, the cytoplasm ribosomes look homogenously distributed (Pachmann et al., 2013). That could indicate a change in the composition of the cytoplasm because of the observed membrane rupture that could affect the homeostasis of the cell.

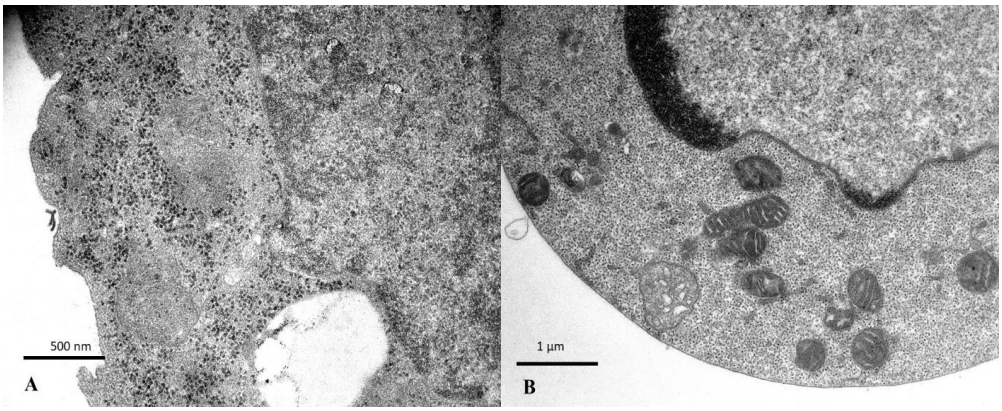

Figure 14. The difference in the cytoplasm in AML MOLM13 cells. A is the control cell line. B shows a MOLM13 cell treated with compound **4**.

4.2.2. Determination of membrane permeability.

In order to find if the cell death observed by TEM could be due to the saponins interfering with the cell membrane, we studied their impact on the integrity of liposomes consisting of phosphatidylcholine and cholesterol. This was chosen since the mitochondria appeared intact even if the outer cell membrane was disintegrated. We have shown that this could be due to the cholesterol dependency of membrane-active compounds isolated from cyanobacteria (Oftedal et al., 2012; Humisto et al., 2019). The lipid membrane permeabilisation assay was performed with the three saponins and their aglycone sarsasapogenin. Because sarsasapogen-in-3-*O*-(2′-*O*-*β*-glucopyranosyl-3′-*O*-*α*-arabinopyranosyl-*β*-galactopyranoside) was the most potent compound described previously (Carpinteyro Diaz, et al., 2019), an experiment with a concentration of 5 µM of this compound was performed. During this experiment, there was no leakage from the liposomes until the synthetic detergent (Tween 20) was added (data not shown). Therefore, the saponins were tested with the highest concentration possible (1 mM, Figure 15).

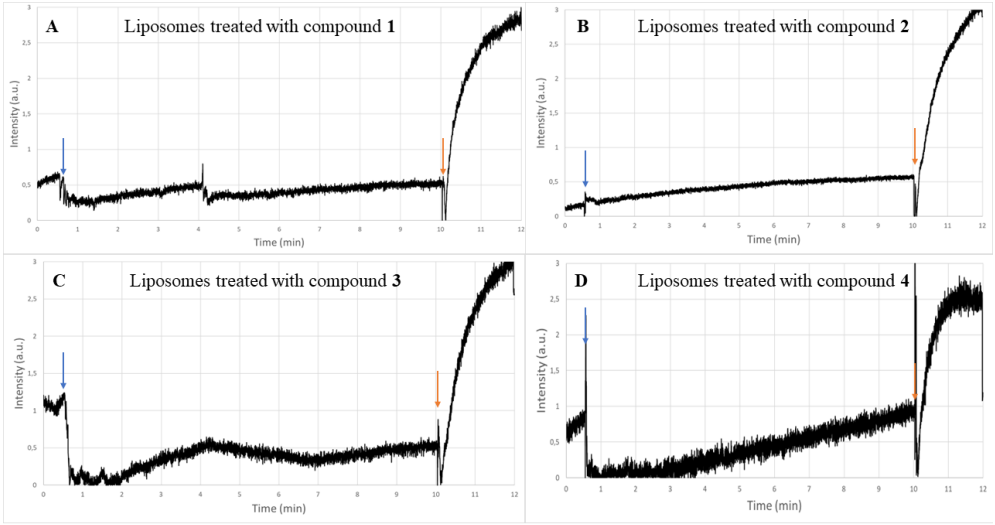

Figure 15. Calcein leakage assay between liposome and four different saponins with a final concentration of 1 mM. The injection of the saponin was 30 seconds after the experiment started (marked with a blue arrow), while the injection of 10% Tween 20 was after 10 minutes (marked with an orange arrow). A: lipid membrane treated with compound **1**; B: lipid membrane treated with compound **2**; C: lipid membrane treated with compound **3**; D: lipid membrane treated with compound **4**.

The lipid concentration of the liposome suspension used during the experiments shown in Figure 15 was 10 µg/mL. It is evident that none of the saponins were able to reach the critical micelle concentration (CMC) to disrupt the membrane. Although there are some indications of a small calcein release, it is far from the maximum release induced by the addition of Tween-20. The fluctuations in fluorescence intensity could indicate that there is a minor release of calcein but that the membrane can reorganise and maintain its integrity. Compound **4** had the highest calcein release but was still modest compared to Tween-20.

These results indicate that there is some interaction between the saponin and the membrane, but not sufficient to induce complete release of calcein. This can be because the saponins create aggregates in solution or that the presence of saponins in the membrane does not change the geometry of the lipid bilayer to an extent that causes breaks.

4.2.3. Haemolysis activity

Since liposomes used in the previous experiment consisted of only PC and cholesterol, it could be that they lack some constituents that are present in cell membranes, which are crucial for saponins to exert their membrane-active action. Red blood cells represent an ideal model for studying cell membrane integrity because of their structural simplicity while still having a complex membrane (Bain, 2004; Hatton, 2013; Lorent et al., 2014). Because of the low membrane disruptive activity observed with the liposome model membranes, individual saponin concentrations of 100-300 µM were applied for the experiments with red blood cells. In Table 2, the haemolytic activity of the four sarsasapogenin derivatives is presented, including the measured haemoglobin content in plasma after adding the four different compounds and the 1:1:1:1 mixture thereof.

Table 2. Haemolytic activity of sarsasapogenin (**1**), sarsasapogenin-3-*O*-*β*-galactopyranoside (**2**), sarsasapogenin-3-*O*-(2'-*O*-*β*-glucopyranosyl-*β*-galactopyranoside) (**3**), and sarsasapogen-in-3-*O*-(2'-*O*-*β*-glucopyranosyl-3'-*O*-*α*-arabinopyranosyl-*β*-galactopyranoside) (**4**), and a 1:1:1:1 mixture of these compounds, isolated from *N. ossifragum*. A voluntary healthy donor provided the blood sample with a haemoglobin value of 14.1 g/dL and 39% of erythrocytes present in the control sample.

Concentration of the saponins (µM)	**Haemolysis activity (%)**				
	1	**2**	**3**	**4**	**Mixture**
100	4	9	4	9	9
150	4	9	9	13	9
200	9	9	9	48	9
250	26	13	9	31	9
300	22	13	9	13	9

Sarsasapogen-in-3-*O*-(2′-*O*-*β*-glucopyranosyl-3′-*O*-*α*-arabinopyranosyl-*β*-galactopyranoside) (compound **4**) was the most potent compound exhibiting a maximum of 48 per cent haemolytic activity (Table 2). The aglycon sarsasapogenin (compound **1**) exhibited haemolytic activity at concentrations of 200 µM, which increases with increasing concentration. Compounds **2** and **3** had intermediate

activity, whereas the 1:1:1:1 mixture of compounds **1**-**4** exhibits the same activity at all applied concentrations (Table 2). Moreover, from the data in Table 2, it appears that higher concentration does not increase haemolytic activity. This could be because a threshold is reached, where maximum activity is induced. However, as is evident by compound **4**, the activity declines with increasing concentrations, suggesting that the saponins become unavailable, presumably due to aggregations or micelle formations at high concentrations.

The haemolytic activity of saponins depends not only on the structure of the aglycon but also on the amount, types, and linkage of sugar moieties (Böttger et al., 2012; Bain, 2004; Hatton, 2013).

The destruction of red blood cells and leakage of substantial amounts of haemoglobin in the blood cause both anaemia and kidney failure. Suzuki et al. (1985) reported that domestic animals which have ingested *N. asiaticum* had a low count of erythrocytes but a high count of white blood cells and gastrointestinal tract bleeding, which was visualised by detection of blood in the fesses. Anaemia created by haemolysis could explain some of the symptoms presented in livestock such as lambs, goats, and cattle (Flåøyen et al., 1995; Suzuki et al., 1985; de Groot & Müller-Goymann, 2016; Greco et al., 2020).

Therefore, it may be reasonable that ruminants that ingest *N. ossifragum* and *N. asiaticum* containing cytotoxic saponins experience toxin-induced non-immune haemolytic anaemia (Hatton, 2013; Lange et al., 2005; Lange et al., 2009).

4.3. Paper III: Cytotoxic Natural Products from the Jurassic Relic *Osmunda regalis* (L).

The royal fern (*Osmunda regalis*) has been widely used for its medicinal properties in traditional medicine for several centuries. Hieronymus Brunschwig, a German surgeon, alchemist, and botanist, wrote about the plant's potential use in the treatment of cancer, fistulas, and fractures in his book Kleines Destillierbuch (Brunschwig, 1500; Schmidt et al., 2017). Moreover, in some regions of Northern Spain, such as Galicia, Asturias, and Cantabria, the plant has been traditionally used to treat bone fractures and alleviate muscular pain (Molina et al., 2009).

Even though *O. regalis* has been utilised as a medicinal plant for more than five centuries, only a few compounds have been identified, including sitosterol, which has been found in different parts of the plant (Sumi, 1929; Jetter & Riederer, 2000), as well as the steroid Ecdysterone (20-hydroxyecdysone) (Ikan & Shulman, 1972). Several relatively nonpolar compounds like saturated fatty acids (Radnuz, 1967; Gemmrich, 1977), alkanediols, ketoaldehydes, methyl palmitate and other fatty acid esters (Hollenbaek & Kuehne, 1974; Jetter & Rieder, 1999) have been reported from this species. Anthocyanins based on the aglycones pelargonidin and cyanidin have also been detected, where the cyanidin derivative is indicated to be an acylated anthocyanin (Price et al., 1939). Further phenolic compounds, like tannis and gallotannins (Lazaro-Carrasco et al., 1987b), as well as a multitude of phenolic acids including caffeic acid, *p*-coumaric acid, *p*-hydroxybenzoic acid, cinnamic acid, and vanillic acid, have previously been identified from this species (Courbet et al., 1971; Lazaro-Carrasco et al., 1987a). Only a few specific compounds to this species, including osmundalactone (Numata et al., 1984) and osmundalin, which is the glucoside of osmundalactone (Hollenbaek & Kuehne, 1974), have hitherto been identified in current literature.

In this work, we describe the characterisation of 17 natural products from the aerial parts of *Osmunda regalis* 15 of these compounds are identified in this species for the first time, which include the six undescribed compounds. In addition, cytotoxic

analysis of some of the isolated compounds was done towards acute monocyte leukaemia cells (MOLM13), as well as towards rat cardiomyoblasts cells (H9c2) and kidney epithelial cells (NRK).

The eleven known compounds chalconaringenin 2'-*O*-*β*-glucopyranoside (**11**), vanillic acid (**14**), *p*-hydroxy-benzoic acid (**15**), *p*-hydroxy-benzoic acid methyl ester (**17**), dihydrodehydrodiconiferyl alcohol 4-*O*-*α*-rhamnopyranoside (**18**), apigenin 7-(2''-*O*-*α*-rhamopyranosyl-*β*-glucopyranoside) (**19**), epoxyconiferyl alcohol (**20**), 5-hydroxy-2-hexen-4-olide (**21**), Blumenol C glucoside (**24**), hexyl-*β*-glucopyranoside (**26**) and 2-hexenoic acid (**27**) (Figures 16) were identified from the fern leaves of *Osmunda regalis* (L). The identifications were based on a combination of several 1D and 2D NMR spectroscopic techniques. Except for vanillic acid and p-hydroxy-benzoic acid, the compounds listed previously were detected in this plant material for the first time.

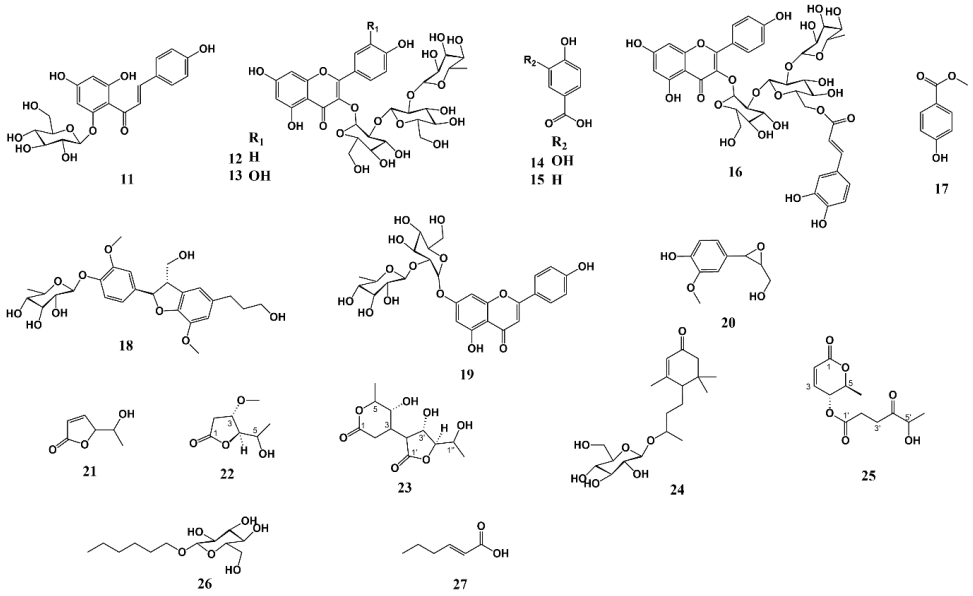

Figure 16. Molecular structures of compounds **11**-**27** characterised from *O. regalis* (L).

The UV spectrum of compound **12** recorded online during HPLC analysis exhibited λ_{max} values at 346 and 266 nm, which is in accordance with a flavonol derivative

(Markham, 1982). The aromatic region of the 1D ^{1}H NMR spectrum of **12** showed a 4H AA'XX' system at δ 8.05 ('d' 8.9 Hz, H-2',6') and δ 6.93 ('d' 8.9 Hz, H-3',5') which is consistent with a *p*-substituted B-ring; and a 2H AX system at δ 6.42 (d 2.0 Hz, H-8) and δ 6.18 (d 2.0 Hz, H-6) which is consistent a kaempferol derivative. The sugar regions of the 1D ^{1}H and 1D ^{13}C CAPT spectrum of **12** showed the presence of three sugar units. All ^{1}H and ^{13}C resonances of these glycosyl substituents were completely assigned by the 1D ^{1}H selective TOCSY spectra of each glycosyl substituent, in addition to the 2D ^{1}H-^{1}H COSY, the 2D ^{1}H-^{13}C HSQC, the 2D ^{1}H-^{13}C HSQC-TOCSY and the 2D ^{1}H-^{13}C H2BC spectra of **12**. The sugar units were identified to be two *β*-glucopyranose units and an *α*-rhamnopyranose unit, respectively, by the observed ^{1}H coupling constants in the 1D ^{1}H and the 1D ^{1}H selective TOCSY spectra, in addition to the 17 ^{13}C chemical shift values belonging to these sugar units observed in the 1D ^{13}C CAPT spectrum of **12**. The anomeric coupling constants revealed the *β*-configurations of the anomeric carbons of the glucosyl substituents and the *α*-configuration of the anomeric carbon of the rhamnosyl substituent, Tables for this structure can be found in the second part of this presented work.

Assignments of the ^{13}C resonances belonging to the aglycone and the inter-residual connections were determined by the 2D ^{1}H-^{13}C HMBC experiment (Figure 17). The cross-peak at δ 5.71/132.98 (H-1''/C-3) confirmed the linkage between the glucopyranosyl unit and the aglycone at the 3-hydroxyl. The downfield chemical shift of C-2'' (δ 77.83) of this glucosyl unit indicated the presence of a sugar substituent at this position. The cross-peaks at δ 4.97/77.83 (H-1'''/C-2'') and δ 3.70/100.2 (H-2''/C-1''') confirmed the linkage between the inner glucosyl substituent and the terminal glucosyl substituent to be at the 2''-position. Cross-peaks at δ 5.05/77.0 (H-1''''/C-2''') and δ 3.23/100.3 (H-2'''/C-1'''') complete the linkage between the terminal glucosyl unit and the rhamnosyl unit to be at the 2'''-position. Thus, compound **12** was identified to be the previously undescribed compound kaempferol 3-*O*-(2''-*O*-(2'''-*α*-rhamnopyranosyl)-*β*-glucopyranosyl)-*β*-glucopyranoside.

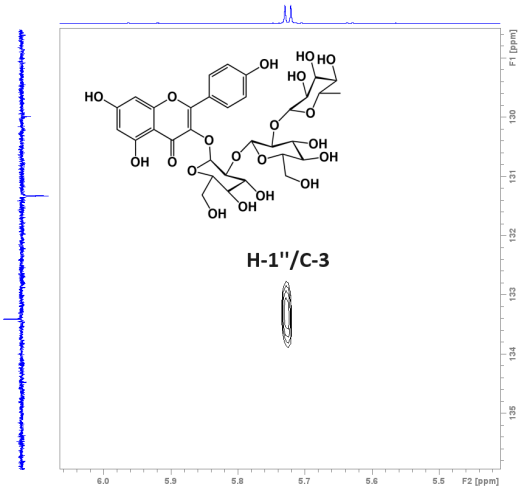

Figure 17. Expanded region of the 2D ^{1}H-^{13}C HMBC spectrum of **12** (kaempferol 3-*O*-(2''-*O*-(2'''-*α*-rhamnopyranosyl)-*β*-glucopyranosyl)-*β*-glucopyranoside) showing the cross-peak between H-1'' and C-3 which confirms the linkage between the inner glucose unit and kaempferol aglycone at the 3-position.

A sodium-added molecular ion $[M+Na]^+$ at *m/z* 779.1999 corresponding to $C_{33}H_{40}O_{20}Na^+$ (calculated: *m/z* 779.2005; Δ = -0.73 ppm) observed in the HRMS of compound **12** confirmed this identification (Figure 16).

Compound **13** exhibited a UV λ_{max} absorption at 352 and 256 nm, which resembles a flavonol derivative (Markham, 1982). The aromatic region of the 1D ^{1}H NMR spectrum of **13** showed a 3H ABX system at δ 7.49 (d 2.3 Hz, H-2',6') and δ 6.89 (d 8.5 Hz, H-3',5') which is consistent to a *m*- and *p*-substituted B-ring; and a 2H AX system at δ 6.38 (d 2.1 Hz, H-8) and δ 6.17 (d 2.1 Hz, H-6) match with a quercetin aglycone. The 1D ^{1}H and 1D ^{13}C CAPT spectrum of **13** indicated the existence of three sugar units in the sugar regions. The ^{1}H and ^{13}C resonances of these glycosyl substituents were fully determined by the 1D ^{1}H selective TOCSY spectra of each glycosyl substituent, in addition to the 2D ^{1}H-^{1}H COSY, the 2D ^{1}H-^{13}C HSQC, the 2D ^{1}H-^{13}C HSQC-TOCSY and the 2D ^{1}H-^{13}C H2BC spectra of **13**. The sugar units were identified to be two *β*-glucopyranose units and an *α*-rhamnopyranose unit, respectively, by the observed ^{1}H coupling constants in the 1D ^{1}H and the 1D ^{1}H selective TOCSY spectra, in addition to the 17 ^{13}C chemical shift values belonging to

these sugar units observed in the 1D ^{13}C CAPT spectrum of **13**. The anomeric coupling constants revealed the *β*-configurations of the anomeric carbons of the glucosyl substituents and the *α*-configuration of the anomeric carbon of the rhamnosyl substituent (Tables in Part **II**).

Assignments of the ^{13}C resonances belonging to the aglycone and the inter-residual connections were determined by the 2D ^{1}H-^{13}C HMBC experiment. The cross-peak at δ 5.70/133.15 (H-1’’/C-3) confirmed the linkage between the glucopyranosyl unit and the aglycone at the 3-hydroxyl. The downfield chemical shift of C-2’’ (δ 77.20) of this glucosyl unit indicated the presence of a sugar substituent at this position. Cross-peaks at δ 4.94/77.20 (H-1’’’/C-2’’) and δ 3.73/100.4 (H-2’’/C-1’’’) confirmed the linkage between the inner glucosyl substituent and the terminal glucosyl substituent to be at the 2’’-position. The cross-peaks at δ 5.06/76.9 (H-1’’’’/C-2’’’) and δ 3.23/100.3 (H-2’’’/C-1’’’’) ratified the linkage between the terminal glucosyl unit and the rhamnosyl unit to be at the 2’’’-position. Thus, compound **13** was identified to be the previously undescribed compound quercetin 3-*O*-(2’’-*O*-(2’’’-*α*-rhamnopyranosyl)-*β*-glucopyranosyl)-*β*-glucopyranoside.

A sodium-added molecular ion $[M+Na]^+$ at *m/z* 795.1951 corresponding to $C_{33}H_{40}O_{21}Na^+$ (calculated: *m/z* 795.1954; Δ = -0.37 ppm) observed in the HRMS of compound **13** confirmed this identification (Figure 16 and Part **II**).

The UV spectrum of compound **16** recorded online during HPLC analysis exhibited UV absorption maxima at 330 and 268 nm with notably strong absorption at 330 nm, in accordance with a flavonol derivative acylated with a cinnamic acid (Markham, 1982). The aromatic region of the 1D ^{1}H NMR spectrum of **16** showed a 4H AA’XX’ system at δ 7.98 (‘d’ 8.8 Hz, H-2’,6’) and δ 6.83 (‘d’ 8.9 Hz, H-3’,5’) in accord with a *p*-substituted B-ring and a 2H AX system at δ 6.37 (d 2.1 Hz, H-8) and δ 6.16 (d 2.1 Hz, H-6) in accordance with a kaempferol derivative. The sugar regions of the 1D and 2D NMR spectra of **16** showed the presence of three sugar units. All ^{1}H and ^{13}C resonances of these glycosyl substituents were completely assigned by the 1D ^{1}H spectrum of **16**, in addition to the combined information from the 2D ^{1}H-^{1}H COSY,

the 2D ^{1}H-^{13}C HMBC, the 2D ^{1}H-^{13}C HSQC, the 2D ^{1}H-^{13}C HSQC-TOCSY and the 2D ^{1}H-^{13}C H2BC spectra of **16**. The sugar units were identified to be two *β*-glucopyranose units and an *α*-rhamnopyranose unit, respectively, by the observed ^{1}H coupling constants in the 1D ^{1}H NMR spectrum, in addition to the 17 ^{13}C chemical shift values belonging to these sugar units observed in the 2D ^{1}H-^{13}C HSQC and H2BC spectra of **16**. The anomeric coupling constants revealed β-configurations of the anomeric carbons of the glucosyl substituents and α-configuration of the anomeric carbon of the rhamnosyl substituent.

Assignments of the ^{13}C resonances belonging to the aglycone and the inter-residual connections were determined by the 2D ^{1}H-^{13}C HMBC experiment. At δ 5.71/133.2 (H-1’’/C-3), this cross-peak confirmed the linkage between the glucopyranosyl unit and the aglycone at the 3-hydroxyl. The downfield chemical shift of C-2’’ (δ 78.2) of this glucosyl unit indicated the presence of a sugar substituent at this position. Cross-peaks at δ 5.02/78.2 (H-1’’’/C-2’’) and δ 3.66/100.4 (H-2’’/C-1’’’) confirmed the linkage between the inner glucosyl substituent and the terminal glucosyl substituent to be at the 2’’-position. The cross-peaks at δ 5.05/77.1 (H-1’’’’/C-2’’’) and δ 3.69/100.4 (H-2’’’/C-1’’’’) definite the linkage between the terminal glucosyl unit and the rhamnosyl unit to be at the 2’’’-position. The acyl moiety was identified as *E*-caffeic acid by the 3H AMX system at δ 6.95 d 2.2 Hz (H-2’’’’’). δ 6.84 dd 8.2; 2.2 Hz (H-6’’’’’) and δ 6.66 d 8.2 Hz (H-5’’’’’), and an 2H AX system at δ 7.36 (H-7’’’’’) and δ 6.16 (H-8’’’’’). A coupling constant of 15.8 Hz between H-7’’’’’ and H-8’’’’’ showed the *E*-configuration. The downfield chemical shift of C-6’’’ (δ 63.4) of the glucose unit indicates the linkage between this sugar unit and the caffeoyl group. The cross-peaks at δ 4.30/166.5 (H-6A’’’/C-9’’’’’) and δ 4.19/166.5 (H-6B’’’/C-9’’’’’) confirmed the linkage between the terminal glucosyl substituent and the caffeoyl unit to be at the 6’’’-position. Thus, compound **16** was identified to be the previously undescribed compound kaempferol 3-*O*-(2’’-*O*-(2’’’-*O*-*α*-rhamnopyranosyl-6’’’-*O*-(*E*)-caffeoyl-)-*β*-glucopyranosyl)-*β*-glucopyranoside (Figure 16). A sodium-added molecular ion $[M+Na]^{+}$ at *m/z* 941.2318 corresponding to

$C_{42}H_{46}O_{23}Na^+$ (calculated: *m/z* at 941.2322; Δ = -0.46 ppm) observed in the HRMS of compound **16** confirmed this identification.

The aromatic region of the 1D ^1H NMR spectrum of **18** showed the presence of a 3H ABX system at δ 6.99 d 2.1 Hz (H-2), 7.04 d 8.3 Hz (H-5), and 6.85 dd 8.3; 2.1 Hz (H-6) and a 2H AB system at δ 6.68 (H-2') and δ 6.67 (H-2') which is consistent with dihydrodehydrodiconiferyl alcohol, where the aromatic rings are connected through a C3 unit showing a 4H spin system at δ 5.46 (H-7), δ 3.42 (H-8), δ 3.71 (H-6A) and δ 3.60 (H-6B). A further 4H spin system of a C3 substituent belonging to dihydrodehydrodiconiferyl was observed at δ 2.52 (H-7'), δ 1.68 (H-8') and δ 3.40 (H-6'). Two 3H signals belonging to methoxy groups were observed at δ 3.73 (3-OCH_3) and 3.76 (3'-OCH_3). The 20 ^{13}C resonances belonging to dihydrodehydrodiconiferyl alcohol aglycone observed in the 1D ^{13}C CAPT spectrum of **18** were assigned by the 2D ^1H-^{13}C HMBC spectrum and the 2D ^1H-^{13}C HSQC spectrum of **18**. The glycosyl unit of **18** was identified as rhamnose by the six 1H signals observed in the 1D ^1H spectrum belonging to this unit and the corresponding six ^{13}C signals belonging to this unit observed in the ^{13}C CAPT spectrum of **18**, which were assigned by the 2D ^1H-^{13}C HSQC spectrum, the 2D ^1H-^{13}C H2BC spectrum and the 2D ^1H-^1H COSY spectrum of **18**. A cross-peak at δ 5.23/144.9 (H-1''/C-4) observed in the 2D ^1H-^{13}C HMBC of **18** confirmed that the rhamnopyranosyl unit was attached to dihydrodehydrodiconiferyl alcohol aglycone at the 4-position. Thus, compound **18** was identified as dihydrodehydrodiconiferyl alcohol 4-*O*-*α*-rhamnopyranoside.

The stereochemistry of this compound was established by circular dichroism (CD) spectroscopy. The CD spectrum of **18** showed a negative Cotton effect at $[\theta]_{279}$, indicating that the configurations of C-7 and C-8 are *R* and *S*, respectively (Miyase et al., 1989; Achenbatch et al., 1987). Henceforth, compound **18** was identified as (7*R*,8*S*)-dihydrodehydrodiconiferyl alcohol 4-*O*-*α*-rhamnopyranoside (Figure 16). Dihydrodehydrodiconiferyl alcohol 4-*O*-*α*-rhamnopyranoside has previously been reported from *Pedicularis torta* (Changzeng & Zhongjian, 1997); however, only incomplete NMR data exist for this compound in current literature.

The UV spectrum compound **22**, which exhibited λ_{max} at 274 and 212 nm combined with its short HPLC retention time, may be indicative of a polar lactone (Sülsen & Martino, 2018; Pignatello et al., 1983), a compound type frequently reported from ferns (Taiz et al., 2015). The 1D ^{1}H NMR spectrum of **22** showed an 8H spin system at δ 4.22 (H-4), δ 4.07 (H-3), δ 3.74 (H-5), δ 2.80 (H-2A), δ 2.39 (H-2B) and δ 1.12 (H-6), in addition to a methoxy group at δ 3.23 (3-OCH3) (Figure 18). The 2D ^{1}H-^{13}C HMBC spectrum assigned the seven ^{13}C signals observed in the 1D ^{13}C CAPT spectrum **22**, the 2D ^{1}H-^{13}C HSQC spectrum, and the 2D ^{1}H-^{13}C H2BC spectrum **22**. The 7H spin system observed in the 1D ^{1}H NMR spectrum of **22** were assigned by the 2D ^{1}H-^{13}C HSQC spectrum, the 2D ^{1}H-^{13}C HSQC-TOCSY spectrum, the 2D ^{1}H-^{13}C H2BC spectrum and the 2D ^{1}H-^{1}H COSY spectrum of **22**. The cross-peaks at δ 2.80/76.0 (H-2A/C-3), δ 2.39/76.0 (H-2B/C-3), δ 4.07/35.0 (H-3/C-2), δ 4.07/88.1 (H-3/C-4), δ 4.22/76.0 (H-4/C-3), δ 4.22/65.6 (H-4/C-5), δ 3.74/88.1 (H-5/C-4), δ 3.74/19.0 (H-5/C-6) and δ 1.12/65.6 (H-6/C-5) observed in the 2D ^{1}H-^{13}C H2BC spectrum of **22** were particularly useful for the assignments of these signals. The cross-peaks established the position of the lactone carbonyl carbon C-1 at δ 2.80/175.9 (H-2A/C-1), δ 2.39/175.9 (H-2B/C-1), δ 4.07/175.9 (H-3/C1) and δ 4.22/175.9 (H-4/C-1) observed in the 2D ^{1}H-^{13}C HMBC spectrum of **22**. A cross-peak at δ 3.23/76.0 (3-OCH3/C-3) observed in the 2D ^{1}H-^{13}C HMBC spectrum of **22** confirmed that the methoxy group was attached to the 3-position. Thus, compound **22** was identified as 3-methoxy-5-hydroxy-4-olide.

The stereochemistry of **22** was established by circular dichroism (CD) spectroscopy. The CD spectrum of **22** showed a positive Cotton effect at $[\theta]_{250}$, which indicates *R* and *S* configurations of C-4 and C-5, respectively, whereas the positive Cotton effect at $[\theta]_{208}$ indicated *S* configuration of C-3 (Numata et al., 1984; Hollenbeak & Kuehn, 1974; Buchanan et al., 1995). Thus, **22** was identified as the previously undescribed natural product (3*S*,5*S*,4*R*)-methoxy-hydroxy-olide (Figure 16). A molecular ion $[M+H]^+$ at *m/z* 161.0809 corresponding to $C_7H_{12}O_4H^+$ (calculated: *m/z* at 161.0808; Δ = -0.1 ppm) observed in the HRMS of compound **22** confirmed this identification.

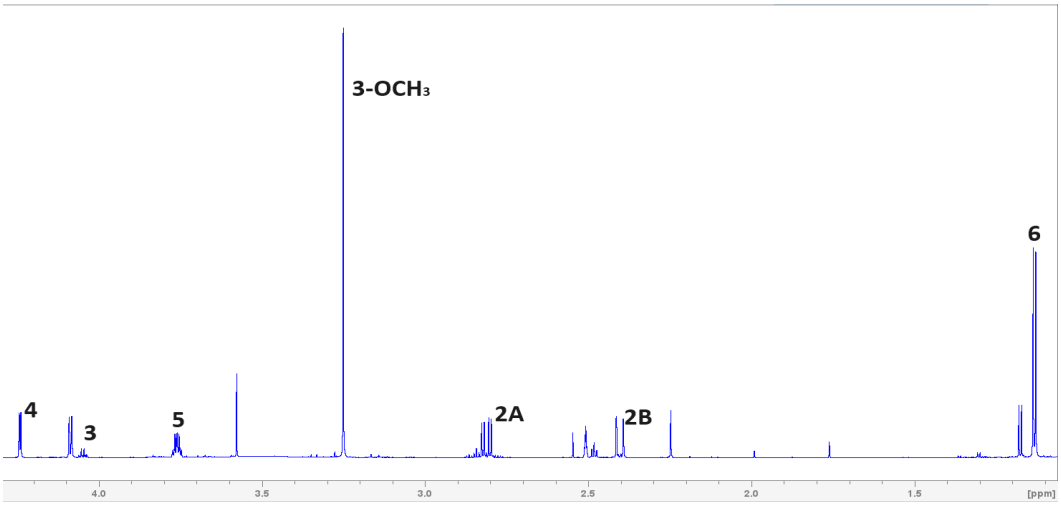

Figure 18. 1D ^{1}H NMR spectrum of 3-methoxy-5-hydroxy-4-olide (**22**) with assignment.

The UV spectrum of **23** showed a λ_{max} at 296 nm, 266 nm, 220 nm and 198 nm that corresponds to a saturated γ,δ-dilactone (Sülsen & Martino, 2018). The 1D ^{1}H NMR spectrum of compound **23** showed the presence of two CH_3 groups at δ 1.29 (5-CH_3) and δ 1.13 (H-2''), one CH_2 group at δ 2.82 (H-2A) and δ 2.66 (H-2B), in addition to seven CH groups at δ 2.91 (H-3), δ 4.04 (H-4), δ 4.39 (H-5), δ 3.21 (H-2'), δ 4.82 (H-3'), δ 4.28 (H-4') and δ 3.78 (H-1''). The corresponding ^{13}C signals were observed at δ 18.19 (5-CH_3), δ 19.02 (C-2''), δ 32.73 (C-2), δ 38.23 (C-3), δ 80.22 (C-4), δ 73.19 (C-5), δ 51.87 (C-2'), δ 78.56 (C-3'), δ 86.97 (C-4') and δ 65.51 (C-1'') in the 1D ^{13}CAPT NMR spectrum of compound **23**, in addition to two ester carbonyls at δ 171.25 (C-1) and δ 176.85 (C-1'), in accordance with two different lactone rings attached through a C-C bond. The 2D ^{1}H-^{13}C HSQC-TOCSY spectrum of compound **23** revealed that the 15 hydrogens observed in the 1D ^{1}H NMR spectrum all belonged to the same spin system. These twelve ^{13}C signals observed in the 1D ^{13}C CAPT spectrum of **23** were assigned by the 2D ^{1}H-^{13}C HMBC spectrum, the 2D ^{1}H-^{13}C HSQC spectrum, and the 2D ^{1}H-^{13}C H2BC spectrum of **23**. The 1H spin systems observed in the 1D ^{1}H NMR spectrum of **23** were assigned by the 2D ^{1}H-^{13}C HSQC spectrum, the 2D ^{1}H-^{13}C HSQC-TOCSY spectrum, the 2D ^{1}H-^{13}C H2BC spectrum and the 2D ^{1}H-^{1}H COSY spectrum. The cross-peaks at δ 2.82/38.2 (H-2A/C-3), δ 2.66/38.2 (H-2B/C-3), δ 2.91/32.7 (H-3/C-2), δ 2.91/80.2 (H-3/C-4), δ 4.04/73.2 (H-

4/C-5), δ 4.04/38.2 (H-4/C-3), δ 4.39/80.2 (H-5/C-4), δ 4.39/18.2 (H-5/C-6), and δ 1.29/73.2 (H-6/C-5) observed in the 2D ^{1}H-^{13}C H2BC spectrum of **23** belonging to the δ-lactone ring and the cross-peaks at δ 3.21/78.6 (H-2'/C-3'), δ 4.82/51.9 (H-3'/C-2'), δ 4.28/65.5 (H-4'/C-5'), δ 3.78/87.0 (H-5'/C-4'), δ 3.78/19.0 (H-5''/C-6') and δ 1.13/65.5 (H-6'/C-5') observed in the 2D ^{1}H-^{13}C H2BC spectrum of **23** belonging to the γ-lactone ring were particularly useful for complete assignment of the non-quaternary carbons of **23**. The ester carbonyls of the γ- lactone ring and the δ-lactone ring were assigned by the observed cross-peaks in the 2D ^{1}H-^{13}C HMBC spectrum of **23**. The cross-peaks at δ 4.04/51.9 (H-4/C-2'), δ 2.82/51.9 (H-2A/C-2'), δ 2.66/51.9 (H-2B/C-2'), δ 2.91/51.9 (H-3/C-2'), δ 2.91/176.9 (H-3/C-1'), δ 2.91/78.6 (H-3/C-3'), δ 3.21/32.7 (H-2'/C-2), δ 3.21/38.2 (H-2'/C-3), and δ 3.21/80.2 (H-2'/C-4) observed in the 2D ^{1}H-^{13}C HMBC spectrum of **23** confirmed the linkage between the γ- lactone ring and the δ- lactone ring from C-3 to C-2'. This was further confirmed by the observation of the cross-peak at δ 2.91/3.21 (H-3/H-2') observed in the 2D ^{1}H-^{1}H COSY spectrum of **23**. The cross-peaks at δ 1.13/87.0 (H-2''/C-4'), δ 4.28/19.02 (H-4'/C-2'') and δ 3.78/87.0 (H-1''/C-4') confirmed that the 1''-hydroxyethyl substituent was attached to C-4'. Thus, compound **23** was identified as the previously undescribed bilactone 4-hydroxy-3-(3'-hydroxy-4'-(hydroxyethyl)-oxotetrafuranone-5-methyl tetrahydropyranone. Completely assigned chemical shift values of this previously undescribed bilactone are shown in the second part of this thesis.

The CD spectrum of compound **23** shows a negative Cotton effect ($[\theta]_{220}$) and a positive Cotton effect ($[\theta]_{255}$) in accordance with (4*R*,5*S*,3'*S,*1''*S*,4'*R*) configuration (Numata et al., 1984; Hollenbeak & Kuehn, 1974; Buchanan et al., 1995: Yu et al., 2009). Thus, compound **23** was identified as (4*R*,5*S*,3'*S*,1''*S*,4'*R*)-4-hydroxy-3-(3'-hydroxy-4'-(1-hydroxyethyl)-oxotetrahydrofuran-5-methyltetrahydropyranone (Figure 16). A molecular ion $[M+H]^{+}$ at *m/z* 275.1124 corresponding to $C_{12}H_{18}O_7H^{+}$ (calculated: *m/z* at 275.1125; Δ = 0.5 ppm) observed in the HRMS of compound **23** confirmed this identification.

Compound **25** showed a UV spectrum like that of a saturated δ-lactone with λ_{max} at 296, 266 and 220 nm (Sülsen & Martino, 2018). The 1D ^{1}H NMR spectrum of **25** showed a 9H spin system at δ 5.30 (H-4), δ 6.87 (H-3), δ 4.60 (H-5), δ 6.11 (H-2), and δ 1.30 (H-6), acylated with a 5'-hydroxy-oxohexanoyl group displaying signals at δ 2.54 (H-2'), 2.86 (H-3'), δ 4.04 (H-5'), and δ 1.16 (H-6'), respectively. The 12 ^{13}C signals observed in the 1D ^{13}C CAPT spectrum **25** were assigned by the 2D ^{1}H-^{13}C HMBC spectrum, the 2D ^{1}H-^{13}C HSQC spectrum, and the 2D ^{1}H-^{13}C H2BC spectrum **25**. The 9H spin system observed in the 1D ^{1}H NMR spectrum of **25** were assigned by the 2D ^{1}H-^{13}C HSQC spectrum, the 2D ^{1}H-^{13}C HSQC-TOCSY spectrum, the 2D ^{1}H-^{13}C H2BC spectrum and the 2D ^{1}H-^{1}H COSY spectrum of **25**. The cross-peaks at δ 6.11/67.3 (H-2/C-4), δ 6.87/122.3 (H-3/C-3), δ 4.07/35.0 (H-3/C-2), δ 5.30/76.0 (H-4/C-5), δ 4.60/67.3 (H-5/C-4), δ 4.60/17.9 (H-5/C-6), δ 3.74/88.1 (H-5/C-4), and δ 1.30/76.0 (H-6/C-5). The cross-peaks of the 5'-hydroxy-oxohexanoyl at δ 2.54/32.1 (H-2'/C-3'), δ 2.86/27.3 (H-3'/C-2'), δ 4.04/19.7 (H-5'/C-6'), and δ 4.04/18.0 (H-5'/C-6) observed in the 2D ^{1}H-^{13}C H2BC spectrum of **25** were particularly useful for the assignments of these signals. The cross-peaks established the position of the lactone carbonyl carbon C-1 at δ 6.11/161.9 (H-2/C-1), δ 6.87/161.9 (H-3/C-1), and δ 4.60/161.9 (H-5/C-1) observed in the 2D ^{1}H-^{13}C HMBC spectrum of **25**. A cross-peak at δ 2.54/171.7 (H-2'/C-1'), δ 2.86/171.7 (H-3'/C-1'), and δ 5.30/171.7 (H-4/C-1') observed in the 2D ^{1}H-^{13}C HMBC spectrum of **25** confirmed that the hydroxy oxohexanoyl group is attached in the 4- position. Thus, compound **25** was identified as 4-*O*-(5'-hydroxy-4'-oxohexanoyl) osmundalactone (Figure 16). The complete chemical shift values of compound **25** are presented in the second part of this work.

The CD spectrum of compound **25** shows a negative band at ($[\theta]_{218}$) and a positive band at ($[\theta]_{260}$) that corresponds to a 4*R*, 5*S* configuration, respectively (Numata et al., 1984; Hollenbeak & Kuehn, 1974). A further negative band was observed at ($[\theta]_{295}$), which could be ascribed to the *R*-configuration of C-5' (Beigi et al., 2012). Thus, compound **25** was identified to be the previously undescribed natural product 4*R*-*O*-(5*S*-hydroxy-4-(5'*R*-hydroxy 4'-oxohexanoyl) osmundalactone. The sodium-added molecular ion $[M+Na]^{+}$ at *m/z* 279.0841 corresponding to $C_{12}H_{16}O_6Na^{+}$ (calculated: *m/z* at 279.0839; Δ = 0.63 ppm) observed in the HRMS of compound **25**

confirmed this identification. Compound **25** represents the first complete assignment of NMR signals of the osmundalactone core structure. The ^{1}H NMR chemical shift values are in good agreement with the previously published incompletely assigned ^{1}H NMR data of osmundalactone (Numata et al., 1984) with exception of the chemical shift value of H-4, which is experiencing a considerable downfield shift because of the effect of acylation of the 4-hydroxyl with 5'-hydroxy4-oxohexanoyl (Andersen & Fossen, 1995).

The previously reported beneficial properties of *Osmunda regalis* as a traditional medicinal plant encouraged studies to determine the potential cytotoxic activity against leukaemia cells of natural products isolated from this plant source. The cytotoxicity of compounds **12**, **13**, **16**, **18**, **20**, **21**, **22**, **23**, **24**, and **25**, which include the six previously undescribed natural products, were tested towards acute myeloid leukaemia cell line MOLM13. Only compounds **21** and **25**, which are γ- and δ-lactones, respectively, exhibited significant cytotoxic activity against the MOLM13 cells with EC_{50} values of 46.2 ± 0.07 μM (11) and 111.9 ± 0.07 μM (15) after 72 hours of incubation. These two compounds were further tested towards the normal cell lines of rat kidney epithelial (NRK) cells and rat cardiomyoblasts H9c2 cells to reveal if the cytotoxic activity was selective towards cancer cells. However, the cytotoxic activity of 5-hydroxy-2-hexen-4-olide lactone (**21**) did not differ between the cell lines tested, and the EC_{50} values were in all instances similar: 46.2 μM for MOML13, 48.7 μM for H9c2 and 49.6 μM for NRK (Table 3). The 4-*O*-(5-hydroxy-4-oxohexanoyl) osmundalactone (**25**) was only cytotoxic towards the heart and AML cells exhibiting similar EC_{50} values for these cell lines (102.7 and 111.9 μM, respectively). We did not detect reduced metabolic activity in the NRK cells at the highest concentration tested (200 μM), indicating lower cytotoxicity of compound **25** towards this cell line. Monolactones such as γ- and δ-lactones have previously been reported to induce DNA damage in the blood and the central nervous systems of rats (Jornada et al., 2010) and to exhibit pro-apoptotic activity against various cancer cells through inhibition of NF-κB (Janecka et al., 2012; Barros et al., 2014). The fact that γ-lactones have been reported to be more cytotoxic against cancer cells than δ-

lactones (Calderon-Montaño et al., 2013) may explain the observed difference in cytotoxic potency between compounds **25** and **21**.

Table 3. Cytotoxicity of compounds **21** and **25** against three mammalian cell lines. The compounds were diluted in DMSO. The cells were tested for metabolic activity after 72 h of incubation. The EC_{50} values were determined by non-linear regression from 3 independent experiments (MOLM-13 and H9c2) described in the methods section. The data from NRK is from 3 experiments. "– "denotes that no data is available due to low or no toxicity.

	MOLM13 (µM)	**H9c2 (µM)**	**NRK(µM)**
21	46.2 ± 0.07	48.7 ± 0.18	49.6 ± 0.11
25	111.9 ± 0.07	102.7± 0.12	-

4.4. Paper IV: Cytotoxic Natural Products Isolated from *Cryptogramma crispa* (L.) R. Br.

In the existing literature regarding *Cryptogramma crispa*, the main results are studies of the botanical characteristics of the plant. However, only a restricted number of studies have explored its phytochemical composition.

In current literature, only relatively volatile compounds, including alkyl esters, fatty acids, primary alcohols, aldehydes, and alkanes, have hitherto been identified by GCMS from *C. crispa* (Guo et al., 2018). Some carotenoid derivatives and shikimic acid derivatives have also been indicated to occur in this plant (Fons et al., 2018). However, the structures of these compounds remain vague, and there are no studies in the current literature about the isolation and identification of pure compounds from this plant species.

As part of our ongoing research in this paper, we have reported the characterisation of 15 natural compounds from the aerial parts of *C. crispa*, which have been identified from this plant species for the first time; this list of compounds includes a novel compound, as well as their cytotoxic activity towards leukaemia cells and normal kidney and heart cell lines.

The fourteen known compounds quercetin (**28**), quercetin 3-*O*-*β*-galactopyranoside (**29**), quercetin 3-*O*-*β*-glucopyranoside (**30**), quercetin 7-*O*-*β*-glucopyranoside (**31**), kaempferol 7-*O*-*β*-glucopyranoside (**32**), ferulic acid (**33**), ferulic acid 4-*O*-*β*-glucopyranoside (**34**), *p*-coumaric acid-4-*O*-*β*-glucopyranoside (**35**), caffeic acid (**36**), methyl chlorogenic acid 4'-*O*-*β*-glucopyranoside (**37**), chlorogenic acid methyl ester (**38**), pteroside D (**39**), pteroside X (**40**), and pterosin D (**42**) (Figure 19) were characterised from aerial parts of *C. crispa*. Compound **40** was previously identified as pteroside X by Murakami et al. (1976) from *Pteris fauriei* Hieron using 1D ^{1}H NMR.

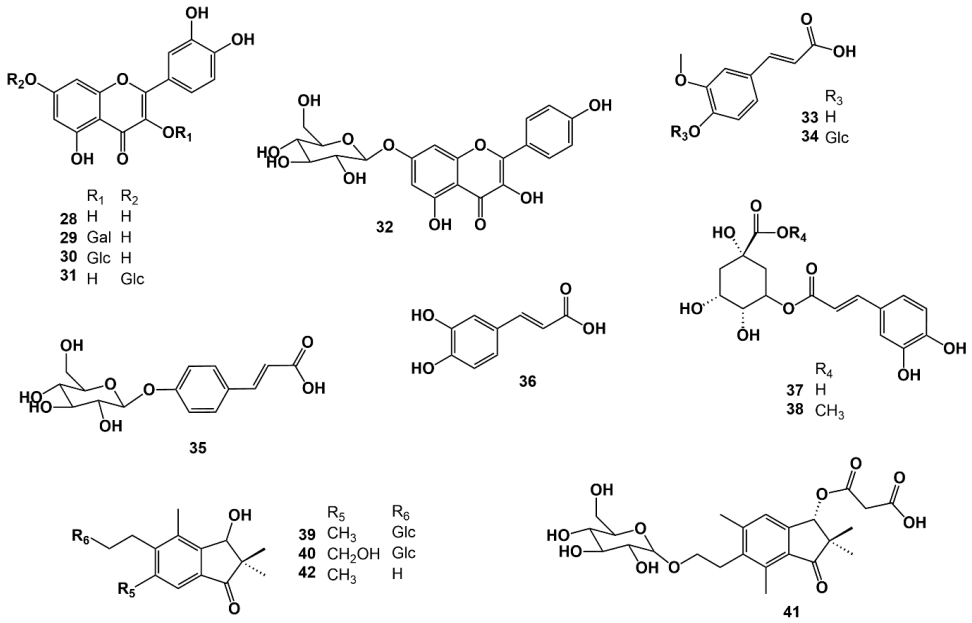

Figure 19. Structures of natural products isolated from *Crytogramma crispa*.

The UV spectrum of compound **41** recorded online during HPLC analysis exhibited λ_{max} values at 260, 215 and 198 nm, which are consistent with a 1-indanone derivative. The 1D ^{1}H NMR spectrum and the 1D ^{13}C NMR spectrum of **41** showed the presence of an extensively substituted 1-indanone derivative with only one aromatic hydrogen observed at δ 7.28 s (H-4) and one aliphatic hydrogen (H-3) observed at δ 5.94 s, directly attached to the 1-indanone ring system. The 1D ^{1}H NMR spectrum and the 1D ^{13}C NMR spectrum of **39** showed the presence of four methyl groups at δ 1.19 (H-10), δ 0.96 (H-11), δ 2.42 (H-12) and δ 2.61 (H-15), respectively. The cross-peaks at δ 1.19/49.8 (H-10/C-2) and δ 0.96/49.8 (H-10/C-2) confirmed that these methyl groups were connected in the C-2 position. The cross-peaks at δ 2.42/145.2 (H-12/C-5) and δ 2.61/137.2 (H-15/C-7) confirmed that these methyl groups were connected to C-5 and C-6 positions, respectively. Moreover, a CH_2 unit was identified at δ 3.00/29.14 (H-13/C-13), δ 3.75/66.79 (H-14A/C-14) and δ 3.56/66.79 (H-14B/C-14). The cross-peaks at δ 3.00/145.2 (H-13/C-5) and δ 3.00/137.2 (H-13/C-7) confirmed that this unit was attached to the C-6 position of the aromatic ring of compound **41**. Furthermore, the 1D ^{1}H NMR spectrum and the 1D

^{13}C NMR spectrum of **41** showed the presence of a glucosyl substituent and a malonyl substituent, respectively. All ^{1}H and ^{13}C resonances belonging to the glucosyl substituent were assigned by the combined information gained from the 1D selective TOCSY spectrum, the 2D ^{1}H-^{13}C HSQC spectrum, the 2D ^{1}H-^{13}C H2BC spectrum and the 2D 1H-1H COSY spectrum of **41.** The cross-peaks at δ 4.20/66.8 (H-1'/C-14), δ 3.75/102.9 (H-14A/C-1') and δ 3.56/102.9 (H-14B/C-1') observed in the 2D ^{1}H-^{13}C HMBC spectrum (Figure 20) of **41** confirmed that the glucosyl substituent was attached to C-14. The sugar unit was identified as glucose with an *β*-configuration because of the large coupling constant (δ 4.20 d 7.8 Hz; H-1'). The cross-peak at δ 5.94/167.2 (H-3/C-1'') confirmed that the malonyl unit was attached to C3. Thus, **39** was identified as the novel natural product 3-*O*-malonyl pteroside D.

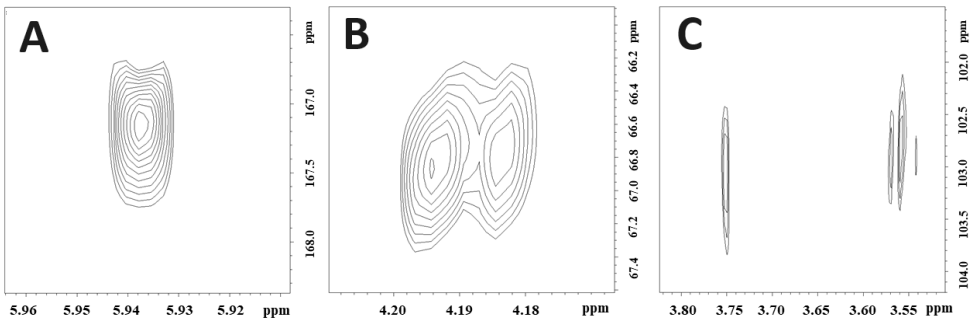

Figure 20. Important HMBC cross-peaks for structure determination of 3(*R*)-*O*-malonyl pteroside D (compound **41**). A: Cross-peak at δ 5.94/167.2 (H-4/C-1'') confirms the malonyl substituent's connection to the 1-indanon core. B: Cross-peak at δ 4.18/66.8 (H-1'/C-14) and C: Cross-peaks detected at δ 3.75/102.9 (H-14A/C-1') and δ 3.56/102.9 /H-14B/C-1') confirming the connection of the glucosyl unit to the alkyl group at C-14.

The stereochemistry of the chiral carbons belonging to C-3 of the 1-indanone core structure was determined by Circular Dichroism (CD) spectroscopy. The CD spectrum of **39** showed a negative Cotton effect at 301 nm and a positive Cotton effect at 333 nm, which is by 3*R* configuration (Kuroyanagi et al., 1974). Therefore, compound **41** was identified as 3(*R*)-*O*-malonyl pteroside D (Figure 19). A molecular ion $[M-H]^-$ at *m/z* 495.1861 corresponding to $C_{24}H_{32}O_{11}$ (calculated at *m/z* 495.1872;

Δ = -2.17 ppm) observed in the HRMS of compound **41** confirmed this identification. All the structures isolated from *C. crispa* can be seen in Figure 19.

Pterosins are sesquiterpenoids with a 1-indanone core structure; the glucoside version is called pterosides. This name originates from the fern *Pteridium aquilinum* var. latiusculum, which is one of the oldest and most common plants in the world and the first plant source from which such compounds were isolated. At the end of the 19th century, reports of lethal intoxication in cattle were established after consuming *P. aquilinum* (Penberthy, 1893; Storrar, 1893). Pterosin D and Pteroside D were first isolated by Yoshihira et al. (1978) from *P. aquilunum* and have later been found in other fern varieties such as *P. aqullinum* subsp wightianum (Wall) Shich, *H. punctata* (Thunb) Mett, *J. scammanae* Tryon, *M. speluncae* (L.) Moore, *M. strigosa* (Thunb) Presl, *D. wilfordii* (Moore) Christ (Cao et al., 2017).

Flavonoids are important natural products of ferns. A multitude of these compounds has hitherto been reported from ferns belonging to Dryopteridaceae, Thelypteridaceae, Selaginellaceae, Equisetaceae, Helminthostachyaceae, Ophioglossaceae, Lygodiaceae, Athyriaceae, and Aspleniaceae species (Cao et al., 2017). In the genus Pteridaceae, flavonoids of the Pteris species have been extensively investigated. The main flavonoids of ferns in this compound class are flavones, flavonols, and flavanones (Harada & Saiki, 1955; Wollenweber, 1989). All flavonoids identified in *C. crispa* during this project are flavonols, where derivatives of quercetin predominate.

In our ongoing research to identify new compounds for future anticancer drugs, the cytotoxic activity of four 1-indanone derivatives (compounds **39**, **40**, **41**, **42**) was tested towards acute myeloid leukaemia cell line MOLM13. Table 4 presents the EC_{50} values after 72h exposure. Moderate and relatively similar cytotoxicity towards this cell line was observed for all compounds, with EC_{50} values ranging from 182.88 ±0.08 μM for compound **39** to 197.88 ± 0.18 μM for compound **41.** The cytotoxicity between pterosin D and pteroside D could be regarded through the sugar moiety;

meanwhile, adding a substituent in the C-3 position and on C-5 decreases the cytotoxicity of these 1-indanone structures (Saito et al., 1975; Yoshihira et al., 1978).

Table 4. Cytotoxicity of compounds **39**-**42** against three mammalian cell lines. The compounds were diluted in DMSO. The cells were tested for metabolic activity after 72 h of incubation. The EC_{50} values were determined by non-linear regression from 3 independent experiments (MOLM13), as described in the methods section. The data from H9c2 and NRK is from three experiment. "–"denotes that no data is available due to low or no toxicity.

	MOLM13 (µM)	**H9c2 (µM)**	**NRK (µM)**
Compound **39**	182.88 ± 0.08	-	-
Compound **40**	191.66 ± 0.13	-	-
Compound **41**	197.88 ± 0.18	-	-
Compound **42**	189.96 ± 0.16	-	-

These compounds exhibited selective cytotoxic activity towards MOLM13, which is illustrated by the fact that none of these compounds were cytotoxic towards normal cell lines (NRK and heart cells, respectively). Pterosides are 1-indanone derivatives structurally related to ptaquiloside derivatives, which are cancer-promoting agents (Hikino et al., 1976). However, cancer-promoting effects are normally not observable within the short timescale of 24 to 72 hours, which was applied in our experiments to determine the cytotoxicity of individual compounds. McMorris et al. (1992), who studied the structure-activity relationship of the structurally related illudins isolated from *Omphalotus illudens* mushroom, reported that illudins have a significant anticancer potential. Illudins are structurally related to ptaquiloside structures with less cytotoxic effects than ptaquiloside. Some of these compounds, for example, illudin M and illudin S, exhibit significant antibacterial activity (Anchel et al., 1950). The latter-mentioned compounds are more potent than the pterosides described in this paper, with cytotoxic effects against myeloid leukaemia HL 60 cells in the range of 6-100nM (Kelner et al., 1987).

Comparing the cytotoxicity of the pterosides presented in this work with other 1-indanone structure-related, the mild and selective toxicity towards AML MOLM13 cells is positive for further investigation.

4.5 Paper V: A novel bicyclic lactone and other polyphenols from the commercially important vegetable *Anthriscus cerefolium*.

Several derivatives of quinic acid, in addition to the phenylpropanoids, where the latter compounds occur in essential oils, have also been reported as phenolic constituents from *A. cerefolium* (Slimestad et al., 2018; Stojkovic et al., 2021; Fejes et al., 2003). These identifications were mainly based on hyphenated mass spectrometry and comparisons with available standards (Slimestad et al., 2018). The observed antimicrobial activity of chervil extracts may be assigned to the content of relatively volatile compounds, including the known antibiotic compound carvacrol (Slimestad et al., 2018; Abdulmanea et al., 2012). Studies of the biological activity of pure compounds isolated from chervil are, however, lacking in current literature.

The major objective of this research industry collaboration is to determine the qualitative and quantitative content of the phenolics of garden chervil by using multidimensional NMR spectroscopic and chromatographic methods to determine the therapeutic potential of the main phenolic constituent towards acute monocytic leukaemia cells.

The dry matter content of chervil, *Anthriscus cerefolium*, was found to be 32.3%, which is higher than the dry matter content of parsley, *Petroselinum crispum*, at 24.7% provided by the same grower (Zwaving et al., 1971). The total phenolic content was found to be 1260 mg gallic acid equivalents (GAE) 100 g^{-1}, quite like that of parsley (1270 mg GAE 100 g^{-1}) (Zwaving et al., 1971). The antiradical potential was 50 ± 5 mg TEAC 100 g^{-1}, similar to the level detected in parsley, 54 mg TEAC 100 g^{-1} (Zwaving et al., 1971) and comparable to previous studies of chervil (Abdulmanea et al., 2012).

From a methanol extract of fresh garden chervil (*Anthriscus cerefolium* L.), four phenolic compounds were detected using UHPLC-DAD-MS analysis. Preparative isolation of the phenolics was achieved by repetitive size-exclusion chromatography (Sephadex LH-20) and preparative HPLC. In total, five compounds were isolated. The aromatic compounds identified in this paper are apigenin 7-*O*-*β*-(2″-

apiofuranosylglucopyranoside) (also known as apiin), luteolin 7-*O*-*β*-glucopyranoside, and apigenin 7-*O*-*β*-(2″-apiofuranosyl-6″-malonylglucopyranoside). These compounds are not part of the scope of this research work. This identification was carried out by a combination of several 1D and 2D NMR experiments and high-resolution mass spectrometry. Apiin and luteolin 7-*O*-*β*-glucopyranoside have previously been identified in chervil (Chizzola, 2011; Milovanović et al., 2009), while apigenin 7-*O*-*β*-(2″-apiofuranosyl-6″-malonylglucopyranoside) is identified in garden chervil for the first time.

In the following sentence, it is presented the novel compound isolated as part of the research collaboration between the Pharmacognosy group and the industry partnership.

The central bicyclic δ-quinide ring system of **43** was assigned by the $^{1}H/^{13}C$ cross-peaks at δ 2.44/69.9 (H-2A/C-3), δ 1.96/69.9 (H-2B/C-3), δ 5.20/35.7 (H-3/C-2), δ 5.20/68.8 (H-3/C-4), δ 3.87/69.9 (H-4/C-3), δ 3.87/72.0 (H-4/C-5), δ 5.32/68.8 (H-5/C-4), δ 5.32/31.8 (H-5/C-6) and δ 2.41/72.0 (H-6/C-5) observed in the 2D $^{1}H–^{13}C$ H2BC spectrum, the $^{1}H/^{1}H$ cross-peaks at δ 2.44/5.20 (H-2A/H-3), δ 1.96/5.20 (H-2B/H-3), δ 2.44/1.96 (H-2A/H-2B), δ 5.20/3.87 (H-3/H-4), δ 3.87/5.32 (H-4/H-5) and δ 5.32/2.41 (H-5/H-6) observed in the 2D $^{1}H–^{1}H$ COSY spectrum. The substituents of the central bicyclic δ-quinide ring system of **43** were identified as two caffeoyl units and a malonyl unit. The $^{1}H/^{13}C$ cross-peaks at δ 6.28/78.8 (H-8′/C-1), δ 6.23/69.9 (H-8″/C-3) and δ 5.20/166.2 (H-3/C-9″) confirmed that the caffeoyl units were attached to the δ-quinide ring system at position -1 and -3, respectively. A cross-peak at δ 5.32/166.7 (H-5/C-1‴) confirmed the linkage between the malonyl substituent and the δ-quinide ring system at position -5. Thus, **43** was identified as the previously undescribed natural product 1,3-dicaffeoyl-5-malonyl-δ-quinide. A molecular ion at *m/z* 585.1234 corresponding to $C_{28}H_{25}O_{14}^{+}$ (calculated *m/z* at 585.1245, $\Delta = -1.9$ ppm) observed in the high-resolution mass spectrum of 1 confirmed this identity (Figure 21).

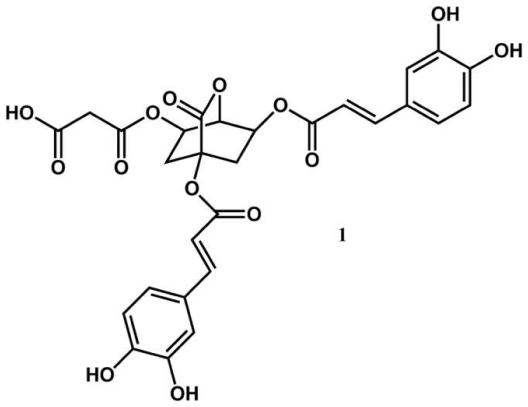

Figure 21. Structure of the previously undescribed compound 1,3-dicaffeoyl-5-malonyl-δ-quinide (**43**) isolated from Anthriscus cerefolium.

A related compound with similar central bicyclic δ-quinide ring system to that of **43**, namely 3,5-O-dicaffeoylepi-δ-quinide, has previously been reported to occur in processed coffee beans, where the identification was solely based on mass spectrometry (Ortan et al., 2015). Recently, Stojkovic et al. reported the presence of several derivatives of quinic acid acylated with caffeoyl and malonyl moieties, which were identified by hyphenated high-resolution mass spectrometry (UHPLC-MS) (Slimestad et al., 2018). However, none of these compounds were lactones.

Previously, extracts of chervil have exhibited weak to moderate cytotoxic activity towards cancer cell lines, including glioblastoma cells, where EC_{50} of 765 µg/mL was observed (Slimestad et al., 2018; Price et al., 1977); however, the cytotoxicity of pure compounds isolated from chervil has not been reported in current literature. The cytotoxicity of the main phenolic compound 1,3-dicaffeoyl-5-malonyl-δ-quinide (**43**) towards MOLM13, OCI-AML3 and MV4-11 acute leukaemia cells and normal cell lines (NRK cells and H9C2). 1,3-dicaffeoyl-5-malonyl-δ-quinide (**43**) exhibited moderate toxicity towards all cell lines tested with EC_{50} values above 1000 µM at 24 h incubation and between 400 and 600 µM at 72 h incubation. The compound did not show selective cytotoxicity towards any of the leukaemia cell lines compared to the non-cancerous cell lines (Figure 22).

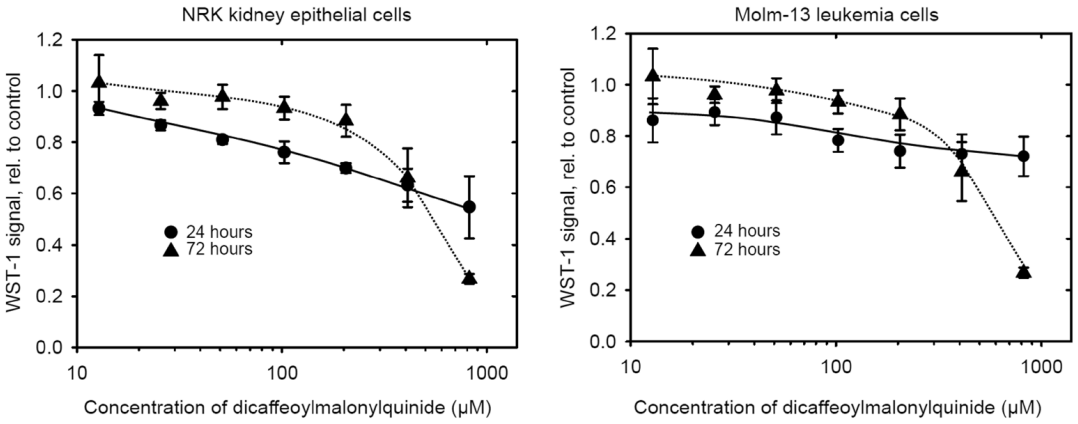

Figure 22. Cytotoxicity of 1,3-dicaffeoyl-5-malonyl-δ-quinide (1) towards NRK kidney epithelial cells and MOLM13 leukaemia cells.

Chapter 5: Conclusions.

This PhD thesis in pharmacognosy has made significant contributions to increased knowledge of several types of bioactive natural compounds isolated from *Narthecium ossifragum*, *Osmunda regalis*, *Cryptogramma crispa* and *Anthriscus cerefolium*.

For the first time, saponins from *N. ossifragum* have been isolated and characterized at atomic resolution. The cytotoxicity of these saponins increased with increasing number of glycosyl substituents. The primary saponin, sarsasapogenin-3-*O*-(2′-*O*-*β*-glucopyranosyl-3′-*O*-*α*-arabinopyranosyl-β galactopyranoside) (**4**), which makes up a significant percentage of the dry weight of *N. ossifragum'*s flowering tops, was found to be the main toxic principle towards all tested cell lines including normal rat kidney cells. This suggests that this compound could be mainly responsible for the kidney and liver damage observed in cattle after consuming *N. ossifragum*. Despite the flowering tops of *N. ossifragum* have been indicated to contain the causative agents of the phototoxic disease alveld, no aromatic compounds have previously been identified. This study reports on the detailed characterisation of five di-*C*-glycosyl flavones, which have been completely characterised for the first time, in addition to a structurally related known compound.

The structures of the saponins of *N. ossifragum* have now been determined, and a protocol for large-scale isolation of these compounds has been presented. This opens for further structure-activity studies of these compounds, including studies of their effects on biological cellular membranes, which are presented in this work, as well as future animal trials. These saponins based on Sarsasapogenin aglycone exhibit non-selective cytotoxicity towards all tested cancer and normal cell lines.

Saponins isolated from *N. ossifragum* can affect different types of cancer cells as well as normal cell lines at similar concentrations, indicating a non-selective cytotoxicity. These findings may help to understand the mechanism of toxicity in connection with ingesting sarsasapogenin derivatives, not only isolated from *N. ossifragum* but also

from other plant sources; therefore, it is suggested not to use these compounds for cancer therapy. (Paper **I** and **II**).

Natural products from the aerial parts of the jurassic relict *Osmunda regalis* L. have for the first time been successfully characterised, leading to the identification of 17 natural products. Among these, six are novel compounds, underscoring the plant's potential as a source of novel natural products. This correlates well with expectations for a unique species like *Osmunda regalis* L., which is one of the few remaining intact representatives of a Jurassic ecosystem.

Two monolactones isolated from Osmunda regalis exhibited cytotoxic activity. Monolactones, specifically γ- and δ-lactones, have been previously found to have different mechanisms for causing cell-death. Interestingly, γ-lactones have been reported to be more cytotoxic against cancer cells than δ-lactones, which could account for the observed difference in cytotoxic potency between compounds **25** and **21**. (Paper **III**).

In Paper **IV**, for the first time, 15 natural products, including the previously undescribed compound 3*R*-*O*-malonyl pteroside D (**41**), have been characterised from *Cryptogramma crispa* (L.) R. Br. The four isolated 1-indanone derivatives were tested for their cytotoxic activity towards the acute myeloid leukaemia cell line MOLM13, and all these compounds exhibited moderate and relatively similar cytotoxicity. This is particularly noteworthy considering that pterosides are 1-indanone derivatives of plants structurally related to ptaquiloside compounds, which are known cancer-promoting agents. Illudins, are natural products with structures related to ptaquiloside and have been reported to have significant anticancer potential and fewer cytotoxic effects than ptaquiloside.

Chervil (*Anthriscus cerefolium* (L.) Hoffm) (Paper **V**) is a very rich source of phenolic compounds, 1260 mg GAE 100^{-1} g DM, and its methanolic extract has a high antiradical capacity. Interestingly, the major phenolic constituent of chervil is a bicyclic lactone; 1,3-dicaffeoyl-5-malonyl-δ-quinide (**43**) and this compound is

reported for the first time. The 1,3-dicaffeoyl-5-malonyl-δ-quinide exhibited moderate cytotoxic activity towards human leukaemia and normal cell lines.

The discovery of a significant number of novel compounds from the above-mentioned unique toxic or edible plant sources encourages further metabolic investigations to reveal their potential as possible drug leads. However, because saponins of *N. ossifragum*, exhibit high and non-selective cytotoxic activity towards all tested cell lines, the potential use of these compounds as anticancer agents indicated in current literature should be reconsidered.

References

Abdelkader, S. V., Čeh, L., Dishington, I. W., & Hange, J. G. (1984). Alveld-Producing Saponins. Acta Veterinaria Scandinavica, 25(1), 76-85. https://doi.org/10.1186/BF03547281

Abdulmanea, K. et al. Immunochemical and HPLC identification of isoflavonoids in the Apiaceae family. Biochem. Syst. Ecol. 45, 237–243 (2012).

Achenbach, H., Grob, J., Dominguez, X. A., Cano, G., Star, J. V., Del Carmen Brussolo, L., Munoz, G., Salgado, F., & Lopez, L. (1987). Lignans neolignans and norneolignans from krameria cystisoides. Phytochemistry (Oxford), 26(4), 1159-1166. https://doi.org/10.1016/S0031-9422(00)82370-5

Aguilar-Santamaría, L., Herrera-Arellano, A., Zamilpa, A., Alonso-Cortés, D., Jiménez-Ferrer, E., Tortoriello, J., & Zúñiga-González, G. (2013). Toxicology, genotoxicity, and cytotoxicity of three extracts of Solanum chrysotrichum. Journal of Ethnopharmacology, 150(1), 275-279. https://doi.org/https://doi.org/10.1016/j.jep.2013.08.039

Anchel, M., Hervey, A., & Robbins, W. J. (1950). Antibiotic substances from Basidiomycetes+. VII. Clitocybe illudens. Proc Natl Acad Sci USA, 36(5), 300-305. https://doi.org/10.1073/pnas.36.5.300

Andersen, Ø. M., & Fossen, T. (1995). Anthocyanins with an unusual acylation pattern from stem of Allium victorialis. Phytochemistry, 40(6), 1809-1812.

Andersen, O. M., & Markham, K. R. (Eds.). (2006). Flavonoids: chemistry, biochemistry and applications. CRC press.

Angell, J., & Ross, T. (2011). Suspected bog asphodel (Narthecium ossifragum) toxicity in cattle in North Wales. Vet Rec, 169(4), 102-102. https://doi.org/10.1136/vr.d3879

Bain, B. J. (2004). A Beginner's Guide to Blood Cells. John Wiley & Sons, Incorporated. http://ebookcentral.proquest.com/lib/bergen-ebooks/detail.action?docID=233065

Bao, W., Pan, H., Lu, M., Ni, Y., Zhang, R., & Gong, X. (2007). The apoptotic effect of sarsasapogenin from Anemarrhena asphodeloides on HepG2 human hepatoma cells. Cell Biol Int, 31(9), 887-892. https://doi.org/10.1016/j.cellbi.2007.02.001

Barros, M. E. S. B., Barros, M. E. S. B., Freitas, J. C. R., Oliveira, J. M., da Cruz, C. H. B., da Silva, P. B. N., de Araújo, L. C. C., Milit?o, G. C. G., da Silva, T. G., Oliveira, R. A., & Menezes, P. H. (2014). Synthesis and evaluation of (-)-Massoialactone and analogues as potential anticancer and anti-inflammatory agents [291-300]. [Amsterdam] :.

Bjorøy, Ø., Rayyan, S., Fossen, T., & Andersen, Ø. M. (2009). Structural Properties of Anthocyanins: Rearrangement of C-Glycosyl-3-deoxyanthocyanidins in Acidic Aqueous Solutions. Journal of Agricultural and Food Chemistry, 57(15), 6668-6677. https://doi.org/10.1021/jf900759q

Bjorøy, Ø., Rayyan, S., Fossen, T., Kalberg, K., & Andersen, Ø. M. (2009). C-glycosylanthocyanidins synthesized from C-glycosylflavones. Phytochemistry, 70(2), 278-287. https://doi.org/https://doi.org/10.1016/j.phytochem.2008.12.012

Bomfleur, B., McLoughlin, S., & Vajda, V. (2014). Fossilized Nuclei and Chromosomes Reveal 180 Million Years of Genomic Stasis in Royal Ferns. Science, 343(6177), 1376-1377. https://doi.org/10.1126/science.1249884

Bouazzi, S., Jmii, H., El Mokni, R., Faidi, K., Falconieri, D., Piras, A., Jaidane, H., Porcedda, S., & Hammami, S. (2018). Cytotoxic and antiviral activities of the essential oils from Tunisian Fern, Osmunda regalis. South African journal of botany, 118, 52-57. https://doi.org/10.1016/j.sajb.2018.06.015

Bouillant, M. L., de Arce, F. F., Favre-Bonvin, J., Chopin, J., Zoll, A., & Mathieu, G. (1979). Nouvelles C-glycosylflavones extraites de Spergularia rubra. Phytochemistry, 18(6), 1043-1047. https://doi.org/https://doi.org/10.1016/S0031-9422(00)91474-2

Brahmkshatriya, P. P., & Brahmkshatriya, P. S. (2013). Terpenes: Chemistry, Biological Role, and Therapeutic Applications. In K. G. Ramawat & J.-M. Mérillon (Eds.), Natural Products: Phytochemistry, Botany and Metabolism of Alkaloids, Phenolics and Terpenes (pp. 2665-2691). Springer Berlin Heidelberg. https://doi.org/10.1007/978-3-642-22144-6_120

Brunschwig, H., & Grüninger, J. (1500). Kleines Destillierbuch. Johann Grüninger. https://books.google.no/books?id=vjyqzgEACAAJ

Buchanan, M. S., Hashimoto, T., Takaoka, S., & Asakawa, Y. (1995). (+)-Osmundalactone, gamma-lactones and spiromentins from the fungus Paxillus atrotomentosus. Phytochemistry (Oxford), 40(4), 1251-1257. https://doi.org/10.1016/0031-9422(95)00467-L

Böttger, S., Hofmann, K., & Melzig, M. (2012). Saponins can perturb biologic membranes and reduce the surface tension of aqueous solutions: A correlation? Bioorganic & Medicinal Chemistry, 20(9), 2822-2828. https://doi.org/https://doi.org/10.1016/j.bmc.2012.03.032

Calderón-Montaño, J. M., Burgos-Morón, E., Orta, M. L., Pastor, N., Austin, C. A., Mateos, S., & López-Lázaro, M. (2013). Alpha, beta-unsaturated lactones 2-furanone and 2-pyrone induce cellular DNA damage, formation of topoisomerase I- and II-DNA complexes and cancer cell death. Toxicol Lett, 222(1), 64-71. https://doi.org/10.1016/j.toxlet.2013.07.007

Cao, H., Chai, T., Wang, X., Morais-Braga, M. F. B., Yang, J. S., Wong, F., Wang, R., Yao, H., Cao, J., Cornara, L., Burlando, B., Wang, Y., Xiao, J., & Coutinho, H. D. M. (2017). Phytochemicals from fern species: potential for medicine applications. Phytochemistry reviews, 16(3), 379-440. https://doi.org/10.1007/s11101-016-9488-7

Carpinteyro Diaz, A. E., Herfindal, L., Rathe, B. A., Sletta, K. Y., Vedeler, A., Haavik, S., & Fossen, T. (2019). Cytotoxic saponins and other natural products from flowering tops of Narthecium ossifragum L. Phytochemistry, 164, 67-77. https://doi.org/10.1016/j.phytochem.2019.04.014

Čeh, L., & Hauge, J. G. (1981). Alveld-Producing Saponins. Acta Veterinaria Scandinavica, 22(3), 391-402. https://doi.org/10.1186/BF03548664

Changzeng, W., & Zhongjian, J. (1997). Lignan, phenylpropanoid and iridoid glycosides from Pedicularis torta. Phytochemistry (Oxford), 45(1), 159-166. https://doi.org/10.1016/S0031-9422(96)00770-4

Choi, Y. H. (2023). Reduction of high glucose-induced oxidative injury in human retinal pigment epithelial cells by sarsasapogenin through inhibition of ROS generation and inactivation of NF-κB/NLRP3 inflammasome pathway. Genes Genomics, 45(9), 1153-1163. https://doi.org/10.1007/s13258-023-01417-2

Courbet, H., & Metche, M. (1971). Extraction and identification of acid phenols from the spores of osmunda regalis p. Comptes Rendus Hebdomadaires des Seances de l'Academie des Sciences Serie D Sciences Naturelles, 272(12), 1686-1689. https://eurekamag.com/research/026/615/026615433.php

Crozier, A., Clifford, M. N., & Ashihara, H. (2006). Plant Secondary Metabolites: Occurrence, Structure and Role in the Human Diet. (1st ed.). John Wiley & Sons, Incorporated.

de Groot, C., & Müller-Goymann, C. C. (2016). Saponin Interactions with Model Membrane Systems - Langmuir Monolayer Studies, Hemolysis and Formation of ISCOMs. Planta Med, 82(18), 1496-1512. https://doi.org/10.1055/s-0042-118387

Dehgan, B. (2022). LYCOPHYES AND MONILOPHYTES (FERNS). In B. Dehgan (Ed.), Garden Plants Taxonomy: Volume 1: Ferns, Gymnosperms, and Angiosperms (Monocots) (pp. 13-56). Springer International Publishing. https://doi.org/10.1007/978-3-031-11561-5_2

del Olmo, A., Calzada, J. & Nuñez, M. (2017) Benzoic acid and its derivatives as naturally occurring compounds in foods and as additives: Uses, exposure, and controversy, Critical Reviews in Food Science and Nutrition, 57:14, 3084-3103, DOI: 10.1080/10408398.2015.1087964

Dias, M. C., Pinto, D. C. G. A., & Silva, A. M. S. (2021). Plant Flavonoids: Chemical Characteristics and Biological Activity. Molecules, 26(17), 5377. https://www.mdpi.com/1420-3049/26/17/5377

Diwan, F. H., Abdel-Hassan, I. A., & Mohammed, S. T. (2000). Effect of saponin on mortality and histopathological changes in mice. East Mediterr Health J, 6(2-3), 345-351.

Fejes, S. et al. Antioxidant activity of different compounds from Anthriscus cerefolium L. (Hoffm). Acta Horticult. 597, 191–198 (2003).

Flåøeyen, A., Borrebaæk, B., & Nordstoga, K. (1991). Glycogen accumulation and histological changes in the livers of lambs with alveld and experimental sporidesmin intoxication. Vet Res Commun, 15(6), 443-453.

Flåøeyen, A., Bratberg, B., Frøslie, A., & Grønstøl, H. (1995). Nephrotoxicity and hepatotoxicity in calves apparently caused by experimental feeding with Narthecium ossifragum. Vet Res Commun, 19(1), 63-73.

Flåøyen, A., Binde, M., Bratberg, B., Djønne, B., Fjølstad, M., Grønstøl, H., Hassan, H., Mantle, P. G., Landsverk, T., & Schönheit, J. (1995). Nephrotoxicity of Narthecium ossifragum in cattle in Norway. Vet Rec, 137(11), 259-263. https://doi.org/10.1136/vr.137.11.259

Flåøyen, A., Bratberg, B., Frøslie, A., Grønstøl, H., Langseth, W., Mantle, P. G., & Von Krogh, A. (1997). Further Studies on the Presence, Qualities and Effects of the Toxic Principles from Narthecium Ossifragum Plants. Veterinary Research Communications, 21(2), 137-148. https://doi.org/10.1023/A:1005781805723

Flåøyen, A., Tønnesen, H. H., Grønstøl, H., & Karlsen, J. (1991). Failure to induce toxicity in lambs by administering saponins from Narthecium ossifragum. Veterinary Research Communications, 15(6), 483-487. https://doi.org/10.1007/BF00346548

Fons, F., Froissard, D., Morel, S., Bessière, J.-M., Buatois, B., Sol, V., Fruchier, A., & Rapior, S. (2018). Pteridaceae Fragrant Resource and Bioactive Potential: A Mini-review of Aroma Compounds. Natural Product Communications, 13(5), 1934578X1801300531. https://doi.org/10.1177/1934578x1801300531

Fossen, T., & Andersen, Ø. (2006). Spectroscopic techniques applied to flavonoids. Flavonoids: chemistry, biochemistry and applications, 37-142.

Fukuoka, M., Kuroyanagi, M., Yoshihira, K., & Natori, S. (1978). Chemical and Toxicological Studies on Bracken Fern, Pteridium aquilinum var. latiusculum. II. Structures of Pterosins, Sesquiterpenes having 1-Indanone Skeleton. Chem. Pharm. Bull., 26(8), 2365-2385. https://doi.org/10.1248/cpb.26.2365

Fægri, K. (1970). Norges planter: blomster og trær i naturen: med et utvalg fra våre nabolands flora: 2 ([2. utg.]. ed., Vol. 2). Cappelen.

Gaffield, W., Horowitz, R. M., Gentili, B., Chopin, J., & Bouillant, M.-L. (1978). Circular dichroism of c-glycosylflavones: A chiroptical method for differentiating 6-C-,8-C- and 6,8-Di-C-β-glycosyl isomers. Tetrahedron, 34(20), 3089-3096. https://doi.org/https://doi.org/10.1016/0040-4020(78)87004-5

Gemmrich, A. R. (1977). Fatty acid composition of fern spore lipids. Phytochemistry, 16(7), 1044-1046. https://doi.org/https://doi.org/10.1016/S0031-9422(00)86721-7

Greco, I., Molchanova, N., Holmedal, E. et al. Correlation between hemolytic activity, cytotoxicity and systemic in vivo toxicity of synthetic antimicrobial peptides. Sci Rep 10, 13206 (2020). https://doi.org/10.1038/s41598-020-69995-9

Guo, Y., Li, J. J., Busta, L., & Jetter, R. (2018). Coverage and composition of cuticular waxes on the fronds of the temperate ferns Pteridium aquilinum, Cryptogramma crispa, Polypodium glycyrrhiza, Polystichum munitum and

Gymnocarpium dryopteris. Annals of Botany, 122(4), 555-568. https://doi.org/10.1093/aob/mcy078

Güclü-Üstündag, O., & Mazza, G. (2007). Saponins: Properties, Applications and Processing. Crit Rev Food Sci Nutr, 47(3), 231-258. https://doi.org/10.1080/10408390600698197

Han, F.-Y., Song, X.-Y., Chen, J.-J., Yao, G.-D., & Song, S.-J. (2018). Timosaponin AIII: A novel potential anti-tumor compound from Anemarrhena asphodeloides. Steroids, 140, 125-130.

Hano, C. F., Dinkova-Kostova, A. T., Davin, L. B., Cort, J. R., & Lewis, N. G. (2021). Editorial: Lignans: Insights Into Their Biosynthesis, Metabolic Engineering, Analytical Methods and Health Benefits [Editorial]. Frontiers in Plant Science, 11. https://doi.org/10.3389/fpls.2020.630327

Harada, T., & Saiki, Y. (1955). Pharmaceutical Studies on Ferns. VIII. Distribution of Flavonoids in Ferns. (2). Pharmaceutical Bulletin, 3(6), 469-472. https://doi.org/10.1248/cpb1953.3.469

Hatton, C. S. R. (2013). Haematology. John Wiley & Sons, Incorporated. http://ebookcentral.proquest.com/lib/bergen-ebooks/detail.action?docID=7103734

Heinrich, M., Barnes, J., Gibbsons, S., & Williamson, E. M. (2012). Fundamentals of pharmacognosy and phytotherapy (2nd. ed.). Elsevier, Churchill Livingstone.

Herfindal, L., & Selheim, F. (2006). Microcystin produces disparate effects on liver cells in a dose dependent manner. Mini reviews in medicinal chemistry, 6(3), 279–285. https://doi.org/10.2174/138955706776073475

Hikino, H., Miyase, T., & Takemoto, T. (1976). Biosynthesis of pteroside B in Pteridium aquilinum var. Latiusculum, proof of the sesquiterpenoid origin of the pterosides. Phytochemistry, 15(1), 121-123. https://doi.org/https://doi.org/10.1016/S0031-9422(00)89065-2

Hollenbeak, K. H., & Kuehne, M. E. (1974). The isolation and structure determination of the fern glycoside osmundalin and the synthesis of its aglycone osmundalactone. Tetrahedron, 30(15), 2307-2316. https://doi.org/10.1016/S0040-4020(01)97097-8

Humisto, A., Jokela, J., Teigen, K., Wahlsten, M., Permi, P., Sivonen, K., & Herfindal, L. (2019). Characterization of the inter-action of the antifungal and cytotoxic cyclic glycolipopeptide hassallidin with sterol-containing lipid membranes. Biochimica et biophysica acta. Biomembranes, 1861(8), 1510–1521. https://doi.org/10.1016/j.bbamem.2019.03.010

Ikan, R., & Shulman, E. (1972). Isolation & identification of ecdysterone from fern Osmunda regalis Osmundaceae. Israel Journal of Botany, 21, 150-152.

Inoue, T., Mimaki, Y., Sashida, Y., & Kobayashi, M. (1995). Structures of Toxic Steroidal Saponins from Narthecium asiaticum MAXIM. CHEMICAL & PHARMACEUTICAL BULLETIN, 43(7), 1162-1166. https://doi.org/10.1248/cpb.43.1162

Janecka, A., Janecka, A., Wyrebska, A., Gach, K., Fichna, J., & Janecki, T. (2012). Natural and synthetic alfa-methylenelactones and alfa-methylenelactams with anticancer potential [561-572]. [Kidlington, Oxford] :.

Jetter, R., & Riederer, M. (1999). Long-chain alkanediols, ketoaldehydes, ketoalcohols and ketoalkyl esters in the cuticular waxes of Osmunda regalis fronds. Phytochemistry (Oxford), 52(5), 907-915. https://doi.org/10.1016/S0031-9422(99)00309-X

Jetter, R., & Riederer, M. (2000). Composition of Cuticular Waxes on Osmunda regalis Fronds. Journal of Chemical Ecology, 26(2), 399-412. https://doi.org/10.1023/A:1005409405771

Jornada, L. K., Valvassori, S. S., Arent, C. O., Leffa, D., Damiani, A. A., Hainzenreder, G., Ferreira, C. L., Moretti, M., Andrade, V. M., & Quevedo, J. (2010).

DNA damage after intracerebroventricular injection of ouabain in rats. Neuroscience Letters, 471(1), 6-9. https://doi.org/https://doi.org/10.1016/j.neulet.2009.12.072

Kelner, M. J., McMorris, T. C., Beck, W. T., Zamora, J. M., & Taetle, R. (1987). Preclinical evaluation of illudins as anticancer agents. Cancer Res, 47(12), 3186-3189.

Kim, K. M., Im, A. R., Kim, S. H., Hyun, J. W., & Chae, S. (2016). Timosaponin AIII inhibits melanoma cell migration by suppressing COX-2 and in vivo tumor metastasis. Cancer science, 107(2), 181-188.

King, F. W., Fong, S., Griffin, C., Shoemaker, M., Staub, R., Zhang, Y.-L., Cohen, I., & Shtivelman, E. (2009). Timosaponin AIII is preferentially cytotoxic to tumor cells through inhibition of mTOR and induction of ER stress. PloS one, 4(9), e7283.

Kobayashi, M., Suzuki, K., Nagasawa, S., & Mimaki, Y. (1993). Purification of Toxic Saponins from Narthecium asiaticum Maxim. Journal of Veterinary Medical Science, 55(3), 401-407. https://doi.org/10.1292/jvms.55.401

Kottenhahn, P., Philipps, G., & Jennewein, S. (2021). Hexanol biosynthesis from syngas by Clostridium carboxidivorans P7 - product toxicity, temperature dependence and in situ extraction. Heliyon, 7(8), e07732. https://doi.org/10.1016/j.heliyon.2021.e07732

Kowalczyk, P., Gawdzik, B., Trzepizur, D., Szymczak, M., Skiba, G., Raj, S., Kramkowski, K., Lizut, R., & Ostaszewski, R. (2021). δ-Lactones—A New Class of Compounds That Are Toxic to E. coli K12 and R2–R4 Strains. Materials, 14(11), 2956. https://www.mdpi.com/1996-1944/14/11/2956

Kurihara, T. & Kikuchi, M. Studies on the constituents of Anthriscus sylvestris Hoffm. II. On the components of flowers and leaves. Yakugaku Zasshi J. Pharm. Soc. Jpn. 99, 602–606 (1979).

Kuroyanagi, M., Fukuoka, M., Yoshihira, K., & Natori, S. (1974). The Absolute Configurations of Pterosins, 1-Indanone Derivatives from Bracken, Pteridium

aquilinum var. latiusculum. CHEMICAL & PHARMACEUTICAL BULLETIN, 22(3), 723-726. https://doi.org/10.1248/cpb.22.723

Lange, Y., Ye, J., Duban, M., & Steck, T. L. (2009). Activation of Membrane Cholesterol by 63 Amphipaths. Biochemistry, 48(36), 8505-8515. https://doi.org/10.1021/bi900951r

Lange, Y., Ye, J., & Steck, T. L. (2005). Activation of Membrane Cholesterol by Displacement from Phospholipids*. Journal of Biological Chemistry, 280(43), 36126-36131. https://doi.org/https://doi.org/10.1074/jbc.M507149200

Lazaro-Carrasco, M. J., Rebuelta, M., Vivas, J. M., & Broncano, F. J. (1987). Study of the phenolic acids and acylphloroglucinol derivates in osmunda regalis lI. Anales de la Real Academia de Farmacia, 53, 97-101.

Lazaro-Carrasco, M. J., Rubuelta, M., Vivas, J. M., & Baraibar, C. (1987). Study of the phenolic acids and acylphloroglucinol derivates in osmunda regalis l. Anales de la Real Academia de Farmacia, 53(1), 91-96. https://eurekamag.com/research/006/529/006529129.php

Lin, Y., Zhao, W.-R., Shi, W.-T., Zhang, J., Zhang, K.-Y., Ding, Q., Chen, X.-L., Tang, J.-Y., & Zhou, Z.-Y. (2020). Pharmacological activity, pharmacokinetics, and toxicity of timosaponin AIII, a natural product isolated from Anemarrhena asphodeloides bunge: a review. Frontiers in pharmacology, 11, 764.

Liu, J., Deng, X., Sun, X., Dong, J., & Huang, J. (2020). Inhibition of autophagy enhances timosaponin AIII-induced lung cancer cell apoptosis and anti-tumor effect in vitro and in vivo. Life Sciences, 257, 118040.

Liu, Z., Cao, Y., Guo, X., & Chen, Z. (2023). The Potential Role of Timosaponin-AIII in Cancer Prevention and Treatment. Molecules, 28(14), 5500.

Lorent, J. H., Quetin-Leclercq, J., & Mingeot-Leclercq, M.-P. (2014). The amphiphilic nature of saponins and their effects on artificial and biological membranes and potential consequences for red blood and cancer cells

[10.1039/C4OB01652A]. Organic & Biomolecular Chemistry, 12(44), 8803-8822. https://doi.org/10.1039/C4OB01652A

Luckey, M. (2014). Membrane structural biology: with biochemical and biophysical foundations. Cambridge University Press.

Malone, F. E., Kennedy, S., Reilly, G. A., & Woods, F. M. (1992). Bog asphodel (Narthecium ossifragum) poisoning in cattle. The Veterinary record, 131(5), 100-103. https://doi.org/10.1136/vr.131.5.100

Markham, K. R. (1982). Techniques of flavonoid identification. Academic press.

Matsuo, Y., MacLeod, R. A. F., Uphoff, C. C., Drexler, H. G., Nishizaki, C., Katayama, Y., Kimura, G., Fujii, N., Omoto, E., Harada, M., & Orita, K. (1997). Two acute monocytic leukemia (AML-M5a) cell lines (MOLM-13 and MOLM-14) with interclonal phenotypic heterogeneity showing MLL-AF9 fusion resulting from an occult chromosome insertion, ins(11;9) (q23;p22p23). Leukemia, 11(9), 1469-1477. https://doi.org/10.1038/sj.leu.2400768

McMorris, T. C., Kelner, M. J., Wang, W., Estes, L. A., Montoya, M. A., & Taetle, R. (1992). Structure-activity relationships of illudins: analogs with improved therapeutic index. The Journal of Organic Chemistry, 57(25), 6876-6883. https://doi.org/10.1021/jo00051a037

Melchert, T. E., & Alston, R. E. (1965). Flavonoids from the Moss Mnium affine Bland. Science, 150(3700), 1170-1171. https://doi.org/doi:10.1126/science.150.3700.1170

Metzgar, J. S., Alverson, E. R., Chen, S., Vaganov, A. V., & Ickert-Bond, S. M. (2013). Diversification and reticulation in the circumboreal fern genus Cryptogramma. Molecular Phylogenetics and Evolution, 67(3), 589-599. https://doi.org/https://doi.org/10.1016/j.ympev.2013.02.020

Miyase, T., Ueno, A., Takizawa, N., Kobayashi, H., & Oguchi, H. (1989). Ionone and lignan glycosides from Epimedium diphyllum. Phytochemistry (Oxford), 28(12), 3483-3485. https://doi.org/10.1016/0031-9422(89)80369-3

Molina, M., Reyes-GarcÍa, V., & Pardo-de-Santayana, M. (2009). Local Knowledge and Management of the Royal Fern (Osmunda regalis L.) in Northern Spain: Implications for Biodiversity Conservation. American Fern Journal, 99(1), 45-55, 11. https://doi.org/10.1640/0002-8444-99.1.45

Moore, S. E. M., Gabarayeva, N., & Hemsley, A. R. (2009). Morphological, developmental and ultrastructural comparison of Osmunda regalis L. spores with spore mimics. Review of palaeobotany and palynology, 156(1), 177-184. https://doi.org/10.1016/j.revpalbo.2008.12.010

Mossberg, B., Stenberg, L., Karlsson, T., Moen, S., & Ryvarden, L. (2018). Gyldendals store nordiske flora (3. utg. ed.). Gyldendal.

Mues, R. (1982). Flavone di-C-glycosides from the liverwort Trichocolea tomentella (L.) Dum. and their taxonomic significance. The Journal of the Hattori Botanical Laboratory, 51, 61-68.

Murakami, T., Taguchi, S., Nomura, Y., Tanaka, N., Satake, T., Saiki, Y., & Chen, C. (1976). Weitere Indan-1-on-Derivate der Gattung Pteris. CHEMICAL & PHARMACEUTICAL BULLETIN, 24, 1961-1964. https://doi.org/https://doi.org/10.1248/cpb.24.1961

Myhren, L., Nilssen, I. M., Nicolas, V., Døskeland, S. O., Barratt, G., & Herfindal, L. (2014). Efficacy of multi-functional liposomes containing daunorubicin and emetine for treatment of acute myeloid leukaemia. European Journal of Pharmaceutics and Biopharmaceutics, 88(1), 186-193. https://doi.org/https://doi.org/10.1016/j.ejpb.2014.04.002

Nguyen, X. H. T., Juvik, O. J., Øvstedal, D. O., & Fossen, T. (2014). 6-Carboxydihydroresveratrol 3-O-b-glucopyranoside- A novel natural product from the

Cretaceous relict Metasequoia glyptostroboides. Fitoterapia, 95, 109-114. https://doi.org/10.1016/j.fitote.2014.03.001

Numata, A., Hokimoto, K., Takemura, T., Katsuno, T., & Yamamoto, K. (1984). Plant constituents biologically active to insects. V. Antifeedants for the larvae of the yellow butterfly, Eurema hecabe mandarina, in Osmunda japonica. (1). Chem. Pharm. Bull., 32(7), 2815-2820. https://doi.org/10.1248/cpb.32.2815

Oftedal, L., Myhren, L., Jokela, J., Gausdal, G., Sivonen, K., Døskeland, S. O., & Herfindal, L. (2012). The lipopeptide toxins anabaenolysin A and B target biological membranes in a cholesterol-dependent manner. Biochimica et Biophysica Acta (BBA) - Biomembranes, 1818(12), 3000-3009. https://doi.org/https://doi.org/10.1016/j.bbamem.2012.07.015

Oftedal, L., Selheim, F., Wahlsten, M., Sivonen, K., Doskeland, S. O., & Herfindal, L. (2010). Marine Benthic Cyanobacteria Contain Apoptosis-Inducing Activity Synergizing with Daunorubicin to Kill Leukemia Cells, but not Cardiomyocytes. Mar Drugs, 8(10), 2659-2672. https://doi.org/10.3390/md8102659

Ortan, A. et al. Innovative phytosynthesized silver nanoarchitectures with enhanced antifungal and antioxidant properties. Appl. Surf. Sci. 358, 540–548 (2015).

Osbourn, A., Goss, R. J. M., & Field, R. A. (2011). The saponins – polar isoprenoids with important and diverse biological activities [10.1039/C1NP00015B]. Natural Product Reports, 28(7), 1261-1268. https://doi.org/10.1039/C1NP00015B

Paulli, S. (1667). Simonis Paulli ... Quadripartitum botanicum de simplicium medicamentorum facultatibus ... additis dosibus purgantium una cum appendice et indicibus necessariis. Impensis auth. fil. P. Paulli. https://books.google.no/books?id=GmpAYAAACAAJ

Paulli, S. Flora Danica, 1648.

Panche, A. N., Diwan, A. D., & Chandra, S. R. (2016). Flavonoids: an overview. Journal of Nutritional Science, 5, e47, Article e47. https://doi.org/10.1017/jns.2016.41

Pechmann, S., Willmund, F., & Frydman, J. (2013). The ribosome as a hub for protein quality control. Molecular cell, 49(3), 411–421. https://doi.org/10.1016/j.molcel.2013.01.020

Penberthy, J. (1893). Vegetable poisoning (?) simulating anthrax in cattle. Journal of Comparative Pathology and Therapeutics, 6, 266-275. https://doi.org/https://doi.org/10.1016/S0368-1742(93)80061-4

Peng, J., Zhao, K., Zhu, J., Wang, Y., Sun, P., Yang, Q., Zhang, T., Han, W., Hu, W., Yang, W., Ruan, J., & Qian, Y. (2020). Sarsasapogenin Suppresses RANKL-Induced Osteoclastogenesis in vitro and Prevents Lipopolysaccharide-Induced Bone Loss in vivo. Drug Des Devel Ther, 14, 3435-3447. https://doi.org/10.2147/dddt.S256867

Pignatello, J. J., Porwoll, J., Carlson, R. E., Xavier, A., Gleason, F. K., & Wood, J. M. (1983). Structure of the antibiotic cyanobacterin, a chlorine-containing .gamma.-lactone from the freshwater cyanobacterium Scytonema hofmanni. J. Org. Chem, 48(22), 4035-4038. https://doi.org/10.1021/jo00170a032

Plaha, N. S., Awasthi, S., Sharma, A., & Kaushik, N. (2022). Distribution, biosynthesis and therapeutic potential of lignans. 3 Biotech, 12(10), 255. https://doi.org/10.1007/s13205-022-03318-9

Plinius Maior, G. Naturalis Historia, 77.

Price, J. R., Sturgess, V. C., Robinson, R., & Robinson, G. M. (1938). Some New Anthocyanin Types. Nature, 142(3590), 356-356. https://doi.org/10.1038/142356a0

Radunz, A. (1967). Über die lipide der pteridophyten-I. : Die isolierung und identifizierung der polyensäuren. Phytochemistry (Oxford), 6(3), 399-406. https://doi.org/10.1016/S0031-9422(00)86297-4

Rayyan, S., Fossen, T., Nateland, H. S., & Andersen, Ø. M. (2005). Isolation and identification of flavonoids, including flavone rotamers, from the herbal drug 'crataegi folium cum flore' (hawthorn). Phytochemical Analysis, 16(5), 334-341. https://doi.org/https://doi.org/10.1002/pca.853

Robinson, S. L., Christenson, J. K., & Wackett, L. P. (2019). Biosynthesis and chemical diversity of β-lactone natural products [10.1039/C8NP00052B]. Natural Product Reports, 36(3), 458-475. https://doi.org/10.1039/C8NP00052B

Saito, M., Umeda, M., Enomoto, M., Hatanaka, Y., Natori, S., Yoshihira, K., Fukuoka, M., & Kuroyanagi, M. (1975). Cytotoxicity and carcinogenicity of pterosins and pterosides, 1-indanone derivatives from bracken (Pteridium aquilinum). Experientia, 31, 829-831. https://doi.org/https://doi.org/10.1007/BF01938490

Sakakibara, M., Mabry, T. J., Bouillant, M.-L., & Chopin, J. (1977). 6,8-di-C-glucosylflavones from Larrea trident at a (Zygophyllaceae). Phytochemistry, 16(7), 1113-1114. https://doi.org/https://doi.org/10.1016/S0031-9422(00)86763-1

Salmenkallio, M., McCormick, S., Mabry, T., Dellamonica, G., & Chopin, J. (1982). flavonoids of Trichophorum cespitosum. Phytochemistry.

Schmidt, M., Skaf, J., Gavril, G., Polednik, C., Roller, J., Kessler, M., & Holzgrabe, U. (2017). The influence of Osmunda regalis root extract on head and neck cancer cell proliferation, invasion and gene expression. BMC Complement Altern Med, 17(1), 518-518. https://doi.org/10.1186/s12906-017-2009-4

Slimestad, R., Hansen, J. S. & Verheul, M. Intake of vegetables and vegetable pigments during a lunch meal in Norwegian canteens with salad bars. J. Food Agric. Environ. 16, 14–21 (2018).

Shen, S., Zhang, Y., Zhang, R., & Gong, X. (2013). Sarsasapogenin induces apoptosis via the reactive oxygen species-mediated mitochondrial pathway and ER stress pathway in HeLa cells. Biochemical and Biophysical Research

Communications, 441(2), 519-524.
https://doi.org/https://doi.org/10.1016/j.bbrc.2013.10.101

Song, X.-Y., Han, F.-Y., Chen, J.-J., Wang, W., Zhang, Y., Yao, G.-D., & Song, S.-J. (2019). Timosaponin AIII, a steroidal saponin, exhibits anti-tumor effect on taxol-resistant cells in vitro and in vivo. Steroids, 146, 57-64.

Stabursvik, A. (1959). A Phytochemical Study of Narthecium Ossifragum (L.) Huds: With Additional Chapters on the Botany and the Veterinary History of the Plant. Organic Chemistry Laboratories, The Technical University of Norway.

Stojkovic, D. et al. Extract of Herba Anthrisci cerefolii: Chemical profiling and insights into its anti-glioblastoma and antimicrobial mechanism of actions. Pharmaceuticals 14, 55 (2021).

Storrar, D. (1893). Cases of vegetable poisoning in cattle. Journal of Comparative Pathology and Therapeutics, 6, 276-279.
https://doi.org/https://doi.org/10.1016/S0368-1742(93)80062-6

Sumi, M. (1929). Sterols Isolated from Several Vegetables. Bull. Inst. Phys. Chem. Res., 8, 228-233.

Summerfield, R. J. (1974). Narthecium Ossifragum (L.) Huds. The Journal of ecology, 62(1), 325-339. https://doi.org/10.2307/2258895

Suzuki, K., Kobayashi, M., Ito, A., & Nakgawa, M. (1985). Narthecium asiaticum Maxim. Poisoning of grazing cattle: observations on spontaneous and experimental cases. The Cornell Veterinarian, 75(2), 348-365.

Sy, L.-K., Lok, C.-N., Wang, J.-Y., Liu, Y., Cheng, L., Wan, P.-K., Leung, C.-T., Cao, B., Kwong, W.-L., Chang, R. C.-C., & Che, C.-M. (2016). Identification of “sarsasapogenin-aglyconed” timosaponins as novel Aβ-lowering modulators of amyloid precursor protein processing [10.1039/C5SC02377G]. Chemical Science, 7(5), 3206-3214. https://doi.org/10.1039/C5SC02377G

Sy, L. K., Yan, S. C., Lok, C. N., Man, R. Y., & Che, C. M. (2008). Timosaponin A-III induces autophagy preceding mitochon-dria-mediated apoptosis in HeLa cancer cells. Cancer Res, 68(24), 10229-10237. https://doi.org/10.1158/0008-5472.Can-08-1983

Sülsen, V. P., & Martino, V. S. (2018). Sesquiterpene Lactones : Advances in their Chemistry and Biological Aspects (1st 2018. ed.). Springer International Publishing : Imprint: Springer.

Taiz, L., Møller, I. M., Murphy, A., & Zeiger, E. (2015). Plant physiology and development (6th ed.). Sinauer.

Takechi, M., Shimada, S., & Tanaka, Y. (1992). Time course and inhibition of saponin-induced hemolysis. Planta Med, 58(2), 128-130. https://doi.org/10.1055/s-2006-961413

Thimmappa, R., Geisler, K., Louveau, T., O'Maille, P., & Osbourn, A. (2014). Triterpene Biosynthesis in Plants. Annu Rev Plant Biol, 65(1), 225-257. https://doi.org/10.1146/annurev-arplant-050312-120229 (Annual Review of Plant Biology)

Tomaselli, M., Petraglia, A., Rossi, G., & Adorni, M. (2005). Contribution to the environmental ecology of Cryptogramma crispa (L.) R. Br. ex Hooker in the Alps. Flora - Morphology, Distribution, Functional Ecology of Plants, 200(2), 175-186. https://doi.org/https://doi.org/10.1016/j.flora.2004.04.002

Trouillas, P., Corbière, C., Liagre, B., Duroux, J., & Beneytout, J. (2005). Structure–function relationship for saponin effects on cell cycle arrest and apoptosis in the human 1547 osteosarcoma cells: a molecular modelling approach of natural molecules structurally close to diosgenin. Bioorganic & Medicinal Chemistry, 13(4), 1141-1149. https://doi.org/https://doi.org/10.1016/j.bmc.2004.11.031

Uhlig, S., Wisløff, H., & Petersen, D. (2007). Identification of Cytotoxic Constituents of Narthecium ossifragum Using Bioassay-Guided Fractionation. J. Agric. Food Chem, 55(15), 6018-6026. https://doi.org/10.1021/jf070776k

Veit, M., Bilger, W., Mühlbauer, T., Brummet, W., & Winter, K. (1996). Diurnal changes in flavonoids. Journal of plant physiology, 148(3-4), 478-482. https://doi.org/https://doi.org/10.1016/S0176-1617(96)80282-3

Viktorsson, E., Melling Grøthe, B., Aesoy, R., Sabir, M., Snellingen, S., Prandina, A., Høgmoen Åstrand, O. A., Bonge-Hansen, T., Døskeland, S. O., Herfindal, L., & Rongved, P. l. (2017). Total synthesis and antileukemic evaluations of the phenazine 5,10-dioxide natural products iodinin, myxin and their derivatives. Bioorg Med Chem, 25(7), 2285-2293. https://doi.org/10.1016/j.bmc.2017.02.058

Wang, G.-J., Lin, L.-C., Chen, C.-F., Cheng, J.-S., Lo, Y.-K., Chou, K.-J., Lee, K.-C., Liu, C.-P., Wu, Y.-Y., Su, W., Chen, W.-C., & Jan, C.-R. (2002). Effect of timosaponin A-III, from Anemarrhenae asphodeloides Bunge (Liliaceae), on calcium mobilization in vascular endothelial and smooth muscle cells and on vascular tension. Life Sciences, 71(9), 1081-1090. https://doi.org/https://doi.org/10.1016/S0024-3205(02)01794-0

Wang, N., Feng, Y., Zhu, M., Siu, F.-M., Ng, K.-M., & Che, C.-M. (2013). A novel mechanism of XIAP degradation induced by timosaponin AIII in hepatocellular carcinoma. Biochimica et Biophysica Acta (BBA)-Molecular Cell Research, 1833(12), 2890-2899.

Wang, Y., Zhang, Y., Zhu, Z., Zhu, S., Li, Y., Li, M., & Yu, B. (2007). Exploration of the correlation between the structure, hemolytic activity, and cytotoxicity of steroid saponins. Bioorganic & Medicinal Chemistry, 15(7), 2528-2532. https://doi.org/https://doi.org/10.1016/j.bmc.2007.01.058

Wellman, K. M., Laur, P. H. A., Briggs, W. S., Moscowitz, A., & Djerassi, C. (1965). Optical Rotatory Dispersion Studies. XCIX.1 Superposed Multiple Cotton Effects of Saturated Ketones and Their Significance in the Circular Dichroism Measurement of

(-)-Menthone2. Journal of the American Chemical Society, 87(1), 66-72. https://doi.org/10.1021/ja01079a013

Winkel-Shirley, B. (2001). Flavonoid Biosynthesis. A Colorful Model for Genetics, Biochemistry, Cell Biology, and Biotechnology. Plant Physiology, 126(2), 485-493. http://www.jstor.org/stable/4279912

Wisløff, H., Flåøyen, A., Ottesen, N., & Hovig, T. (2003). Narthecium ossifragum (L.) huds. causes kidney damage in goats: morphologic and functional effects. Vet Pathol, 40(3), 317-327. https://doi.org/10.1354/vp.40-3-317

Wollenweber, E. (1989). Exudate flavonoids in ferns and their chemosystematic implication. Biochemical Systematics and Ecology, 17(2), 141-144. https://doi.org/https://doi.org/10.1016/0305-1978(89)90071-9

Yoshihira, K., Fukuoka, M., Kuroyanagi, M., Natori, S., Umeda, M., Morohoshi, T., Enomoto, M., & Saito, M. (1978). Chemical and Toxicological Studies on Bracken Fern, Pteridium aquilinum var. latiusculum. I. Introduction, Extraction and Fractionation of Constituents, and Toxicological Studies including Carcinogenicity Tests. CHEMICAL & PHARMACEUTICAL BULLETIN, 26(8), 2346-2364. https://doi.org/10.1248/cpb.26.2346

You, Y., Ray, R., Halitschke, R., Baldwin, G., & Baldwin, I. T. (2023). Arbuscular mycorrhizal fungi-indicative blumenol-C-glucosides predict lipid accumulations and fitness in plants grown without competitors. New Phytologist, 238(5), 2159-2174. https://doi.org/https://doi.org/10.1111/nph.18858

Yu, Y. M., Yang, J. S., Peng, C. Z., Caer, V., Cong, P. Z., Zou, Z. M., Lu, Y., Yang, S. Y., & Gu, Y. C. (2009). Lactones from Angiopteris caudatiformis. J Nat Prod, 72(5), 921-924. https://doi.org/10.1021/np900027m

Zhang, J., Meng, Z., Zhang, M., Ma, D., Xu, S., & Kodama, H. (1999). Effect of six steroidal saponins isolated from anemarrhenae rhizoma on platelet aggregation and

hemolysis in human blood. Clinica Chimica Acta, 289(1), 79-88. https://doi.org/https://doi.org/10.1016/S0009-8981(99)00160-6

Zhang, M., Qu, J., Gao, Z., Qi, Q., Yin, H., Zhu, L., Wu, Y., Liu, W., Yang, J., & Huang, X. (2021). Timosaponin AIII induces G2/M arrest and apoptosis in breast cancer by activating the ATM/Chk2 and p38 MAPK signaling pathways. Frontiers in pharmacology, 11, 601468.

Zwaving, J. H., Smith, D. & Bos, R. The essential oil of chervil Anthriscus cerefolium (L.) Hoffm. Pharm. Weekblad 106, 182–189 (1971).

Part II

1. Appendix:

1.1. List of compounds isolated and presented in this thesis.

1.2. NMR tables of isolated compounds.

1.3. Papers I-V including supplementary data.

1. Appendix

1.1. List of compounds isolated and presented in this thesis.

List of compounds isolated from *Narthecium ossifragum*.

Saponins:

1. Sarsasapogenin
2. Sarsasapogenin-3-*O*-*β*-galactopyranoside
3. Sarsasapogenin-3-*O*-(2′-*O*-*β*-glucopyranosyl-*β*-galactopyranoside)
4. Sarsasapogenin-3-*O*-(2′-*O*-*β*-glucopyranosyl-3′-*O*-*α*-arabinopyranosyl-*β*-galactopyranoside)

Aromatic compounds:

5. Chrysoeriol 6-*C*-*β*-arabinofuranoside-8-*C*-*β*-glucopyranoside
6. Chrysoeriol 6-*C*-*β*-arabinopyranosyl-8-*C*-*β*-glucopyranoside
7. Chrysoeriol 6-*C*-*β*-xylopyranosyl-8-*C*-*β*-galactopyranoside
8. Chrysoeriol 6-*C*-*β*-galactopyranosyl-8-*C*-*β*-glucopyranoside
9. Chrysoeriol 6-*C*-*β*-glucopyranosyl-8-*C*-*β*-galactopyranoside
10. Chrysoeriol 6,8-di-*C*-*β*-glucopyranoside

List of compounds isolated from *Osmunda regalis*.

Aromatic compounds:

11. Chalconaringenin 2'-*O*-*β*-glucopyranoside
12. Kaempferol 3-*O*-(2''-*O*-(2'''-*α*-rhamnopyranosyl)-*β*-glucopyranosyl)-*β*-glucopyranoside
13. Quercetin 3-*O*-(2''-*O*-(2'''-*α*-rhamnopyranosyl)-*β*-glucopyranosyl)-*β*-glucopyranoside
14. Vanillic acid
15. *p*-Hydroxy-benzoic acid

16. Kaempferol 3-*O*-(2’’-*O*-(2’’’-*O*-*α*-rhamnopyranosyl-6’’’-*O*-(*E*)-caffeoyl-)-*β*-glucopyranosyl)-*β*-glucopyranoside
17. *p*-Hydroxy-benzoic acid methyl ester.
18. Dihydrodehydrodiconiferyl alcohol 4-*O*-*α*-rhamnopyranoside
19. Apigenin 7-(2’’-*O*-*α*-rhamopyranosil-*β*-glucopyranoside)
20. Epoxyconiferyl alcohol

Terpenoids derivatives:

21. 5-hydroxy-2-hexen-4-olide
22. 3-methoxy-5-hydroxy-4-olide
23. 4-hydroxy-3(3’-hydroxy-4’(hydroxyethyl)-oxotetrafuranone-5-methyl tetrahydropyranone
24. Blumenol C glucoside
25. 4-*O*-(5’-hydroxy-4’-oxohexanoyl) osmundalactone

Fatty acid and related compounds:

26. Hexyl-*β*-glucopyranoside
27. 2-Hexenoic acid

List of compounds isolated from *Cryptogramma crispa*

Aromatic compounds:

28. Quercetin
29. Quercetin 3-*O*-*β*-galactopyranoside
30. Quercetin 3-*O*-*β*-glucopyranoside
31. Quercetin 7-*O*-*β*-glucopyranoside
32. Kaempferol 7-*O*-*β*-glucopyranoside
33. Ferulic acid
34. Ferulic acid-4-*O*-*β*-glucopyranoside
35. *p*-cumeric acid-4-*O*-*β*-glucopyranoside

36. Caffeic acid
37. Chlorogenic acid methyl ester 4'-*O*-*β*-glucopyranoside
38. Chlorogenic acid methyl ester

Terpenoids

39. Pteroside D
40. Pteroside X
41. 3-manolyl-pteroside D
42. Pterosin D

List of novel compounds isolated from *Anthriscus cerefolium*

43. 1,3-dicaffeoyl-5-malonyl-δ-quinide

1.2. NMR tables of the isolated compounds.

NMR tables of the isolated compounds from *Narthecium ossifragum*.

Table 1. ^{1}H NMR chemical shift values (ppm) and coupling constants (Hz) for saponins **1**-**4** isolated from flowering tops of *N. ossifragum* in DMSO-D_6 at 298K. s = singlet; d = doublet; dd = double doublet; dt = double triplet; p = pentet; m = multiplet.

	1	**2**	**3**	**4**
1A	1.37	1.40	1.41	1.48
1B	1.33	1.35	1.34	1.30
2A	1.38	1.51	1.55	1.48
2B	1.31	1.40	1.38	1.41
3	3.86 *m*	3.88 *m*	3.89 *m*	3.88 *m*
4A	1.81	1.71	1.71	1.67
4B	1.16	1.41	1.42	1.39
5	1.67	1.71	1.71	1.84
6A	1.81	1.79	1.78	1.76
6B	1.06	1.08	1.09	1.06
7A	1.35	1.36	1.35	1.34
7B	1.02	1.03	1.02	1.02
8	1.51	1.51	1.51	1.51
9	1.32	1.34	1.33	1.33
10				
11A	1.32	1.33	1.33	1.33
11B	1.17	1.18	1.17	1.14
12A	1.65	1.66	1.65	1.65
12B	1.12	1.13	1.12	1.12
14	1.13	1.14	1.14	1.14
15A	1.88	1.89	1.89	1.88
15B	1.13	1.13	1.13	1.13
16	4.26 *m*	4.27 *m*	4.27 *m*	4.27 *m*
17	1.65	1.65	1.65	1.65
18	0.69 *s*	0.70 *s*	0.70 *s*	0.70 *s*
19	0.89 *s*	0.90 *s*	0.89 *s*	0.89 *s*
20	1.75 *p* 6.8Hz	1.75 *p* 6.8Hz	1.75 *p* 6.5Hz	1.75 *p* 6.9Hz
21	0.92 *d* 7.0Hz	0.92 *d* 7.0Hz	0.92 *d* 7.0Hz	0.92 *d* 7.0Hz
22				
23A	1.88	1.88	1.88	1.88
23B	1.33	1.33	1.34	1.34
24A	1.79	1.79	1.79	1.79
24B	1.26	1.26	1.26	1.26

25	1.63	1.63	1.63	1.63
26A	3.77 *dd* 2.9, 11.0Hz	3.77 *dd* 2.8, 11.0Hz	3.78 *dd* 2.8, 11.1Hz	3.78 *dd* 2.8, 11.0Hz
26B	3.20 *dt* 11.0, 1.8Hz	3.20 *dt* 11.0, 1.8	3.20 *dt* 1.7,11.1Hz	3.20 *dt* 1.9, 11.4Hz
27	1.00 *d* 7.1Hz	1.00 *d* 7.1Hz	1.00 *d* 7.1Hz	1.00 *d* 7.1Hz
3-OH	4.15 *d* 3.1Hz			
3-*O*-*β*-Galactopyranoside				
1’		4.08 *d* 7.5Hz	4.24 *d* 5.9Hz	4.27 *d* 7.7Hz
2’		3.24	3.57	3.75 *d* 2.0Hz
3’		3.24	3.48	3.56 *dd* 3.1, 9.8Hz
4’		3.61	3.65	3.81
5’		3.27 *dt* 6.2, 1.0Hz	3.30	3.34
6A’		3.50 *dd* 6.2, 11.0Hz	3.50	3.48
6B’		3.40 *dd* 6.2, 11.0Hz	3.40 *p* 5.6Hz	3.38
2’-*O*-*β*- Glucopyranosyl				
1’’			4.39 *d* 7.9Hz	4.64 *d* 7.9Hz
2’’			2.97	2.86
3’’			3.15	3.11
4’’			3.11 *d* 4.6Hz	2.96
5’’			3.03	3.07
6A’’			3.62 *m*	3.68
6B’’			3.49	3.43
3’-*O*-*β*-xylopyranosyl				
1’’’				4.41 *d* 7.2Hz
2’’’				3.42
3’’’				3.28
4’’’				3.62
5A’’’				3.68
5B’’’				3.38

Table 2. ^{13}C NMR chemical shift values (ppm) for saponins **1**-**4** isolated from flowering tops of *N. ossifragum* in DMSO-D_6 at 298K.

	1	**2**	**3**	**4**
1	29.8	30.16	30.14	29.88
2	27.5	26.08	25.96	26.19
3	64.6	72.79	73.90	72.99
4	33.4	29.59	29.97	29.43
5	36.0	35.97	36.00	34.42
6	26.4	26.40	26.34	26.40
7	26.2	26.22	26.22	26.25
8	35.0	34.95	34.95	34.98
9	39.4	39.50	39.50	39.50
10	34.8	34.65	34.58	34.61
11	20.5	20.51	20.50	20.51
12	39.7	39.70	39.7	39.7
13	40.2	40.0	40.27	40.29
14	55.8	55.73	55.77	55.79
15	31.5	31.47	31.47	31.49
16	80.5	80.45	80.46	80.48
17	61.9	61.91	61.91	61.92
18	16.2	16.24	16.25	16.29
19	23.8	23.63	23.63	23.51
20	41.6	41.62	41.62	41.64
21	14.5	14.53	14.53	14.55
22	108.9	108.91	108.91	108.93
23	25.5	25.50	25.50	25.50
24	25.6	25.59	25.59	26.61
25	26.5	26.50	26.51	26.52
26	64.3	64.31	64.32	64.32
27	16.0	15.99	15.99	16.01
3-*O*-β- Galactopyranoside				
1’		101.83	100.81	99.83
2’		70.76	79.21	75.49
3’		73.65	73.27	82.10
4’		68.19	67.72	68.02
5’		75.05	74.78	74.62
6’		60.42	60.30	60.09
2’-*O*-β- Glucopyranosyl				
1’’			103.90	102.20
2’’			75.21	74.68
3’’			76.22	76.79
4’’			70.08	71.10
5’’			77.02	76.65
6’’			61.12	61.89

3'-*O*-β-xylopyranosyl	
1'''	104.70
2'''	70.97
3'''	72.88
4'''	67.94
5'''	65.85

Table 3. ^{1}H NMR chemical shift values (ppm) and coupling constants (Hz) of chrysoeriol 6-*C*-β-arabinofuranosyl-8-*C*-β-glucopyranoside (**5**), chrysoeriol 6-*C*-β-arabinopyranosyl-8-*C*-β-glucopyranoside (**6**), chrysoeriol 6-*C*-β-xylopyranosyl-8-*C*-β-galactopyranoside (**7**), chrysoeriol 6-*C*-β-galactopyranosyl-8-*C*-*β*-glucopyranoside (**8**), chrysoeriol 6-*C*-β-glucopyranosyl-8-*C*-β-galactopyranoside (**9**) and chrysoeriol 6,8-di-*C*-β-*D*-glucopyranoside (**10**) in DMSO-D_6 at 298K. Top: Signals of major rotamer. Bottom: Signals of minor rotamer. s = singlet; d = doublet; dd = double doublet; ddd = double double doublet; t = triplet; br = broad; m = multiplet.

	5	**6**	**7**	**8**	**9**	**10**
3	6.94 *s*	6.94 *s*	6.86 *s*	6.94 *s* (6.91 *s*)	6.86 *s* (7.00 *s*)	6.95 (6.87)
2'	7.55 *d* 2.2Hz	7.54 *d* 2.2Hz	7.65 *d* 2.1Hz	7.54 *d* 2.3Hz (7.59 *d* 2.2Hz)	7.65 *d* 2.2Hz (7.56)	7.55 (7.64)
5'	6.88 *d* 8.3Hz	6.89 *d* 8.4Hz	6.92 *d* 8.4Hz	6.89 *d* 8.4Hz (6.95)	6.92 *d* 8.4Hz (6.88)	6.88 (6.95)
6'	7.73 *dd* 8.3, 2.2Hz	7.70 *dd* 8.4, 2.2Hz	7.58 *dd* 2.1, 8.4Hz	7.70 *dd* 2.3, 8.4Hz (7.56 *dd* 2.2, 8.4Hz)	7.58 *dd* 2.2, 8.4Hz (8.27)	7.71 (7.57)
5-OH	13.81 *s*	13.71	13.74	13.71 *s*	13.75 *s* (13.86 *s*)	13.75 (13.73)
7-OH	10.52 *s*	9.18	9.23	9.18 *s*	9.24 *s* (br) (9.03 *s* (br))	9.36 (9.36)
4'-OH	10.00 *s*	9.99 *s*	9.96	10.00 *s*	9.96 *s* (9.83 *s*)	
3'-OCH$_3$	3.88 *s*	3.88 *s*	3.90 *s*	3.88 *s* (3.90 *s*)	3.90 *s* (3.88 *s*)	3.88 *s* (3.90 *s*)
	6-*C*-β-Arabinofuranosyl	**6-*C*-β-Arabinopyranosyl**	**6-*C*-β-Xylopyranosyl**	**6-*C*-β-Galactopyranosyl**	**6-*C*-β-Glucopyranosyl**	**6-*C*-*β*-Glucopyranosyl**
1''	5.44 *d* 3.2Hz	4.71 *d* 9.2 Hz	4.55 *d* 9.8Hz	4.77*d* 9.7Hz (4.70 d 9.7Hz)	4.62 *d* 10.0Hz (4.80)	4.80 *d* 9.9Hz (4.66 *d*)
2''	4.09 *dd* 3.2, 0.8Hz	3.80 *m*	4.09 *m*	3.80 *dd* 9.7, 9.5Hz	4.12 (3.48 (br))	3.48 *m* (3.98)

3''	3.93 *dd* 0.8, 3.0Hz	3.46 *m*	3.13 *t* 8.7Hz	3.45 *m*	3.19 *t* 8.6Hz (3.30)	3.30 *t* 8.8Hz (3.22)
4''	3.89 *m*	3.81 *m*	3.38 *m*	3.79	3.08 *t* 9.0Hz	3.37 *t* 9.4Hz
5A''	3.67 *dd* 6.6, 11.3Hz	3.83 *dd* 11.9, 2.7Hz	3.74 *m*	3.56	3.15 *m* (3.32)	3.32 *m*
5B''	3.64 *dd* 4.8, 11.3Hz	3.64 *d* 11.9Hz	3.05 *t* 10.8Hz			
6A''				3.53 *m*	3.70 *dd* 2.0, 12.0Hz (3.63)	3.63 *m*
6B''					3.37 *m*	
	8-*C*-β-Glucopyranoside	**8-*C*-β-Glucopyranoside**	**8-*C*-β-Galactopyranoside**	**8-*C*-β-Glucopyranoside**	**8-*C*-β-Galactopyranoside**	**8-*C*-*β*-Glucopyranoside**
1'''	4.70 *d* 9.9Hz	4.74 *d* 9.8 Hz	5.00 *d* 9.6	4.74 *d* 10.00Hz (4.91 d 10.0Hz)	5.00 *d* 9.6 Hz (4.69 *d* 9.9Hz)	4.75 *d* 9.9Hz (5.04 *d*)
2'''	3.88 *m*	3.93 *dd* 9.8, 8.7Hz	3.80 *t* 9.3Hz	3.94 *dd* 10.0, 9.0Hz (3.89)	3.83 *m* (4.24 *t* 9.4Hz)	3.92 *dd* 8.7, 9.8Hz (3.56)
3'''	3.24 *t* 8.8Hz	3.27 *t* 8.7Hz	3.47 *dd* 2.8, 9.3Hz	3.27 *t* 8.8Hz	3.47 *dd* 3.9, 9.1Hz (3.41 *dd* 3.2, 8.9Hz)	3.26 *t* 8.7Hz (3.31)
4'''	3.35 *dd* 8.8, 9.6Hz	3.36 *dd* 8.7, 9.6Hz	3.83 *d* 2.8Hz	3.34 *dd* 9.6, 8.8Hz	3.83 *br d* 2.9Hz (3.85)	3.34 *t* 9.1Hz (3.34)
5'''	3.23 *ddd* 2.1, 6.1, 9.6Hz	3.23 *ddd* 2.0, 6.0, 9.6Hz	3.71 *t* 6.2Hz	3.23 *ddd* 2.0, 6.3, 9.6Hz	3.71 *m*	3.22 *ddd* 1.9, 6.2, 9.5Hz (3.18)
6A''	3.76 *dd* 2.1, 12.1Hz	3.73 *dd* 2.0, 12.1Hz	3.55 *d* 6.2Hz	3.75 *dd* 2.0, 12.4Hz (3.71)	3.56 *m* (3.56)	3.74 *dd* 1.9, 12.0Hz (3.69)
6B''	3.48 *dd* 6.1, 12.1Hz	3.47 *dd* 6.0, 12.1Hz		3.46 *dd* 6.3, 12.1Hz (3.46)		3.47 *dd* 6.2, 12.0Hz (3.46)

Table 4. ^{13}C NMR chemical shift values (ppm) and coupling constants (Hz) of chrysoeriol 6-*C*-β-arabinofuranosyl-8-*C*-β-glucopyranoside (**5**), chrysoeriol 6-*C*-β-arabinopyranosyl-8-*C*-β-glucopyranoside (**6**), chrysoeriol 6-*C*-β-xylopyranosyl-8-*C*-β-galactopyranoside (**7**), chrysoeriol 6-*C*-β-galactopyranosyl-8-*C*-*β*-glucopyranoside (**8**), chrysoeriol 6-*C*-β-glucopyranosyl-8-*C*-β-galactopyranoside (**9**) and chrysoeriol 6,8-di-*C*-β-*D*-glucopyranoside (**10**) in DMSO-D_6 at 298K. Top: Signals of major rotamer. Bottom: Signals of minor rotamer. nd = not detected.

	5	**6**	**7**	**8**	**9**	**10**
Chrysoeriol						
2	164.0	163.9	163.2	164.1	163.2	164.1
				(163.5)	(164.1)	(163.5)
3	102.8	103.0	102.6	103.0	102.6	103.1
				(102.8)	(103.4)	(102.8)
4	182.2	182.1	181.9	182.2	182.2	182.5
				(182.2)	(182.2)	(182.4)
5	157.1	158.0	159.8	158.1	nd	158.6
					(158.5)	(159.9)
6	103.3	107.9	109.1	108.2	109.2	107.6
					(107.1)	(109.0)
7	162.7	160.7	161.4	160.8	161.5	160.9
					(160.7)	(161.5)
8	104.5	104.7	103.8	105.0	103.4	105.3
					(105.2)	
9	154.9	155.1	153.1	155.1	153.2	155.1
					(155.2)	
10	103.1	103.5	102.9	103.6	103.0	103.7
				(102.9)	(103.8)	(103.3)
1’	121.9	121.6	121.5	121.7	121.4	121.8
				(121.6)	(120.9)	(121.7)
2’	110.6	110.5	110.0	110.7	110.1	110.7
				(109.9)	(109.9)	(110.2)
3’	148.0	147.8	147.8	148.0	147.7	148.1
				(147.9)	(147.7)	(147.8)
4’	150.8	150.6	150.3	150.8	150.3	150.9
				(150.5)	(150.6)	(150.4)
5’	115.5	115.1	115.4	115.4	115.6	115.5
				(115.8)	(115.7)	(115.7)
6’	121.2	121.0	120.5	121.1	120.3	121.3
				(120.3)	(123.0)	(120.5)
3’-OCH_3	56.2	56	55.5	56.1	55.6	56.2
				(55.6)	(55.9)	(55.7)
	6-*C*-β-Arabinofur	**6-*C*-β-Arabinopyr**	**6-*C*-β-Xylopyranos**	**6-*C*-β-Galactopyr**	**6-*C*-β-Glucopyran**	**6-*C*-*β*-Glucopyra**

	anosyl	**anosyl**	**yl**	**anosyl**	**osyl**	**nosyl**
1''	79.9	73.9	73.4	73.5 (73.6)	72.7 (73.9)	74.0 (73.1)
2''	77.3	68.1	77.2	69.6 (68.5)	69.7 (71.8)	71.9
3''	77.4	73.6	79.1	74.4 (74.7)	79.1 (77.7)	77.8 (78.9)
4''	87.0	69.3	69.7	68.3	70.7	69.0
5''	61.1	69.9	70.0	79.0	81.7 80.7)	80.9
6''				60.7	61.5 (59.7)	59.7
	8-*C*-β-Glucopyranoside	**8-*C*-β-Glucopyranoside**	**8-*C*-β-Galactopyranoside**	**8-*C*-β-Glucopyranoside**	**8-*C*-β-Galactopyranoside**	**8-*C*-*β*-Glucopyranoside**
1'''	73.0	72.9	74.8	73.0 (74.5)	74.9 (73.7)	73.2 (75.1)
2'''	70.7	70.6	69.8	70.7 (70.7)	68.2 (68.8)	70.8 (72.0)
3'''	78.7	78.7	74.3	78.8 (79.0)	74.4 (75.5)	78.8 (78.3)
4'''	70.5	70.4	68.1	70.6 (70.5)	69.7 (69.1)	70.6 (69.2)
5'''	81.9	81.7	79.2	81.9 (82.0)	79.4	82.0 (81.8)
6'''	61.4	61.1	60.5	61.3 (61.6)	60.7 (60.8)	61.3 (61.3)

NMR tables of the isolated compounds from *Osmunda regalis*.

Table 5. ^{1}H and ^{13}C chemical shift values (ppm) and coupling constants (Hz) of chalconaringenin 2'-*O*-β-glucopyranoside (**11**) in DMSO-D_6 at 298K.

	Compound **11** δ ^{1}H	Compound **11** δ ^{13}C
1		130.0
2/6	7.88 'd' 8.8	130.5
3/5	6.36 'd' 8.8	115.3
4		161.3
1'		104.2
2'		159.1
3'	6.12 d 2.3	94.3
4'		160.9
5'	6.10 d 2.3	96.5
6'		159.9
α	7.97 d 15.7	120.0
β	8.01 d 15.7	135.1
C=O		188.5
4-OH	10.22 *s*	
4'-OH	9.90 *s*	
6'-OH	10.20 *s*	
2'-O-β-glc		
1''	4.93 d 7.7	100.2
2''	3.34 m	73.6
3''	3.31 m	77.0
4''	3.22 dd 9.8; 9.0	69.6
5''	3.24 ddd 2.2; 5.4; 9.7	60.6
6A''	3.69 dd 2.2; 11.9	60.6
6B''	3.49 dd 5.4; 11.9	

Table 6. ^{1}H chemical shift values (ppm) and coupling constants (Hz) of kaempferol 3-*O*-(2''-*O*-(2'''-α-rhamnopyranosyl)-β-glucopyranosyl)-β-glucopyranoside (Compound **12**), quercetin 3-*O*-(2''-*O*-(2'''-α-rhamnopyranosyl)-β-glucopyranosyl)-β-glucopyranoside (Compound **13**), and kaempferol 3-*O*-(2''-*O*-(2'''-α-rhamnopyranosyl-6'''-*O*-(E)-caffeoyl-)-β-glucopyranosyl)-β-glucopyranoside (Compound **16**) in DMSO-D_6 at 298 K.

	Compound **12** δ ^{1}H	Compound **13** δ ^{1}H	Compound **16** δ ^{1}H
2			
3			
4			
5			
6	6.18 d 2.0	6.17 d 2.1	6.16 d 2.1
7			
8	6.42 d 2.0	6.38 d 2.1	6.37 d 2.1
9			

10			
1’			
2’	8.05 ‘d’ 8.9	7.49 d 2.3	7.98 ‘d’ 8.8
3’	6.93 ‘d’ 8.9		6.83 ‘d’ 8.8
4’			
5’	6.93 ‘d’ 8.9	6.89 d 8.5	6.83 ‘d’ 8.8
6’	8.05 ‘d’ 8.9	7.66 d 8.5	7.98 ‘d’ 8.8
5-OH	12.76 s	12.78 s	12.74 s
7-OH	10.83 s	10.81 s	10.78 s
3’-OH		9.20 s	9.02 s
4’-OH	10.13 s	9.63 s	9.52 s
3-*O*-β-glc			
1’’	5.71 d 7.41	5.70 d 7.3	5.71 d 7.3
2’’	3.70 dd 8.5, 7.4	3.73	3.66 dd 8.5, 7.3
3’’	3.49 t 8.5	3.49	3.50 t 8.5
4’’	3.05 dd 9.8, 8.5	3.08	3.04 m
5’’	3.03 ddd 9.8, 5.7, 2.0	3.04	3.04 m
6A’’	3.50 m	3.51	3.49 dd 11.8, 1.9
6B’’	3.19 dd 11.3. 5.7	3.20	3.19 m
2’’-*O*-β-glc			
1’’’	4.97 d 7.8	4.94 d 7.8	5.02 d 7.7
2’’’	3.23 dd 9.0, 7.8	3.23	3.27 dd 9.1, 7.7
3’’’	3.29 t 9.0	3.29	3.31 t 9.1
4’’’	3.11 dd 9.8, 9.0	3.11	3.22 dd 9.8, 9.1
5’’’	3.07 ddd 9.8, 5.4, 2.4	3.06	3.35 ddd 9.8, 4.8, 2.2
6A’’’	3.67 dd 11.9, 2.4	3.64	4.30 dd 11.8, 2.2
6B’’’	3.48 dd 11.9, 5.4	3.47	4.19 dd 11.8, 4.8
2’’’-*O*-α-rha			
1’’’’	5.05 d 1.8	5.06 d 1.7	5.05 d 1.7
2’’’’	3.69 dd 3.4, 1.8	3.69	3.69 dd 3.4, 1.7
3’’’’	3.53 dd 9.3, 3.4	3.54	3.53 dd 9.4, 3.4
4’’’’	3.18 t 9.3	3.18	3.19 t 9.4
5’’’’	4.00 dd 9.3, 6.2	3.99	3.98 dd 9.4, 6.2
6’’’’	1.17 d 6.2	1.17 d 6.2	1.17 d 6.2
6’’’-*O*-(*E*)-caffeoyl			
1’’’’’			
2’’’’’			6.95 d 2.2
3’’’’’			
4’’’’’			
5’’’’’			6.66 d 8.2
6’’’’’			6.84 dd 8.2, 2.2
7’’’’’			7.36 d 15.8
8’’’’			6.16 d 15.8
9’’’’’			

Table 7. ^{13}C chemical shift values (ppm) of kaempferol 3-*O*-(2''-*O*-(2'''-α-rhamnopyranosyl)-β-glucopyranosyl)-β-glucopyranoside (Compound **12**), quercetin 3-*O*-(2''-*O*-(2'''-α-rhamnopyranosyl)-β-glucopyranosyl)-β-glucopyranoside (Compound **13**), and kaempferol 3-*O*-(2''-*O*-(2'''-α-rhamnopyranosyl-6'''-*O*-(E)-caffeoyl-)-β-glucopyranosyl)-β-glucopyranoside (Compound **16**) in DMSO-D_6 at 298 K.

	Compound **12** δ ^{13}C	Compound **13** 6 δ ^{13}C	Compound **16** δ ^{13}C
2	155.66	155.71	155.7
3	132.98	133.15	133.2
4	177.55	177.52	177.6
5	161.38	161.40	161.4
6	98.61	98.58	98.6
7	164.04	164.02	164.1
8	93.57	93.38	93.6
9	156.30	156.24	156.3
10	104.01	103.99	104.1
1'	121.12	121.36	121.1
2'	130.90	115.61	130.7
3'	115.38	144.87	115.2
4'	159.94	148.48	160.0
5'	115.38	115.58	115.2
6'	130.90	122.34	130.7
5-OH			
7-OH			
3'-OH			
4'-OH			
3-*O*-β-glc			
1''	98.19	98.26	98.1
2''	77.83	77.20	78.2
3''	77.51	77.44	77.3
4''	70.34	77.30	70.3
5''	77.35	77.37	77.5
6A''	60.77	60.89	60.7
6B''			
2''-*O*-β-glc			
1'''	100.19	100.35	100.3
2'''	77.03	76.94	77.1
3'''	77.82	77.80	77.6
4'''	70.46	70.42	70.0
5'''	76.74	76.57	73.7
6A'''	61.33	61.26	63.4
6B'''			
2'''-*O*-α-rha			
1''''	100.29	100.25	100.4
2''''	70.58	70.55	70.6

3’’’’	70.64	70.61	70.7
4’’’’	72.36	72.38	72.3
5’’’’	68.29	68.29	68.4
6’’’’	17.78	17.80	17.8
6’’’-*O*-(*E*)-caffeoyl			
1’’’’’			125.6
2’’’’’			115.00
3’’’’’			145.5
4’’’’’			148.3
5’’’’’			115.7
6’’’’’			121.3
7’’’’’			145.3
8’’’’			113.8
9’’’’’			166.5

Table 8. ^{1}H and ^{13}C chemical shift values (ppm) and coupling constants (Hz) of vanillic acid (**14**) in DMSO-D_6 at 298K.

	Compound **14** δ ^{1}H	Compound **14** δ ^{13}C
1		121.66
2	7.42 d 1.9	112.78
3		147.28
4		151.16
5	6.82 d 8.1	115.08
6	7.42 dd 8.1; 1.9	123.52
7		167.25
7-COOH	12.46 s (br)	
4-OH	9.81 s	
3-OCH_3	3.79 s	55.60

Table 9. ^{1}H and ^{13}C chemical shift values (ppm) and coupling constants (Hz) of *p*-hydroxy-benzoic acid (**15**) and *p*-hydroxy-benzoic acid methyl ester (**17**) in DMSO-D_6 at 298K.

	Compound **5** δ ^{1}H	Compound **7** δ ^{1}H	Compound **5** δ ^{13}C	Compound **7** δ ^{13}C
1			121.41	120.32
2/6	7.77 ‘d’ 8.6	7.80 ‘d’ 8.9	131.58	131.47
3/5	6.80 ‘d’ 8.6	6.83 ‘d’ 8.9	115.17	115.40
4			161.60	162.02
7			167.21	166.11
7-COOH	12.39 s (br)	3.77 s		51.68
4-OH	10.19 s	10.31 s (br)		

Table 10. ^{1}H and ^{13}C chemical shift values (ppm) and coupling constants (Hz) of Dihydrodehydrodiconiferyl alcohol 4-O-α-rhamnopyranoside (Compound **18**) in DMSO-D_6 at 298K.

	Compound **18** δ ^{1}H	Compound **18** δ ^{13}C
1		136.58
2	6.99 d 2.1	110.61
3		150.10
4		144.85
5	7.04 d 8.3	117.90
6	6.85 dd 8.3, 2.1	118.04
7	5.46 d 6.5	86.56
8	3.42 dddd 7.4, 6.5, 5.3, 0.8	53.51
9A	3.71 dd 10.8, 5.3	63.20
9B	3.60 dd 10.8, 7.4	
1’		135.27
2’	6.68 d 1.8	112.56
3’		143.43 (w)
4’		145.53 (s)
5’		128.82 (w)
6’	6.67 dd 1.8, 0.8	116.53
7’	3.40 d 6.5	60.26
8’	1.68 m	34.79
9’	2.52 m	31.62
3-OCH_3	3.73 s	55.85
3’-OCH_3	3.76 s	55.75
	4-*O*-*α*-rha	
1’’	5.23 d 2.0	99.71
2’’	3.83 dd 3.4, 2.0	70.33
3’’	3.63 dd 9.4, 3.4	70.47
4’’	3.26 t 9.4	71.80
5’’	3.57 dd 9.4, 6.2	69.66
6’’	1.08 d 6.2	17.92

Table 11. ^{1}H and ^{13}C chemical shift values (ppm) and coupling constants (Hz) of apigenin 7-(2’’-O-α-rhamopyranosyl-β-glucopyranoside) (**19**) in DMSO-D_6 at 298K.

	Compound **19** δ ^{1}H	Compound **19** δ ^{13}C
2		164.33
3	6.87 s	103.26
4		182.05
5		161.19
6	6.37 d 2.2	99.39
7		162.61
8	6.78 d 2.2	94.57
9		157.05

10		105.49
1’		121.08
2’/6’	7.93 ‘d’ 8.8	128.65
3’/5’	6.93 ‘d’ 8.8	116.09
4’		161.45
7-*O*-β-glc		
1’’	5.22 d 7.7	97.88
2’’	3.50 dd 9.2, 7.7	76.32
3’’	3.46 t 9.2	77.28
4’’	3.19 t 9.2	69.71
5’’	3.48 ddd 9.2, 5.8, 1.9	77.09
6A’’	3.70 dd 11.8, 1.9	60.54
6B’’	3.46 m	
2’’-*O*-α-rha		
1’’’	5.12 d 1.9	100.52
2’’’	3.68 dd 3.3, 1.9	70.46
3’’’	3.32 dd 9.3, 3.3	70.54
4’’’	3.20 t 9.3	71.92
5’’’	3.74 dd 9.3, 6.2	68.40
6’’’	1.19 d 6.2	18.14

Table 12. ^{1}H and ^{13}C chemical shift values (ppm) and coupling constants (Hz) of epoxyconiferyl alcohol (**20**) in DMSO-D_6 at 298K.

	Compound 2**0** δ ^{1}H	Compound 2**0** δ ^{13}C
1		132.30
2	6.88 d 2.0	110.48
3		147.59
4		145.98
5	6.71 d 8.1	115.20
6	6.74 ddd 8.1, 2.0, 0.6	118.69
7	4.59 dd 4.6, 0.6	85.22
8	3.02 m	53.65
9A	4.11 dd 9.1, 7.1	70.96
9B	3.71 dd 9.1, 3.9	
3-OCH_3	3.75 s	55.67
4-OH	8.88 s (br)	

Table 13. ^{1}H and ^{13}C chemical shift values (ppm) and coupling constants (Hz) of 5-hydroxy-2-hexen-4-olide (**21**) in DMSO-D_6 at 298K.

	Isomer 1		**Isomer 2**	
	Compound **21** δ ^{1}H	Compound **21** δ ^{13}C	Compound **21** δ ^{1}H	Compound **21** δ ^{13}C
1	-	173.33	-	173.40
2	6.20 dd 5.8, 2.0	121.58	6.20 dd 5.8, 2.0	121.57
3	7.78 dd 5.8, 1.5	156.16	7.69 dd 5.8, 1.6	156.50
4	4.94 m	87.30	4.98 m	87.12
5	3.79 dd 6.4, 4.8	66.60	3.84 dd 6.4, 4.5	66.16
6	1.11 d 6.4	19.17	1.08 dd 6.4, 0.6	19.15

Table 14. ^{1}H and ^{13}C NMR chemical shift values (ppm) and coupling constants (Hz) of the novel lactone 3-methoxy-5-hydroxy-4-olide (Compounds **22**) in DMSO-D_6 at 298 K.

	Compound **22** δ ^{1}H	Compound **22** δ ^{13}C
1		175.86
2A	2.80 dd 18.2, 6.8	35.04
2B	2.39 dd 18.2, 1.3	
3	4.07 dt 6.8, 4.3	76.00
4	4.22 dd 4.2, 1.3	88.13
5	3.74 dd 6.5, 4.2	65.57
6	1.12 d 6.5	18.98
3-OCH_3	3.23 s	55.65

Table 15. ^{1}H and ^{13}C NMR chemical shift values (ppm) and coupling constants (Hz) of the novel bilactone 4-hydroxy-3-(3-hydroxy-4-(1-hydroxyethyl)-oxotetrahydroifuran-5-methyltetrahydropyranone (Compound **23**) in DMSO-D_6 at 298 K.

	Compound **23** δ ^{1}H	Compound **23** δ ^{13}C
1		171.25
2A	2.82 dd 15.2, 11.5	32.73
2B	2.66 dd 15.2, 6.6	
3	2.91 dddd 11.5, 8.0, 6.6, 1.4	38.23
4	4.04 dd 8.7, 8.0	80.22
5	4.39 dd 8.7, 6.3	73.19
5-CH_3	1.29 d 6.3	18.19
1’		176.85
2’	3.21 dd 5.3, 1.4	51.87
3’	4.82 d 5.3	78.56
4’	4.28 d 3.7	86.97
4’-1’’-hydroxyethyl		
1’’	3.78 dd 6.6, 3.7	65.51
2’’	1.13 d 6.6	19.02

Table 16. ^{1}H and ^{13}C chemical shift values (ppm) and coupling constants (Hz) of Blumenol C glucoside (**24**) in DMSO-D_6 at 298K.

	Compound **24** δ ^{1}H	Compound **24** δ ^{13}C
1		35.99
2A	2.33	47.04
2B	1.87	
3		198.09
4	5.71	124.26
5		166.04
6	1.90 t 5.4	50.20
7A	1.78	25.10
7B	1.37	
8A	1.52	36.23
8B	1.49	
9	3.74 q 6.0	73.30
10	1.08 d 6.1	19.57
11	0.99 s	26.82
12	0.92 s	28.53
13	1.96 d 1.2	24.15
9-*O*-β-glc		
1’	4.16 d 7.8	100.76
2’	2.88 dd 9.0, 7.8	73.59
3’	3.11 t 9.0	76.93
4’	3.01 dd 9.7, 9.0	70.32
5’	3.06 ddd 9.7, 6.0, 2.2	76.82
6A’	3.64 dd 11.6, 2.2	61.34
6B’	3.40 dd 11.6, 6.0	

Table 17. ^{1}H and ^{13}C NMR chemical shift values (ppm) and coupling constants (Hz) of the novel lactone 4-*O*-(5’-hydroxy-4’-oxohexanoyl) osmundalactone (Compound **15**) in DMSO-D_6 at 298 K.

	Compound **25** δ ^{1}H	Compound **25** δ ^{13}C
1		161.88
2	6.11 dd 9.9, 1.5	122.25
3	6.87 dd 9.9, 3.4	143.83
4	5.30 ddd 6.6, 3.4, 1.5	67.25
5	4.60 p 6.6	76.02
6	1.30 d 6.6	17.90
	4-*O*-(5’-hydroxy-4’-oxohexanoyl)	
1’		171.71
2’	2.54 m	27.31
3’	2.86 m	32.12
4’		212.85
5’	4.04 q 6.9	72.18
6’	1.16 d 6.9	19.66

Table 18. ^{1}H and ^{13}C chemical shift values (ppm) and coupling constants (Hz) of hexyl-β-glucopyranoside (**26**) in DMSO-D_6 at 298K.

	Compound **26** δ ^{1}H	Compound **26** δ ^{13}C
1A	3.73 m	68.62
1B	3.39 m	
2	1.50 m	29.31
3	1.30 m	25.27
4	1.24 m	31.23
5	1.26 m	22.15
6	0.85 t 7.0	14.01
1’	4.08 d 7.8	102.91
2’	2.91 dd 9.0, 7.8	73.51
3’	3.10 dd 9.0, 8.6	76.89
4’	3.02 dd 9.8, 8.6	70.16
5’	3.05 ddd 9.8, 5.8, 2.1	76.86
6A’	3.64 dd 11.8, 2.1	61.16
6B’	3.41 dd 11.8, 5.8	

Table 19. ^{1}H and ^{13}C chemical shift values (ppm) and coupling constants (Hz) of 2-hexenoic acid (**27**) in DMSO-D_6 at 298K.

	Compound **27** δ ^{1}H	Compound **27** δ ^{13}C
1		167.17
2	5.75 dt 15.7, 1.6	122.15
3	6.80 dt 15.7, 6.9	148.68
4	2.14 m	33.43
5	1.42 p 7.4	20.87
6	0.87 t 7.4	13.56

NMR tables of the isolated compounds from *Cryptogramma* crispa.

Table 20. ^{1}H chemical shift values (ppm) and coupling constants (Hz) of quercetin (**28**), quercetin 3-O-β-galactopyranoside (**29**), quercetin 3-O-β-glucopyranoside (**30**) and quercetin 7-O-β-glucopyranoside (**31**) in DMSO-D_6 at 298K.

	Compound **28** δ ^{1}H	Compound **29** δ ^{1}H	Compound **30** δ ^{1}H	Compound **31** δ ^{1}H
2				
3				
4				
5				
6	6.17 d 2.1	6.20 d 2.1	6.40 d 2.0	6.41 d 2.1
7				
8	6.39 d 2.1	6.40 d 2.1	6.76 d 2.3	6.75 d 2.1
9				
10				
1’				
2’	7.66 d 2.2	7.54 d 2.2	7.73 d 3.0	7.71 d 2.3
3’				
4’				
5’	6.87 d 8.4	6.82 d 8.4	6.82 d 8.5	6.89 d 8.4
6’	7.53 dd 8.4, 2.2	7.66 dd 8.4, 2.2	7.5 d 2.3	7.54 dd 8.4, 2.3
3-OH		12.62 s		9.48 s
5-OH		10.84 s	12.60 s	12.50 s
7-OH		9.39 s		
3’-OH		9.39 s		9.28 s
4’-OH				9.63 s
3-O-β		**galactopyranoside**	**glucopyranoside**	
7-O-β				**glucopyranoside**
1’’		5.37 d 7.7	5.30 d 7.8	5.06 d 7.7
2’’		3.58 dd 9.5, 7.7		3.25 dd 9.0, 7.7
3’’		3.38 dd 9.5, 3.4		3.29 t 9.0
4’’		3.66 dd 3.4, 1.0		3.17 dd 9.8, 9.0
5’’		3.34 dt 6.0, 1.0	3.45 m	3.44 ddd 9.8, 5.9, 2.1
6A’’		3.46 dd 10.7, 6.0	3.11 dd 12.0, 2.5	3.70 dd 11.8, 2.1
6B’’		3.30 dd 10.7, 6.0	3.37 m	3.47 dd 11.8, 5.8

Table 21. ^{13}C chemical shift values (ppm) of quercetin (**28**), quercetin 3-O-β-galactopyranoside (**29**), quercetin 3-O-β-glucopyranoside (**30**) and quercetin 7-O-β-glucopyranoside (**31**) in DMSO-D_6 at 298K.

	Compound **28** δ ^{13}C	Compound **29** δ ^{13}C	Compound **30** δ ^{13}C	Compound **31** δ ^{13}C
2	146.89	156.47	146.0	147.6
3	135.82	133.70	136.0	136.0
4	175.92	177.70	174.1	176.1
5	160.81	161.42	160.5	160.5
6	98.26	98.88	98.8	98.8
7	163.96	164.32	162.7	162.7
8	93.43	93.70	94.3	94.3
9	156.22	156.51	155.8	155.8
10	103.10	104.13	104.8	104.8
1’	122.04	121.32	121.9	121.9
2’	115.15	116.20	115.5	115.5
3’	145.14	145.01	145.1	145.1
4’	147.79	148.65	148.1	148.1
5’	115.69	115.39	115.7	115.7
6’	120.06	122.17	120.1	120.1
3-OH				
5-OH				
7-OH				
3’-OH				
4’-OH				
3-O-β		**galactopyranoside**	**glucopyranoside**	
7-O-β				**glucopyranoside**
1’’		102.04	102.3	100.0
2’’		71.42		73.2
3’’		73.40		76.5
4’’		68.14		69.6
5’’		76.02	77.8	77.3
6A’’		60.36	60.5	60.7
6B’’				

Table 22. ^{1}H and ^{13}C chemical shift values (ppm) and coupling constants (Hz) of kaempferol 7-O-β-glucopyranoside (**32**) in DMSO-D_6 at 298K.

	Compound **32** δ ^{1}H	Compound **32** δ ^{13}C
2		147.60
3		136.10

4		176.17
5		160.43
6	6.41 d 2.1	98.83
7		162.77
8	6.79 d 2.1	94.44
9		155.83
10		104.76
1’		121.60
2’/6’	8.06 ‘d’ 9.0	129.72
3’/5’	6.93 ‘d’ 9.0	115.54
4’		159.46
3-OH	9.53 s	
5-OH	12.48 s	
4’-OH	10.15 s	
7-*O*-β-glc		
1’’	5.06 d 7.7	99.96
2’’	3.25 dd 9.0, 7.7	73.18
3’’	3.29 t 9.0	76.51
4’’	3.17 dd 9.8, 9.0	69.63
5’’	3.44 ddd 9.8, 5.9, 2.1	77.24
6A’’	3.70 dd 11.8, 2.1	60.68
6B’’	3.47 dd 11.8. 5.9	

Table 23. ^{1}H and ^{13}C NMR chemical shift values (ppm) and coupling constants (Hz) of (*E*) + (*Z*) Ferulic acid (**33**) in DMSO-D_6 at 298K.

	Compound **32 δ ^{1}H Major (E)**	Compound **32 δ ^{13}C Major (E)**	Compound **32 δ ^{1}H Minor (Z)**	Compound **32 δ ^{13}C Minor (Z)**
1		125.90		126.3
2	7.26 d 2.1	111.20	7.64 d 2.1	114.30
3		148.00		146.90
4		140.10		148.20
5	6.77 d 8.2	115.6	6.74 d 8.2	115.00
6	7.07 dd 8.2, 2.1	122.90	7.14 dd 8.2, 2.1	125.00
7	7.47 d 15.9	144.60	6.75 d 12.9	142.1
8	6.34 d 15.9	115.7	5.72 d 12.9	117.00
9		168.0		167.90
3-OCH_3	3.80 s	55.80	3.74 s	55.50
4-OH	9.52 s		9.44 s	
COOH	12.11 s		12.11 s	

Table 24. ^{1}H and ^{13}C NMR chemical shift values (ppm) and coupling constants (Hz) of (*E*) + (*Z*) Ferulic acid 4-*O*-β-glucopyranoside (**34**) in DMSO-D_6 at 298K.

	δ ^{1}H Major (E)	**δ ^{13}C Major (E)**	**δ ^{1}H Minor (Z)**	**δ ^{13}C Minor (Z)**

1		128.19		128.57
2	7.33 d 2.0	111.24	7.57 d 2.1	114.30
3		149.17		148.15
4		148.43		147.43
5	7.08 d 8.5	114.98	7.06 d 8.6	114.46
6	7.17 dd 8.5, 2.0	122.30	7.20 dd 8.6, 2.1	123.86
7	7.51 d 15.9	144.05	6.81 d 12.9	141.05
8	6.45 d 15.9	117.25	5.82 d 12.9	118.71
9		167.89		167.73
3-OCH_3	3.80 s	55.79	3.75 s	55.56
	4-*O*-*β*-glc		4-*O*-*β*-glc	
1’	4.96 d 7.5	99.68	4.95 m	99.72
2’	3.25 m	73.19	3.24 m	73.21
3’	3.26 m	76.90	3.26 m	76.93
4’	3.15 dd 9.8, 9.0	69.66	3.16 m	69.70
5’	3.32 ddd 9.8, 5.8, 2.3	77.14	3.32 m	77.11
6A’’	3.65 dd 11.8, 2.3	60.68	3.66 m	60.70
6B’’	3.43 dd 11.8, 5.8		3.44 m	

Table 25. ^{1}H and ^{13}C NMR chemical shift values (ppm) and coupling constants (Hz) of *p*-Coumaric acid 4-*O*-β-glucopyranoside (**35**) in DMSO-D_6 at 298K.

	Compound **35** δ ^{1}H	Compound **35** δ ^{13}C
1		128.00
2/6	7.62 ‘d’ 8.8	129.83
3/5	7.03 ‘d’ 8.8	116.51
4		159.03
7	7.54 d 15.9	143.66
8	6.39 d 15.9	117.12
9		167.83
COOH	12.24 s (br)	
	4-*O*-*β*-glc	
1’	4.92 d 7.7	100.07
2’	3.23 dd 9.1, 7.7	73.25
3’	3.26 dd 9.0, 8.7	76.63
4’	3.15 dd 9.8, 8.7	69.73
5’	3.34 ddd 9.8, 5.9, 2.2	77.17
6A’	3.68 dd 11.9, 2.2	60.72
6B’	3.44 dd 11.9, 5.9	

Table 26. ^{1}H and ^{13}C NMR chemical shift values (ppm) and coupling constants (Hz) of caffeic acid (**36**) in DMSO-D_6 at 298K.

	Compound **36** δ ^{1}H	Compound **36** δ ^{13}C
1		125.77
2	7.00	114.99
3		145.63
4		148.22
5	6.95	115.85
6	6.95	121.13
7	7.45	144.45

8	6.18	115.12
9		166.14
3-OH	9.12 s	
4-OH	9.51 s	

Table 27. ^{1}H and ^{13}C NMR chemical shift values (ppm) and coupling constants (Hz) of methyl chlorogenic acid 4'-O-β-glucopyranoside (**37**) and chlorogenic acid methyl ester (**38**) in DMSO-D_6 at 298K.

	Compound **37** δ ^{1}H	Compound **37** δ ^{13}C	Compound **38** δ ^{1}H	Compound **38** δ ^{13}C
1		74.6		71.8
2A	1.92	37.7	1.98	35.3
2B	1.69		1.85	
3	3.85	67.7	3.83	68.4
4	3.32	73.7	3.17	73.0
5	3.77	67.3	3.76	67.8
6A	1.81	39.5	1.89	39.2
6B	1.81		1.89	
7	3.57	51.5	3.54	51.8
1'		129.0		125.9
2'	7.12 d 2.1	114.9	7.05 d 2.5	114.5
3'		144.1		145.1
4'		147.2		148.5
5'	7.10 d 8.4	116.0	7.03 d 2.1	116.3
6'	7.06 dd 8.4, 2.1	120.9	7.02 d 2.2	121.5
7'	7.45 d 16.0	144.1	7.48 dd 15.8, 10.2	145.9
8'	6.31 d 16.0	117.3	6.22 d 15.8	115.5
9'		167.7		166.6
7-OCH_3	3.57 s	51.5	1.77 s	51.8
4'-O-β-glc				
1''	4.76 d 7.5	101.7		
2''	3.29 m	73.3		
3''	3.27 t 9.0	75.9		
4''	3.16 dd 9.8, 8.8	69.8		
5''	3.34 ddd 9.8, 6.0, 2.1	77.4		
6A''	3.70 dd 11.8, 2.1	60.8		
6B''	3.46 m			

Table 28. ^{1}H chemical shift values (ppm) and coupling constants (Hz) of Pteroside D (**39**), Pteroside X (**40**), 3-malonyl-pteroside D (**41**) and Pterosin D (**42**) dissolved in DMSO-D6 at 298K.

	Compound **39** δ ^{1}H	Compound **40** δ ^{1}H	Compound **41** δ ^{1}H	Compound **42** δ ^{1}H
1				
2				
3	4.64	4.66	5.94 s	4.64
4	7.30 s	7.62 s	7.28 s	7.30 s
5				
6				
7				

8				
9				
10	1.08 s	1.10 s	1.19 s	1.08 s
11	0.91 s	0.92	0.96 s	0.91 s
12	2.41 s	4.65 s	2.42 s	2.40 s
13	2.97 m	2.95 t 7.9	3.00 m	2.84 dd 8.5, 7.3
14A	3.75 m	3.75 m	3.75 m	3.45 dd 8.5, 7.3
14B	3.55 m	3.54 dt 10.1, 7.9	3.56 m	
15	2.57	2.58 s	2.61 s	2.56 s
14-*O*-*β*-glc				
1’	4.20 d 7.8	4.18 d 7.8	4.20 d 7.8	
2’	2.98 dd 2.8; 9.1	2.95 dd 9.0, 7.8	2.94 dd 9.0, 7.8	
3’	3.15 dd 8.5; 9.1	3.12 t 8.9	3.12 t 8.9	
4’	3.06 dd 8.5; 9.7	3.03 dd 9.7, 8.8	3.02 dd 9.8, 8.8	
5’	3.09 ddd 2.2; 5.8; 9.7	3.08 ddd 9.7, 6.0, 2.2	3.08 ddd 9.8, 6.0, 2.2	
6A’	3.66 dd 2.2; 11.8	3.64 dd 11.8, 2.2	3.64 dd 11.8, 2.2	
6B’	3.44 dd 5.8; 11.8	3.42 dd 11.8, 6.0	3.41 dd 11.8, 6.0	
3-*O*-malonyl				
1’’				
2’’			3.50 s	
3’’				

Table 29. ^{13}C chemical shift values (ppm) and coupling constants (Hz) of Pteroside D (**39**), Pteroside X (**40**), 3-malonyl-pteroside D (**41**) and Pterosin D (**42**) dissolved in DMSO-D6 at 298K.

	Compound **39**	Compund **40**	Compound **41**	Compound **42**
	δ ^{13}C	δ ^{13}C	δ ^{13}C	δ ^{13}C
1	209.26	209.23	207.21	209.12
2	51.06	51.01	49.77	50.88
3	75.45	75.35	77.61	75.25
4	125.18	121.75	125.42	124.92
5	144.48	148.08	145.19	144.20
6	136.60	134.93	138.15	137.19
7	136.55	136.25	137.15	136.15
8	129.62	129.88	129.91	129.39
9	153.19	153.12	147.74	152.81
10	23.04	22.85	23.46	22.95
11	20.67	20.64	20.11	20.59
12	21.03	61.38	20.96	20.95
13	29.22	28.10	29.14	32.22
14A	67.13	67.43	66.79	59.81
14B				
15	13.58	13.22	13.4	13.50
14-*O*-*β*-glc				
1’	103.08	102.95	102.91	
2’	73.73	73.56	73.56	

3’	77.07	76.87	76.90
4’	70.33	70.15	70.19
5’	77.10	76.99	77.02
6A’	61.31	61.14	61.16
6B’			
3-*O*-malonyl			
1’’			167.18
2’’			41.62
3’’			168.00

NMR table of the isolated compound from *Anthriscus cerefolium*

Table 30. ^{1}H and ^{13}C NMR chemical shift values (ppm) and coupling constants (Hz) of 1,3-dicaffeoyl-5-malonyl-δ-quinide (**43**) in DMSO-D_6 at 298K.

	Compound **43** δ ^{1}H	Compound **43** δ ^{13}C
1		78.82
2A	2.44 dd 14.0, 4.4	35.7
2B	1.96 m	
3	5.20 dt 9.0, 4.4	69.86
4	3.87 dd 8.8, 3.7	68.8
5	5.32 dd 8.1, 4.4	71.98
6	2.41 m	31.83
7		172.08
1-*O*-caffeoyl		
1’		125.59
2’	7.08 d 2.1	115.25
3’		145.80
4’		116.02
5’	6.78 d 8.2	121.67
6’	7.02 dd 8.2, 2.1	146.26
7’	7.49 d 15.7	113.89
8’	6.28 d 15.7	165.43
9’		
3’-OH	9.19 s	
4’-OH	9.67 s	
3-*O*-*Z*-caffeoyl		
1’’		125.70
2’’	7.06 d 2.1	114.98
3’’		145.80
4’’		148.69
5’’	6.77 d 8.2	115.99
6’’	6.99 dd 8.2, 2.1	121.67
7’’	7.49 d 15.7	145.66
8’’		114.13
9’’		166.17
3’’-OH	9.21 s	
4’’-OH	9.63 s	
5-*O*-malonyl		
1’’’		166.65
2A’’’	3.31 d 15.9	41.74
2B’’’	3.22 d 15.9	
3’’’		167.94
3’’’-OH	12.5 s (very broad)	

1.3. Papers I-V including supplementary data.

Paper I

Phytochemistry 164 (2019) 67–77

Contents lists available at ScienceDirect

Phytochemistry

journal homepage: www.elsevier.com/locate/phytochem

Cytotoxic saponins and other natural products from flowering tops of *Narthecium ossifragum* L

Andrea Estefanía Carpinteyro Díaz[a], Lars Herfindal[b], Bendik Auran Rathe[b], Kristine Yttersian Sletta[b], Anni Vedeler[c], Svein Haavik[b], Torgils Fossen[a,*]

[a] Department of Chemistry and Centre for Pharmacy, University of Bergen, Allégt. 41, N-5007 Bergen, Norway
[b] Department of Clinical Science and Centre for Pharmacy, University of Bergen, Norway
[c] Department of Biomedicine, University of Bergen, Norway

ARTICLE INFO

Keywords:
Narthecium ossifragum (L.) huds
Nartheciaceae
Flowers
Cytotoxicity
Toxicity
Saponins
di-C-Glycosylflavones
2D NMR

ABSTRACT

For more than four centuries, the intake of *Narthecium ossifragum* has been associated with poisoning in domesticated animals. Saponins occurring in flowering tops of the plant are considered to cause kidney damage in calves. At present, there are more than 30 papers on the saponins of *N. ossifragum* in the literature, although the structures of these compounds have hitherto not been determined. Here, we identify the saponins of *N. ossifragum* as sarsasapogenin, sarsasapogenin-3-*O*-*β*-galactopyranoside, sarsasapogenin-3-*O*-(2′-*O*-*β*-glucopyranosyl-*β*-galactopyranoside) and sarsasapogenin-3-*O*-(2′-*O*-*β*-glucopyranosyl-3′-*O*-*α*-arabinopyranosyl-*β*-galactopyranoside). Moreover, six aromatic natural products were isolated and characterized from the methanolic extract from flowers of *N. ossifragum*. Five of these aromatic compounds, chrysoeriol 6-*C*-*β*-arabinofuranoside-8-*C*-*β*-glucopyranoside, chrysoeriol 6-*C*-*β*-arabinopyranosyl-8-*C*-*β*-glucopyranoside, chrysoeriol 6-*C*-*β*-xylopyranosyl-8-*C*-*β*-galactopyranoside, chrysoeriol 6-*C*-*β*-galactopyranosyl-8-*C*-*β*-glucopyranoside and chrysoeriol 6-*C*-*β*-glucopyranosyl-8-*C*-*β*-galactopyranoside are undescribed. All compounds were tested for cytotoxicity in mammalian cell lines derived from the heart, kidney, and haematological tissues. The saponins exhibited cytotoxicity in the micromolar range, with proportionally increasing cytotoxicity with increasing number of glycosyl substituents. The most potent compound was the main saponin sarsasapogenin-3-*O*-(2′-*O*-*β*-glucopyranosyl-3′-*O*-*α*-arabinopyranosyl-*β*-galactopyranoside), which produced cell death at concentrations below 3–4 μM in all three cell lines tested. This indicates that the saponins are the toxicants mainly responsible for kidney damage observed in cattle after ingestion of *N. ossifragum*. Our findings also pave the way for analysis of individual compounds isolated during the biopsies of intoxicated animals.

1. Introduction

Narthecium ossifragum (L.) Huds. (Nartheciaceae) is a perennial flowering plant (Fig. 1), which natively grows on bogs in western and north-western Europe. Flowering of this species occurs between July and August (Mossberg et al., 1995). The bright yellow flowers are 10–16 mm wide and occur in clusters with 6–20 flowers (Feilberg, 1999). The first available information about the potential toxicity of this plant was published in 1667 by the physician and botanist Simon Paulli in what is known to be the first Norwegian scientific publication (Paulli, 1667). The plant has in several instances been associated with toxic effects in grazing animals (Stabursvik, 1953; Flåøyen et al., 1995a; Wisløff et al., 2003) and is considered to cause the phototoxic disease alveld in lambs (Stabursvik, 1953). This livestock poisoning is both economically important and an animal welfare problem especially in the Nordic countries (Bernhoft, 2010). It has been suggested that alveld may be caused by metabolite(s) produced by *N. ossifragum* (Abdelkader et al., 1984), an associated fungus (di Menna et al., 1992) or cyanobacteria (Tønnesen et al., 2013). However, an explanation for the observed toxic effects associated with intake of *N. ossifragum* at the molecular level has not been provided in the current literature.

In numerous publications, the flowering tops of *N. ossifragum* have been reported to contain significant amounts of saponins, which are considered to be toxic components of the plant (Uhlig et al., 2007). Saponins occurring in the flowering tops of the plant are presumed to cause kidney damage in calves (Flåøyen et al., 1997). These compounds have been suggested as playing a role in the development of hypothesized secondary phototoxicity although this view has been challenged

* Corresponding author. .
E-mail address: Torgils.Fossen@uib.no (T. Fossen).

https://doi.org/10.1016/j.phytochem.2019.04.014
Received 18 January 2019; Received in revised form 17 April 2019; Accepted 24 April 2019

Fig. 1. Flowers of *N. ossifragum*. Photo: Andrea Estefanía Carpinteyro Díaz.

(Flåøyen et al., 1991). Even though more than thirty publications in the current literature deal with saponins of *N. ossifragum*, none of these compounds has hitherto been characterized in detail from this plant source and their molecular structures remain unknown. Stabursvik (1959) identified the aglycone of the saponins of *N. ossifragum* to be sarsasapogenin (Stabursvik, 1959). Ceh and Hauge (1981) tentatively identified two saponins from *N. ossifragum* based on sarsasapogenin (spirostan-3-ol) aglycone. Both of these saponins were indicated to be glycosylated with trisaccharides consisting of galactose-glucose-arabinose (major compound) and galactose-glucose-xylose (minor compound), respectively, where the trisaccharide moiety was attached at C-3 of the aglycone. The names narthecin and xylosin were suggested for these saponins. However, the linkages between the individual sugar units were not determined (Ceh and Hauge, 1981) and the structures were not confirmed by NMR spectroscopy and HR-MS. Using LC-MS Uhlig et al. (2007) tentatively identified saponins based on smilagenin and sarsasapogenin with two and three sugar units. However, neither the sugar composition nor the individual glycosyl substituents could be identified (Uhlig et al., 2007). Even though the connection between the intake of *N. ossifragum* and the occurrence of alveld in lambs seems to be well documented (Abdelkader et al., 1984; Ceh and Hauge, 1981) the original assumption about a potential connection between saponins of this plant species and the phototoxic disease is controversial and has been challenged (Flåøyen et al., 1991). Abdelkader et al. (1984) reported that lambs fed with a crude mixture of saponins developed alveld. However, the same authors reported that the most purified fraction of saponins did not induce alveld in lambs. Moreover, Flåøyen et al. (1991) reported that lambs fed with large quantities of freeze-dried *N. ossifragum*, containing significant amounts of saponins, did not develop alveld. Surprisingly, the possibility that alveld may be caused by aromatic compounds unique to *N. ossifragum* with the ability to fluoresce has not been considered in current literature. Further progress in research into the potential structure-activity role of the saponins of *N. ossifragum* in connection with their potential role as nephrotoxins poisoning cattle is severely hampered by the fact that their structures have not yet been determined and the lack of methodology for large-scale isolation of these compounds.

In this paper we report on structure determination and cytotoxicity of individual saponins of *N. ossifragum*. A methodology for large-scale separation and isolation of these compounds in the pure state is provided for the first time. Although the content of aromatic compounds of the fruits of *N. ossifragum* has been thoroughly characterized (Vu et al., 2016) no aromatic compound has hitherto been identified from the plant at the flowering stage, i.e. at the development stage where intake of *N. ossifragum* has been associated with lifestock toxicity. As part of our on-going research concerning the characterization of aromatic compounds from *N. ossifragum*, several di-*C*-glycosylflavones, including several previously undescribed compounds, were isolated for the first time from this plant source.

2. Results and discussion

The methanolic extracts of 1.7 kg of flowering tops of *N. ossifragum* were concentrated under reduced pressure and subjected to liquid/liquid separation with petroleum ether followed by ethyl acetate.

A total of 7.1546 g white precipitate was collected from the concentrated petroleum ether and ethyl acetate phases, corresponding to approximately 2.3% of the total dry weight of the plant material. The white precipitate was identified as a mixture of saponins by the recorded 1D and 2D NMR spectra, where glycosyl substituents attached to an aliphatic aglycone were observed. One gram of this mixture was further purified by Sephadex LH-20 column chromatography. Individual pure saponins were then isolated by silica column chromatography. The individual pure saponins were identified as sarsasapogenin (**1**), sarsasapogenin-3-*O*-*β*-galactopyranoside (**2**), sarsasapogenin-3-*O*-(2′-*O*-*β*-glucopyranosyl-*β*-galactopyranoside) (**3**) and sarsasapogenin-3-*O*-(2′-*O*-*β*-glucopyranosyl-3′-*O*-*α*-arabinopyranosyl-*β*-galactopyranoside) (**4**) by 1D and 2D NMR spectroscopy (Tables 2 and 3, Fig. 2 and Supplementary Figs. S1–S34) and high resolution mass spectrometry (Supplementary Figs. S70–72). The 1D ^{1}H NMR spectrum of compound **4** showed the presence of sarsasapogenin aglycone in addition to three glycosyl substituents (Figure S26) The glycosyl units were identified to be galactopyranosyl, glucopyranosyl and arabinopyranosyl by the 17 ^{13}C signals observed in the 1D^{13}C CAPT NMR spectrum of **4**. The ^{13}C signals belonging to these sugar units were in agreement with reference values of galactopyranosyl, glucopyranosyl and arabinopyranosyl, respectively (Inoue et al., 1995; Fossen and Andersen, 2006). The combined information in the 2D ^{1}H–^{1}H COSY spectrum and the 2D ^{1}H–^{13}C edited HSQC spectrum, the 2D ^{1}H–^{13}C HSQC-TOCSY spectrum and the 2D ^{1}H–^{13}C H2BC spectrum were of paramount importance with respect to complete assignments of all ^{1}H and ^{13}C resonances belonging to the glycosyl substituents (Figs. S28–S34 and Tables 1 and 2). The identities of the glycosyl substituents were further confirmed by the observed coupling constants in the 1D ^{1}H NMR spectrum and the 1D ^{1}H selective TOCSY spectra of **4** (Table 1). The configurations of C-1′, C-1″ and C-1‴ belonging to the galactopyranosyl, the glucopyranosyl and the arabinopyranosyl units, respectively, were determined to be in *β*-configuration for the former two units and in *α*-configuration for the latter, by the observed large $^{3}J_{HH}$ vicinal coupling constants of 7.7 Hz, 7.9 Hz and 7.2 Hz (Table 1). The configurations of the anomeric carbons were

Table 1
^{1}H NMR chemical shift values (ppm) and coupling constants (Hz) for saponins **1–4** isolated from flowering tops of *N. ossifragum* in DMSO-D_6 at 298K. s = singlet; d = doublet; dd = double doublet; dt = double triplet; p = pentet; m = multiplet.

	1	2	3	4
1A	1.37	1.40	1.41	1.48
1B	1.33	1.35	1.34	1.30
2A	1.38	1.51	1.55	1.48
2B	1.31	1.40	1.38	1.41
3	3.86 *m*	3.88 *m*	3.89 *m*	3.88 *m*
4A	1.81	1.71	1.71	1.67
4B	1.16	1.41	1.42	1.39
5	1.67	1.71	1.71	1.84
6A	1.81	1.79	1.78	1.76
6B	1.06	1.08	1.09	1.06
7A	1.35	1.36	1.35	1.34
7B	1.02	1.03	1.02	1.02
8	1.51	1.51	1.51	1.51
9	1.32	1.34	1.33	1.33
10				
11A	1.32	1.33	1.33	1.33
11B	1.17	1.18	1.17	1.14
12A	1.65	1.66	1.65	1.65
12B	1.12	1.13	1.12	1.12
14	1.13	1.14	1.14	1.14
15A	1.88	1.89	1.89	1.88
15B	1.13	1.13	1.13	1.13
16	4.26 *m*	4.27 *m*	4.27 *m*	4.27 *m*
17	1.65	1.65	1.65	1.65
18	0.69 *s*	0.70 *s*	0.70 *s*	0.70 *s*
19	0.89 *s*	0.90 *s*	0.89 *s*	0.89 *s*
20	1.75 *p* 6.8	1.75 *p* 6.8	1.75 *p* 6.5	1.75 *p* 6.9
21	0.92 *d* 7.0	0.92 *d* 7.0	0.92 *d* 7.0	0.92 *d* 7.0
22				
23A	1.88	1.88	1.88	1.88
23B	1.33	1.33	1.34	1.34
24A	1.79	1.79	1.79	1.79
24B	1.26	1.26	1.26	1.26
25	1.63	1.63	1.63	1.63
26A	3.77 dd 2.9, 11.0	3.77 dd 2.8, 11.0	3.78 dd 2.8, 11.1	3.78 dd 2.8, 11.0
26B	3.20 dt 11.0, 1.8	3.20 dt 11.0, 1.8	3.20 dt 1.7,11.1	3.20 dt 1.9, 11.4
27	1.00 *d* 7.1	1.00 *d* 7.1	1.00 *d* 7.1	1.00 *d* 7.1
3-OH	4.15 *d* 3.1			
3-*O*-*β*-Galactopyranoside				
1'		4.08 *d* 7.5Hz	4.24 *d* 5.9Hz	4.27 *d* 7.7
2'		3.24	3.57	3.75 dd 9.8, 7.7
3'		3.24	3.48	3.56 dd 3.1, 9.8Hz
4'		3.61	3.65	3.81 dd 3.1, 1.0
5'		3.27 dt 6.2, 1.0	3.30	3.34
6A'		3.50 dd 6.2, 11.0	3.50	3.48 dd 12.0, 6.1
6B'		3.40 dd 6.2, 11.0	3.40 *p* 5.6Hz	3.38 dd 12.0, 1.6
2′-*O*-*β*-Glucopyranosyl				
1''			4.39 *d* 7.9Hz	4.64 *d* 7.9
2''			2.97	2.86 dd 7.9, 9.0
3''			3.15	3.11 t 9.0
4''			3.11 *d* 4.6Hz	2.96 dd 9.6, 9.0
5''			3.03	3.07 ddd 9.6, 6.3, 2.7
6A''			3.62 *m*	3.68 dd 12.2, 2.7
6B''			3.49	3.43
3′-*O*-*α*-arabinopyranosyl				
1'''				4.41 *d* 7.2
2'''				3.42
3'''				3.28
4'''				3.62
5A'''				3.68
5B'''				3.38

Table 2
^{13}C NMR chemical shift values (ppm) for saponins **1–4** isolated from flowering tops of *N. ossifragum* in DMSO-D_6 at 298K.

	1	2	3	4
1	29.8	30.16	30.14	29.88
2	27.5	26.08	25.96	26.19
3	64.6	72.79	73.90	72.99
4	33.4	29.59	29.97	29.43
5	36.0	35.97	36.00	34.42
6	26.4	26.40	26.34	26.40
7	26.2	26.22	26.22	26.25
8	35.0	34.95	34.95	34.98
9	39.4	39.50	39.50	39.50
10	34.8	34.65	34.58	34.61
11	20.5	20.51	20.50	20.51
12	39.7	39.70	39.7	39.7
13	40.2	40.0	40.27	40.29
14	55.8	55.73	55.77	55.79
15	31.5	31.47	31.47	31.49
16	80.5	80.45	80.46	80.48
17	61.9	61.91	61.91	61.92
18	16.2	16.24	16.25	16.29
19	23.8	23.63	23.63	23.51
20	41.6	41.62	41.62	41.64
21	14.5	14.53	14.53	14.55
22	108.9	108.91	108.91	108.93
23	25.5	25.50	25.50	25.50
24	25.6	25.59	25.59	26.61
25	26.5	26.50	26.51	26.52
26	64.3	64.31	64.32	64.32
27	16.0	15.99	15.99	16.01
3-*O*-*β*-Galactopyranoside				
1'		101.83	100.81	99.83
2'		70.76	79.21	75.49
3'		73.65	73.27	82.10
4'		68.19	67.72	68.02
5'		75.05	74.78	74.62
6'		60.42	60.30	60.09
2′-*O*-*β*-Glucopyranosyl				
1''			103.90	102.20
2''			75.21	74.68
3''			76.22	76.79
4''			70.08	71.10
5''			77.02	76.65
6''			61.12	61.89
3′-*O*-*α*-arabinopyranosyl				
1'''				104.70
2'''				70.97
3'''				72.88
4'''				67.94
5'''				65.85

Table 3
UV data for compounds **5–10** isolated from flowering tops of *N. ossifragum*.

Compound	λ_{max} I	λ_{max} II
5	346	271
6	347	270
7	347	269
8	347	270
9	346	270
10	346	270

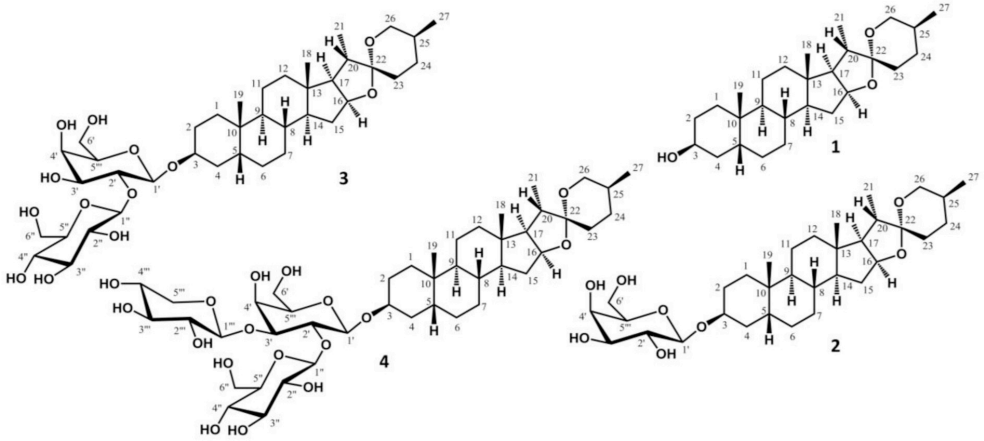

Fig. 2. Structures of sarsasapogenin (**1**), sarsasapogenin-3-O-*β*-galactopyranoside (**2**), sarsasapogenin-3-*O*-(2′-*O*-*β*-glucopyranosyl-*β*-galactopyranoside) (**3**) and sarsasapogenin-3-*O*-(2′-*O*-*β*-glucopyranosyl-3′-*O*-*α*-arabinopyranosyl-*β*-galactopyranoside) (**4**) isolated from flowering tops of *N. ossifragum*.

further confirmed by the $^{1}H–^{13}C$ coupling constants of H-1'/C-1' (163 Hz), H-1''/C-1'' (162 Hz) and H-1‴/C-1‴ (164 Hz), which are in agreement with literature values for *β*-galactopyranosyl, *β*-glucopyranosyl and *α*-arabinopyranosyl, respectively (Pedersen et al., 1995). The crosspeaks at δ 4.27/73.0 (H-1'/C-3), δ 3.88/99.8 (H-3/C-1′) observed in the HMBC spectrum and the crosspeaks at δ 4.27/3.88 (H-1'/H-3), δ 4.27/1.67 (H-1'/H-4A), δ 4.27/1.48 (H-1'/H-2A) and δ 4.27/1.39 (H-1'/H–4B) observed in the ROESY spectrum confirmed the linkage between the galactopyranosyl unit and the aglycone to be at the 3-position. The crosspeaks at δ 4.64/75.5 (H-1''/C-2′), δ 3.75/102.2 (H-2'/C-1″) observed in the HMBC spectrum and the crosspeak at δ 4.64/3.75 (H-1''/H-2′) observed in the ROESY spectrum confirmed the linkage between the glucopyranosyl and the galactopyranosyl units to be at the 2′-position. The crosspeaks at δ 4.41/82.1 (H-1‴/C-3′), δ 3.56/104.7 (H-3'/C-1‴) observed in the HMBC spectrum and the crosspeak at δ 4.41/3.56 (H-1‴/H-3′) observed in the ROESY spectrum confirmed the linkage between the arabinopyranosyl and the galactopyranosyl units to be at the 3′-position. Thus, **4**, which is the main saponin of *N. ossifragum*, was identified as sarsasapogenin-3-*O*-(2′-*O*-*β*-glucopyranosyl-3′-*O*-*α*-arabinopyranosyl-*β*-galactopyranoside). A sodiated molecular ion [MNa^{+}] at *m/z* 895.46624 (calculated: 895.46681; Mass difference: −0.53 ppm) observed in the high-resolution mass spectrum of **4** (Fig. S72) corresponding to $C_{27}H_{30}O_{15}Na$ confirmed this identity. Following a similar strategy, compounds **1**, **2** and **3** were identified as sarsasapogenin (**1**), sarsasapogenin-3-*O*-*β*-galactopyranoside (**2**) and sarsasapogenin-3-*O*-(2′-*O*-*β*-glucopyranosyl-*β*-galactopyranoside) (**3**), respectively.

The stereochemistry of the sapogenin aglycones of compounds **1–4** were determined to be (3β,5β,25R/S)-spirostan-3-ol by 2D ^{1}H ROESY NMR (Fig. 3); with the same stereochemistry as the aglycone sarsasapogenin reported in the literature (Inoue et al., 1995). Inoue et al. (1995) reported that compound **4**, which is also present in *N. asiaticum* occurred as a racemic mixture of compounds with R/S configurations of C25, respectively. The specific rotation of compound **4** isolated from *N. ossifragum* was −2.86°, indicating that compound **4** occur as a similar racemic mixture (Inoue et al., 1995). According to Li et al. (2013) L-glucose does not occur naturally in higher living organisms. The same applies to L-galactose (Li et al., 2013), whereas the prevalent L-arabinose is the structural equivalent to D-glucose (Gaffield et al., 1977).

Stabursvik (1959) indicated the presence of sarsasapogenin, as well as unidentified glycosylated derivatives thereof, in flowering tops of *N. ossifragum* (Stabursvik, 1959). Ceh and Hauge (1981) previously tentatively identified two saponins from *N. ossifragum* based on sarsasapogenin (spirostan-3-ol) aglycone. Without determining the linkages between the individual glycosyl units, these saponins were indicated to be glycosylated with trisaccharides consisting of galactose-glucose-arabinose (major compound) and galactose-glucose-xylose (minor compound), respectively, where the trisaccharide moiety was attached at C-3 of the aglycone (Ceh and Hauge, 1981). We identified sarsasapogenin-3-*O*-(2′-*O*-*β*-glucopyranosyl-3′-*O*-*α*-arabinopyranosyl-*β*-galactopyranoside) as the main saponin of *N. ossifragum*. This compound, in addition to sarsasapogenin-3-*O*-(2′-*O*-*β*-glucopyranosyl-*β*-galactopyranoside), has previously been identified in the related Asian species *N. asiaticum* (Inoue et al., 1995). Sarsasapogenin-3-*O*-*β*-galactopyranoside is identified for the first time in the genus Narthecium. The compound has previously been identified in *Anemarrhena asphodeloides* (Bge) (Sy et al., 2016).

Brine shrimp lethality assay is a simple *in vivo* test for the cytotoxicity of biochemicals (Wu, 2014) where the test organisms are *Artemia salina* nauplii (Harwig and Scott, 1971; Meyer et al., 1982). Initial toxicity tests indeed revealed that a mixture of the above described saponins of *N. ossifragum* proved to be potent toxins for *Artemia salina* nauplii with LC_{50} value of 8.7 μg/mL, which encouraged more extensive and through-depth studies of their cytotoxic potential, as described below.

The components of the aqueous phase were further separated by gradient XAD-7 adsorption chromatography, Sephadex LH-20 gel filtration chromatography and preparative HPLC. The UV spectra of compounds **5–10** recorded on-line during HPLC analysis (Table 3) showed UV maximum absorptions at 346–347 nm and 269–271 nm indicating that these compounds have a flavone core structure. These six compounds were identified by a combination of 1D and 2D NMR spectroscopic techniques and high resolution mass spectrometry, as described below. Compound **10** was identified as the known compound chrysoeriol 6,8-di-*C*-*β*-glucopyranoside (**10**) by a combination of 1D and 2D NMR spectroscopy and high-resolution mass spectrometry. A di-C-glycoside of chrysoeriol was first indicated to occur in the moss *Mnium affine* Bland (Melchert and Alston, 1965). Chrysoeriol 6,8-di-*C*-*β*-glucopyranoside was originally identified in *Larrea tridentata* (Sakakibara et al., 1977). The compound has also been identified in several quite diverse sources such as *Spergularia rubra* (Bouillant et al., 1979), the liverwort *Trichocolea tomentella* (Mues, 1982) and *Tricophorum cespitosum* (Salmenkallio et al., 1982).

The downfield region of the 1D ^{1}H NMR spectrum of compound **5**

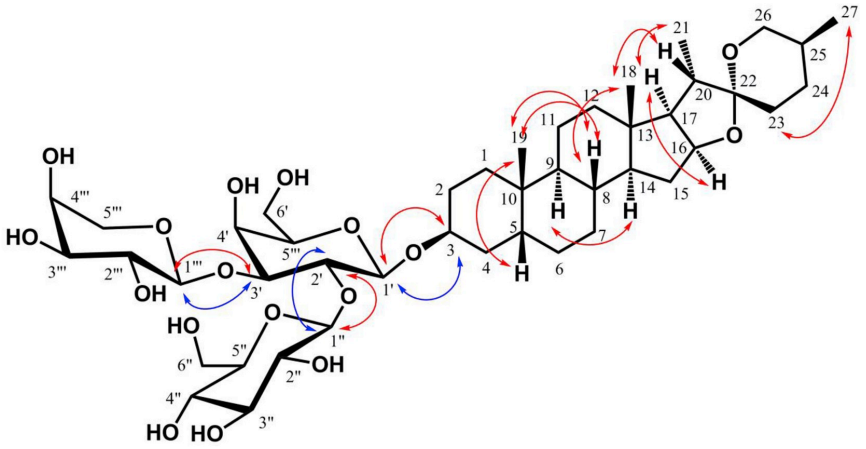

Fig. 3. HMBC correlations (blue curved arrows) and ROE correlations (red curved arrows) important for complete structure determination of sarsasapogenin-3-*O*-(2′-*O*-*β*-glucopyranosyl-3′-*O*-*α*-arabinopyranosyl-*β*-galactopyranoside) (**4**) isolated from flowering tops of *N. ossifragum*. (For interpretation of the references to colour in this figure legend, the reader is referred to the Web version of this article.)

showed a 3H ABX system at δ 7.55 (d 2.2 Hz; H-2′), δ 7.73 (dd 8.3, 2.2 Hz; H-6′) and δ 6.88 (d 8.3 Hz; H-5′), in addition to a 1H singlet at δ 6.94 (H-3), which is in accord with chrysoeriol aglycone with substituents at C-6 and C-8. A 3H signal corresponding to a methoxy group attached to the 3′-position of the aglycone of **5** was observed at δ 3.88 ppm. The methoxy group was confirmed to be attached to C-3′ of the aglycone by the crosspeak at δ 3.88/148.0 (3′-OCH_3/C-3′) observed in the HMBC spectrum of **5** and the crosspeak at δ 3.88/7.55 (3′-OCH_3/H-2′) observed in the ROESY spectrum of **5**. The glycosyl substituent attached to the 6-position of the aglycone was identified as arabinofuranose by the observed ^{1}H–^{1}H coupling constants in the 1D 1H NMR spectrum, in addition to the characteristic downfield shifts of C-2″, C-3″ and C-4″ of this glycosyl unit (Fossen and Andersen, 2006). The linkage between the arabinofuranosyl and chrysoeriol aglycone was confirmed to be at the 6-position by the observed crosspeaks at δ 5.44/162.7 (H-1″/C-7), δ 5.44/157.1 (H-1″/C-5) and δ 5.44/103.3 (H-1″/C-6) in the 2D ^{1}H–^{13}C HMBC spectrum of **5** (Fig. S38) and the crosspeak at δ 5.44/13.81 (H-1″/5-OH) observed in the 2D 1H ROESY spectrum of **5** (Fig. S41).

The glycosyl unit attached to the 8-position of the aglycone of **5** was identified as glucose by observation of seven proton resonances, where large axial-axial coupling constants between the ring protons of the glycosyl were found, and the characteristic values (Fossen and Andersen, 2006) of the six ^{13}C resonances belonging to this unit (Table 5). The anomeric coupling constant (9.9 Hz) observed in the 1D ^{1}H NMR spectrum of **5** confirmed the *β*-configuration of H-1‴. The linkage between the glucopyranosyl and chrysoeriol aglycone was confirmed to be at the 8-position by the observed crosspeaks at δ 4.70/162.7 (H-1‴/C-7), δ 4.70/154.9 (H-1‴/C-9) and δ 4.70/104.5 (H-1‴/C-8) in the 2D ^{1}H–^{13}C HMBC spectrum of **5** (Fig. S38). Thus, **5** was identified as the previously undescribed compound chrysoeriol 6-*C*-*β*-arabinofuranosyl-8-*C*-*β*-glucopyranoside (Fig. 4). A sodiated molecular ion $[M+Na]^+$ at *m/z* 617.14848 (calculated: 617.14832; Mass difference: 0.39 ppm) observed in the high resolution mass spectrum of **5** (Fig. S73) corresponding to $C_{27}H_{30}O_{15}Na$ confirmed this identity.

The 1D and 2D NMR spectra of **6** shared many similarities to that of **5**, showing chrysoeriol aglycone glycosylated with an arabinosyl unit at the 6-position and a glucopyranosyl substituent at the 8-position, respectively. The arabinosyl substituent of compound **6** was, however, determined to be in the pyranose form by the characteristic carbon signals at δ 73.9 (C-1″), δ 68.1 (C-2″), δ 73.6 (C-3″), δ 69.3 (C-4″) and δ 69.9 (C-5″) which are accord with an arabinopyranosyl unit (Fossen and Andersen, 2006). Thus, **6** was identified as the previously undescribed di-*C*-glycosylflavone chrysoeriol 6-*C*-*β*-arabinopyranosyl-8-*C*-*β*-glucopyranoside (Fig. 4). The sodiated molecular ion $[M+Na]^+$ at *m/z* 617.14867 (calculated: 617.14832; Mass difference: 0.71 ppm) observed in the high-resolution mass spectrum of **6** (Fig. S74) corresponding to $C_{27}H_{30}O_{15}Na$ confirmed this identity.

Two chrysoeriol di-C-glycosides found in quince seeds (*Cydonia oblonga* Miller) have previously been tentatively identified as chrysoeriol 6-*C*-pentosyl-8-*C*-glucoside and Chrysoeriol 6-*C*-pentosyl-8-*C*-glucoside by mass spectrometry (Ferreres et al., 2003; Silva et al., 2005), without identification of the pentose sugar unit. Interestingly, extracts of *Cydonia oblonga* seeds exhibited anticancer effect against human kidney and colon cancer cells (Carvalho et al., 2010). Salmenkallio et al. (1982) reported chrysoeriol 6-*C*-arabinosyl-8-*C*-glucoside from stems of *Trichophorum cespitosum*, without determining if the arabinosyl was present in the furanose or pyranose form. Chrysoeriol 6-*C*-arabinosyl-8-*C*-glucoside has also been indicated to occur in several *Arrhenaterum* spp. (Jay and Ismaili, 1989). No NMR data exist for these compounds in current literature, which would have allowed for the exact identification of the ring forms of their glycosyl substituents.

The 1D and 2D NMR spectra of **7** shared many similarities to that of **5**, showing chrysoeriol aglycone glycosylated with a pentose at the 6-position and a hexose at the 8-position, respectively. The 6-glycosyl substituent of **7** was identified as *β*-xylopyranose by comparing the five ^{1}H resonances in the region 4.55–3.05 in the 1D ^{1}H NMR spectrum of **7** and the corresponding five ^{13}C resonances belonging to this unit (Tables 4 and 5 and Supplementary Figs. S48–S51). The 8-glycosyl substituent of **6** was identified as *β*-galactopyranose by the signals corresponding to seven hydrogens in the region 5.00–3.47 in the 1D ^{1}H NMR spectrum of **7** and the corresponding six ^{13}C resonances belonging to this unit (Tables 4 and 5 and Supplementary Figs. S48–S51). The observed characteristic small axial-equatorial coupling constant for the coupling between H-3‴ and H-4‴ (2.8 Hz) verified the identification of the galactopyranose unit of **7**. Thus, **7** was identified as the previously undescribed compound chrysoeriol 6-*C*-*β*-xylopyranosyl-8-*C*-*β*-galactopyranoside) (Fig. 4). A sodiated molecular ion $[M+Na]^+$ at *m/z* of 617.14855 (calculated: 617.14832; Mass difference: 0.51 ppm) was observed in the high resolution mass spectrum of **7** corresponding to $C_{27}H_{30}O_{15}Na$. A further sodiated molecular ion $[M+2Na–H]^+$ at *m/z*

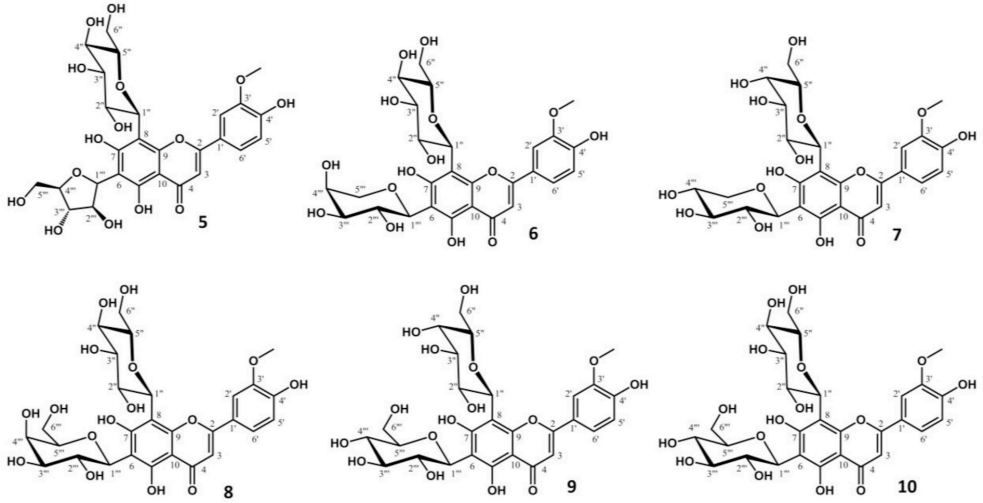

Fig. 4. Structures of the aromatic compounds chrysoeriol 6-*C*-*β*-arabinofuranosyl-8-*C*-*β*-glucopyranoside (**5**), chrysoeriol 6-*C*-*β*-arabinopyranosyl-8-*C*-*β*-glucopyranoside (**6**), chrysoeriol 6-*C*-*β*-xylopyranosyl-8-*C*-*β*-galactopyranoside (**7**), chrysoeriol 6-*C*-*β*-galactopyranosyl-8-*C*-*β*-glucopyranoside (**8**), chrysoeriol 6-*C*-*β*-glucopyranosyl-8-*C*-*β*-galactopyranoside (**9**) and chrysoeriol 6,8-di-*C*-*β*-*D*-glucopyranoside (**10**) isolated for the first time from flowering tops of *N. ossifragum*.

Table 4
^{1}H NMR chemical shift values (ppm) and coupling constants (Hz) of chrysoeriol 6-*C*-*β*-arabinofuranosyl-8-*C*-*β*-glucopyranoside (**5**), chrysoeriol 6-*C*-*β*-arabinopyranosyl-8-*C*-*β*-glucopyranoside (**6**), chrysoeriol 6-*C*-*β*-xylopyranosyl-8-*C*-*β*-galactopyranoside (**7**), chrysoeriol 6-*C*-*β*-galactopyranosyl-8-*C*-*β*-glucopyranoside (**8**), chrysoeriol 6-*C*-*β*-glucopyranosyl-8-*C*-*β*-galactopyranoside (**9**) and chrysoeriol 6,8-di-*C*-*β*-*D*-glucopyranoside (**10**) in DMSO-D_6 at 298K. Top: Signals of major rotamer. Bottom: Signals of minor rotamer. s = singlet; d = doublet; dd = double doublet; ddd = double double doublet; t = triplet; br = broad; m = multiplet.

	5	6	7	8	9	10
3	6.94 *s*	6.94 *s*	6.86 *s*	6.94 *s* (6.91 *s*)	6.86 *s* (7.00 *s*)	6.95 (6.87)
2'	7.55 *d* 2.2	7.54 *d* 2.2	7.65 *d* 2.1	7.54 *d* 2.3 (7.59 *d* 2.2)	7.65 *d* 2.2 (7.56)	7.55 (7.64)
5'	6.88 *d* 8.3	6.89 *d* 8.4	6.92 *d* 8.4	6.89 *d* 8.4 (6.95)	6.92 *d* 8.4 (6.88)	6.88 (6.95)
6'	7.73 dd 8.3, 2.2	7.70 dd 8.4, 2.2	7.58 dd 8.4, 2.1	7.70 dd 8.4, 2.3 (7.56 dd 8.4, 2.2)	7.58 dd 8.4, 2.2 (8.27)	7.71 (7.57)
5-OH	13.81 *s*	13.71	13.74	13.71 *s*	13.75 *s* (13.86 *s*)	13.75 (13.73)
7-OH	10.52 *s*	9.18	9.23	9.18 *s*	9.24 *s* (br) (9.03 *s* (br))	9.36 (9.36)
4'-OH	10.00 *s*	9.99 *s*	9.96	10.00 *s*	9.96 *s* (9.83 *s*)	
3'-OCH_3	3.88 *s*	3.88 *s*	3.90 *s*	3.88 *s* (3.90 *s*)	3.90 *s* (3.88 *s*)	3.88 *s* (3.90 *s*)
	6-*C*-*β*-Arabinofuranosyl	**6-*C*-*β*-Arabinopyranosyl**	**6-*C*-*β*-Xylopyranosyl**	**6-*C*-*β*-Galactopyranosyl**	**6-*C*-*β*-Glucopyranosyl**	**6-*C*-*β*-Glucopyranosyl**
1''	5.44 *d* 3.2	4.71 *d* 9.2	4.55 *d* 9.8	4.77*d* 9.7 (4.70 d 9.7)	4.62 *d* 10.0 (4.80)	4.80 *d* 9.9 (4.66 *d*)
2''	4.09 dd 3.2, 0.8	3.80 *m*	4.09 *m*	3.80 dd 9.7, 9.5	4.12 (3.48 (br))	3.48 *m* (3.98)
3''	3.93 dd 3.0, 0.8	3.46 *m*	3.13 *t* 8.7	3.45 *m*	3.19 *t* 8.6 (3.30)	3.30 *t* 8.8 (3.22)
4''	3.89 *m*	3.81 *m*	3.38 *m*	3.79	3.08 *t* 9.0	3.37 *t* 9.4
5A''	3.67 dd 11.3, 6.6,	3.83 dd 11.9, 2.7	3.74 *m*	3.56	3.15 *m* (3.32)	3.32 *m*
5B''	3.64 dd 4.8, 11.3	3.64 *d* 11.9	3.05 *t* 10.8			
6A''				3.53 *m*	3.70 dd 12.0, 2.0 (3.63)	3.63 *m*
6B''					3.37 *m*	
	8-*C*-*β*-Glucopyranoside	**8-*C*-*β*-Glucopyranoside**	**8-*C*-*β*-Galactopyranoside**	**8-*C*-*β*-Glucopyranoside**	**8-*C*-*β*-Galactopyranoside**	**8-*C*-*β*-Glucopyranoside**
1'''	4.70 *d* 9.9	4.74 *d* 9.8	5.00 *d* 9.6	4.74 *d* 10.00 (4.91 d 10.0)	5.00 *d* 9.6 (4.69 *d* 9.9)	4.75 *d* 9.9 (5.04 *d*)
2'''	3.88 *m*	3.93 dd 9.8, 8.7	3.80 *t* 9.3	3.94 dd 10.0, 9.0 (3.89)	3.83 *m* (4.24 *t* 9.4)	3.92 dd 9.8, 8.7, (3.56)
3'''	3.24 *t* 8.8	3.27 *t* 8.7	3.47 dd 9.3, 2.8	3.27 *t* 8.8	3.47 dd 9.1, 3.9 (3.41 dd 8.9, 3.2)	3.26 *t* 8.7 (3.31)
4'''	3.35 dd 9.6, 8.8	3.36 dd 9.6, 8.7	3.83 *d* 2.8	3.34 dd 9.6, 8.8	3.83 *br d* 2.9 (3.85)	3.34 *t* 9.1 (3.34)
5'''	3.23 ddd 9.6, 6.1, 2.1	3.23 ddd 9.6, 6.0, 2.0	3.71 *t* 6.2	3.23 ddd 9.6, 6.3, 2.0	3.71 *m*	3.22 ddd 9.5, 6.2, 1.9 (3.18)
6A'''	3.76 dd 12.1, 2.1	3.73 dd 12.1, 2.0	3.55 *d* 6.2	3.75 dd 12.4, 2.0 (3.71)	3.56 *m* (3.56)	3.74 dd 12.0, 1.9 (3.69)
6B'''	3.48 dd 12.1, 6.1	3.47 dd 12.1, 6.0		3.46 dd 12.1, 6.3 (3.46)		3.47 dd 12.0, 6.2 (3.46)

*proton signals overlapping in the 1D ^{1}H NMR spectra are reported without designated multiplicity.

Table 5
^{13}C NMR chemical shift values (ppm) and coupling constants (Hz) of chrysoeriol 6-*C*-*β*-arabinofuranosyl-8-*C*-*β*-glucopyranoside (**5**), chrysoeriol 6-*C*-*β*-arabinopyranosyl-8-*C*-*β*-glucopyranoside (**6**), chrysoeriol 6-*C*-*β*-xylopyranosyl-8-*C*-*β*-galactopyranoside (**7**), chrysoeriol 6-*C*-*β*-galactopyranosyl-8-*C*-*β*-glucopyranoside (**8**), chrysoeriol 6-*C*-*β*-glucopyranosyl-8-*C*-*β*-galactopyranoside (**9**) and chrysoeriol 6,8-di-*C*-*β*-*D*-glucopyranoside (**10**) in DMSO-D_6 at 298K. Top: Signals of major rotamer. Bottom: Signals of minor rotamer. nd = not detected.

	5	6	7	8	9	10
Chrysoeriol						
2	164.0	163.9	163.2	164.1 (163.5)	163.2 (164.1)	164.1 (163.5)
3	102.8	103.0	102.6	103.0 (102.8)	102.6 (103.4)	103.1 (102.8)
4	182.2	182.1	181.9	182.2 (182.2)	182.2 (182.2)	182.5 (182.4)
5	157.1	158.0	159.8	158.1	nd (158.5)	158.6 (159.9)
6	103.3	107.9	109.1	108.2	109.2 (107.1)	107.6 (109.0)
7	162.7	160.7	161.4	160.8	161.5 (160.7)	160.9 (161.5)
8	104.5	104.7	103.8	105.0	103.4 (105.2)	105.3
9	154.9	155.1	153.1	155.1	153.2 (155.2)	155.1
10	103.1	103.5	102.9	103.6 (102.9)	103.0 (103.8)	103.7 (103.3)
1'	121.9	121.6	121.5	121.7 (121.6)	121.4 (120.9)	121.8 (121.7)
2'	110.6	110.5	110.0	110.7 (109.9)	110.1 (109.9)	110.7 (110.2)
3'	148.0	147.8	147.8	148.0 (147.9)	147.7 (147.7)	148.1 (147.8)
4'	150.8	150.6	150.3	150.8 (150.5)	150.3 (150.6)	150.9 (150.4)
5'	115.5	115.1	115.4	115.4 (115.8)	115.6 (115.7)	115.5 (115.7)
6'	121.2	121.0	120.5	121.1 (120.3)	120.3 (123.0)	121.3 (120.5)
3'-OCH_3	56.2	56	55.5	56.1 (55.6)	55.6 (55.9)	56.2 (55.7)
	6-*C*-*β*-Arabinofuranosyl	**6-*C*-*β*-Arabinopyranosyl**	**6-*C*-*β*-Xylopyranosyl**	**6-*C*-*β*-Galactopyranosyl**	**6-*C*-*β*-Glucopyranosyl**	**6-*C*-*β*-Glucopyranosyl**
1''	79.9	73.9	73.4	73.5 (73.6)	72.7 (73.9)	74.0 (73.1)
2''	77.3	68.1	77.2	69.6 (68.5)	69.7 (71.8)	71.9
3''	77.4	73.6	79.1	74.4 (74.7)	79.1 (77.7)	77.8 (78.9)
4''	87.0	69.3	69.7	68.3	70.7	69.0
5''	61.1	69.9	70.0	79.0	81.7	80.9
					80.7)	
6''				60.7	61.5 (59.7)	59.7
	8-*C*-*β*-Glucopyranoside	**8-*C*-*β*-Glucopyranoside**	**8-*C*-*β*-Galactopyranoside**	**8-*C*-*β*-Glucopyranoside**	**8-*C*-*β*-Galactopyranoside**	**8-*C*-*β*-Glucopyranoside**
1'''	73.0	72.9	74.8	73.0 (74.5)	74.9 (73.7)	73.2 (75.1)
2'''	70.7	70.6	69.8	70.7 (70.7)	68.2 (68.8)	70.8 (72.0)
3'''	78.7	78.7	74.3	78.8 (79.0)	74.4 (75.5)	78.8 (78.3)
4'''	70.5	70.4	68.1	70.6 (70.5)	69.7 (69.1)	70.6 (69.2)
5'''	81.9	81.7	79.2	81.9 (82.0)	79.4	82.0 (81.8)
6'''	61.4	61.1	60.5	61.3 (61.6)	60.7 (60.8)	61.3 (61.3)

639.13064 (calculated: 639.13027; Mass difference: 0.71 ppm) observed in the high resolution mass spectrum of **7** corresponding to $C_{27}H_{29}O_{15}Na_2$ confirmed this identification.

The 1D and 2D NMR spectra of **9** shared many similarities to that of **7**, showing chrysoeriol aglycone glycosylated at positions 6 and 8 of the aglycone, with galactopyranose as the 8-glycosyl substituent (Fig. 4 and Tables 4 and 5). The 6-*C*-glycosyl substituent of **9** was, however, identified as glucopyranosyl (Fig. 4 structure and Tables 4 and 5). Thus, **9** was identified as the previously undescribed flavonoid chrysoeriol 6-*C*-*β*-glucopyranosyl-8-*C*-*β*-galactopyranoside) (Fig. 4). The sodiated molecular ion $[M+Na]^+$ at *m/z* 647.15899 (calculated: 647.15889; Mass difference: 0.29 ppm) observed in the high resolution mass spectrum corresponding to $C_{28}H_{32}O_{16}Na$, and $[M+2Na–H]^+$ at *m/z* 669.14084 (calculated: 669.14084; Mass difference: 0.34 ppm) observed in the high resolution mass spectrum of **9** (Fig. S77) corresponding to $C_{28}H_{31}O_{16}Na_2$ confirmed this identification.

The 1D and 2D NMR spectra of **8** shared many similarities to that of **9**, showing chrysoeriol aglycone *C*-glycosylated with glucose and galactose at positions 6 and 8 of the aglycone, although the positions of the *C*-glycosyl substituents were interchanged as compared to those of **9**. Thus, **8** was identified as the previously undescribed flavonoid chrysoeriol 6-*C*-*β*-galactopyranosyl-8-*C*-*β*-glucopyranoside (Fig. 4). The sodiated molecular ions $[M+Na]^+$ at *m/z* 647.15868 (calculated: 647.15889; Mass difference: −0.19 ppm) observed in the high resolution mass spectrum (Fig. S76) of **8** corresponding to $C_{28}H_{32}O_{16}Na$, and $[M+2Na–H]^+$ at *m/z* 669.14138 (calculated: 669.14084; Mass difference: 0.94 ppm) corresponding to $C_{28}H_{31}O_{16}Na_2$ confirmed **8** to be the previously undescribed compound chrysoeriol 6-*C*-*β*-galactopyranosyl-8-*C*-*β*-glucopyranoside.

Circular Dichroism (CD) spectra of all isolated di-*C*-glycosylflavones were recorded. All these compounds are based on the same chrysoeriol aglycone. According to Gaffield et al. (1978) the CD bands of di-*C*-glycosylflavones are often relatively weak as a result of overlapping of oppositely signed adjacent CD bands (Wellman et al., 1965). The similarity of the recorded CD spectra of compounds **6–10** indicate that the configurations of C-1 of the glycosyl substituents are similar for these compounds (Gaffield et al., 1978). The fact that the CD spectrum of compound **5**, which exhibited a strong negative band at 275 nm, differed from the CD-spectra recorded of compounds **6–10** may not be unexpected since compound **5** is the only di-*C*-glycosylflavone among the isolated compounds which is substituted by an arabinofuranosyl moiety.

Compounds **8–10** exhibit most of their ^{1}H and ^{13}C-NMR signals (Tables 4 and 5) in double sets. These signals reveal two conformational isomers created by rotational hindrance at the *C* (sp^3)–*C* (sp^2) glucosyl–flavone linkage in each of these 6,8-di-C-substituted flavones (Rayyan et al., 2005). The equilibrium between the rotamers was supported by observations of strong exchange peaks between equivalent protons of each of the rotameric pairs in their ROESY spectra (Supplementary Fig. S57, S63 and S69).

Isomerisation of di-*C*-glycosyl flavones by Wessely Moser rearrangement was demonstrated to occur by the fact that during the final isolation of pure compounds by preparative HPLC, compound **5** was isolated at two different retention times from the same mixture. This

Table 6
Cytotoxicity of compounds **1–10** against three mammalian cell lines. The compounds were diluted in DMSO or water and a dilution series made on each cell line. The cells were tested for metabolic activity after 72 h of incubation. The EC_{50} values were determined by non-linear regression from 3 to 5 independent experiments (NRK and MOLM13) as described in the methods section. The data from H9c2 is from one experiment. "– " denotes that no data is available due to low toxicity.

	NRK		Molm13		H9c2	
	EC_{50} (mM)	R^2	EC_{50} (mM)	R^2	EC_{50} (mM)	R^2
1	0.5–1	–	0.4	0.66	> 0.3	–
2	0.12	0.86	0.22	0.69	0.2–0.6	–
3	0.05	0.77	0.08	0.74	0.02	0.92
4	0.007	0.94	0.002	0.85	0.006	0.96
5	> 1	–	0.5–1.0	–	–	–
6	> 1	–	0.5–1.0	–	–	–
7	> 1	–	> 1	–	–	–
8	> 1	–	> 1	–	–	–
9	> 1	–	> 1	–	–	–
10	> 1	–	0.5–1	–	–	–

may not be surprising since we have previously observed similar isomerisation of *C*-glycosyl-3-deoxyanthocyanins occurring under similar mild experimental conditions (Bjorøy et al. 2009a, 2009b).

To investigate if any of the compounds could be responsible for the death of sheep and cattle, their cytotoxic potential was investigated on three cell lines. The rat kidney epithelial cell line NRK, the rat cardiomyoblast H9c2, and the human AML cell line Molm13. The flavonoids (compounds **5–10**) exhibited no, or very low toxicity towards the cell lines, with either activity above 0.5 mM, or no detectable cytotoxic activity at 1 mM (Table 6). The saponins (compounds **1–4**) were more potent. Interestingly, the cytotoxic potential increased proportionally with the increasing number of glycosyl substituents, where compound **4** (sarsasapogenin-3-*O*-(2′-*O*-*β*-glucopyranosyl-3′-*O*-*α*-arabinopyranosyl-*β*-galactopyranoside)) showed an EC_{50} (concentration leading to 50% cell death) between 2 and 8 μM after 72 h of incubation (Table 6 and Fig. 5). Incubation time for 24 h gave higher EC_{50} values (Table 6 and Fig. 5), but for compound **4**, the EC_{50} values for the different cell lines were still between 3 and 10 μM.

The results presented in Table 6 and Fig. 5 indicate that the saponins, and particularly the main saponin, compound **4**, are responsible for some of the toxic effects observed in livestock after ingestion of flowering tops of *N. ossifragum*. All cell lines were severely affected by the main saponin compound **4**, indicating that the presence of this substance in the vascular system might affect the function of the heart, leukocytes, and kidneys. Furthermore, our data suggests that compounds **3** and **4** induce both a sub-acute and protracted toxicity, since we found significant cell death at 24 h, which increased after 72 h (Fig. 5). It has previously been shown that orally administered saponins induced damage in the intestinal mucosa, as well as causing liver and kidney necrosis (Aguilar-Santamaría et al. (2013); Diwan et al. (2000)). Moreover, case reports of cattle with suspected *N. ossifragum* poisoning showed hepatic fibrosis and reduced renal function (Flåøyen et al., 1995a Flåøyen et al., 1995b; Angell and Ross (2011)). Interestingly, Angell and Ross (2011) observed that the condition of one of the cattle exacerbated even after treatment was initiated (Angell and Ross, 2011), indicating irreparable damage, or a protracted toxic effect. The kidney and liver might be particularly vulnerable to compounds like compound **3** and **4** due to their high perfusion rate, and their ability to actively take up (hepatocytes) or concentrate (kidney tubules) xenobiotics.

3. Concluding remarks

For the first time, saponins from *N. ossifragum* have been characterized at atomic resolution. The cytotoxicity of the saponins increased proportionally with the increasing number of glycosyl substituents. The fact that the main saponin, sarsasapogenin-3-*O*-(2′-*O*-*β*-glucopyranosyl-3′-*O*-*α*-arabinopyranosyl-*β*-galactopyranoside) (**4**), which comprises several percent of the dry weight of flowering tops of *N. ossifragum*, proved to be the main toxic principle towards all tested cell lines may indicate that this compound is responsible for the observed kidney and liver damage seen in cattle after ingestion of *N. ossifragum*. The fact that the structures of the saponins of *N. ossifragum* have now been determined, in addition to the presentation of a protocol for large-scale isolation of these compounds paves the way for further extensive structure-activity studies of these compounds. Even although the flowering tops of *N. ossifragum* have been indicated to contain the causative agents of the phototoxic disease alveld, no aromatic compounds have previously been identified therefrom. Here, we report on the detailed characterization of five di-*C*-glycosylflavones, which have been completely characterized for the first time, in addition to a structurally related known compound.

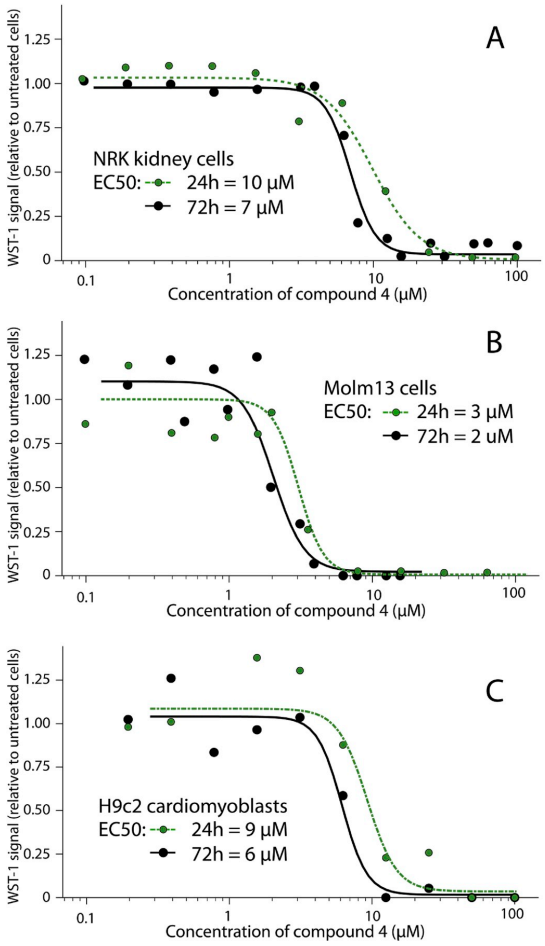

Fig. 5. EC_{50} values of the main saponin (**4**) isolated from flowering tops of *N. ossifragum* towards normal rat kidney (NRK) cells, MOLM13 cells and H9c2 cardiomyoblasts.

4. Experimental

4.1. Plant material

Fresh plant material of *Narthecium ossifragum* (L.) Huds. (Nartheciaceae) was collected in the summer season (collection date 07/2016) in a bog area located at south western part of Ulriken, Bergen, Norway at 350m above sea level (coordinates 60.36884N 005.38237E). Voucher specimen of *N. ossifragum* has been deposited at the ARBOHA, University of Bergen (accession number BG/S-162115). Prior to extraction, the plant material was stored at −80 °C. The water content of the plant material was determined to be 81.3% of the weight.

4.2. Extraction of compounds and partitions with organic solvents

Flowering tops (1.7 kg) of *N. ossifragum* were extracted with 15 L methanol for 72 h at room temperature. The extraction yield was 7.6% of the wet weight. When taking into account that the water content was 81.3%, the dry weight extraction yield was 40.5%. The methanolic extract was filtered through glass wool and concentrated by rotary evaporator under reduced pressure. The resulting concentrated aqueous extract was partitioned (three times) with petroleum ether (3 L), followed by partition (three times) with ethyl acetate (3 L). The residual aqueous phase was concentrated by rotavapor to a volume of 500 mL. The petroleum ether and the ethyl acetate phases provided a white precipitate, which was collected and dried before further purification and separation as described below.

4.3. Amberlite XAD-7 column chromatography

The concentrated residual aqueous partition (500 mL) was applied to an Amberlite XAD-7 column (column dimensions 50 × 1000 mm, containing 500g XAD-7 stationary phase). The mobile phase gradient consisted of 5 L distilled water (fractions 1–5), followed by 1L water-methanol 90:10; v/v (fraction 6), 1 L water-methanol 75:25; v/v (fraction 7), 3 L water-methanol 50:50; v/v (fraction 8–10) and finally 4 L methanol 100% (fractions 11–14). The flow rate was 5 mL/min. This gave a total of 14 fractions with volumes of 1 L, which were analysed individually by analytical HPLC.

4.4. Sephadex LH-20 column chromatography

Fractions 8–10 from the Amberlite XAD-7 column chromatography were combined, concentrated to a volume of 20 mL and further separated on a Sephadex LH-20 column (column dimensions 50 × 1000 mm, containing 500 g Sephadex LH-20 stationary phase) using a gradient of water and methanol containing 0.2% of TFA. The gradient consisted of 650 mL water-methanol-TFA 80:20:0.2; v/v/v (fractions 1–13), followed by 900 mL water-methanol-TFA 50:50:0.2 v/v/v (fractions 14–32) and finally 800 mL water-methanol-TFA 30:70:0.2 v/v/v (fractions 33–49). The flow rate was 5 mL/min. A total of 49 fractions, each with a volume of 50 mL were collected.

4.5. Preparative HPLC

Compounds of the combined fractions 4–6 from the Sephadex LH-20 column chromatography were isolated by preparative HPLC (Gilson 321 preparative HPLC equipped with a Dionex Ultimate 3000 variable wavelength detector). The HPLC instrument was equipped with a C_{18} Ascentis column (250 × 20 mm; 5 µm, spherical particles). Chromatograms were recorded at 360 nm. Two solvents were used for elution; mobile phase A (water-TFA 99.9:0.1 v/v) and mobile phase B (methanol-TFA 99.9:0.1 v/v). The flow rate was 12 mL/min. Prior the analysis the combined fractions were evaporated to dryness and dissolved in a mixture of 1:1; v/v of the two mobile phases. Portions of 200 µL were manually injected into the HPLC column. Fractions were collected manually based on peaks appearing in the on-line chromatogram recorded at 360 nm. The collected fractions were transferred to HPLC vials for purity control using analytical HPLC. Following this strategy 16.4 mg of compound **5**, 6.2 mg of compound **6**, 1.8 mg of compound **7**, 3.4 mg of compound **8**, 8.5 mg of compound **9** and 2.2 mg of compound **10** were obtained.

4.6. Analytical HPLC

The HPLC instrument (Dionex P680) was equipped with a multi-diode array detector, an autoinjector and a 250 × 4.6 mm, 5 µm Thermo Scientific Hypersil GOLD column. Two solvents were used for elution; A (water-TFA 99.5:0.5; v/v) and B (acetonitrile-TFA 99.5:0.5; v/v). The flow rate was 1 mL/min. Aliquots of 20 µl were injected.

4.7. Isolation of pure saponins from crystallized mixture of saponins

7.1546 g of crystals from the extract of flowering tops of *N. ossifragum* were precipitated and collected from the concentrated petroleum ether and ethyl acetate partitions of the crude extract. The 1D and 2D NMR spectra of 20 mg of these crystals dissolved in DMSO-D_6 indicated that they consisted of a mixture of saponins. Subsequently, 1g of these crystals was dissolved in 5 mL of DMSO and further purified by Sephadex LH-20 chromatography.

4.8. Purification of saponins by Sephadex LH-20 column chromatography

1 g of crystals dissolved in 5 mL DMSO was purified on a Sephadex LH-20 column (500 × 50 mm containing 200 g column material) using a gradient of 600 mL water-methanol-TFA 50:50:0.2 v/v/v, followed by 4450 mL of methanol-TFA 100:0.2 and finally 1750 mL of acetone 100%. The flow rate was 5 mL/min 138 fractions, each with volumes of 25 mL, were collected, evaporated to dryness under nitrogen and analysed by TLC.

4.9. Silica gel column chromatography

Fractions 35–55 from the Sephadex LH-20 column chromatography were combined, concentrated to a volume of 5 mL and further separated on a Silica gel column (200 × 50 mm containing 300 g column material) using a gradient of ethyl acetate-methanol-water as mobile phase. The gradient consisted of 3000 mL of ethyl acetate-methanol-water 80:20:4 v/v/v, followed by 3000 mL ethyl acetate-methanol-water 50:50:4; v/v/v and finally by 575 mL of ethyl acetate-methanol-water 20:80:4; v/v/v. The flow rate was 8 mL/min. The silica chromatographic separation resulted in collection of 275 fractions, each with a volume of 25 mL. The resulting fractions were concentrated to dryness under nitrogen and analysed by TLC. Following this strategy 4.6 mg of sarsasapogenin (**1**), 13.1 mg of sarsapogenin-3-*O*-*β*-galactopyranoside (**2**), 56.1 mg of sarsasapogenin-3-O-(2′-*O*-*β*-glucopyranosyl)-*β*-galactopyranoside (**3**), and 260.7 mg of sarsapogenin-3-*O*-*β*-(2′-*O*-*β*-glucopyranosyl-3′-*O*-*α*-arabinopyranosyl-*β*-galactopyranoside) (**4**) were obtained.

4.10. Analytical TLC

Purified mixtures of saponins and isolated pure saponins were analysed by a TLC method modified from the procedures described by Kobayashi et al., 1993 and Miles et al., 1991. The chromatographic separation was performed on silica TLC plates. The mobile phase consisted of ethyl acetate-methanol-water 80:20:4; v/v/v. Detection of colourless compounds after TLC separation was achieved using Ehrlich's solution (4-(dimethylamino)benzaldehyde in hydrochloric acid solution provided by Sigma Aldrich) and 5% sulfuric acid on methanol as spray reagent.

4.11. Spectroscopy

High resolution mass spectra were recorded using a JEOL AccuTOF JMS T100LC instrument fitted with an electrospray ion source. The spectrum was recorded over the mass range 50–1000 *m/z*.

UV–Vis absorption spectra were recorded on-line during HPLC analysis over the wavelength range 240–600 nm in steps of 2 nm.

Specific rotations of compounds **1**–**4** were determine on a Rudolph Research Analytical Autopol IV instrument. Samples dissolved in DMSO were transferred to a 600 µl cell. Measurements were performed at 589 nm. The specific rotations were determined to be −2.86° for compound **4**, -22.33° for compound **3**, -10.83° for compound **2** and -2.00° for compound **1**.

Circular Dichroism (CD) spectra were recorded at 20 °C in a Jasco J-810 spectropolarimeter equipped with a Peltier temperature control unit. 5 mM of compounds **5**, **7** and **9**, 1 mM of compounds **6** and **8** and 0.5 mM of compound 10 solubilised in 100% DMSO were used to obtain the spectra. The spectra obtained were the average of 6 scans. Buffer scans (100% DMSO) were subtracted from the spectra. The spectra were scanned from 185 nm to 450 nm, but only the relevant region of the scans (250–400 nm) is shown. A 1-mm pathlength cell was used.

NMR samples were prepared by dissolving the isolated compounds in deuterated dimethylsulfoxide (DMSO-D_6; 99.96 atom % D, Sigma-Aldrich). The 1D ^{1}H and the 2D ^{1}H–^{13}C HMBC, the 2D ^{1}H–^{13}C HSQC, the 2D ^{1}H–^{13}C HSQC-TOCSY, the 2D ^{1}H–^{13}C H2BC, the 2D ^{1}H–^{1}H COSY and 2D ^{1}H–^{1}H ROESY NMR experiments were obtained at 850 MHz at 298K on a Bruker 850 MHz instrument equipped with a ^{1}H,^{13}C,^{15}N triple resonance cryogenic probe.

4.12. Brine shrimp lethality assay

The stock solution was prepared by dissolving 124 mg of the crystallized mixtures of saponins in 1 mL DMSO. 20 µL of this stock solution was transferred to a beaker containing 10 mL of seawater (distilled water containing 35.5 g/l dissolved sea salt) to make the stock solution. A volume of 0, 2, 5, 7, 9, 12.5 µL of the stock solution of saponin were used in each well containing 10–20 *Artemia salina* nauplii, having a total volume of 200 µL seawater. Individual concentrations in each well were 2.5, 5, 8.8, 11.3 and 15.6 µg/mL, respectively. Three parallels of each concentration and controls were performed. After 24 h the number of surviving *A. salina* nauplii in each well were counted using a computer-connected Veho 400x USB microscope with 20 times magnification.

4.13. Cytotoxicity towards mammalian cell lines

Stock solutions were prepared by dissolving pure compounds to a final concentration of 100 mM in DMSO. The normal rat kidney epithelial cells (NRK, ATCC no.: CRL-6509) and rat cardiomyoblasts (H9c2, ATCC no.: CRL-1446) were cultured in DMEM supplemented with 10% fetal bovine serum (FBS, Invitrogen, Carlsbad, CA). When the cells reached 80% confluence, they were detached by mild trypsin treatment (0.33 mg/mL trypsin for 5 min at 37 °C), centrifuged (160 × *g*, 4 min) and reseeded in fresh medium to 25% confluence. The AML cell line MOLM13 (Matsuo et al., 1997; Quentmeier et al., 2003) were cultured in RPMI 1640 medium enriched with 10% FBS. The cells were kept in suspension cultures at a density of between 150,000 and 600,000 cells/mL. All media were supplemented with 1 IU/mL penicillin and 1 mg/mL streptomycin (both from Cambrex, Belgium), and incubated in a humidified atmosphere (37 °C, 5% CO_2).

For cytotoxicity experiments with compounds **1**–**10**, the NRK and H9c2 cells were seeded in 96 well tissue culture plates (5000 cells/well, 0.1 mL) and left overnight to attach before adding compounds. The MOLM13 cells were seeded in 96 well tissue culture plates at 15,000 cells/well in 0.1 mL on the day of the experiment. Compounds dissolved in DMSO were added to the cells, and the plates were kept overnight before addition of the tetrazolium salt WST-1 according to the manufacturer instructions. The plates were further incubated for 2 h before the signal was recorded at 450 nm with reference at 620 nm. For blank subtraction, medium added only WST-1 and compound was used. In some of the experiments involving coloured compounds, the fluorescent dye resazurin, which is converted to the reporter product by the same enzyme as WST-1, was used as an alternative. The protocol is identical, except that viability was assessed by measuring fluorescence at 480/520 nm. After recording of WST-1 or resazurin conversion, the cells were next fixed 2% buffered formaldehyde (pH 7.4) with 0.01 mg/mL of the DNA-specific fluorescent dye, Hoechst 33342. The presence of dead (apoptotic or necrotic) cells was verified by differential interference contrast and fluorescence microscopy as previously described (Oftedal et al., 2010; Myhren et al., 2014). EC_{50} values were determined by a four-parameter regression analysis as described previously (Viktorsson et al. (2017)), using IBM SPSS® statistic software (ver. 25). For comparison the corresponding EC_{50} values of the standard compound quercetin 3-(6″-rhamnosylglucoside) (rutin) was 40 ± 12 µM for MOLM13 cells and 245 ± 19 µM for NRK cells.

Acknowledgements

The authors acknowledge Dr. Bjarte Holmelid for recording the high-resolution mass spectra, Professor George W. Francis for proofreading the manuscript and Centre for Pharmacy at the University of Bergen, the Western Norway Health authorities (912052), and the Norwegian Cancer Society (112502) for financial support. This work was partly supported by the Research Council of Norway through the (226244/F50).

Appendix A. Supplementary data

Supplementary data to this article can be found online at https://doi.org/10.1016/j.phytochem.2019.04.014.

References

Abdelkader, S.V., Ceh, L., Dishington, I.W., Hauge, J.G., 1984. Alveld-producing saponins. II: toxicological studies. Acta Vet. Scand. 25, 76–85.
Aguilar-Santamaría, L., Herrera-Arellano, A., Zamilpa, A., Alonso-Cortés, D., Jiménez-Ferrer, E., Tortoriello, J., Zúñiga-González, G., 2013. Toxicity, genotoxicity, and cytotoxicity of three extracts of *Solanum chrysotrichum*. J. Ethnopharmacol. 150, 275–279.
Angell, J., Ross, T., 2011. Suspected bog asphodel (*Narthecium ossifragum*) toxicity in cattle in North Wales. Vet. Rec. 169, 101. https://doi.org/10.1136/vr.d3879.
Bernhoft, A. (Ed.), 2010. Bioactive Compounds in Plants - Benefits and Risks for Man and Animals. The Norwegian Academy of Science and Letters, Oslo, Norway (Novus forlag, Oslo).
Bjorøy, Ø., Rayyan, S., Fossen, T., Kalberg, K., Andersen, Ø.M., 2009a. Anthocyanin *C*-glycosides from flavone *C*-glycosides. Phytochemistry 70, 278–287.
Bjorøy, Ø., Rayyan, S., Fossen, T., Andersen, Ø.M., 2009b. Detailed properties of anthocyanins – rearrangement of *C*-glycosyl-3-deoxyanthocyanidins in acidic aqueous solutions. J. Agric. Food Chem. 57, 6668–6677.
Bouillant, M.-L., Ferreres de Arce, F., Favre-Bonvin, J., Chopin, J., Zoll, A., Mathieu, G., 1979. Nouvelles *C*-glycosylflavones extraites de *Spergularia rubra*. Phytochemistry 18, 1043–1047.
Carvalho, M., Silva, B.M., Silva, R., Valentao, P., Andrade, P.B., Bastos, M.L., 2010. First report on *Cydonia oblonga* Miller anticancer potential: differential antiproliferative effect against human kidney and colon cancer cells. J. Agric. Food Chem. 58, 3366–3370.
Ceh, L., Hauge, J.G., 1981. Alveld-producing saponins. I. Chemical studies. Acta Vet. Scand. 22, 391–402.
di Menna, M.E., Flåøyen, A., Ulvund, M.J., 1992. Fungi on *Narthecium ossifragum* leaves and their potential involvement in alveld disease of Norwegian lambs. Vet. Res. Commun. 16, 117–124.
Diwan, F.H., Abdel-Hassan, I.A., Mohammed, S.T., 2000. Effect of saponin on mortality and histopathological changes in mice. East. Mediterr. Health J. 6, 345–351.
Feilberg, J., 1999. Blomster I Norge. Aschehoug, Oslo.
Ferreres, F., Silva, B.M., Andrade, P.B., Seabra, R.M., Ferreira, M.A., 2003. Approach to the study of *C*-glycosyl flavones by ion trap HPLC-PAD-ESI/MS/MS: application so seeds of quince (*Cydonia oblonga*). Phytochem. Anal. 14, 352–359.
Flåøyen, A., Hjorth Tønnesen, H., Grønstøl, H., Karlsen, J., 1991. Failure to induce toxicity in lambs by administering saponins from *Narthecium ossifragum*. Vet. Res. Commun. 15, 483–487.

Flåøyen, A., Bratberg, B., Frøslie, A., Grønstøl, H., 1995a. Nephrotoxicity and hepatotoxicity in calves apparently caused by experimental feeding with *Narthecium ossifragum*. Vet. Res. Commun. 19, 63–73.
Flåøyen, A., Binde, M., Bratberg, B., Djønne, B., Fjølstad, M., Grønstøl, H., Hassan, H., Mantle, P.G., Landsverk, T., Schönheit, J., 1995b. Nephrotoxicity of *Narthecium ossifragum* in cattle in Norway. Vet. Rec. 137, 259–263.
Flåøyen, A., Bratberg, B., Frøslie, A., Grønstøl, H., Langseth, W., Mantle, P.G., von Krogh, A., 1997. Further studies on the presence, qualities and effects of the toxic princliples from *Narthecium ossifragum* plants. Vet. Res. Commun. 21, 137–148.
Fossen, T., Andersen, Ø.M., 2006. Spectroscopic techniques applied to flavonoids. In: Flavonoids: Chemistry, Biochemistry, and Applications. CRC Press, pp. 37–142.
Gaffield, W., Horowitz, R., Gentili, B., Chopin, J., Bouillant, M.L., 1978. Circular dichroism of C-glycosylflavones. A chiroptical method for differentiating 6-C, 8-C- and 6,8-di-C-β-glycosyl isomers. Tetrahedron 34, 3089–3096.
Harwig, J., Scott, P.M., 1971. Brine shrimp (*Artemia salina* L.) larvae as a screening system for fungal toxins. Appl. Microbiol. 21, 1011–1016.
Inoue, T., Mimaki, Y., Sashida, Y., Kobayashi, M., 1995. Structures of toxic steroidal saponins from *Narthecium asiaticum*. Chem. Pharm. Bull. 43, 1162–1166.
Jay, M., Ismaili, A., 1989. Flavones and *C*-glycosylflavones from the leaves of some *Arrhenatherum* species. Phytochemistry 28, 3035–3037.
Kobayashi, M., Suzuki, K., Nagasawa, S., Mimaki, Y., 1993. Purification of toxic saponins from *Narthecium asiaticum* Maxim. J. Vet. Med. Sci. 55, 401–407.
Li, Z., Gao, Y., Nakanishi, H., Gao, X., Cai, L., 2013. Biosynthesis of rare hexoses using microorganisms and related enzymes. Beilstein J. Org. Chem. 9, 2434–2445.
Matsuo, Y., MacLeod, R.A.F., Uphoff, C.C., Drexler, H.G., Nishizaki, C., Katayama, Y., Kimura, G., Fujii, N., Omoto, E., Harada, M., Orita, K., 1997. Two acute monocytic leukemia (AML-M5a) cell lines (MOLM-13 and MOLM-14) with interclonal phenotypic heterogeneity showing MLL-AF9 fusion resulting from an occult chromosome insertion, ins(11;9)(q23;p22p23). Leukemia 11, 1469–1477.
Melchert, T.E., Alston, R.E., 1965. Flavonoids from the moss *Mnium affine* Bland. Science 150, 1170–1171.
Meyer, B.N., Ferrighi, N.R., Putnam, J.E., Jacobsen, L.B., Nichols, D.E., McLaughlin, J.L., 1982. Brine shrimp: a convenient general bioassay for active plant constituents. Planta Med. 45, 31–34.
Miles, C., Munday, S., Holland, P.L.M., Wilkins, A., 1991. Identification of a sapogenin glucuronide in the bile of sheep affected by *Panicum dichoromiflorum* toxicosis. N. Z. Vet. J. 39, 150–152.
Mossberg, B., Stenberg, L., Ericsson, S., 1995. Gyldendals Store Nordiske Flora. GYLDENDAL NORSK FORLAG.
Mues, R., 1982. Flavone di-*C*-glycosides from the liverwort *Trichocolea tomentella* (L.) Dum. and their taxonomic significance. J. Hattori Bot. Lab. 51, 61–68.
Myhren, L., Mostrøm Nilssen, I., Nicolas, V., Døskeland, S.O., Barratt, G., Herfindal, L., 2014. Efficacy of multi-functional liposomes containing daunorubicin and emetine for treatment of acute myeloid leukaemia. Eur. J. Pharm. Biopharm. 88, 186–193.
Oftedal, L., Selheim, F., Wahlsten, M., Sivonen, K., Døskeland, S.O., Herfindal, L., 2010. Marine benthic cyanobacteria contain apoptosis-inducing activity synergizing with Daunorubicin to kill leukemia cells, but not cardiomyocytes. Mar. Drugs 8, 2659–2672.
Paulli, S., 1667. A Quadripartitum botanicum de simplicum medicamentorum. Argentorati: Impensis Fil. Simonis Paulli, pp. 690.
Pedersen, A.T., Andersen, Ø.M., Aksnes, D.W., Nerdal, W., 1995. Anomeric sugar configurations of anthocyanin *O*-pyranosides determined from heteronuclear one-bond coupling constants. Phytochem. Anal. 6, 313–316.
Quentmeier, H., Reinhardt, J., Zaborski, M., Drexler, H.G., 2003. FLT3 mutations in acute myeloid leukemia cell lines. Leukemia 17, 120–124.
Rayyan, S., Fossen, T., Nateland, H.S., Andersen, Ø.M., 2005. Isolation and identification of flavonoids, including flavone rotamers, from the herbal drug 'Crataegi Folium Cum Flore' (Hawthorn). Phytochem. Anal. 16, 334–341.
Sakakibara, M., Mabry, T.J., Bouillant, M.-L., Chopin, J., 1977. 6,8-di-*C*-glucosylflavones from *Larrea tridentate* (Zygophyllaceae). Phytochemistry 16, 1113–1114.
Salmenkallio, M., McCormick, S., Mabry, T.J., Dellamonica, G., Chopin, J., 1982. The flavonoids of *Trichophorum cespitosum*. Phytochemistry 21, 2990–2991.
Silva, B.M., Andrade, P.B., Ferreres, F., Seabra, R.M., Beatriz, M., Oliveira, P.P., Ferreira, M.A., 2005. Composition of Quince (*Cydonia oblonga* Miller) seeds: phenolics, organic acids and free amino acids. Nat. Prod. Res. 19, 275–281.
Stabursvik, A., 1953. A steroidal glycol, 22-Hydroxy-cholesterol from *Narthecium ossifragum* Huds. Acta Chem. Scand. 7 1220–1220.
Stabursvik, A., 1959. A Phytochemical Study of Narthecium Ossifragum (L.) Huds. Doctoral thesis NTH. Technical University of Norway, Trondheim.
Sy, L.K., Lok, C.N., Wang, J.Y., Liu, Y., Cheng, L., Wan, P.K., Leung, C.T., Cao, B., Kwong, W.L., Chang, R.C.C., Che, C.M., 2016. Identification of "sarsapogenin-aglyconed" timosaponins as novel Abeta-lowering modulators of amyloid precursor protein processing. Royal Soc. Chem. 7, 3206–3214.
Tønnesen, H.H., Mysterud, I., Karlsen, J., Skulberg, O.M., Laane, C.M.M., Schumacher, T., 2013. Identification of singlet oxygen photosensitizes in lambs drinking water in an alveld risk area in West Norway. J. Photochem. Photobiol. B Biol. 119, 37–45.
Uhlig, S., Wisløff, H., Petersen, D., 2007. Identification of cytotoxic constituents of *Narthecium ossifragum* using bioassay-guided fractionation. J. Agric. Food Chem. 55, 6018–6026.
Viktorsson, E.Ö., Grøthe, B.M., Aesoy, R., Sabir, M., Snellingen, S., Prandina, A., Åstrand, O.A.H., Bonge-Hansen, T., Døskeland, S.O., Herfindal, L., Rongved, P., 2017. Total synthesis and antileukemic evaluations of the phenazine 5,10-dioxide natural products iodinin, myxin and their derivatives. Bioorg. Med. Chem. 25, 2285–2293.
Vu, M., Herfindal, L., Juvik, O.J., Vedeler, A., Haavik, S., Fossen, T., 2016. Toxic aromatic compounds from fruits of *Narthecium ossifragum* L. Phytochemistry 132, 76–85.
Wellman, K., Laur, P.H.A., Briggs, W.S., Moscowitz, A., Djerassi, C., 1965. Optical Rotatory Dispersion Studies. XCIX. Superposed multiple cotton effects of saturated ketones and their significance in the circular dichroism measurement of (-)-menthone. J. Am. Chem. Soc. 87, 66–72.
Wisløff, H., Flåøyen, A., Ottesen, N., Hovig, T., 2003. *Narthecium ossifragum* (L.) Huds. Causes kidney damage in goats: morphologic and functional effects. Vet. Pathol. 40, 317–327.
Wu, C., 2014. An important player in brine shrimp lethality bioassay: the solvent. "J. Adv. Pharm. Technol. Research"" (JAPTR)" 5, 57–58.

Cytotoxic saponins and other natural products from flowering tops of *Narthecium ossifragum* L.

Andrea Estefanía Carpinteyro Díaz, Lars Herfindal, Bendik Auran Rathe, Kristine Yttersian Sletta, Anni Vedeler, Svein Haavik and Torgils Fossen*

Supplementary material

NMR spectra

High resolution mass spectra

Table of content

Figure S1. 1D ^{1}H NMR spectrum of sarsasapogenin (1)

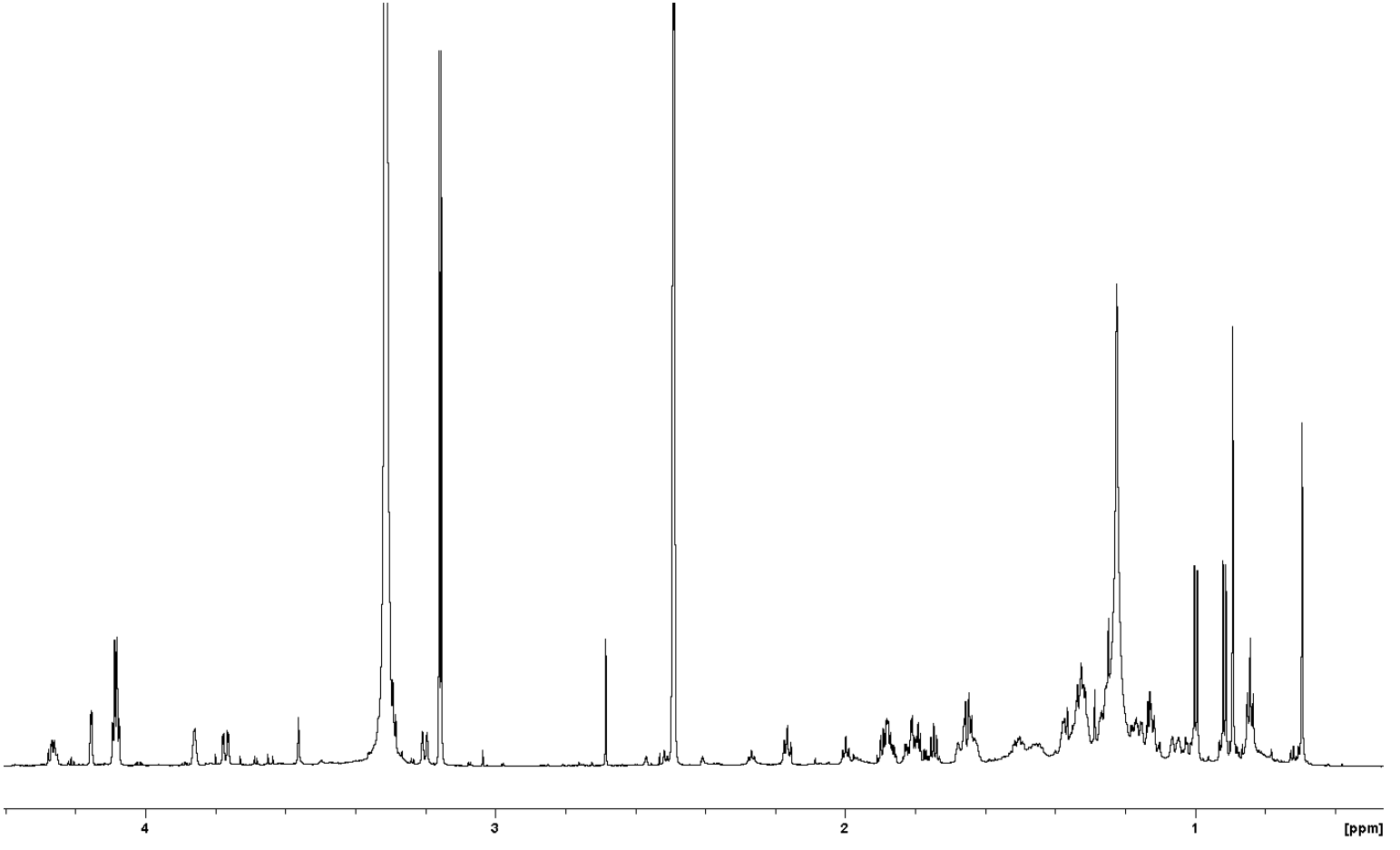

Figure S2. 2D ^{1}H-^{13}C HSQC NMR spectrum of sarsasapogenin (1)

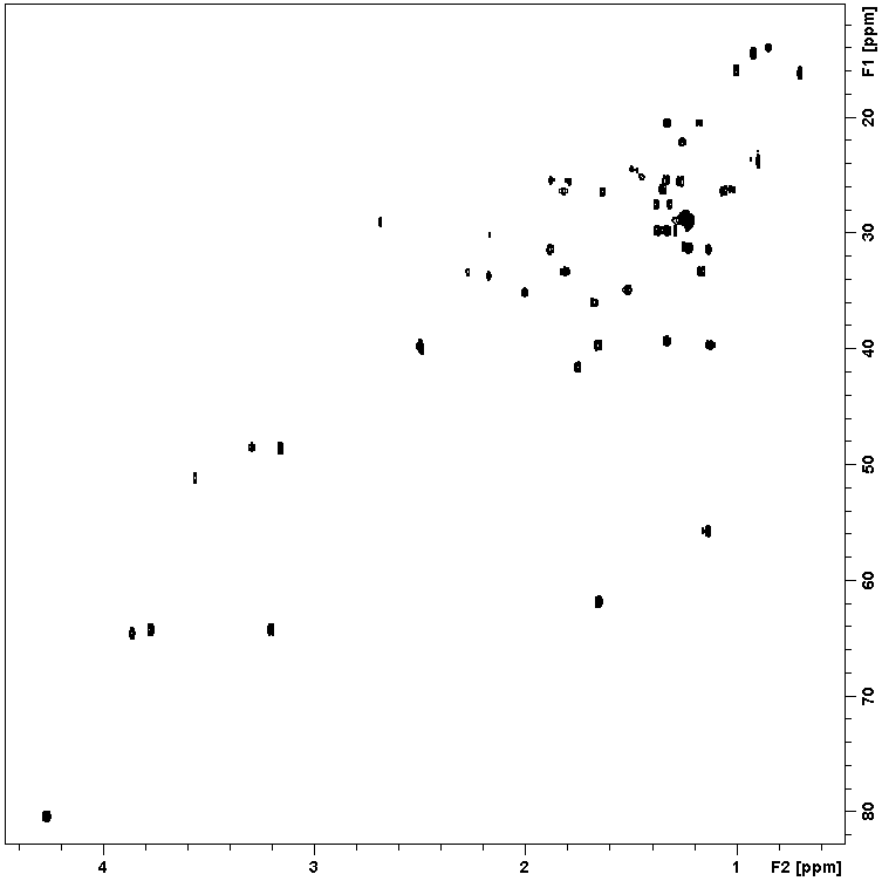

Figure S3. 2D Edited ^{1}H-^{13}C HSQC NMR spectrum of sarsasapogenin (1)

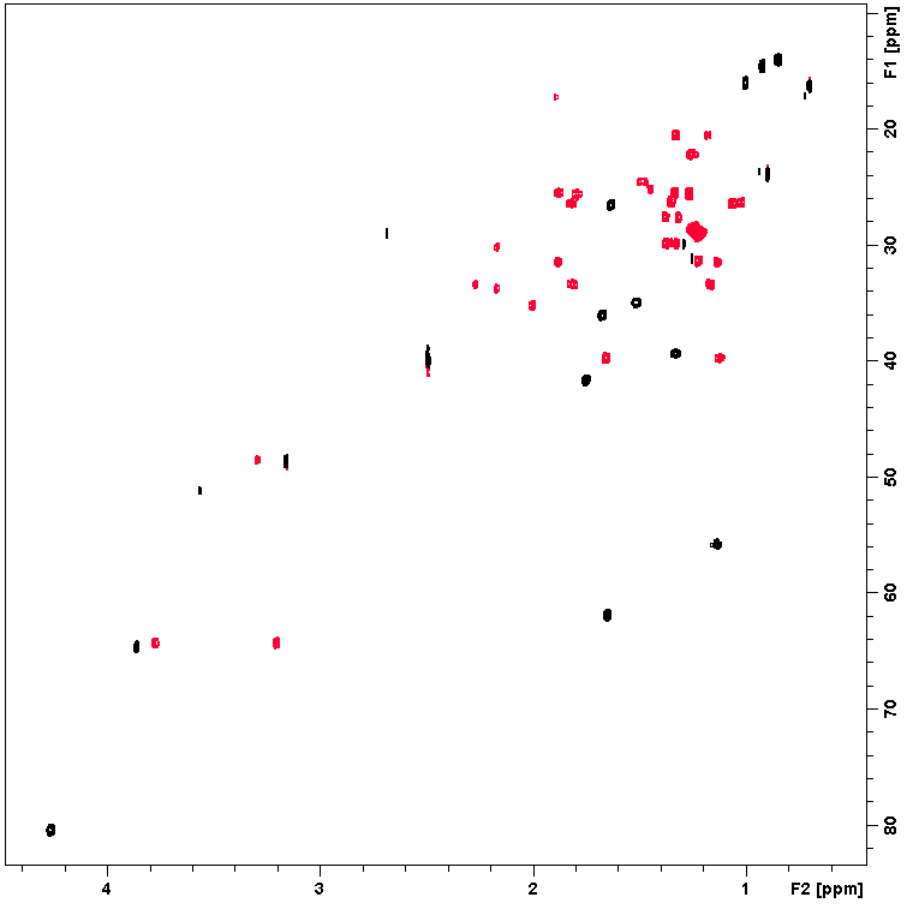

Figure S4. 2D ^{1}H-^{13}C HMBC NMR spectrum of sarsasapogenin (1)

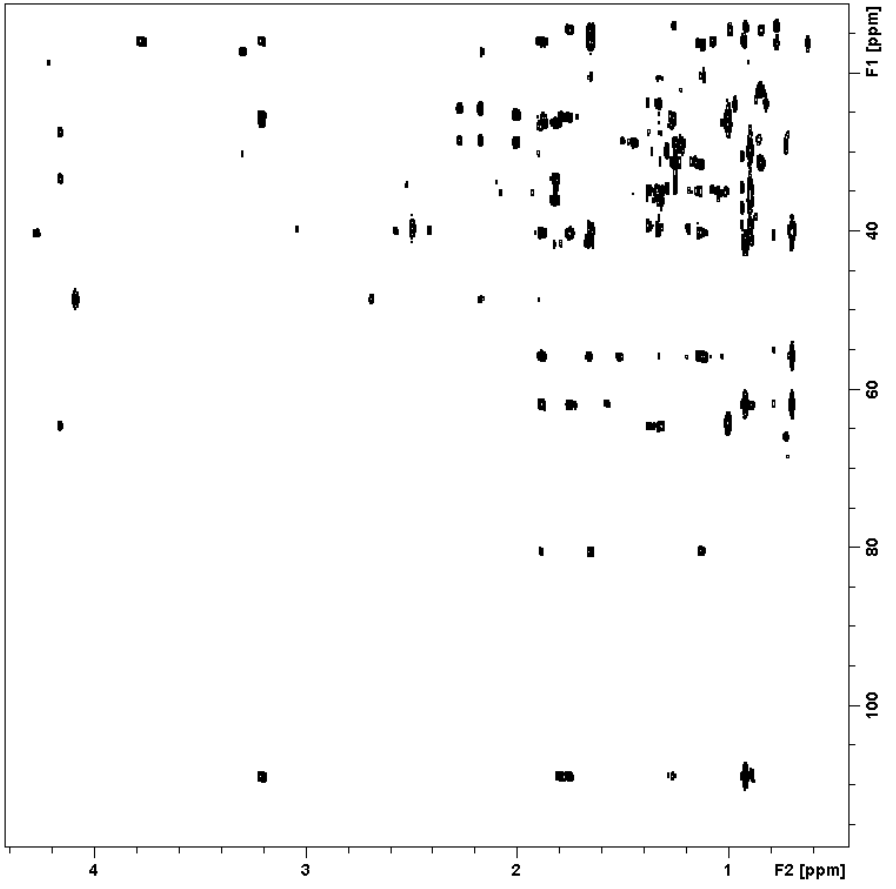

Figure S5. 2D ^{1}H-^{13}C HSQC-TOCSY NMR spectrum of sarsasapogenin (1)

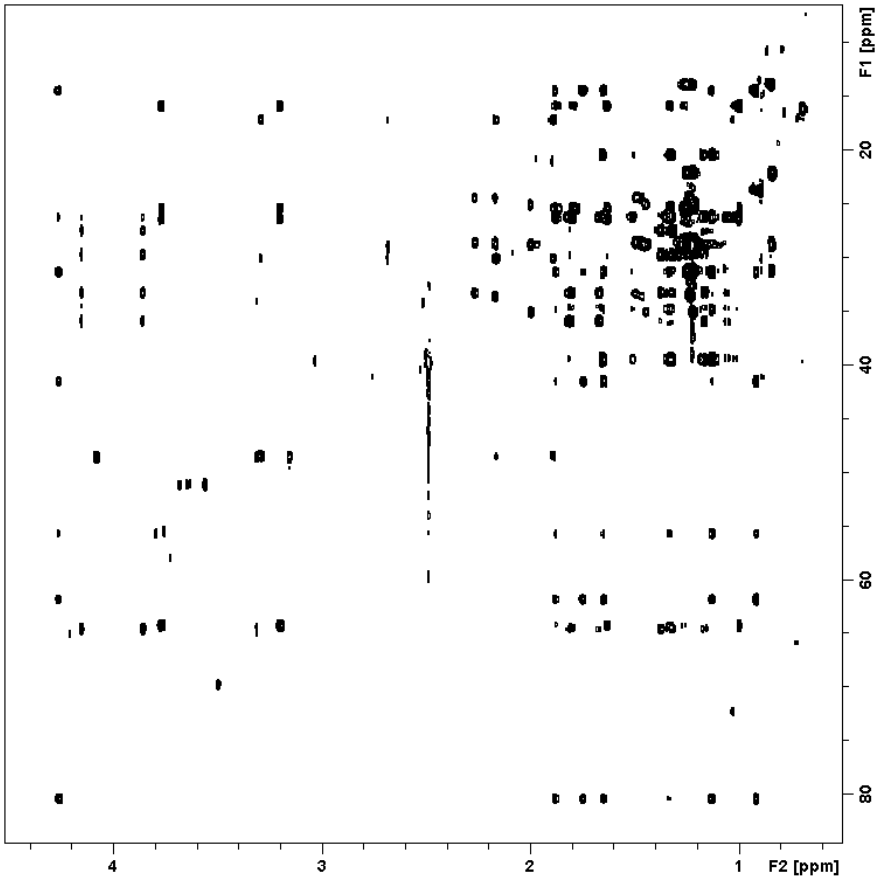

Figure S6. 2D ^{1}H-^{13}C H2BC NMR spectrum of sarsasapogenin (1)

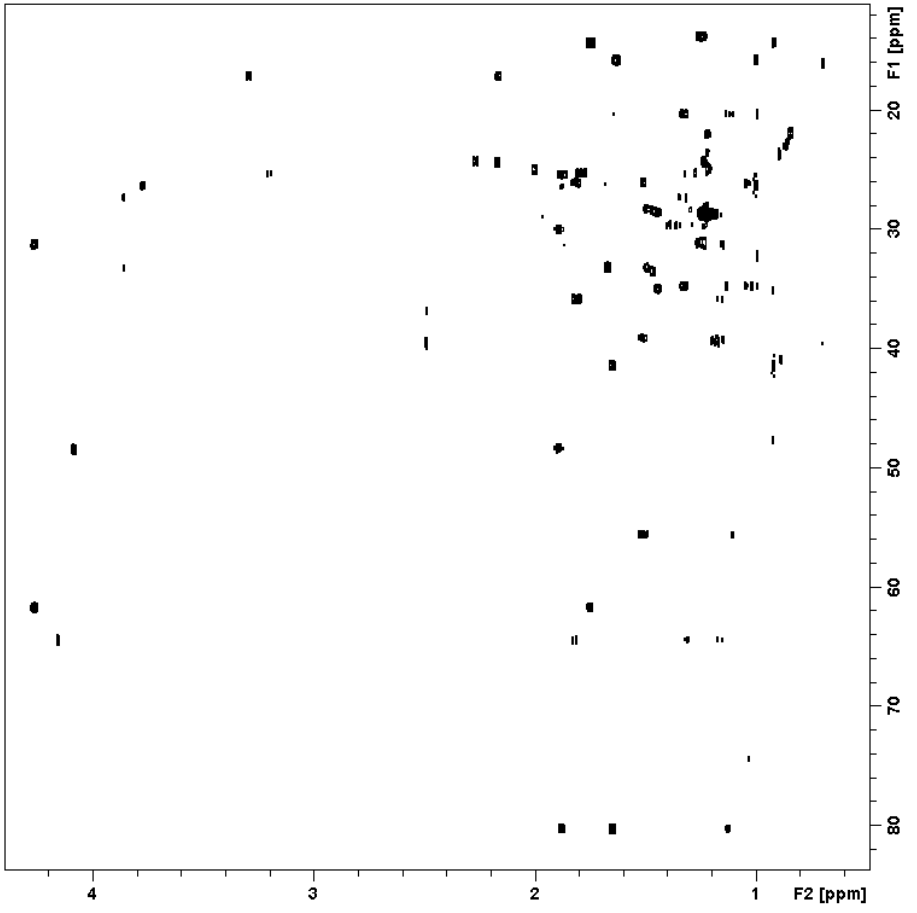

Figure S7. 2D ^{1}H-^{1}H COSY NMR spectrum of sarsasapogenin (1)

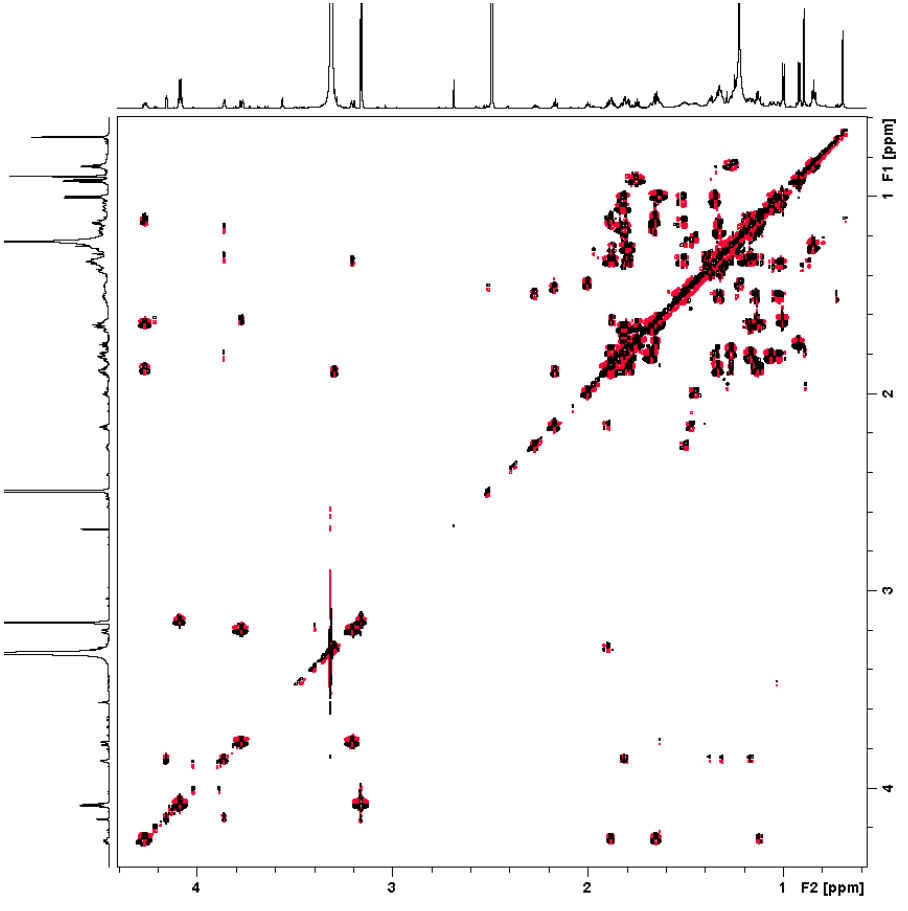

Figure S8. 2D ^{1}H-^{1}H ROESY NMR spectrum of sarsasapogenin (1)

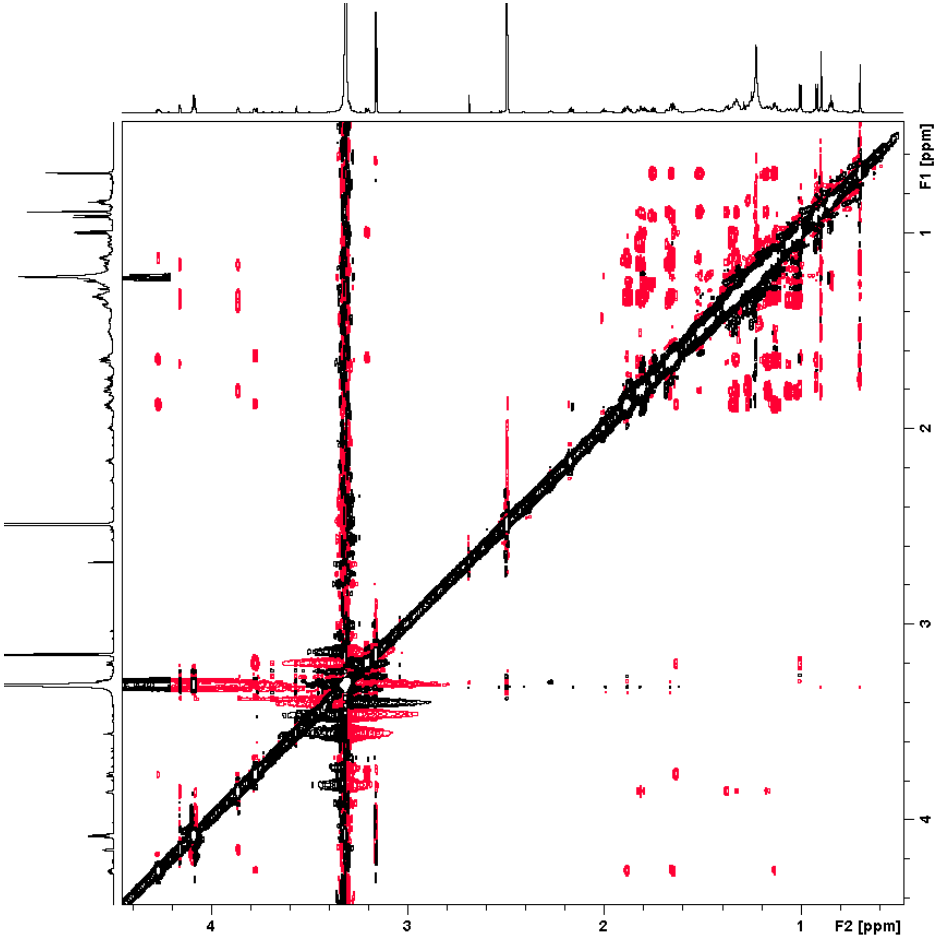

Figure S9. 1D ^{1}H NMR spectrum of sarsasapogenin 3-O-β-galactopyranoside (2)

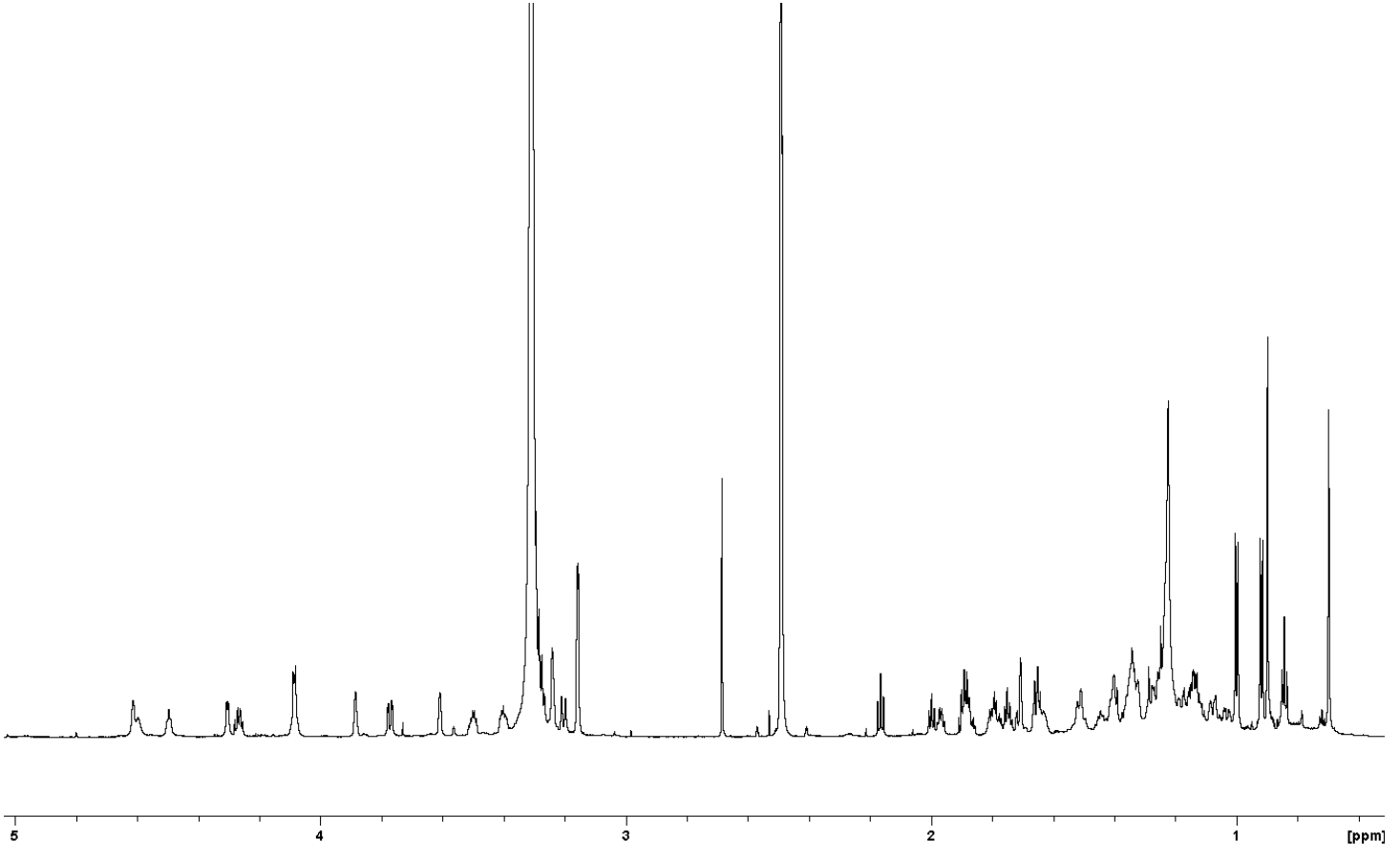

Figure S10. 2D ^{1}H-^{13}C HSQC NMR spectrum of sarsasapogenin 3-O-β-galactopyranoside (2)

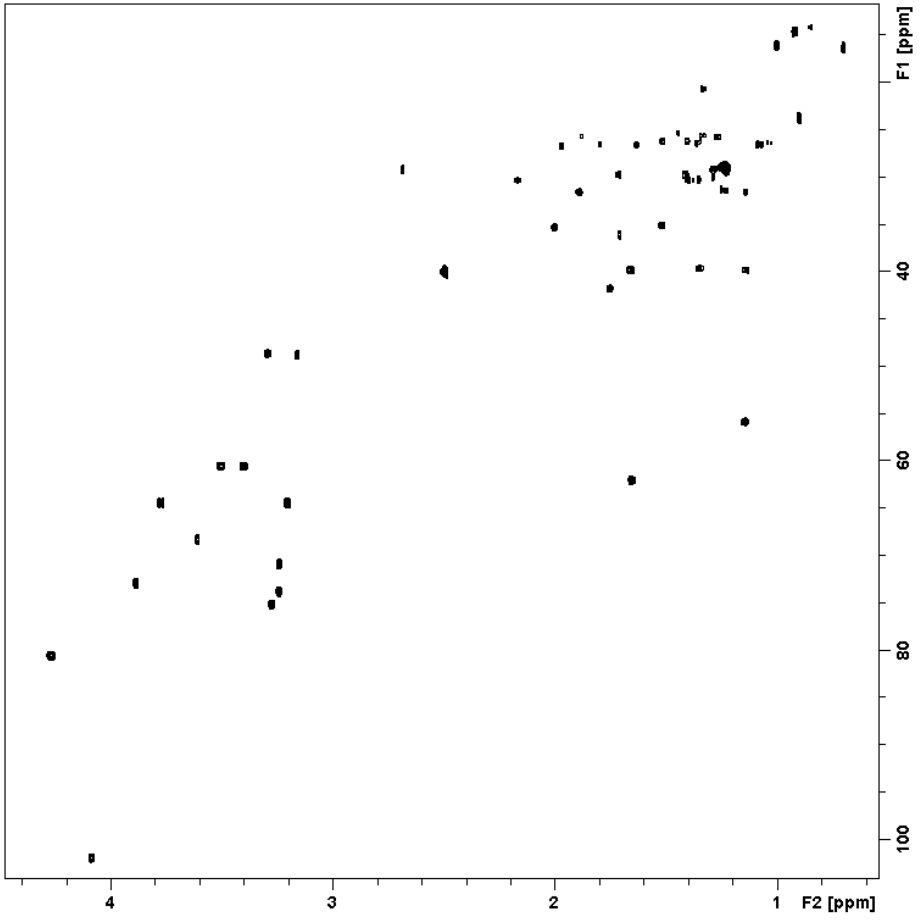

Figure S11. 2D Edited ^{1}H-^{13}C HSQC NMR spectrum of sarsasapogenin 3-O-β-galactopyranoside (2)

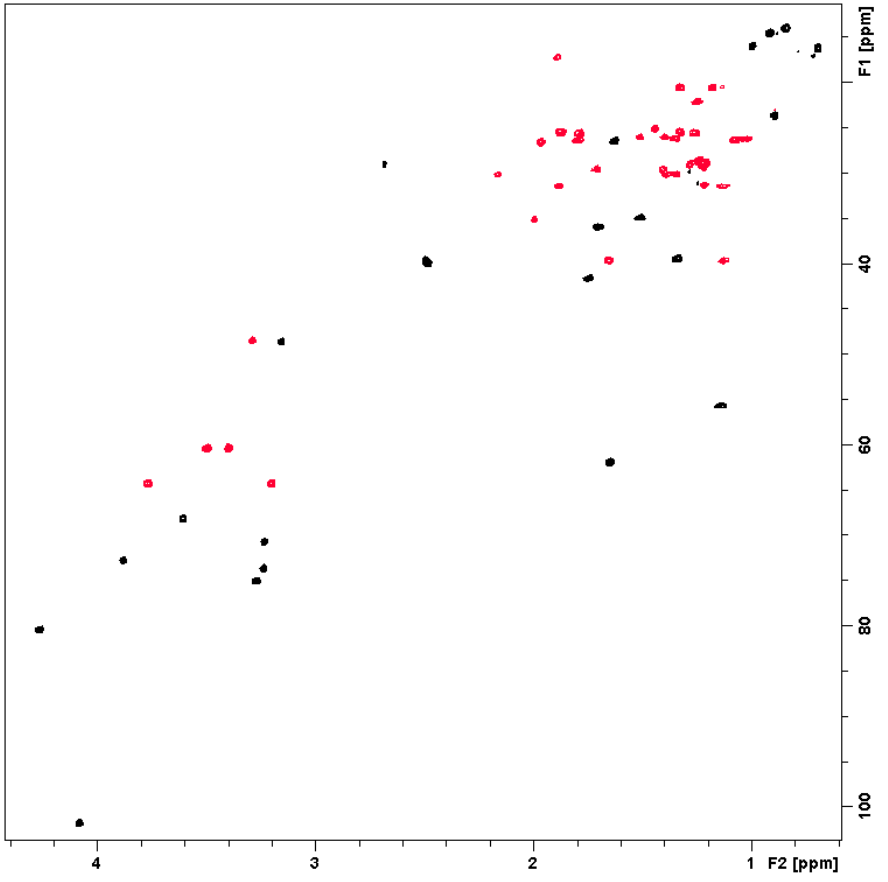

Figure S12. 2D ^{1}H-^{13}C HMBC NMR spectrum of sarsasapogenin 3-O-β-galactopyranoside (2)

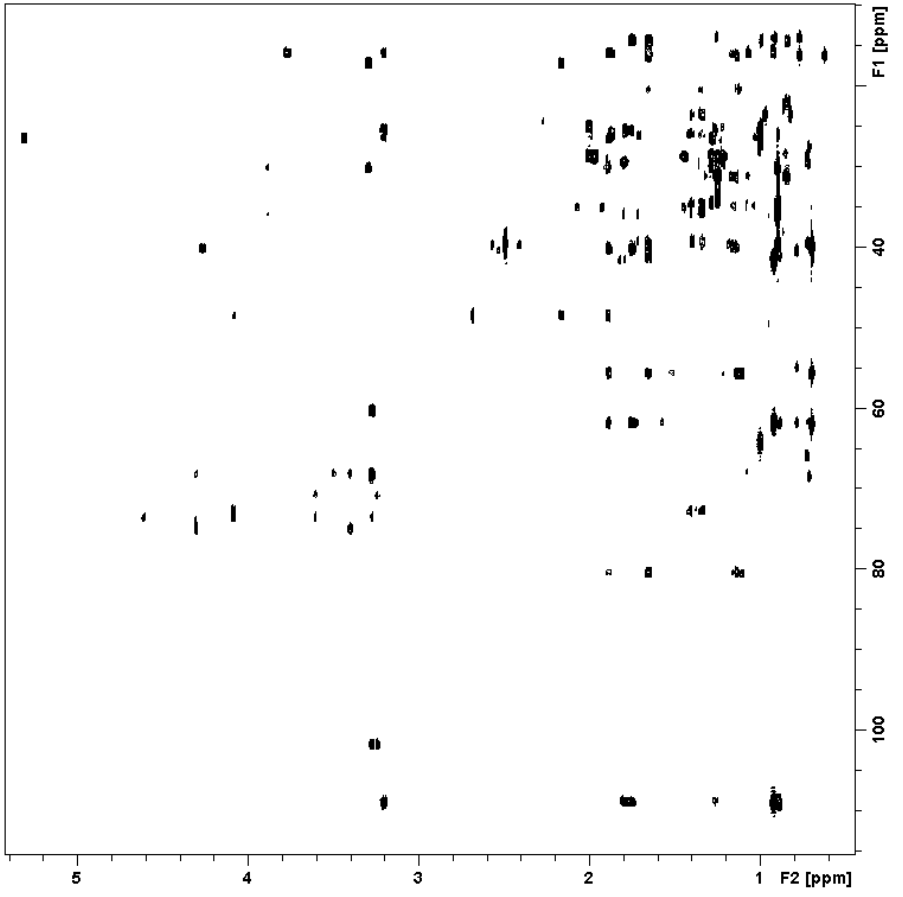

Figure S13. 2D ^{1}H-^{13}C HSQC-TOCSY NMR spectrum of sarsasapogenin 3-O-β-galactopyranoside (2)

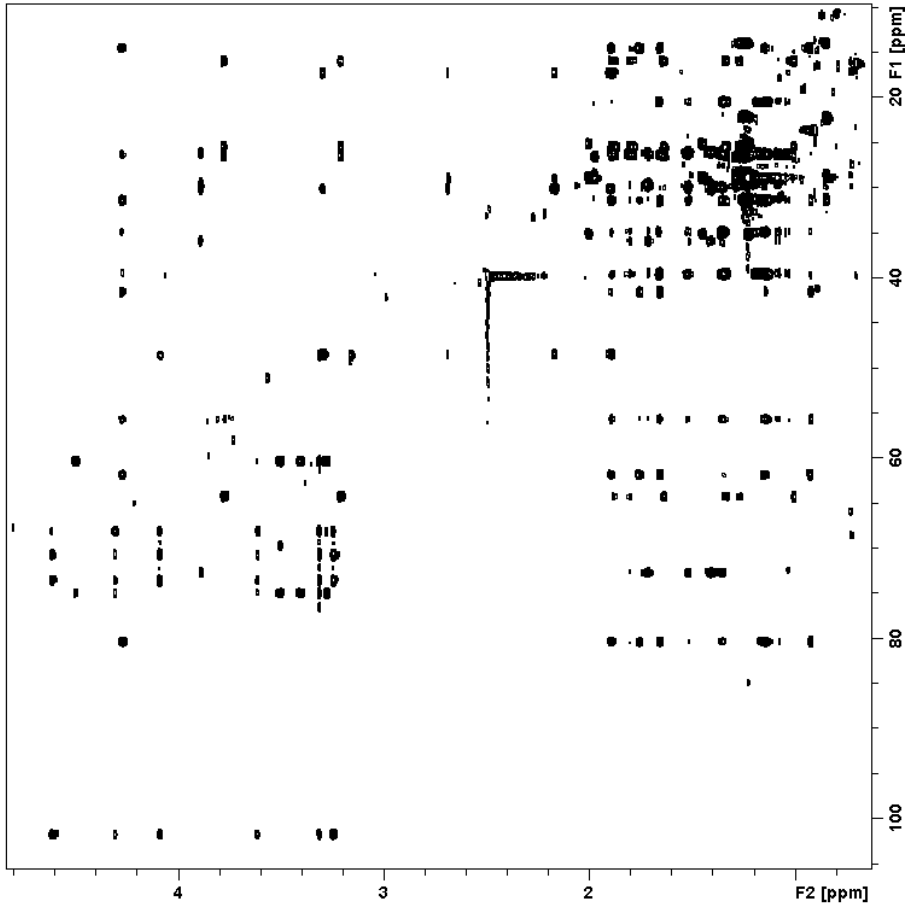

Figure S14. 2D ^{1}H-^{13}C H2BC NMR spectrum of sarsasapogenin 3-O-β-galactopyranoside (2)

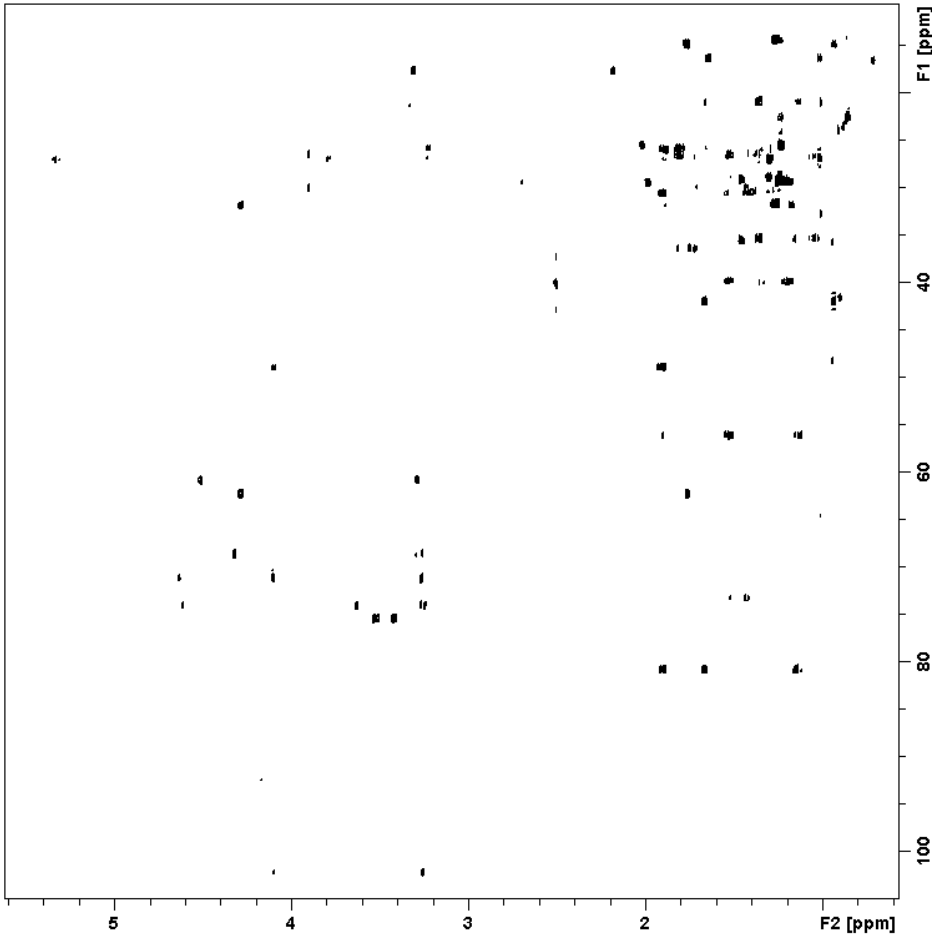

Figure S15. 2D ^{1}H-^{1}H COSY NMR spectrum of sarsasapogenin 3-O-β-galactopyranoside (2)

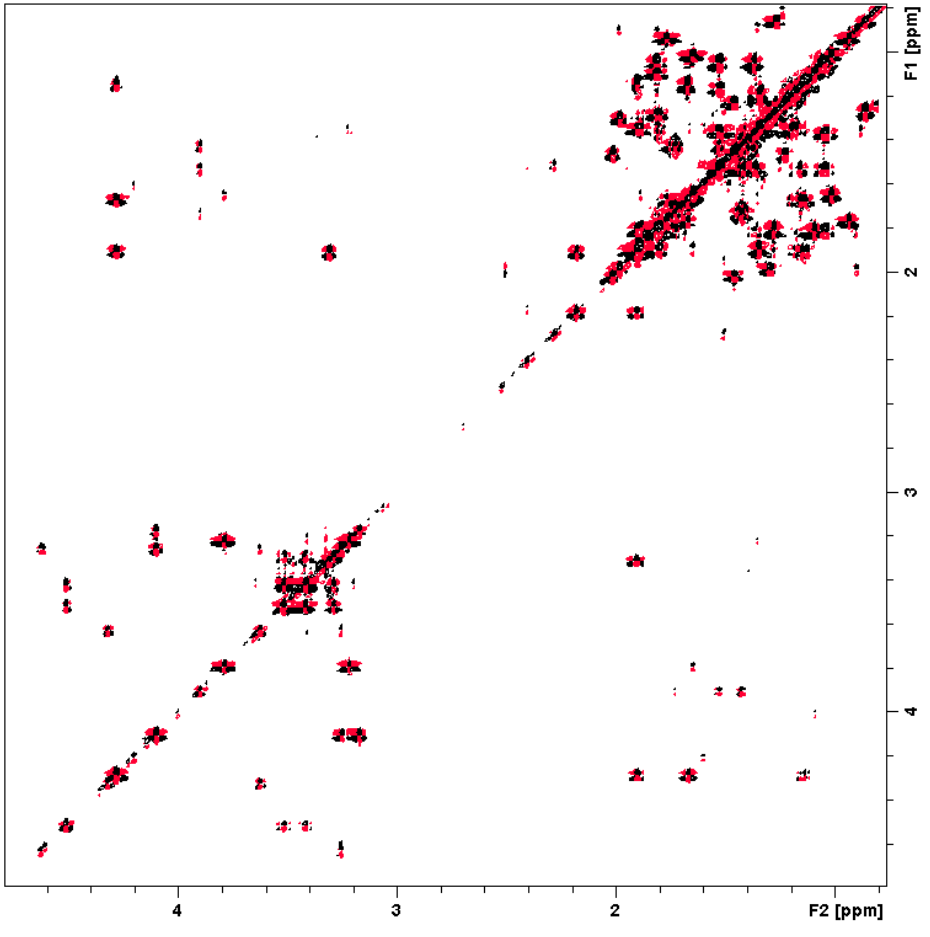

Figure S16. 2D ^{1}H-^{1}H ROESY NMR spectrum of sarsasapogenin 3-O-β-galactopyranoside (2)

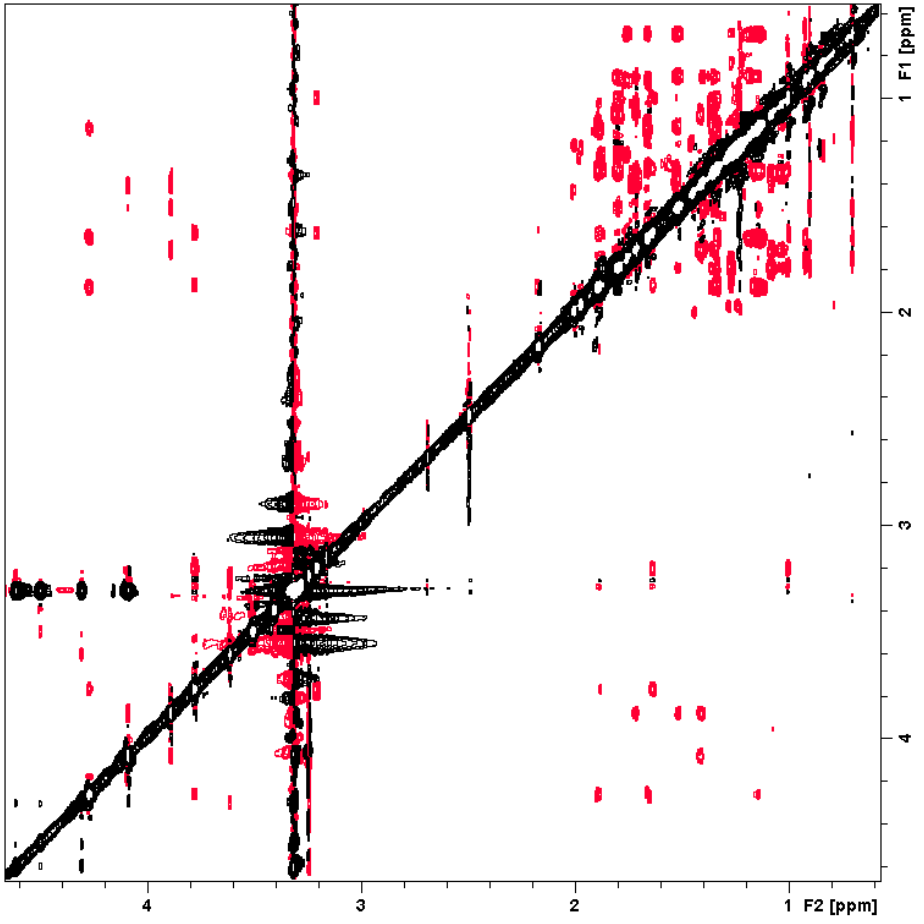

Figure S17. 1D ^{1}H NMR spectrum of sarsasapogenin 3-O-(2'-O-β-glucopyranosyl-β-galactopyranoside) (3)

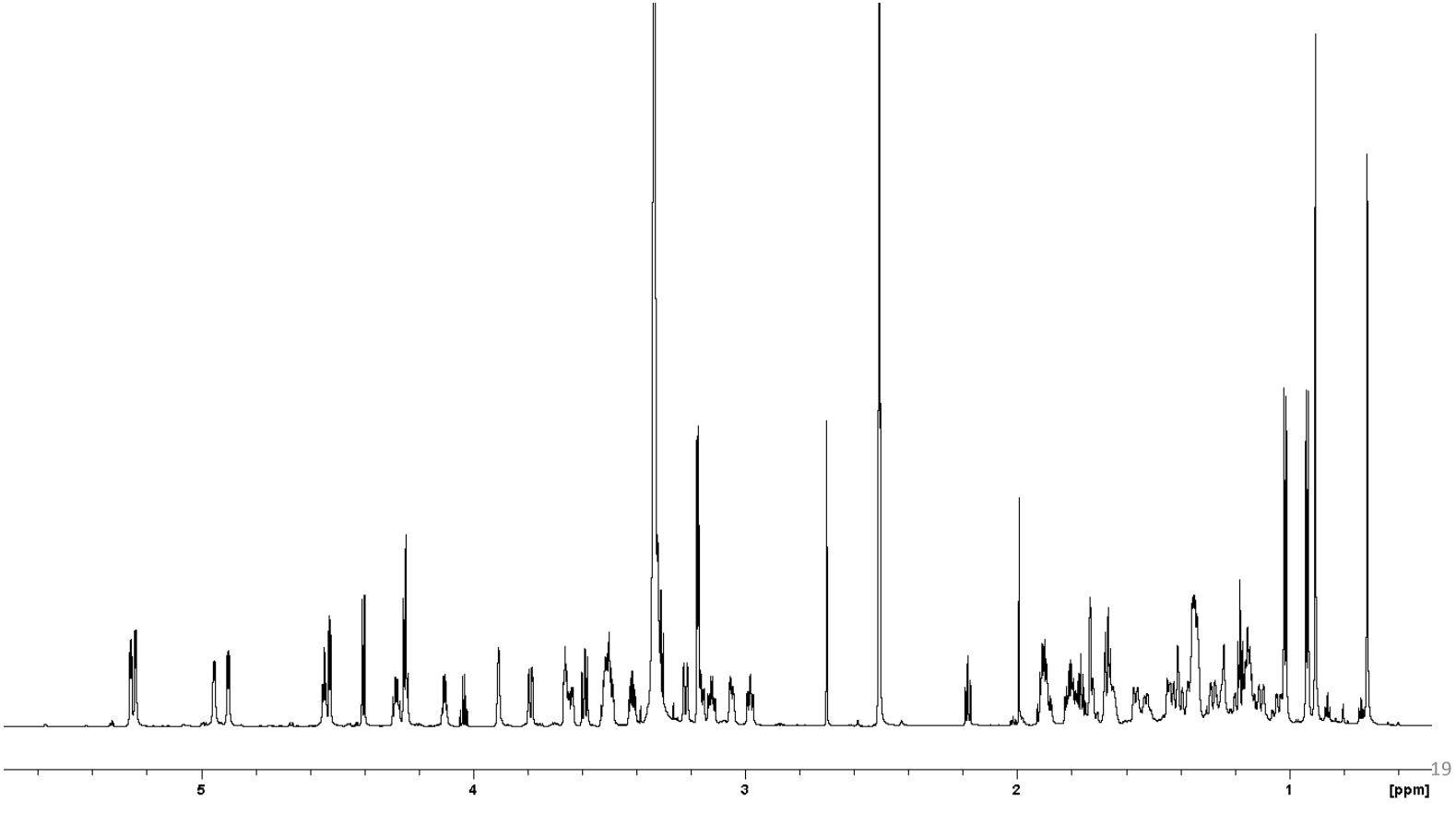

Figure S18. 1D ^{13}C CAPT NMR spectrum of sarsasapogenin 3-O-(2'-O-β-glucopyranosyl-β-galactopyranoside) (3)

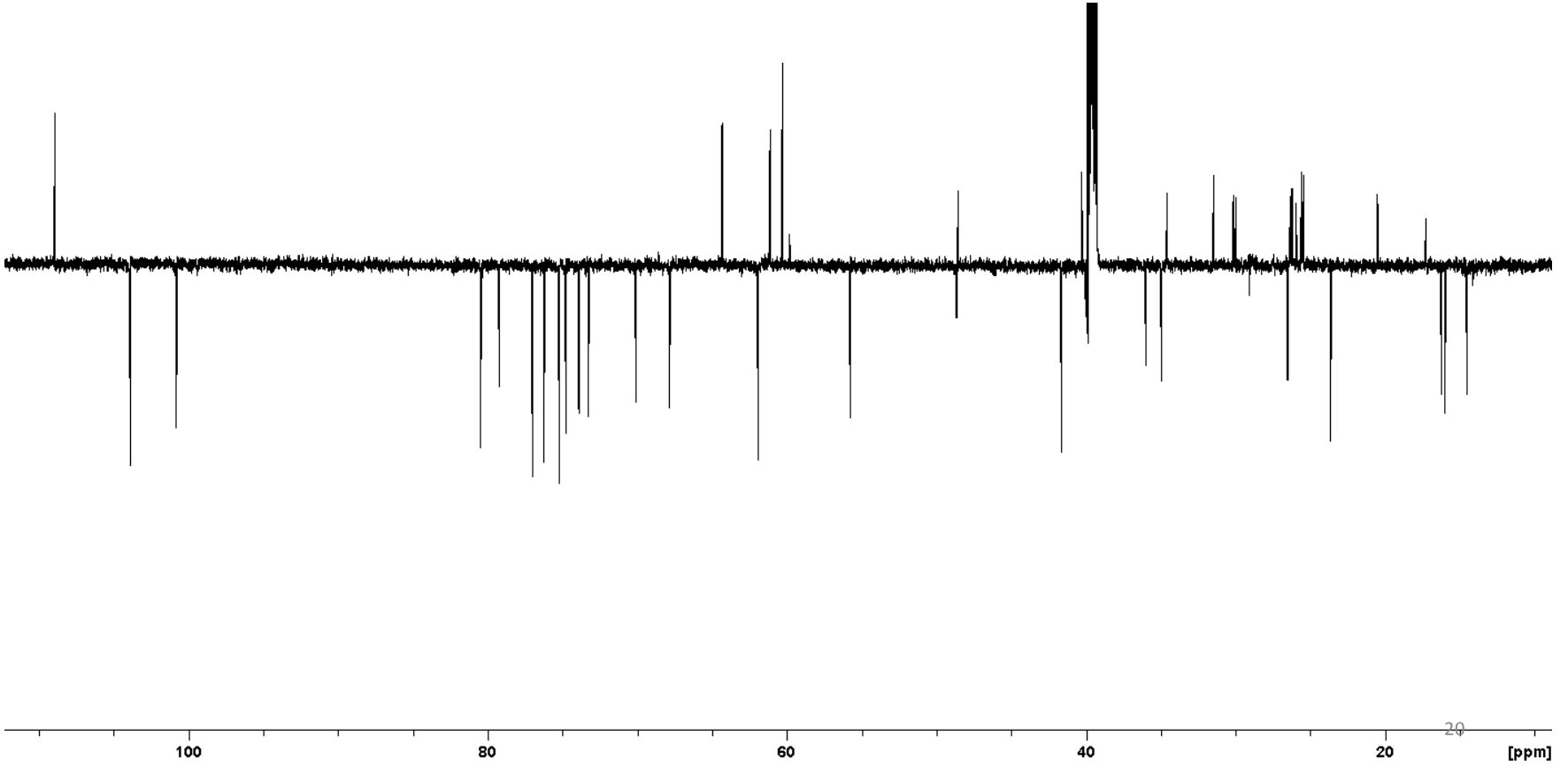

Figure S19. 2D ^{1}H-^{13}C HSQC NMR spectrum of sarsasapogenin 3-O-(2'-O-β-glucopyranosyl-β-galactopyranoside) (3)

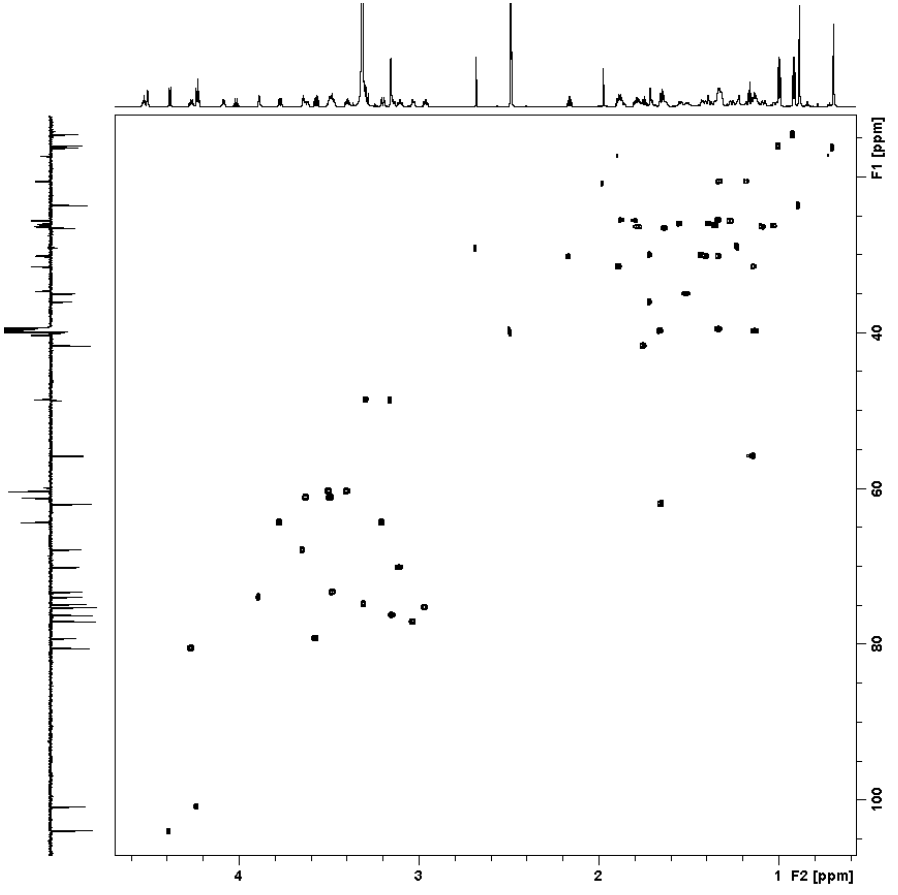

Figure S20. 2D Edited ^{1}H-^{13}C HSQC NMR spectrum of sarsasapogenin 3-O-(2'-O-β-glucopyranosyl-β-galactopyranoside) (3)

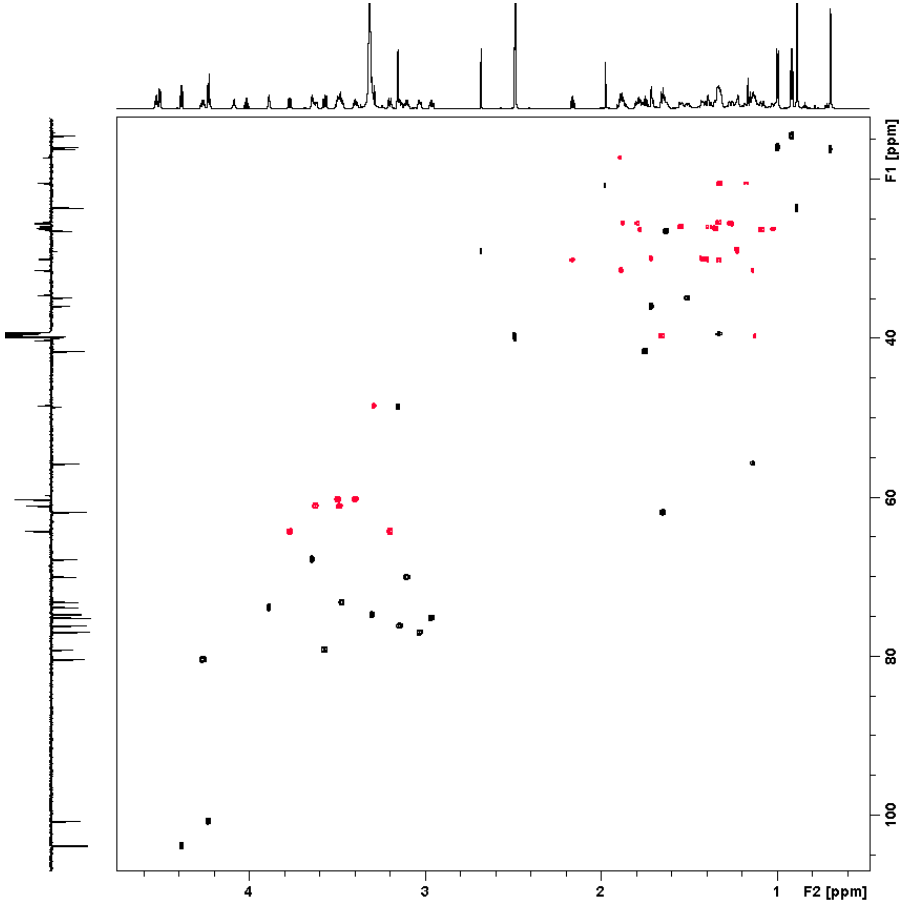

Figure S21. 2D ^{1}H-^{13}C HMBC NMR spectrum of sarsasapogenin 3-O-(2'-O-β-glucopyranosyl-β-galactopyranoside) (3)

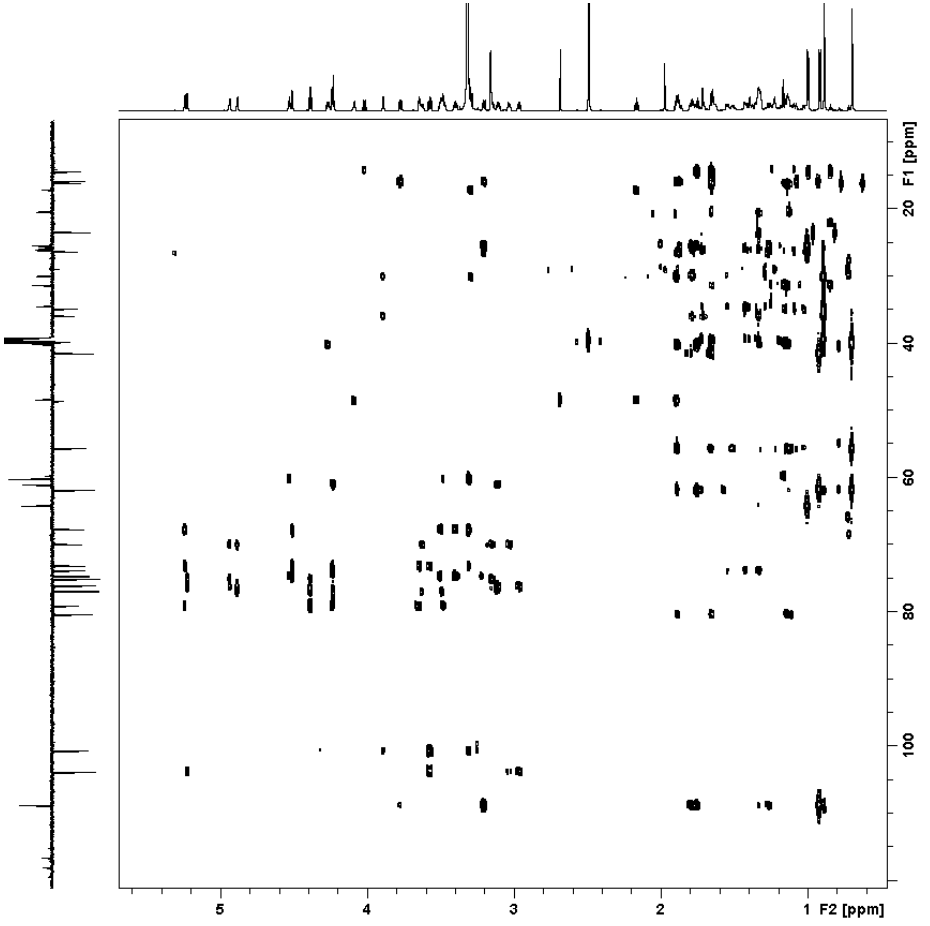

Figure S22. 2D ^{1}H-^{13}C HSQC-TOCSY NMR spectrum of sarsasapogenin 3-O-(2'-O-β-glucopyranosyl-β-galactopyranoside) (3)

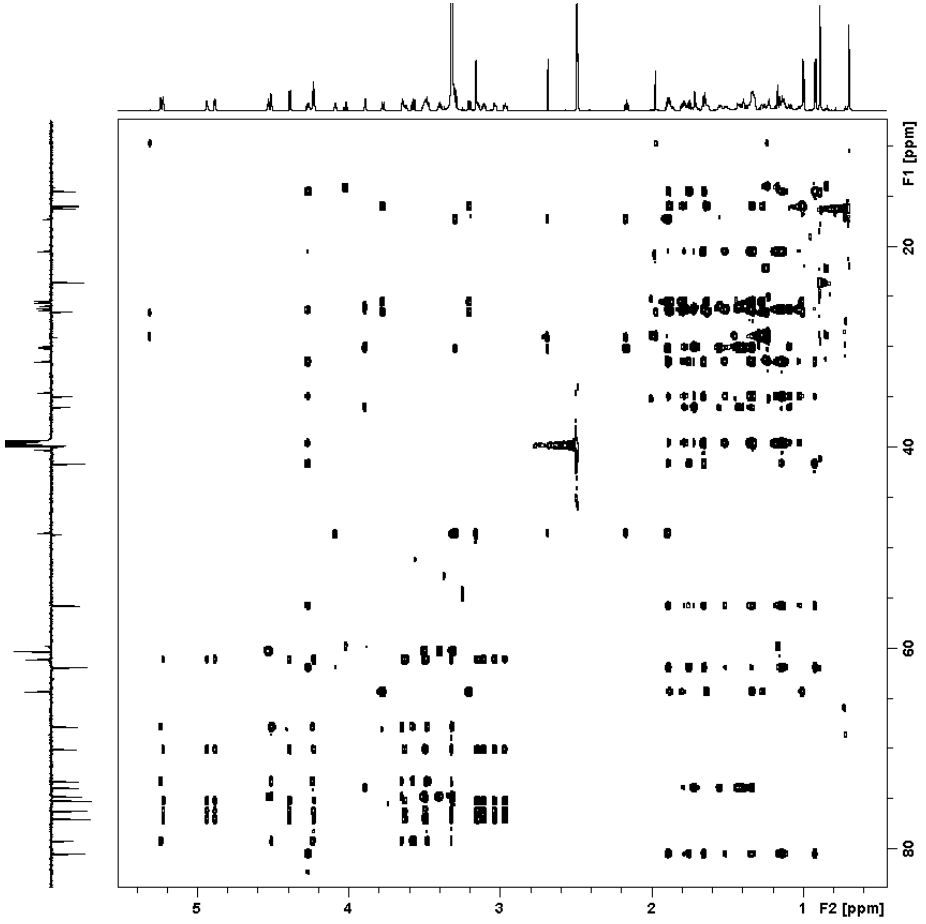

Figure S23. 2D ^{1}H-^{13}C H2BC NMR spectrum of sarsasapogenin 3-O-(2'-O-β-glucopyranosyl-β-galactopyranoside) (3)

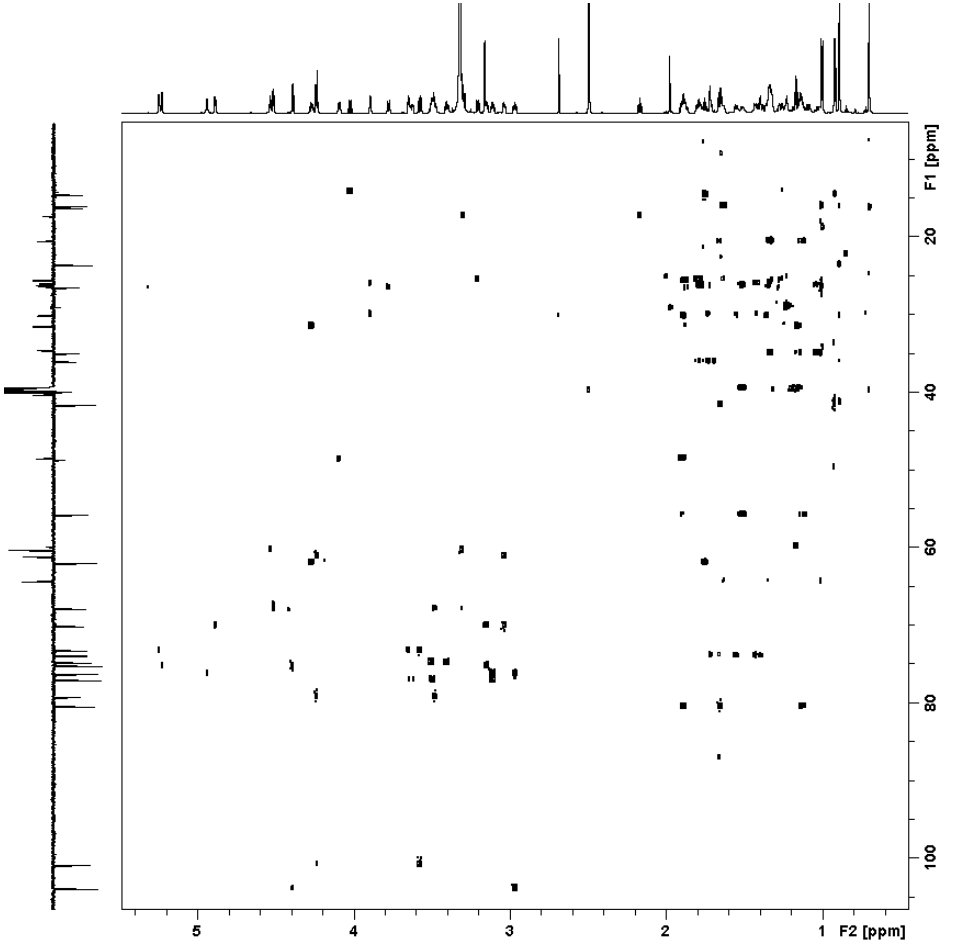

Figure S24. 2D ^{1}H-^{1}H COSY NMR spectrum of sarsasapogenin 3-O-(2'-O-β-glucopyranosyl-β-galactopyranoside) (3)

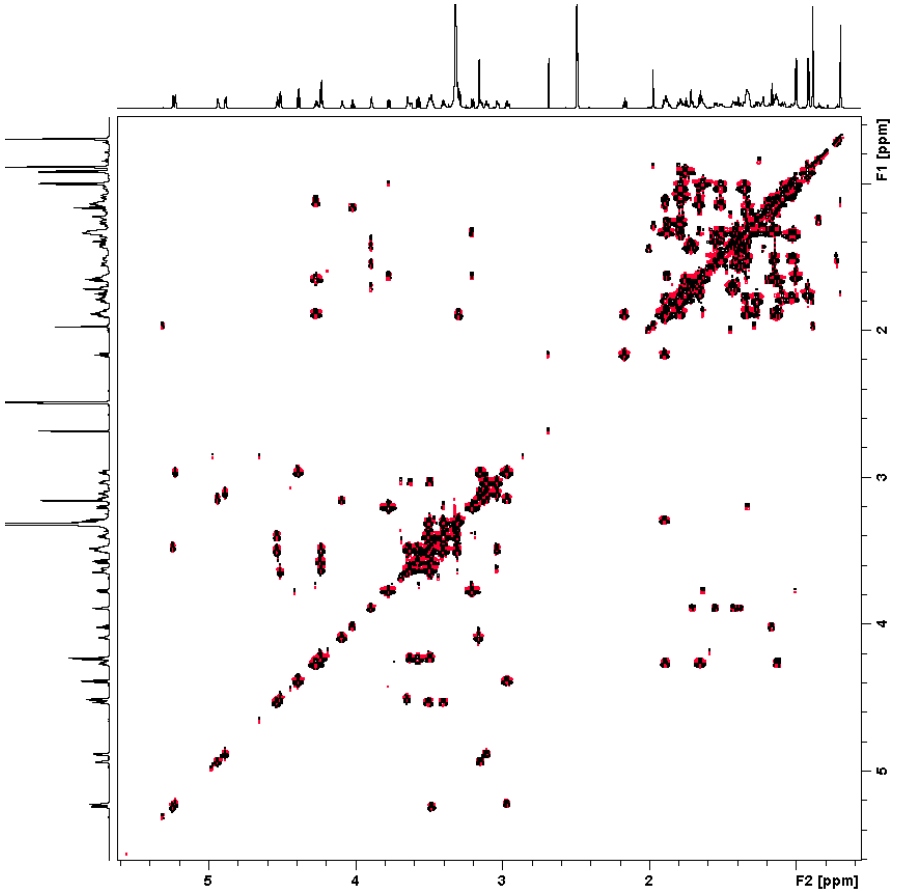

Figure S25. 2D ^{1}H-^{1}H ROESY NMR spectrum of sarsasapogenin 3-O-(2'-O-β-glucopyranosyl-β-galactopyranoside) (3)

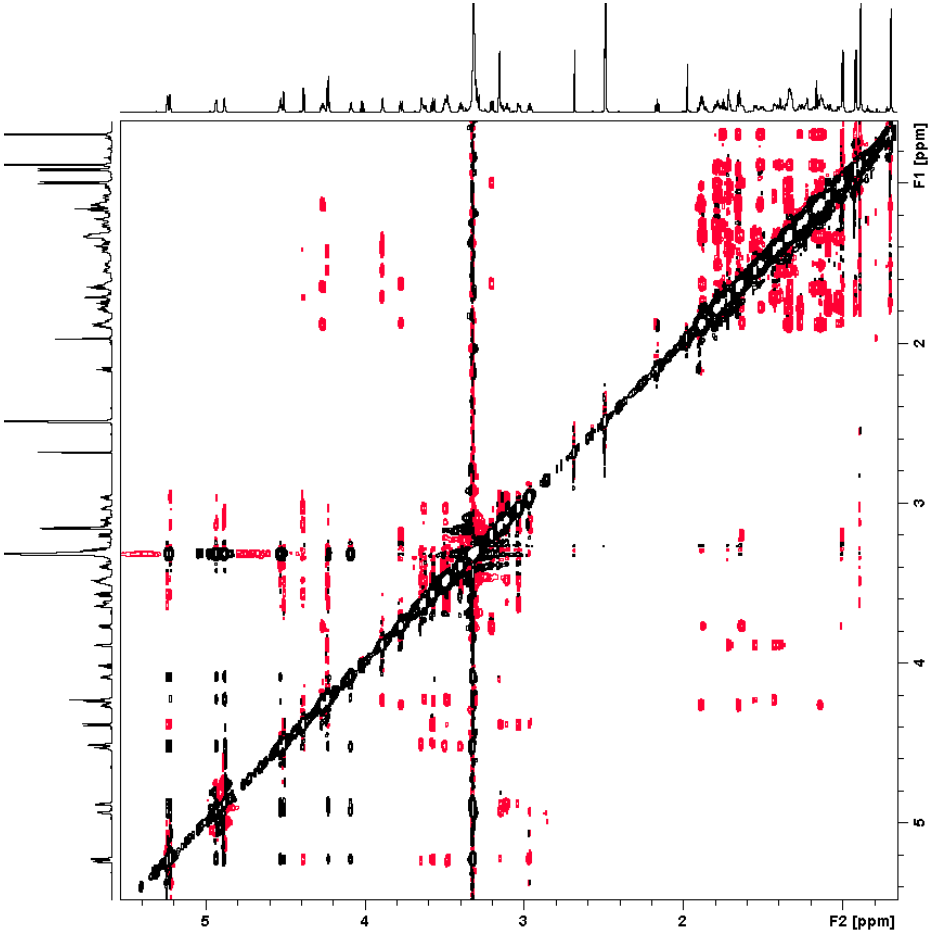

Figure S26. 1D ^{1}H NMR spectrum of sarsasapogenin 3-O-(2'-O-β-glucopyranosyl-3'-O-α-arabinopyranosyl-β-galactopyranoside) (4)

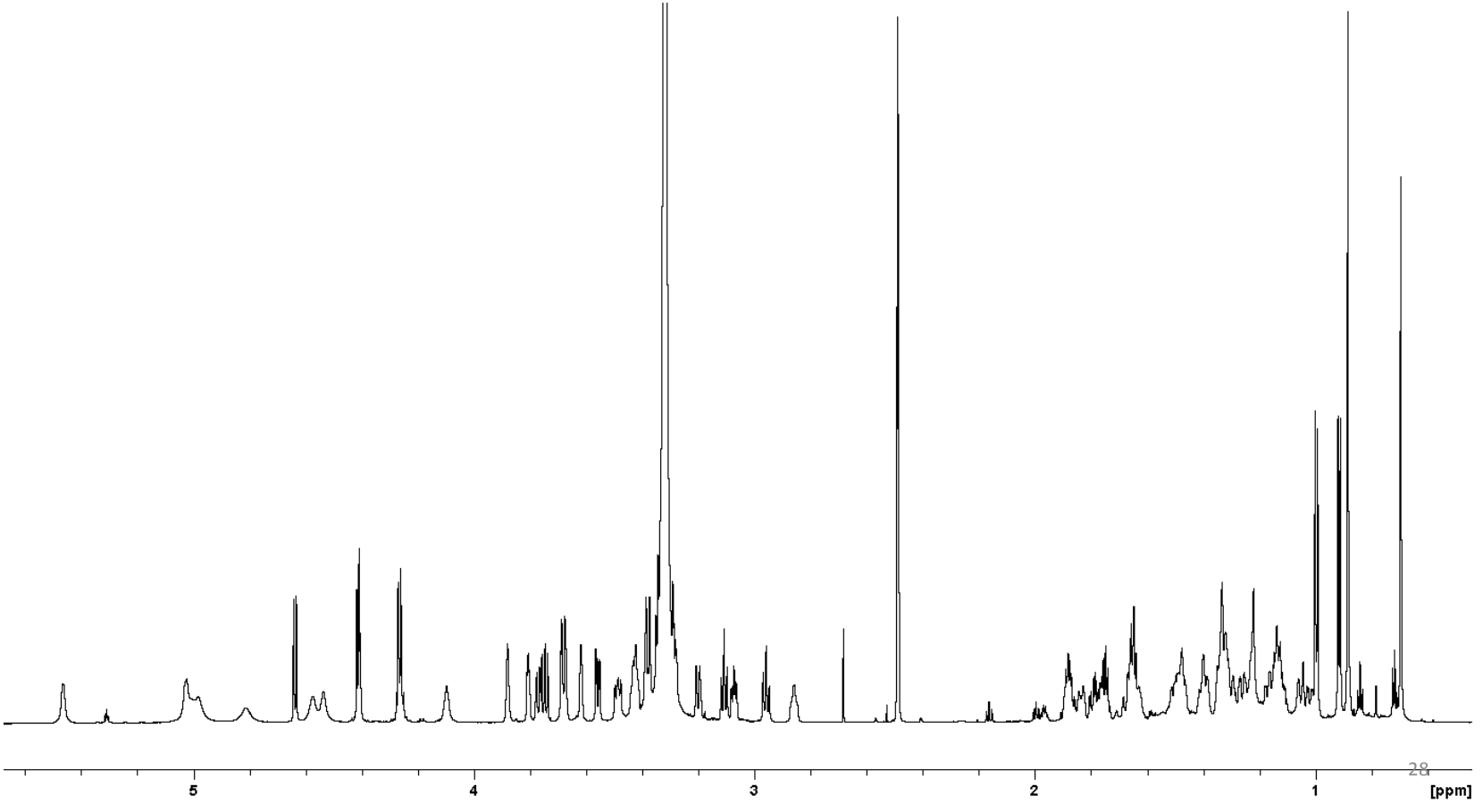

Figure S27. 1D ^{13}C CAPT NMR spectrum of sarsasapogenin 3-O-(2'-O-β-glucopyranosyl-3'-O-α-arabinopyranosyl-β-galactopyranoside) (4)

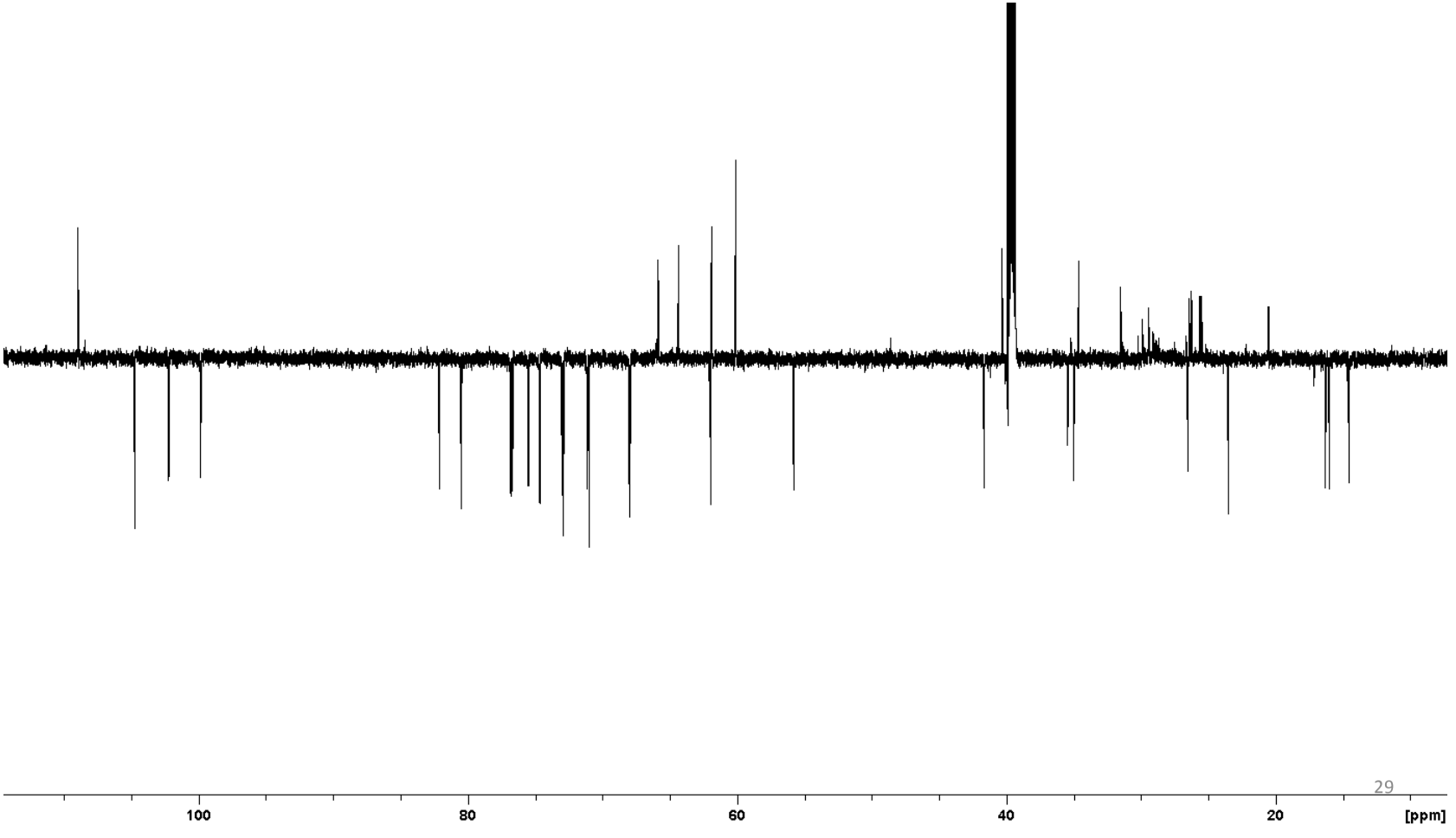

Figure S28. 2D ^{1}H-^{13}C HSQC spectrum of sarsasapogenin 3-O-(2'-O-β-glucopyranosyl-3'-O-α-arabinopyranosyl-β-galactopyranoside) (4)

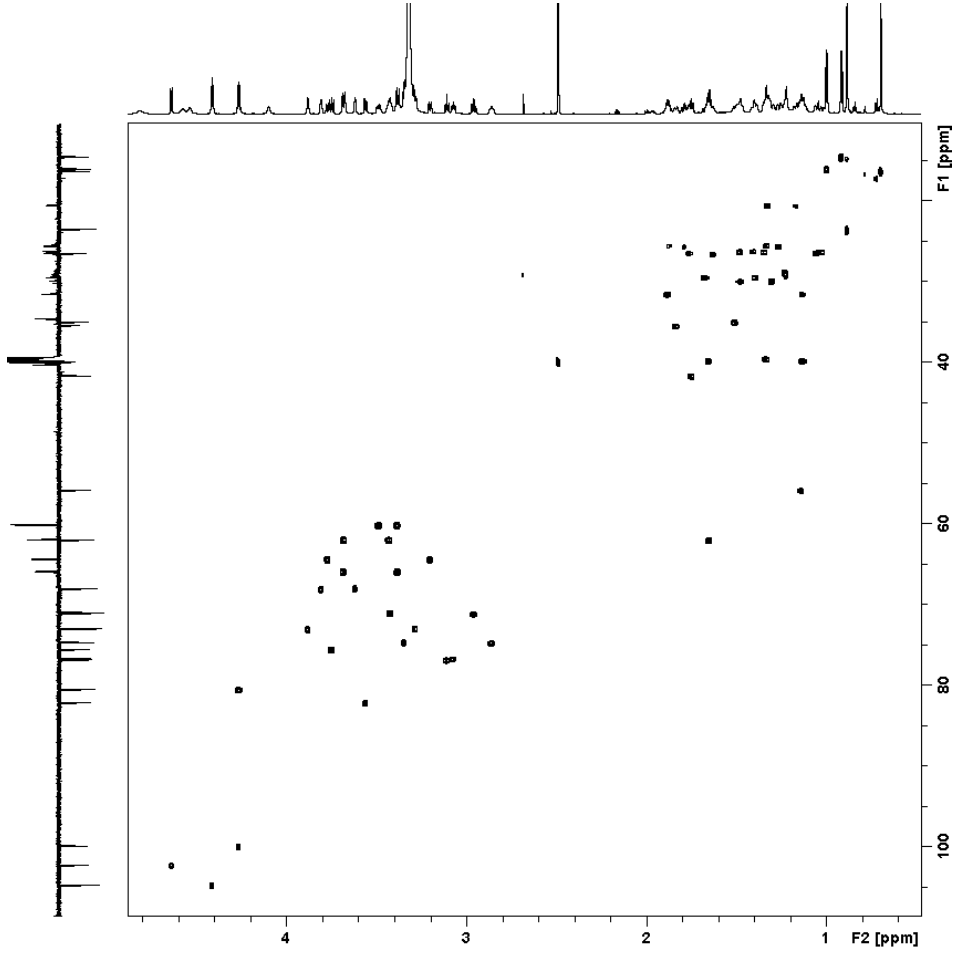

Figure S29. 2D Edited ^{1}H-^{13}C HSQC spectrum of sarsasapogenin 3-O-(2'-O-β-glucopyranosyl-3'-O-α-arabinopyranosyl-β-galactopyranoside) (4)

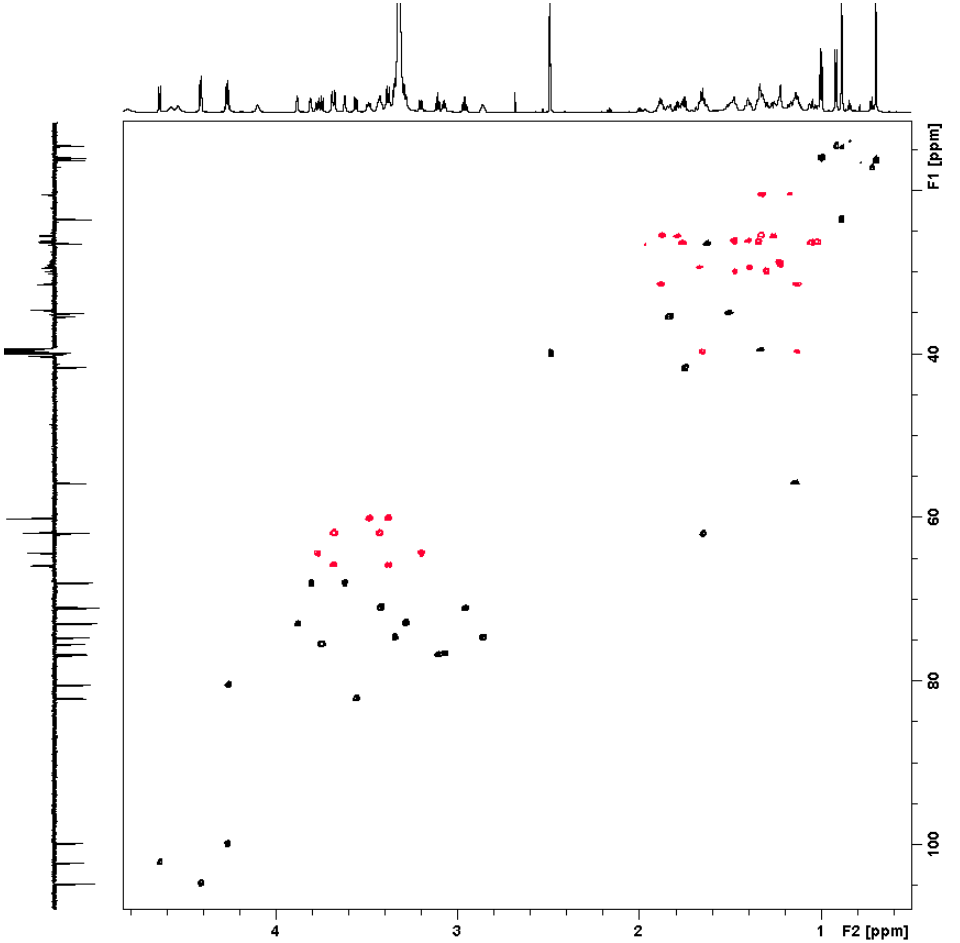

Figure S30. 2D ^{1}H-^{13}C HMBC spectrum of sarsasapogenin 3-O-(2'-O-β-glucopyranosyl-3'-O-α-arabinopyranosyl-β-galactopyranoside) (4)

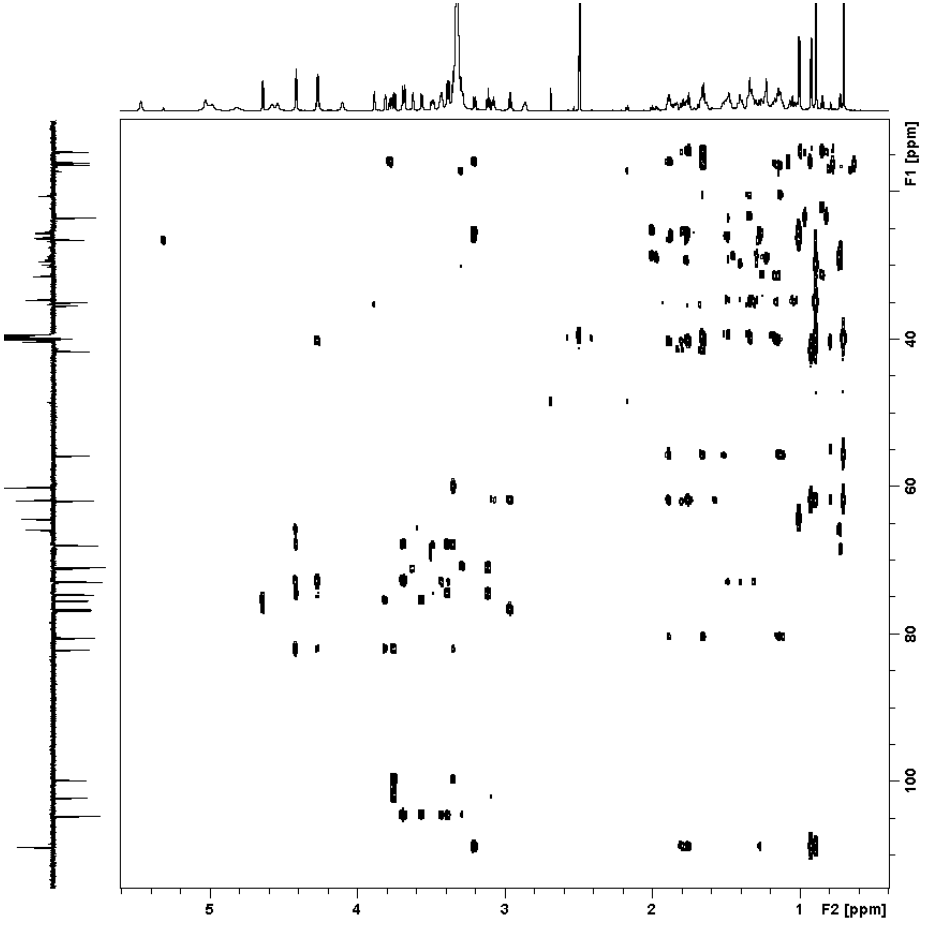

Figure S31. 2D ^{1}H-^{13}C HSQC-TOCSY spectrum of sarsasapogenin 3-O-(2'-O-β-glucopyranosyl-3'-O-α-arabinopyranosyl-β-galactopyranoside) (4)

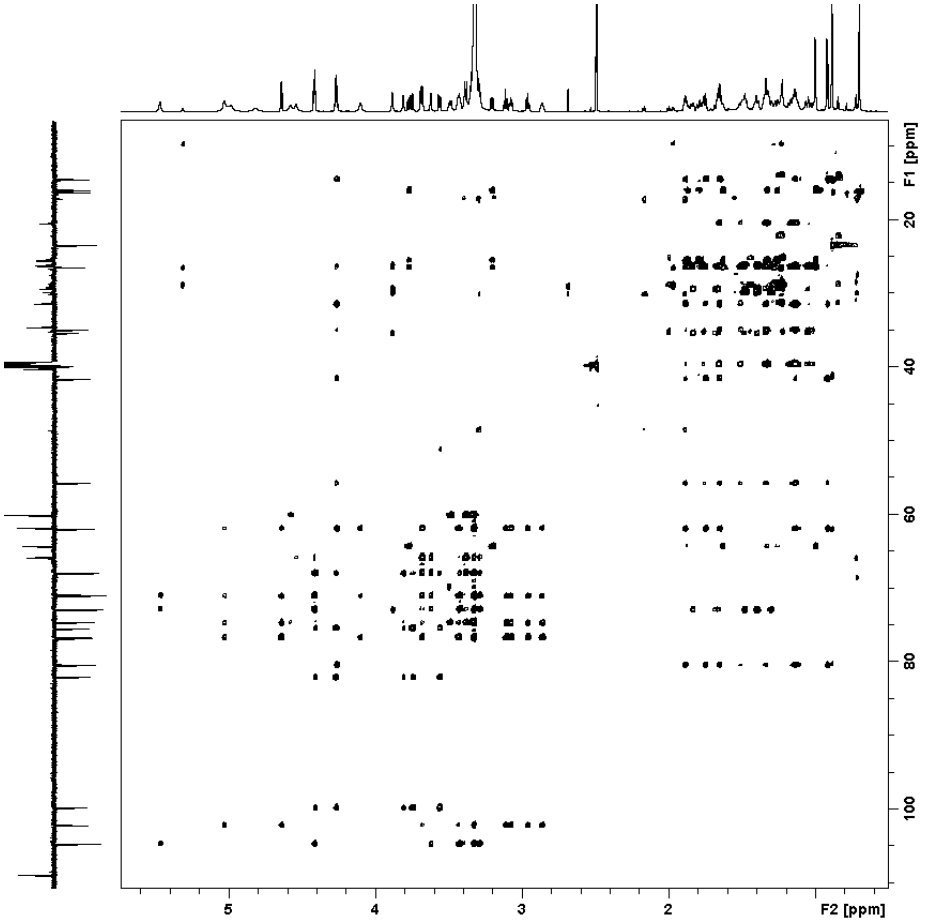

Figure S32. 2D ^{1}H-^{13}C H2BC spectrum of sarsasapogenin 3-O-(2'-O-β-glucopyranosyl-3'-O-α-arabinopyranosyl-β-galactopyranoside) (4)

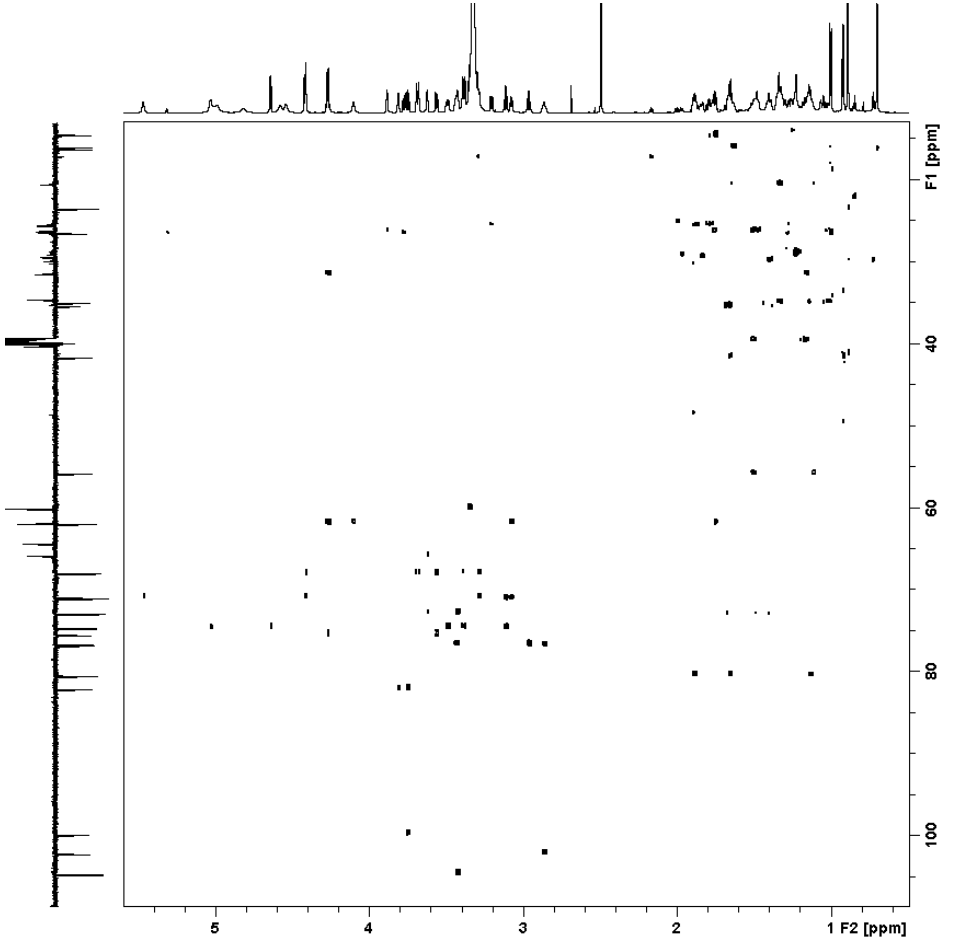

Figure S33. 2D ^{1}H-^{1}H COSY spectrum of sarsasapogenin 3-O-(2'-O-β-glucopyranosyl-3'-O-α-arabinopyranosyl-β-galactopyranoside) (4)

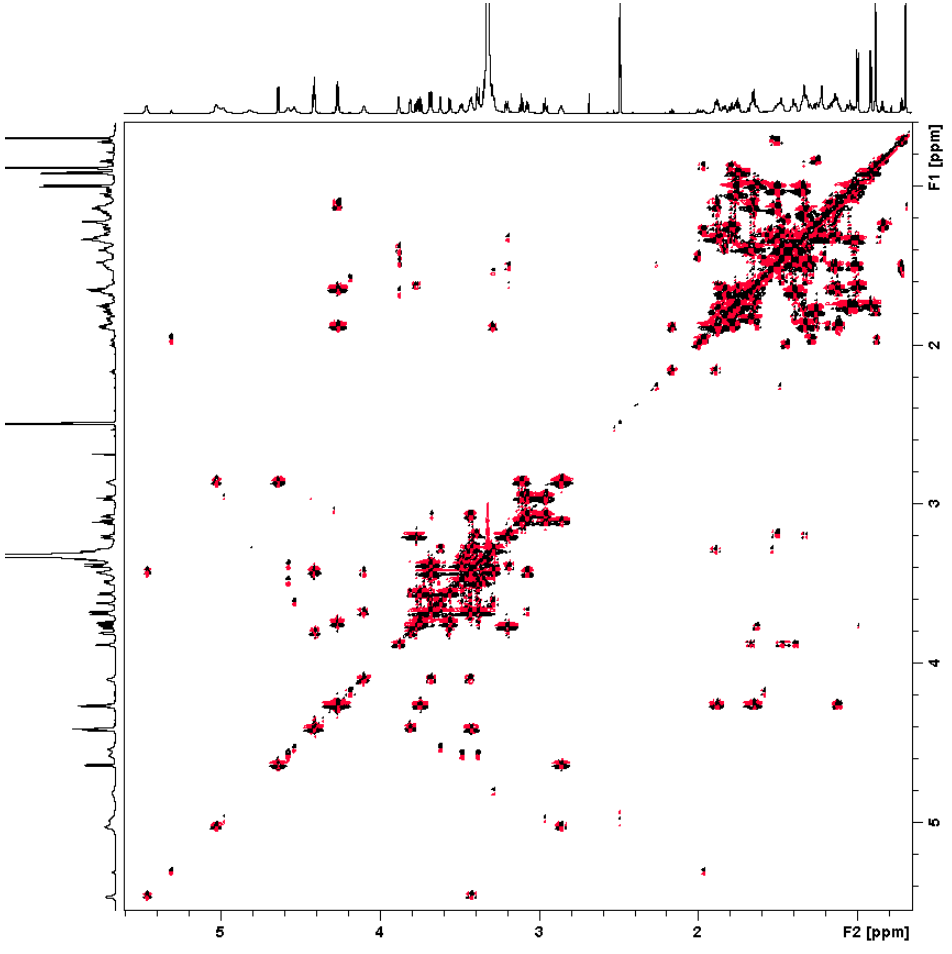

Figure S34. 2D ^{1}H-^{1}H ROESY spectrum of sarsasapogenin 3-O-(2'-O-β-glucopyranosyl-3'-O-α-arabinopyranosyl-β-galactopyranoside) (4)

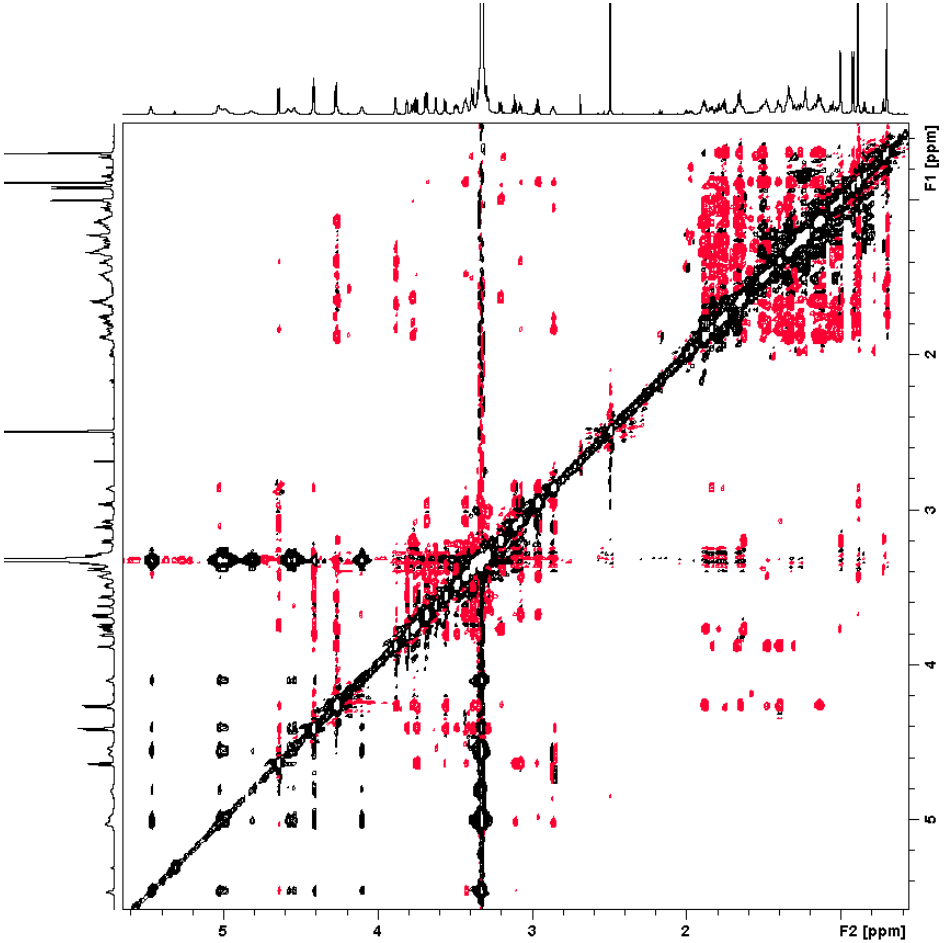

Figure S35. 1D ^{1}H NMR spectrum of Chrysoeriol 6-C-β-arabinofuranosyl-8-C-β-glucopyranoside (5)

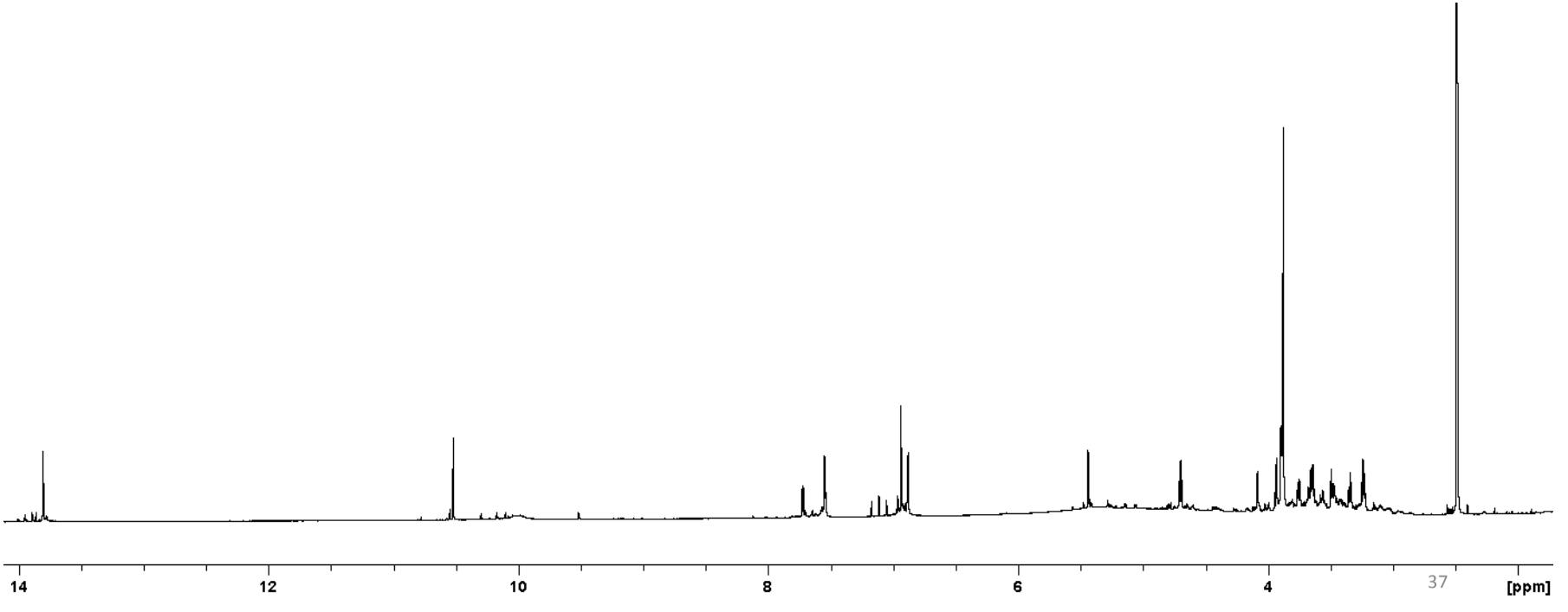

Figure S36. 2D ^{1}H-^{13}C HSQC spectrum of Chrysoeriol 6-C-β-arabinofuranosyl-8-C-β-glucopyranoside (5)

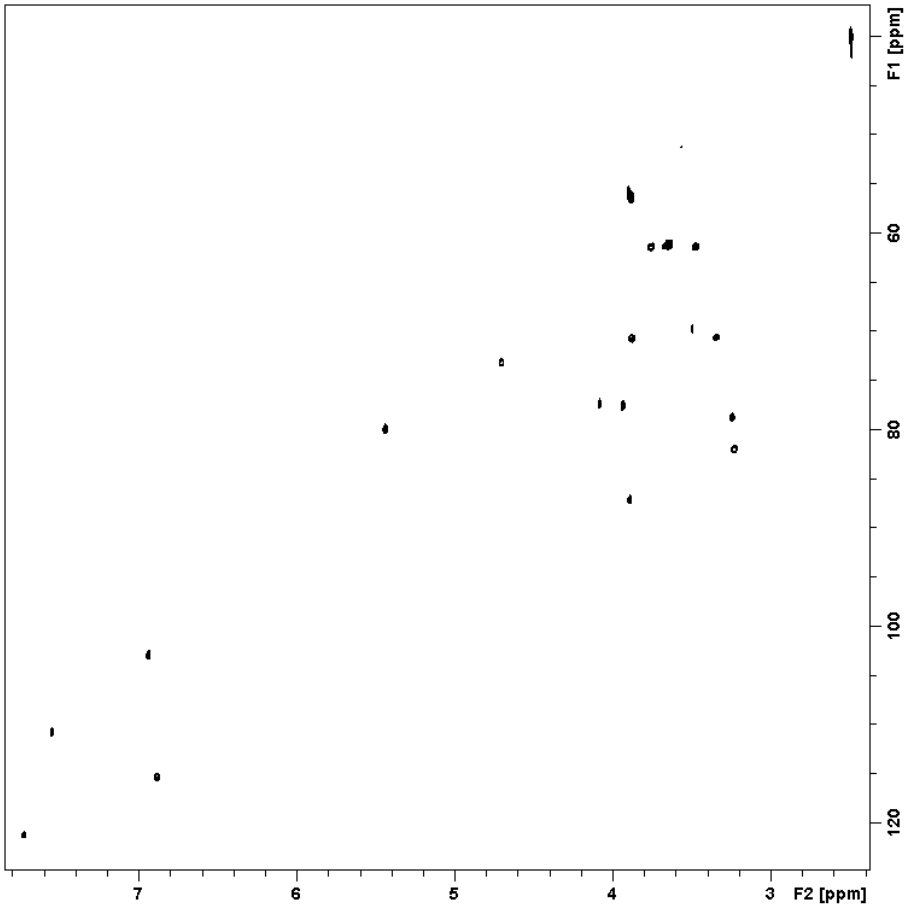

Figure S37. 2D Edited ^{1}H-^{13}C HSQC spectrum of Chrysoeriol 6-C-β-arabinofuranosyl-8-C-β-glucopyranoside (5)

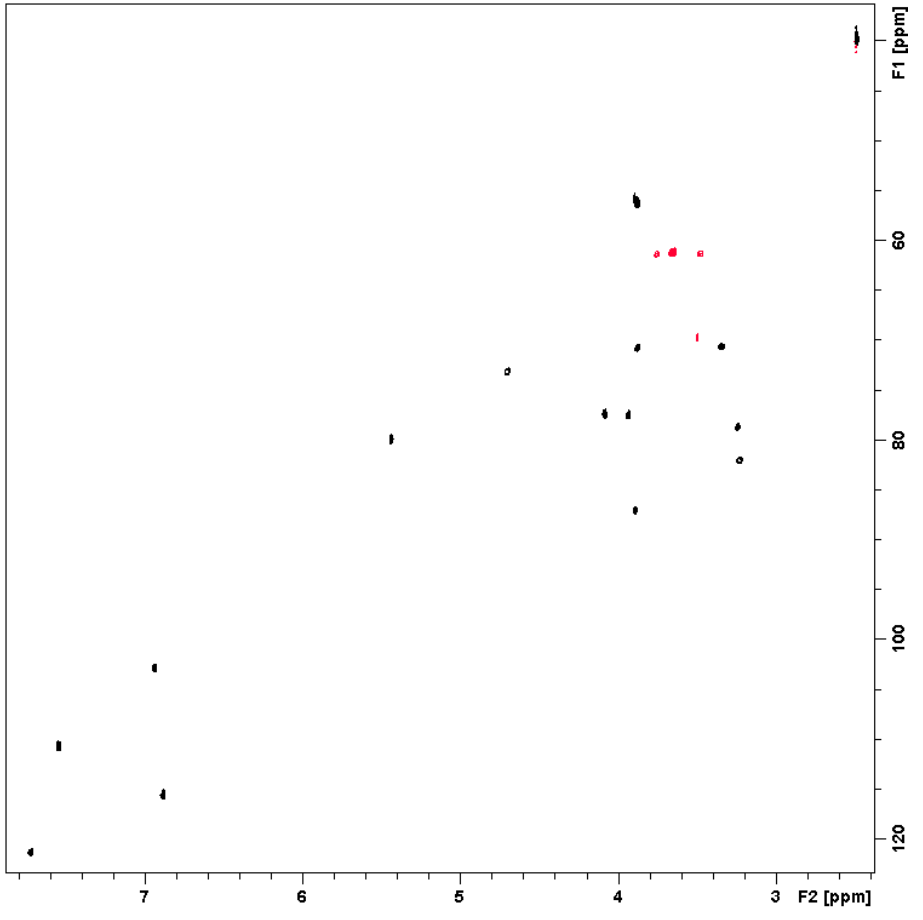

Figure S38. 2D ^{1}H-^{13}C HMBC spectrum of Chrysoeriol 6-C-β-arabinofuranosyl-8-C-β-glucopyranoside (5)

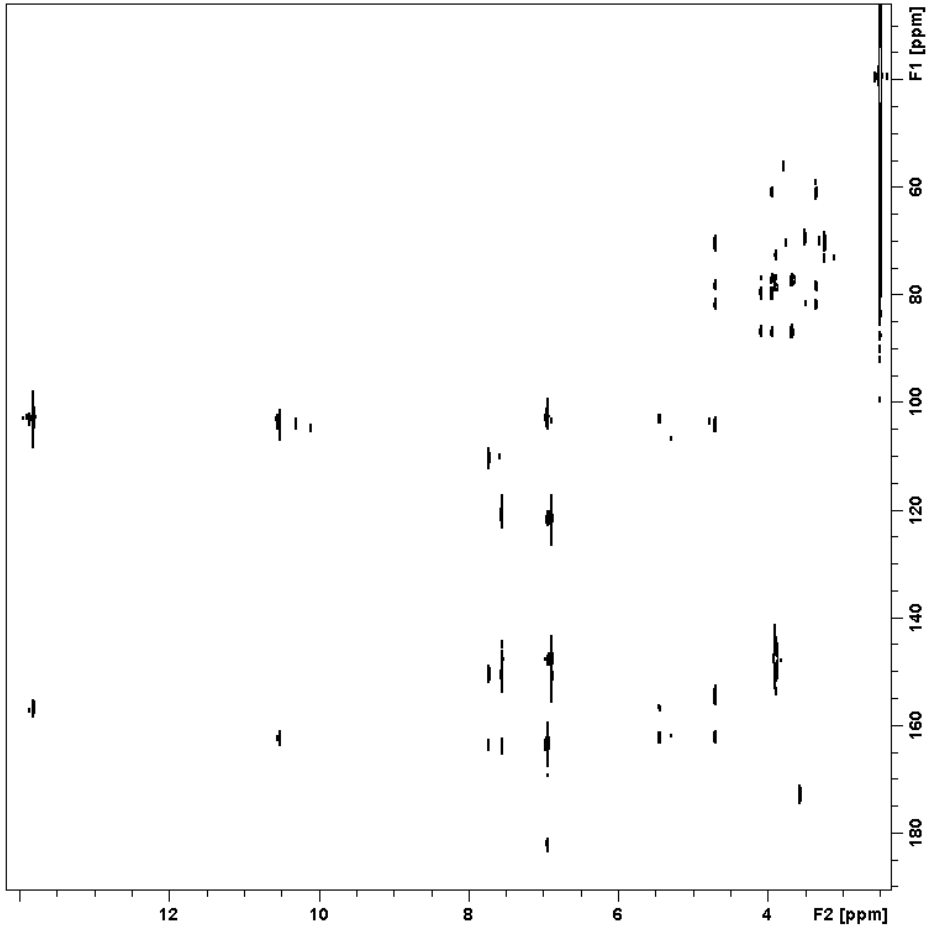

Figure S39. 2D ^{1}H-^{13}C HSQC-TOCSY spectrum of Chrysoeriol 6-C-β-arabinofuranosyl-8-C-β-glucopyranoside (5)

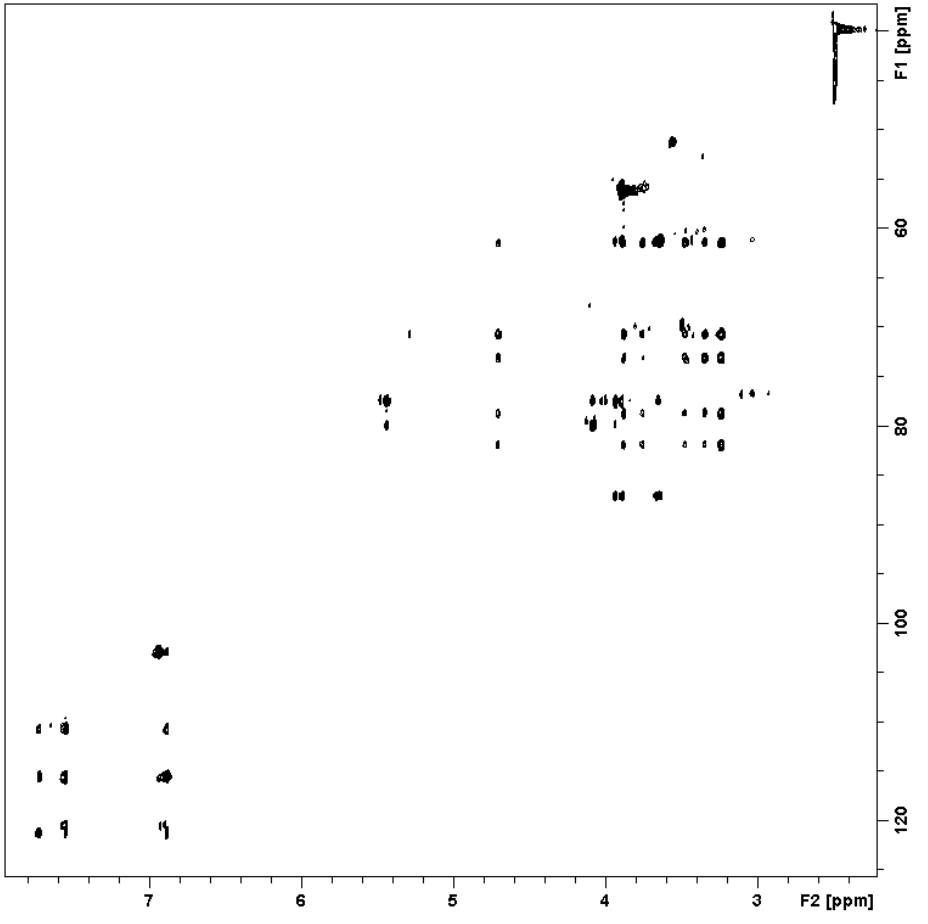

Figure S40. 2D ^{1}H-^{1}H COSY spectrum of Chrysoeriol 6-C-β-arabinofuranosyl-8-C-β-glucopyranoside (5)

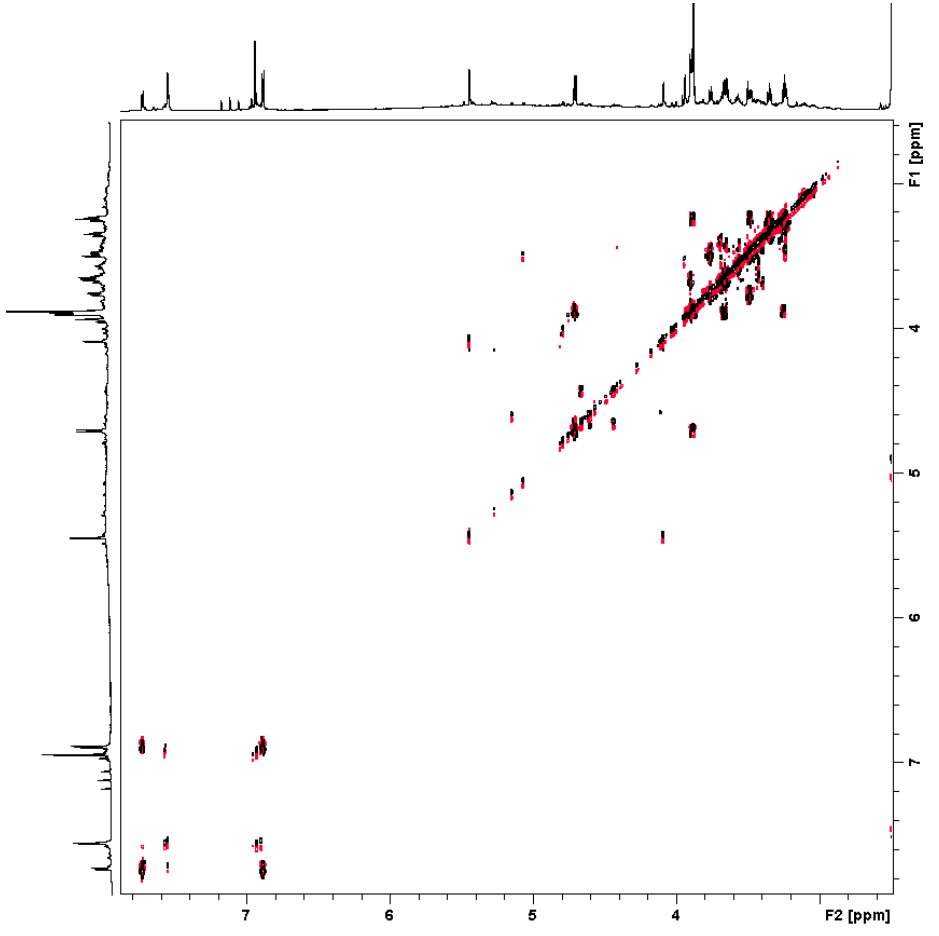

Figure S41. 2D ^{1}H-^{1}H ROESY spectrum of Chrysoeriol 6-C-β-arabinofuranosyl-8-C-β-glucopyranoside (5)

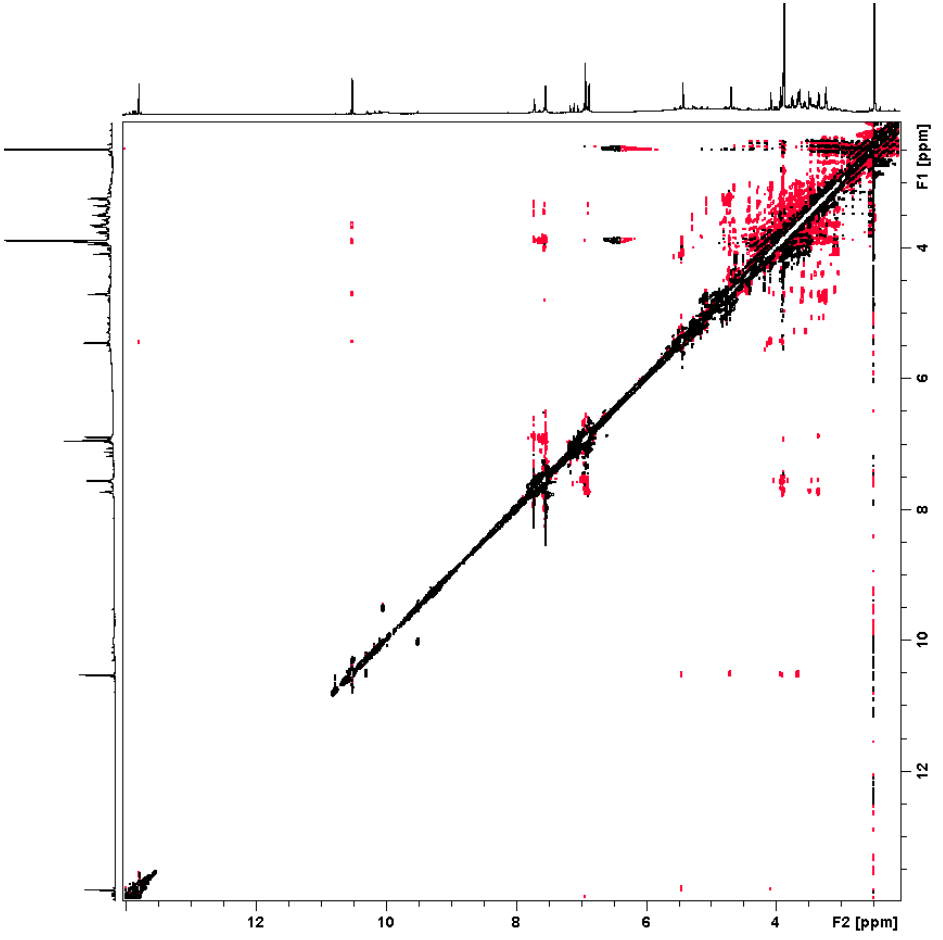

Figure S42. 1D ^{1}H NMR spectrum of Chrysoeriol 6-C-β-arabinopyranosyl-8-C-β-glucopyranoside (6)

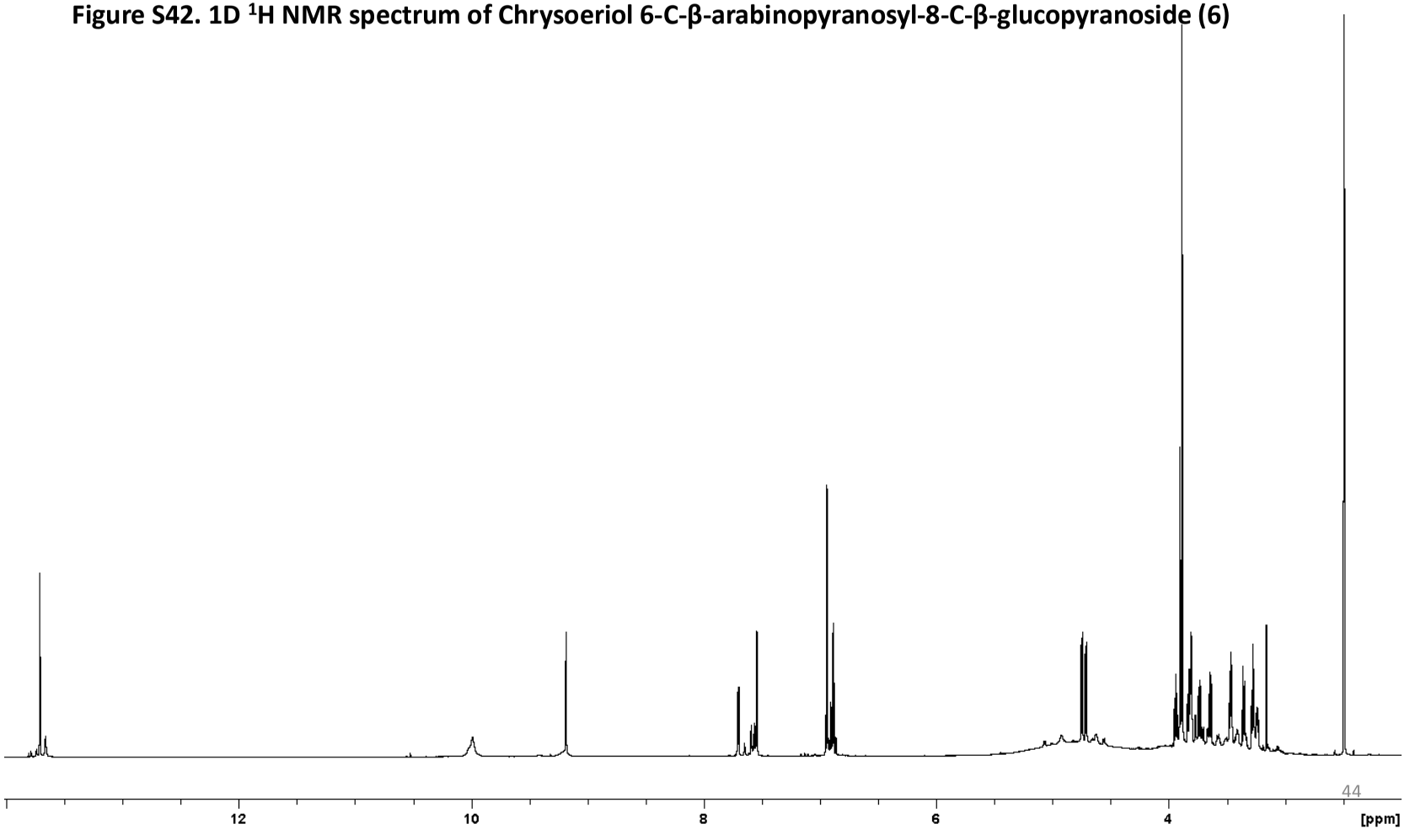

Figure S43. 2D ^{1}H-^{13}C HSQC spectrum of Chrysoeriol 6-C-β-arabinopyranosyl-8-C-β-glucopyranoside (6)

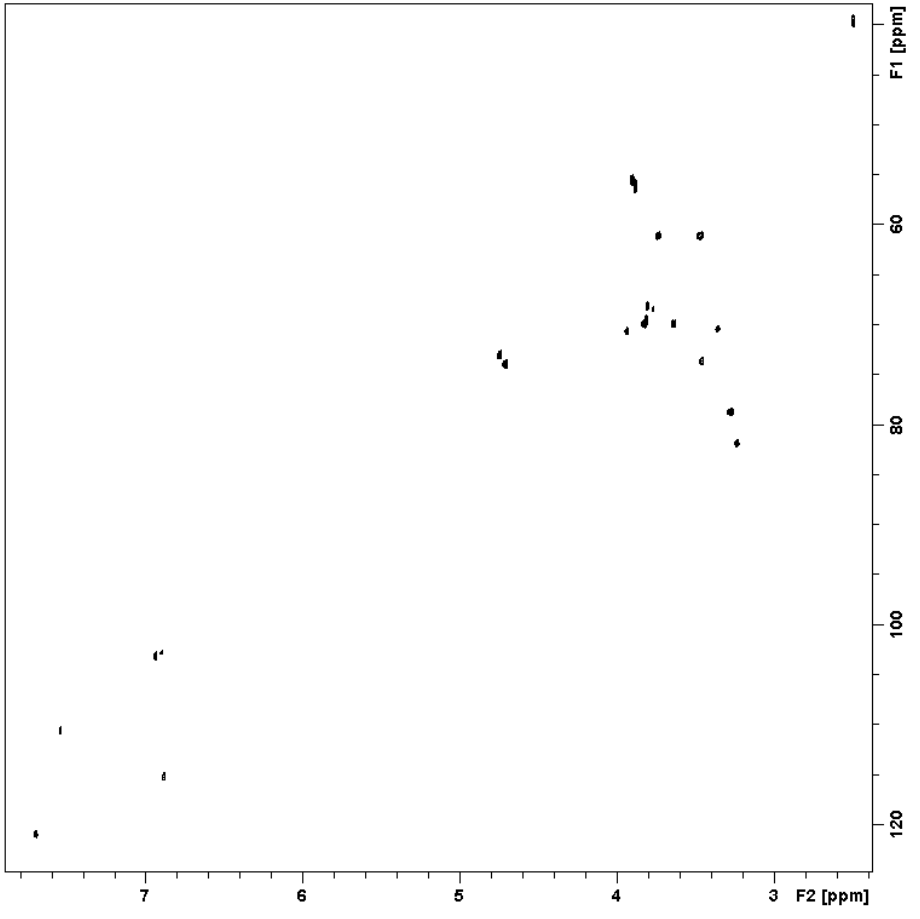

Figure S44. 2D ^{1}H-^{13}C HMBC spectrum of Chrysoeriol 6-C-β-arabinopyranosyl-8-C-β-glucopyranoside (6)

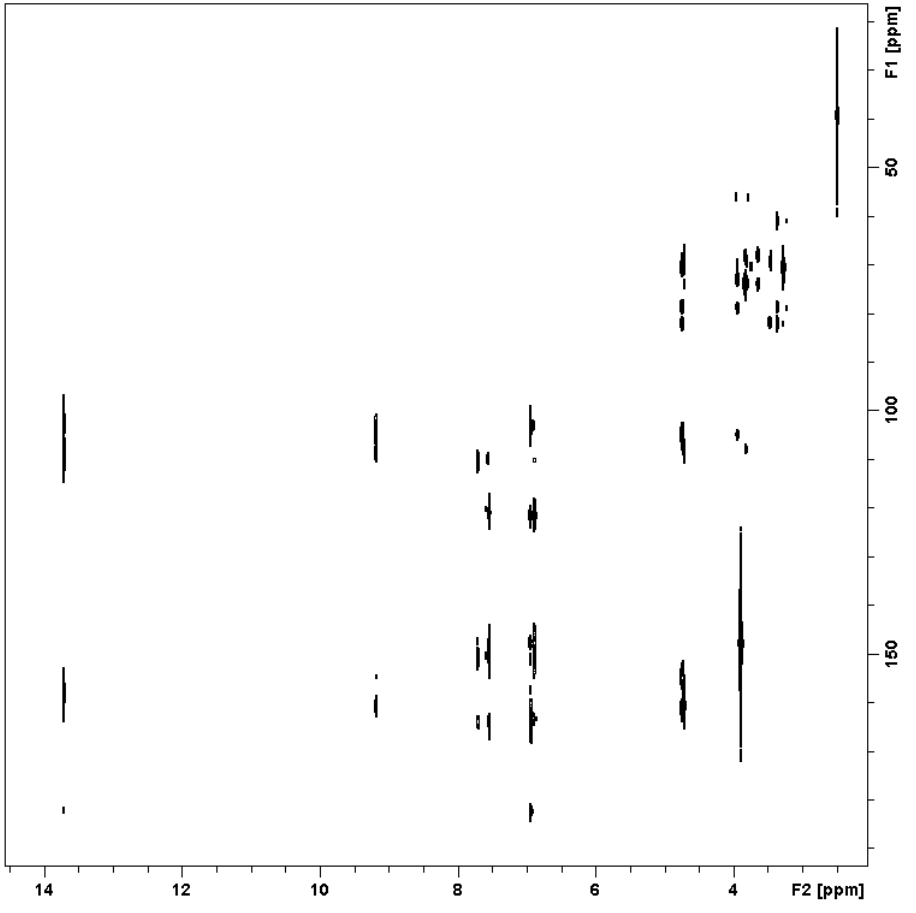

Figure S45. 2D ^{1}H-^{13}C HSQC-TOCSY spectrum of Chrysoeriol 6-C-β-arabinopyranosyl-8-C-β-glucopyranoside (6)

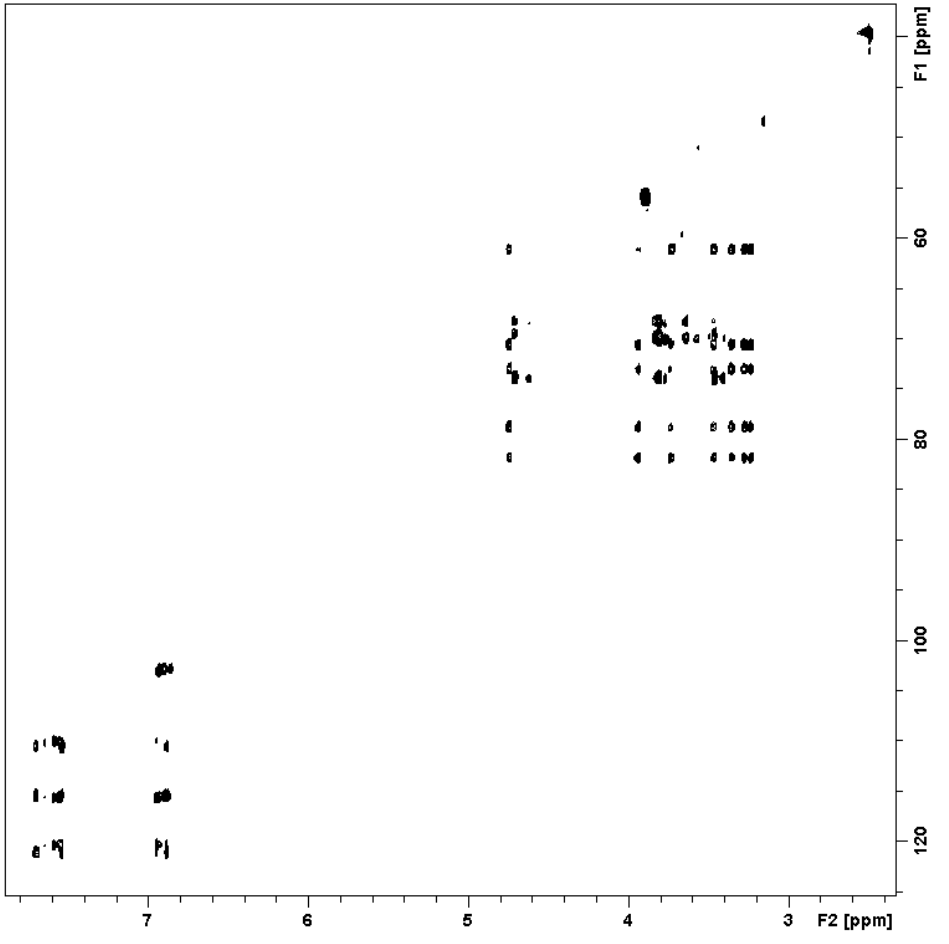

Figure S46. 2D ^{1}H-^{1}H COSY spectrum of Chrysoeriol 6-C-β-arabinopyranosyl-8-C-β-glucopyranoside (6)

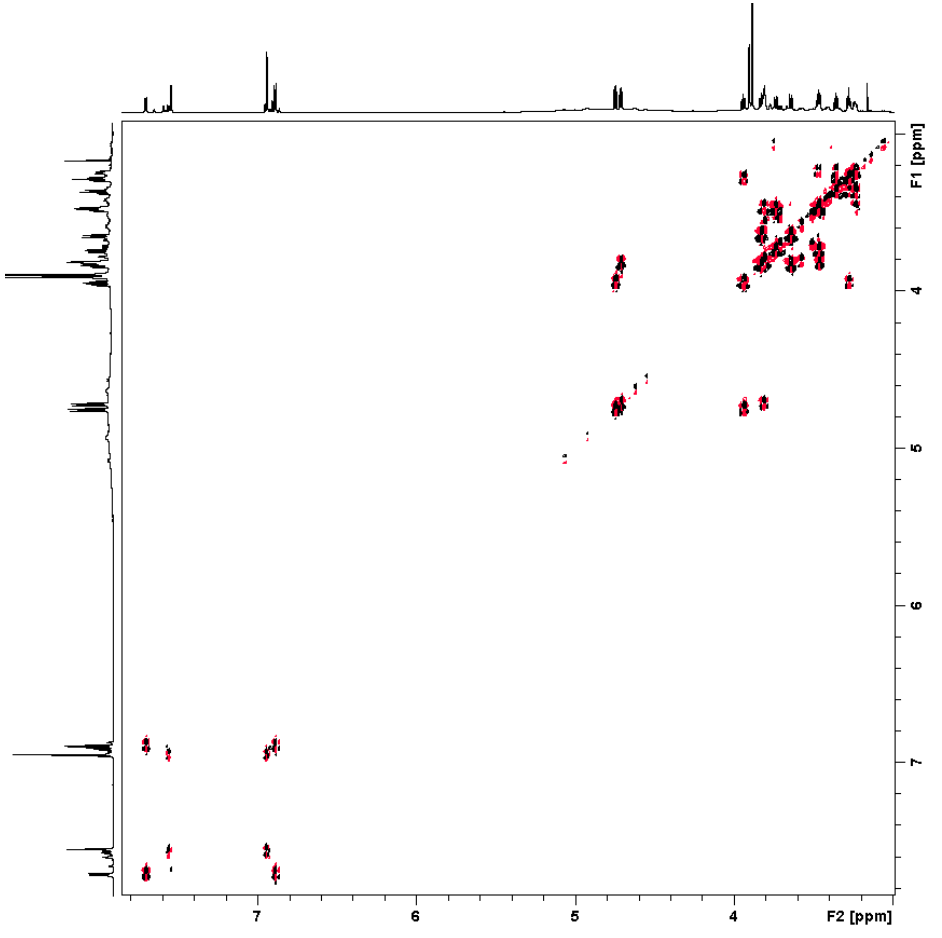

Figure S47. 2D ^{1}H-^{1}H ROESY spectrum of Chrysoeriol 6-C-β-arabinopyranosyl-8-C-β-glucopyranoside (6)

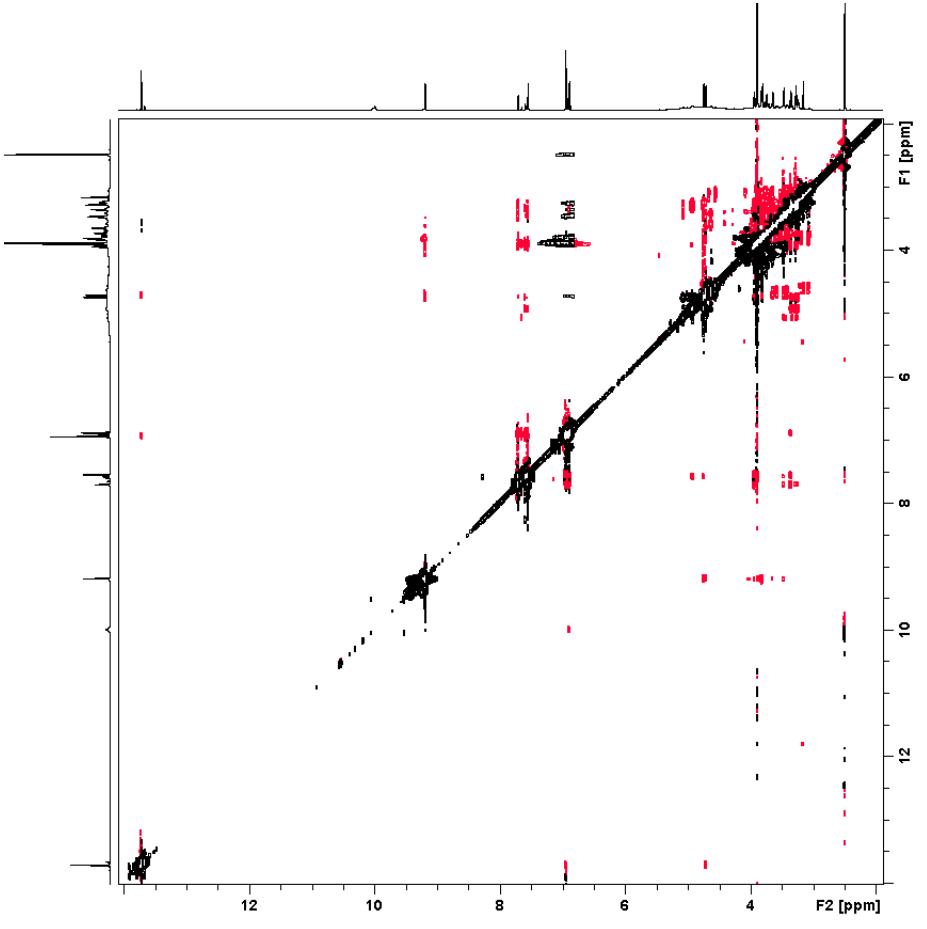

Figure S48. 1D ^{1}H NMR spectrum of Chrysoeriol 6-C-β-xylopyranosyl-8-C-β-galactopyranoside (7)

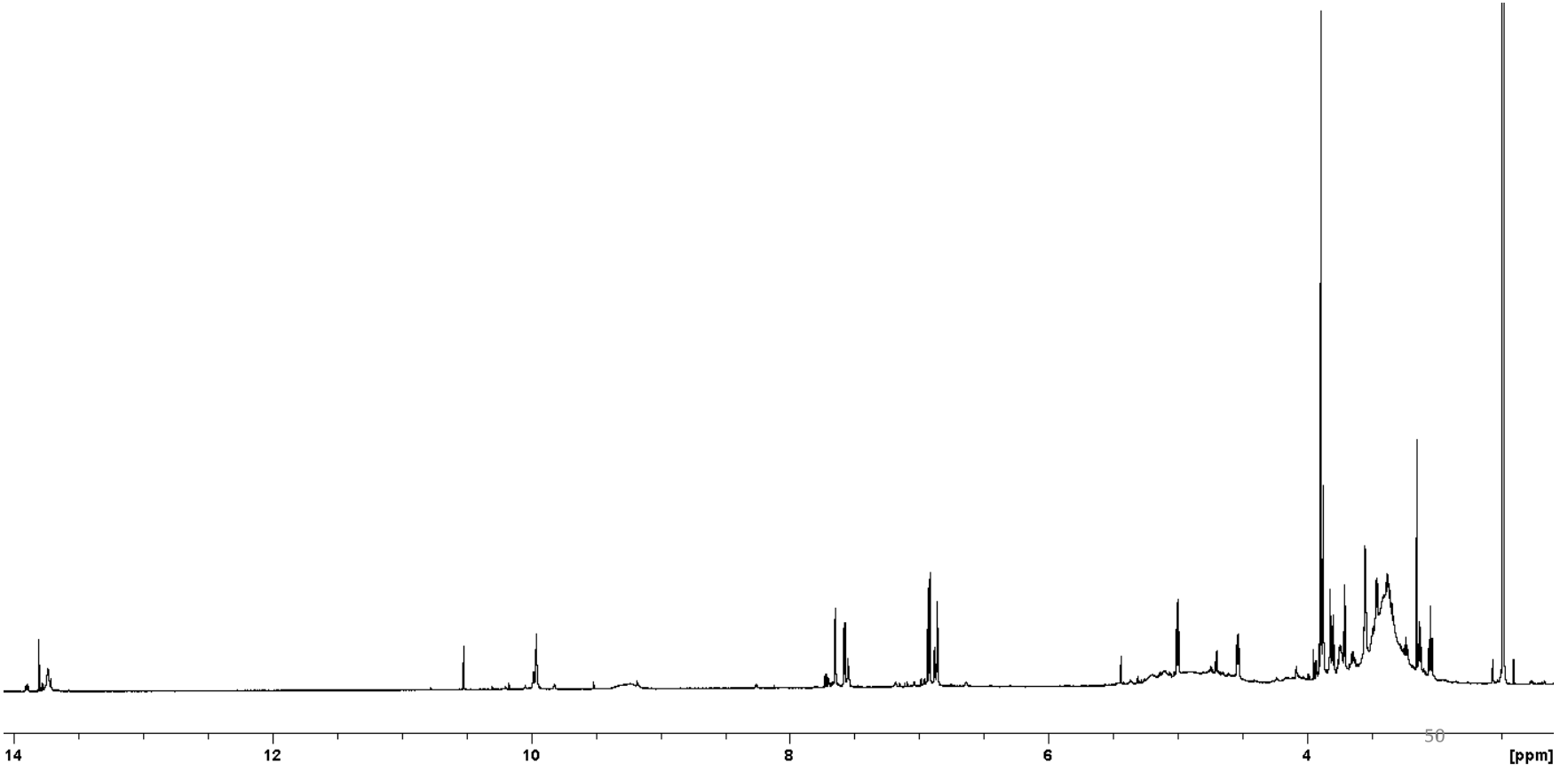

Figure S49. 2D ^{1}H-^{13}C HSQC spectrum of Chrysoeriol 6-C-β-xylopyranosyl-8-C-β-glucopyranoside (7)

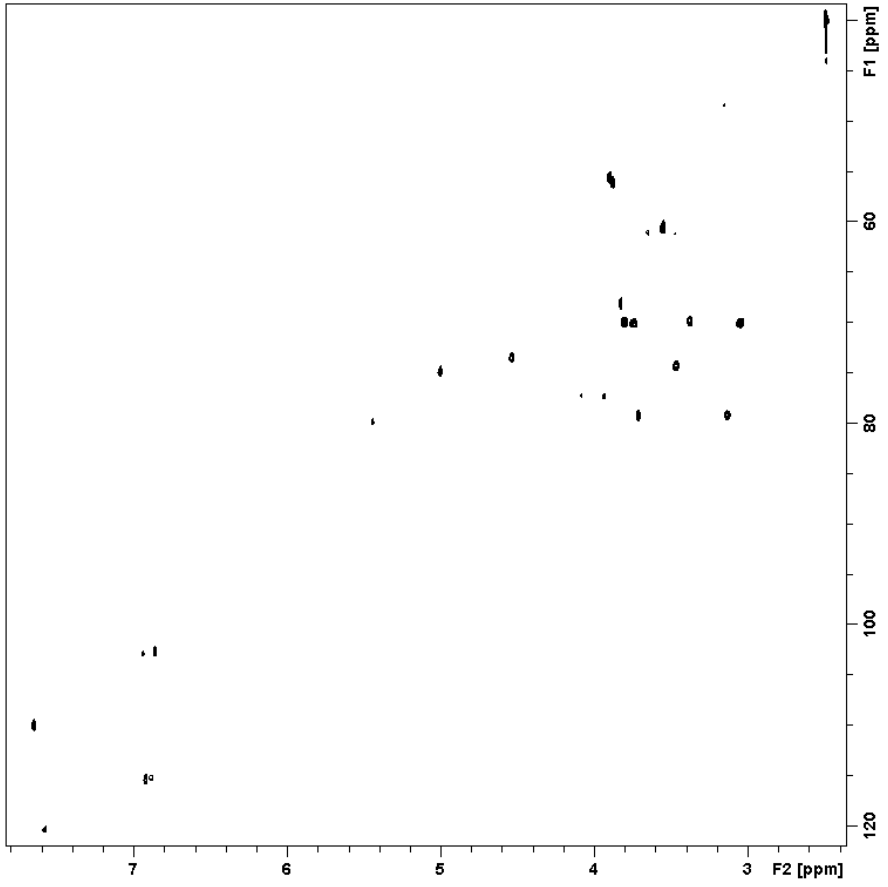

Figure S50. 2D ^{1}H-^{13}C HMBC spectrum of Chrysoeriol 6-C-β-xylopyranosyl-8-C-β-glucopyranoside (7)

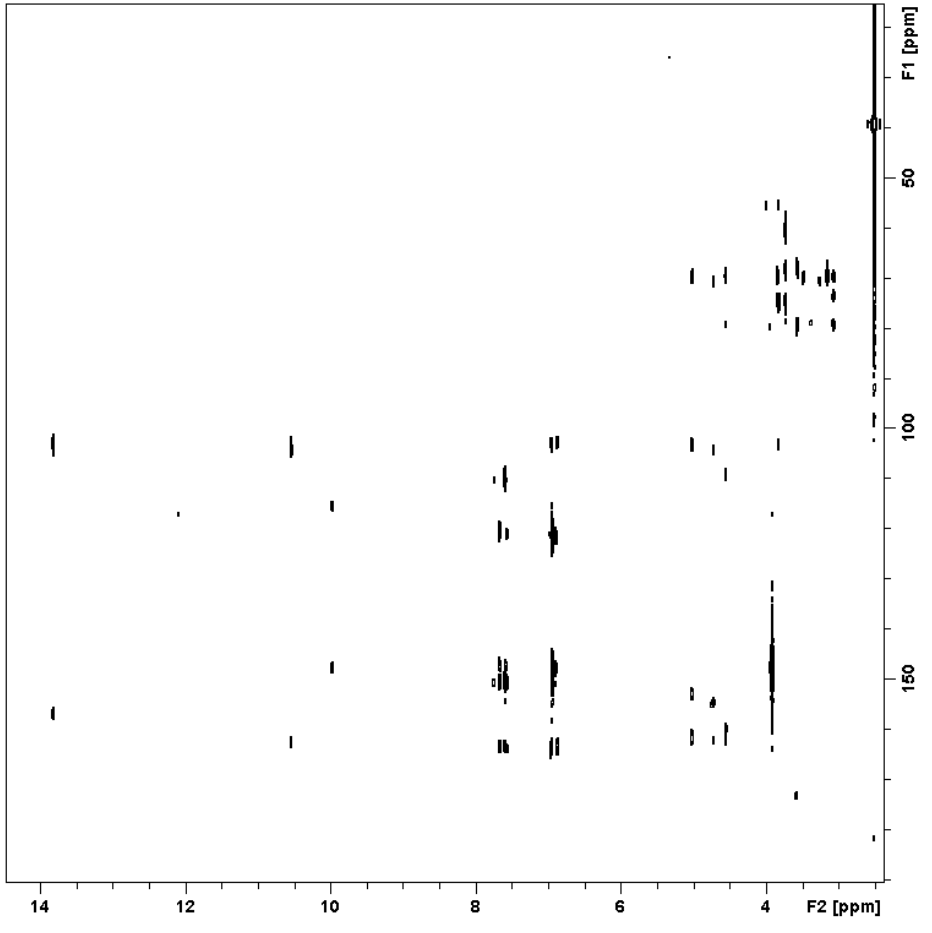

Figure S51. 2D ^{1}H-^{1}H COSY spectrum of Chrysoeriol 6-C-β-xylopyranosyl-8-C-β-glucopyranoside (7)

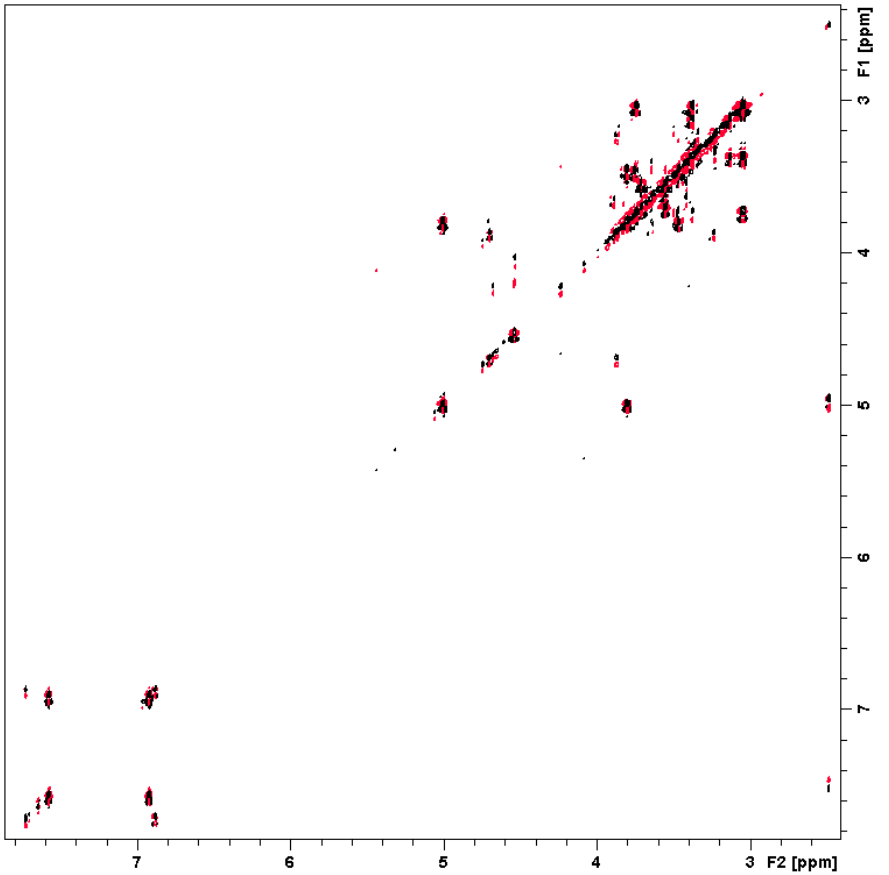

Figure S52. 1D ^{1}H NMR spectrum of Chrysoeriol 6-C-β-galactopyranosyl-8-C-β-glucopyranoside (8)

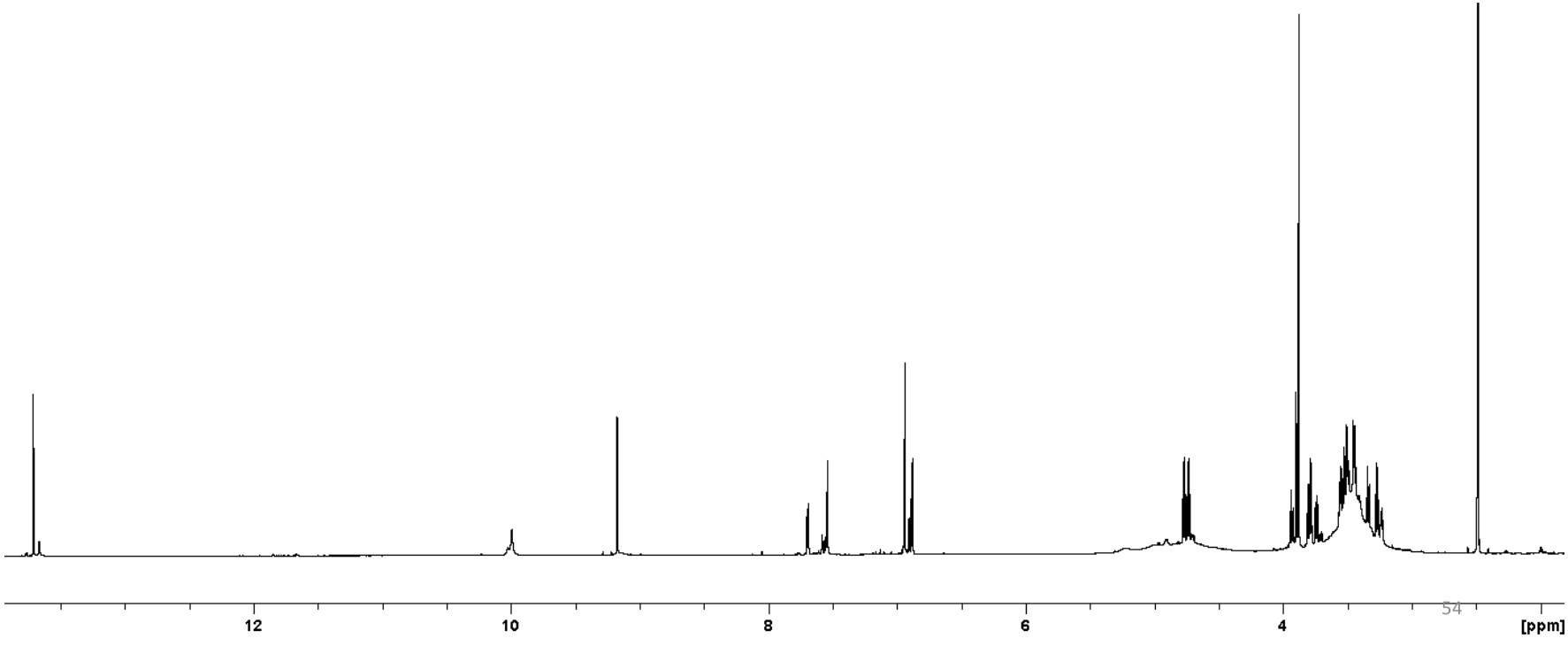

Figure S53. 2D ^{1}H-^{13}C HSQC spectrum of Chrysoeriol 6-C-β-galactopyranosyl-8-C-β-glucopyranoside (8)

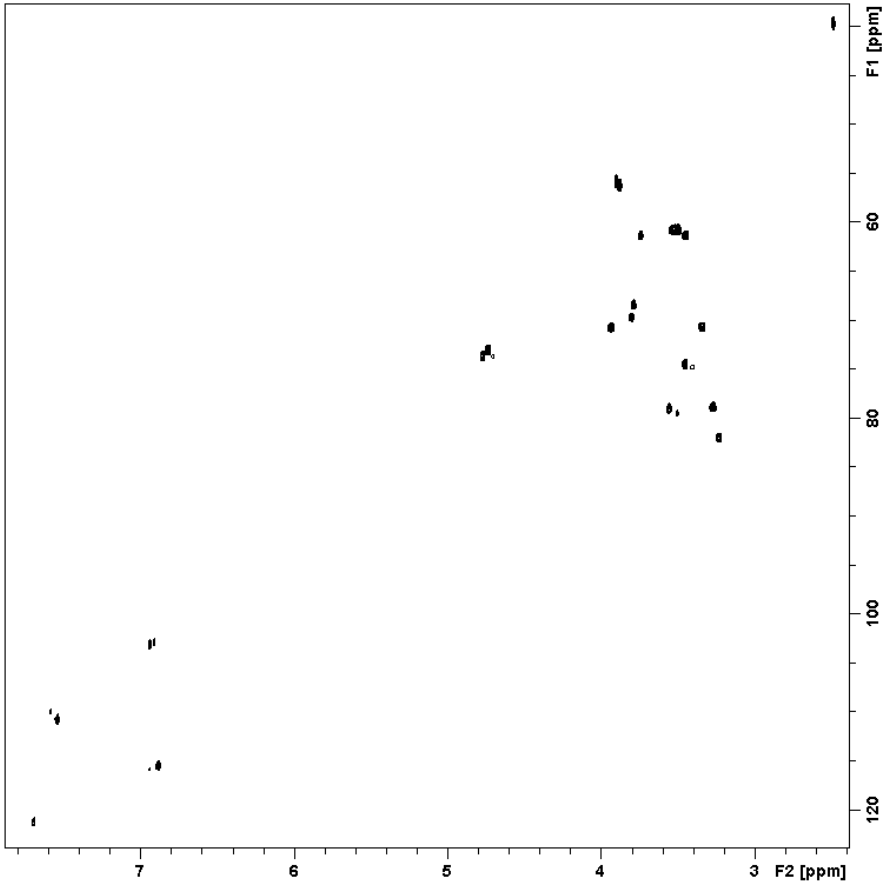

Figure S54. 2D ^{1}H-^{13}C HMBC spectrum of Chrysoeriol 6-C-β-galactopyranosyl-8-C-β-glucopyranoside (8)

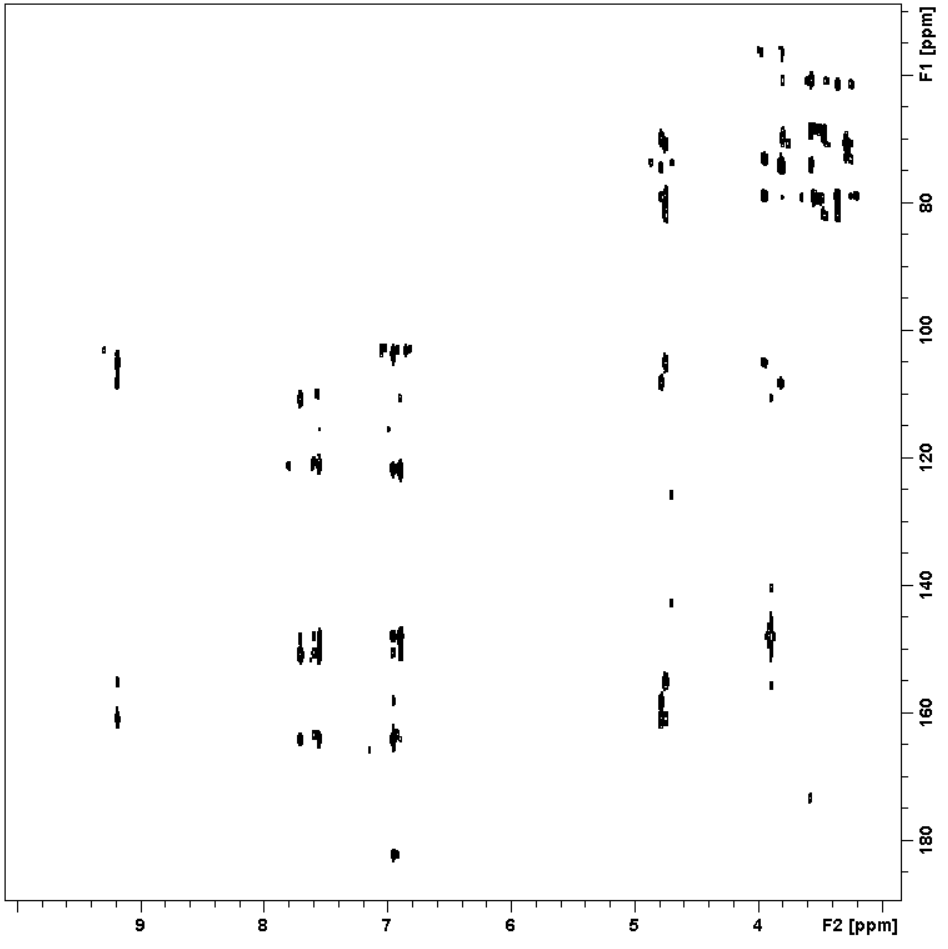

Figure S55. 2D ^{1}H-^{13}C HSQC-TOCSY spectrum of Chrysoeriol 6-C-β-galactopyranosyl-8-C-β-glucopyranoside (8)

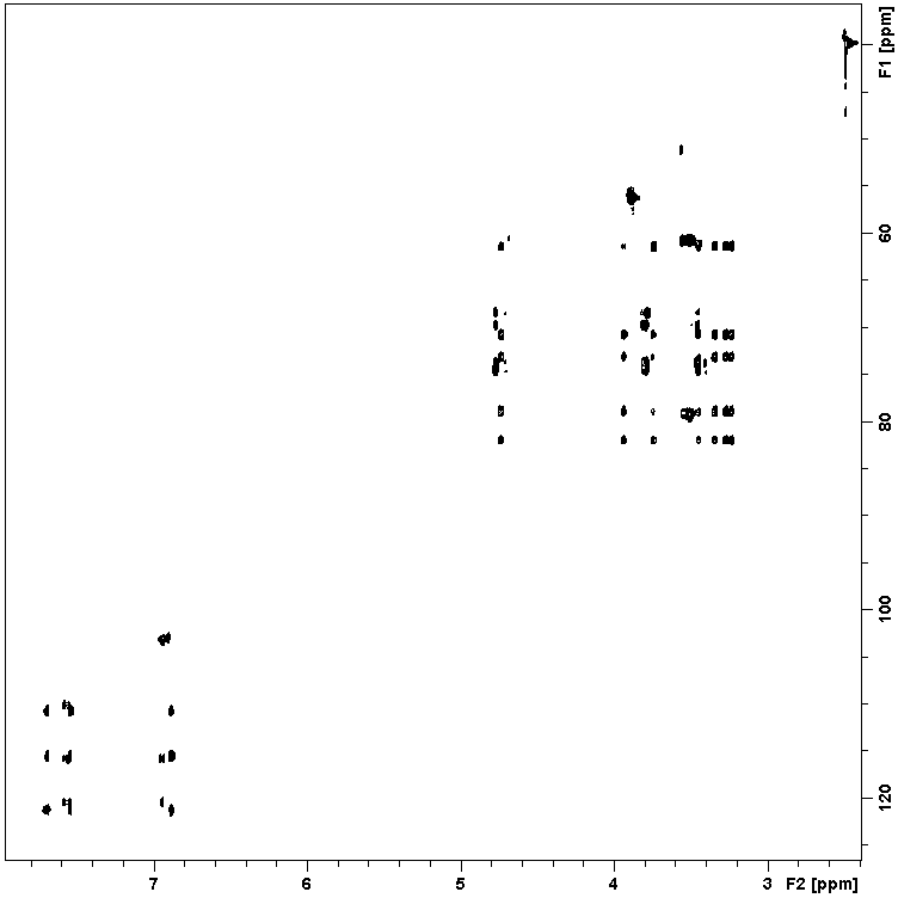

Figure S56. 2D ^{1}H-^{1}H COSY spectrum of Chrysoeriol 6-C-β-galactopyranosyl-8-C-β-glucopyranoside (8)

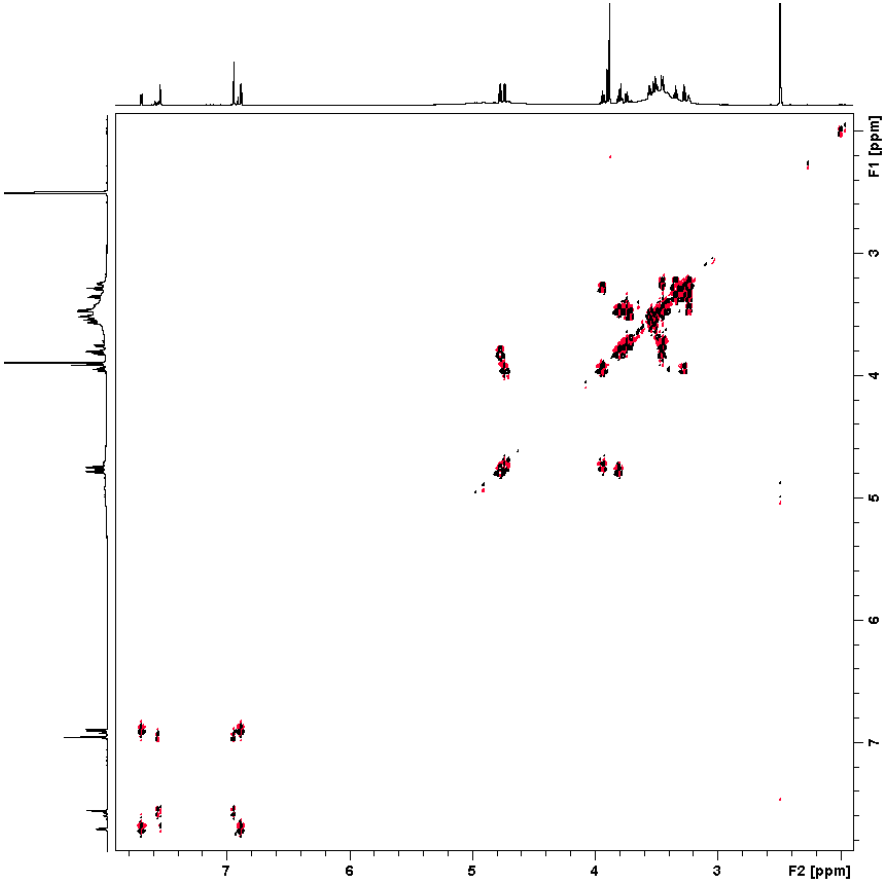

Figure S57.
2D ^{1}H-^{1}H ROESY spectrum of Chrysoeriol 6-C-β-galactopyranosyl-8-C-β-glucopyranoside (8)

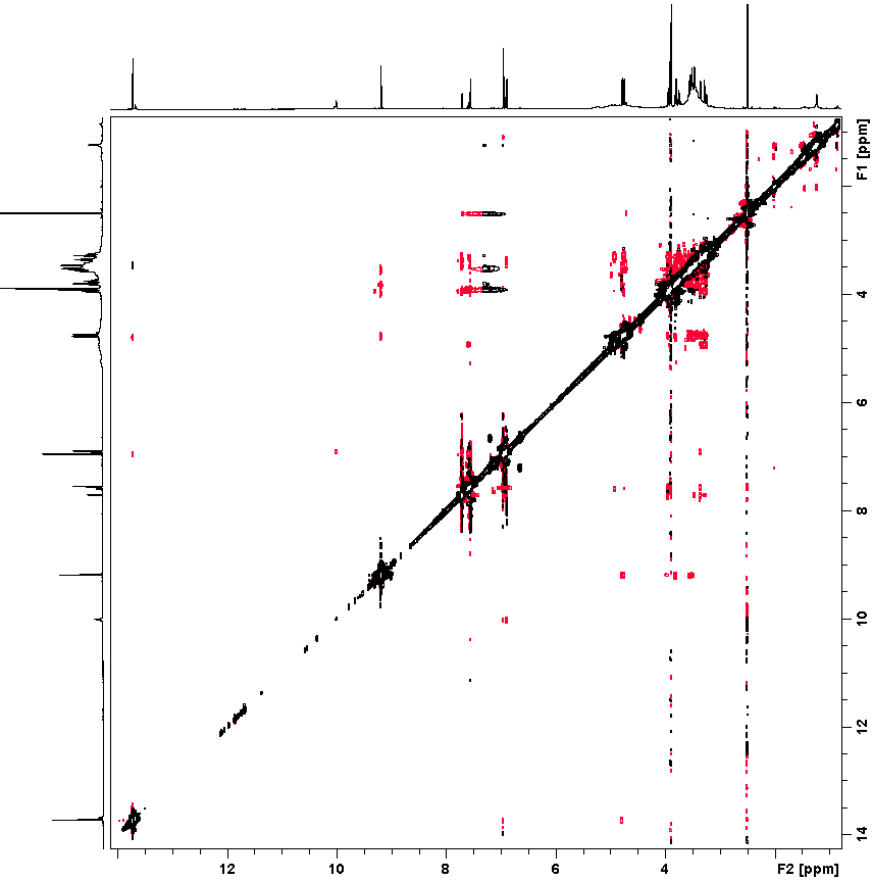

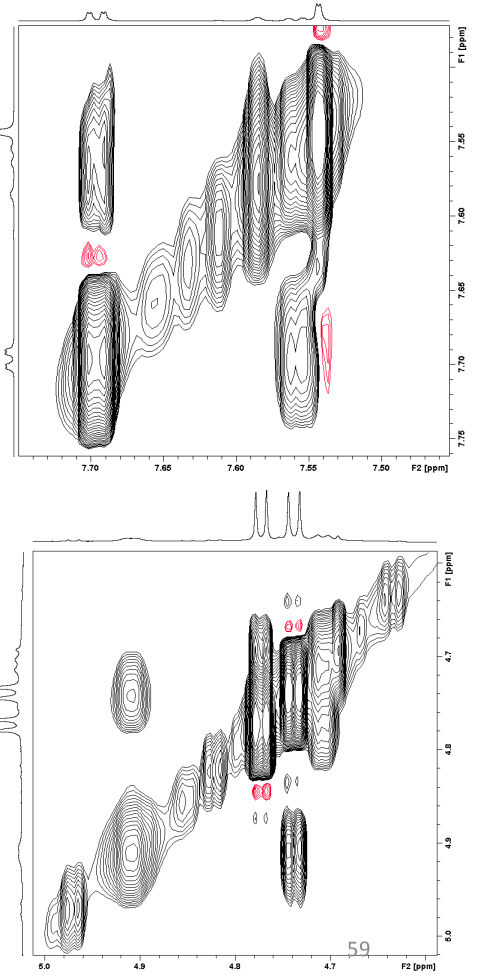

Figure S58. 1D ^{1}H NMR spectrum of Chrysoeriol 6-C-β-glucopyranosyl-8-C-β-galactopyranoside (9)

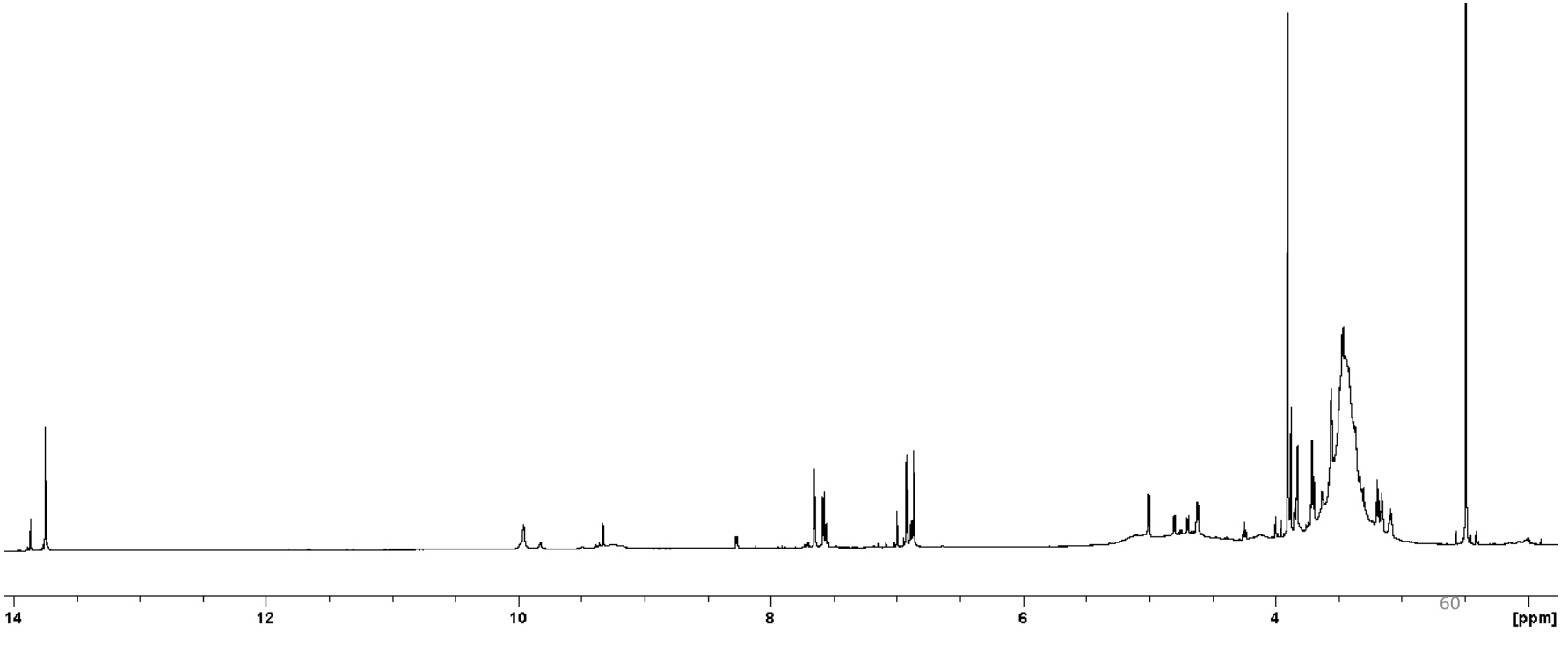

Figure S59. 2D ^{1}H-^{13}C HSQC spectrum of Chrysoeriol 6-C-β-glucopyranosyl-8-C-β-galactopyranoside (9)

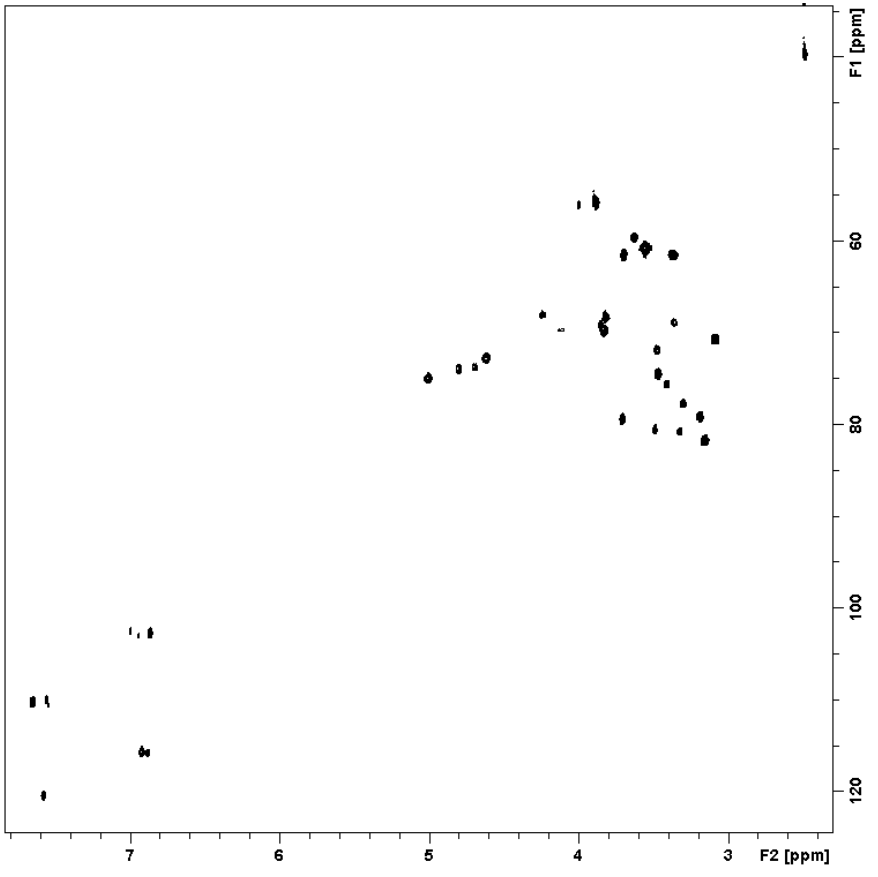

Figure S60. 2D ^{1}H-^{13}C HMBC spectrum of Chrysoeriol 6-C-β-glucopyranosyl-8-C-β-galactopyranoside (9)

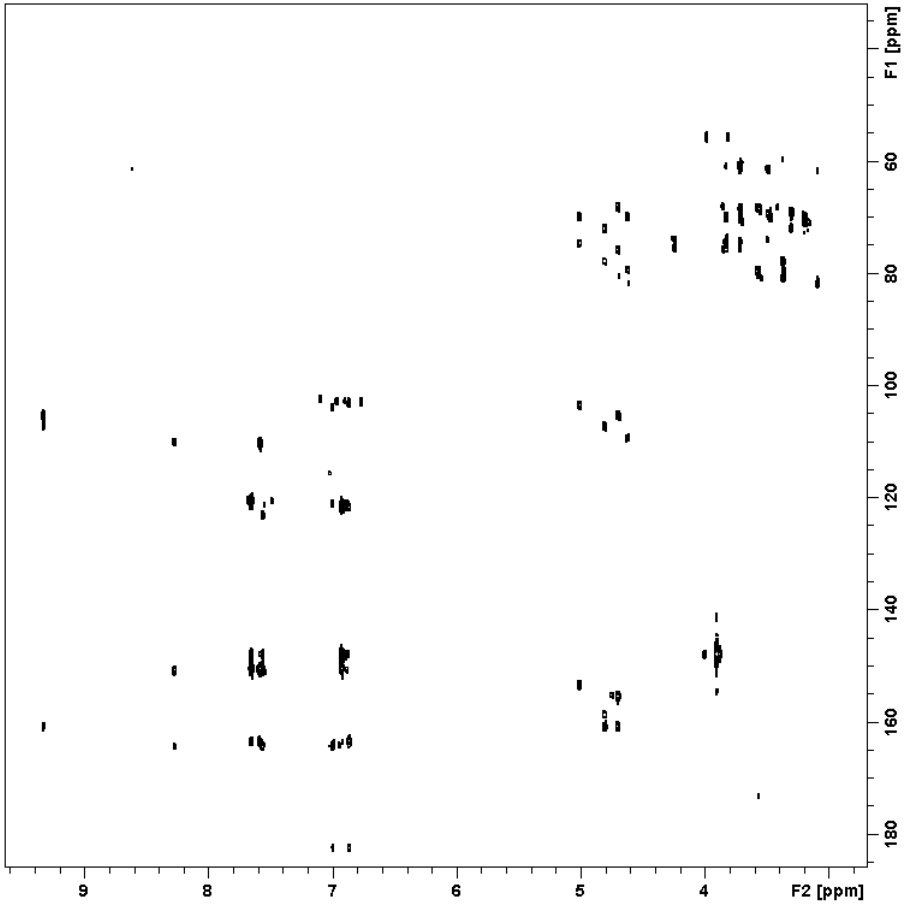

Figure S61. 2D ^{1}H-^{13}C HSQC-TOCSY spectrum of Chrysoeriol 6-C-β-glucopyranosyl-8-C-β-galactopyranoside (9)

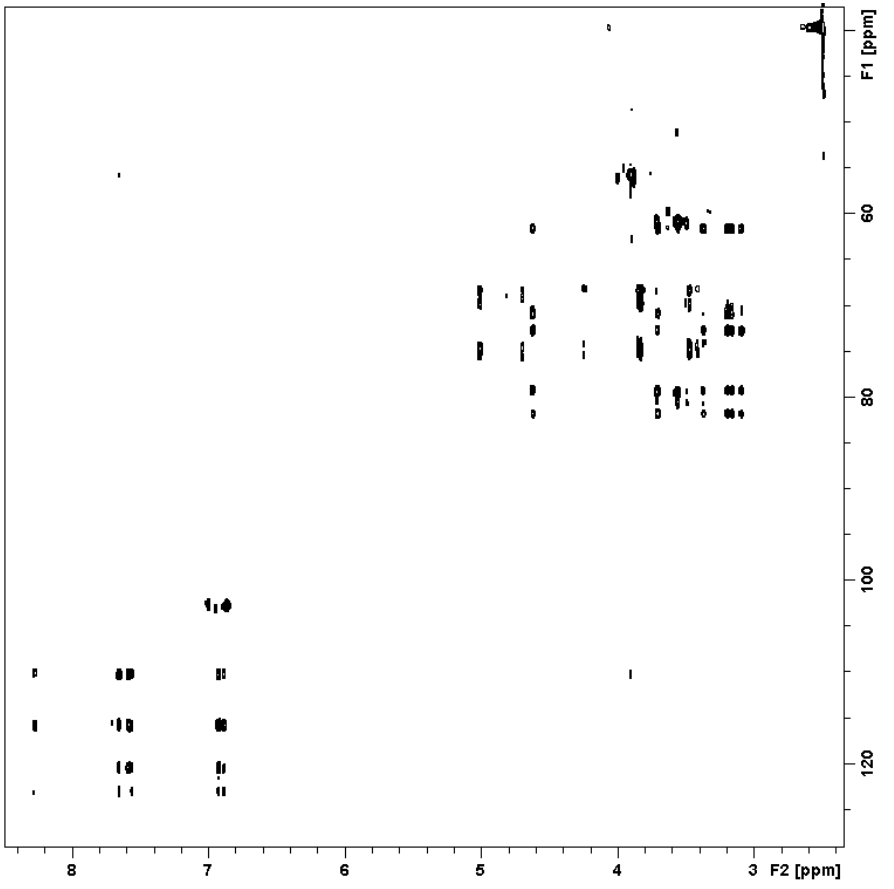

Figure S62. 2D ^{1}H-^{1}H COSY spectrum of Chrysoeriol 6-C-β-glucopyranosyl-8-C-β-galactopyranoside (9)

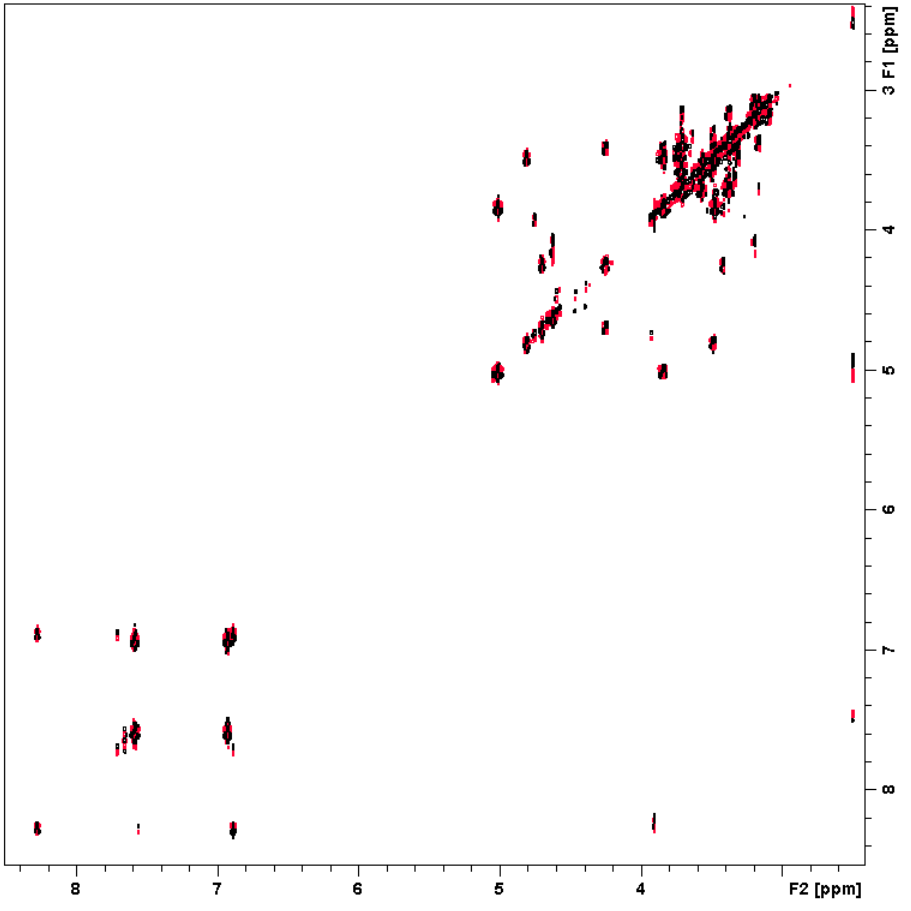

Figure S63.
2D ^{1}H-^{1}H COSY spectrum of Chrysoeriol 6-C-β-glucopyranosyl-8-C-β-galactopyranoside (9)

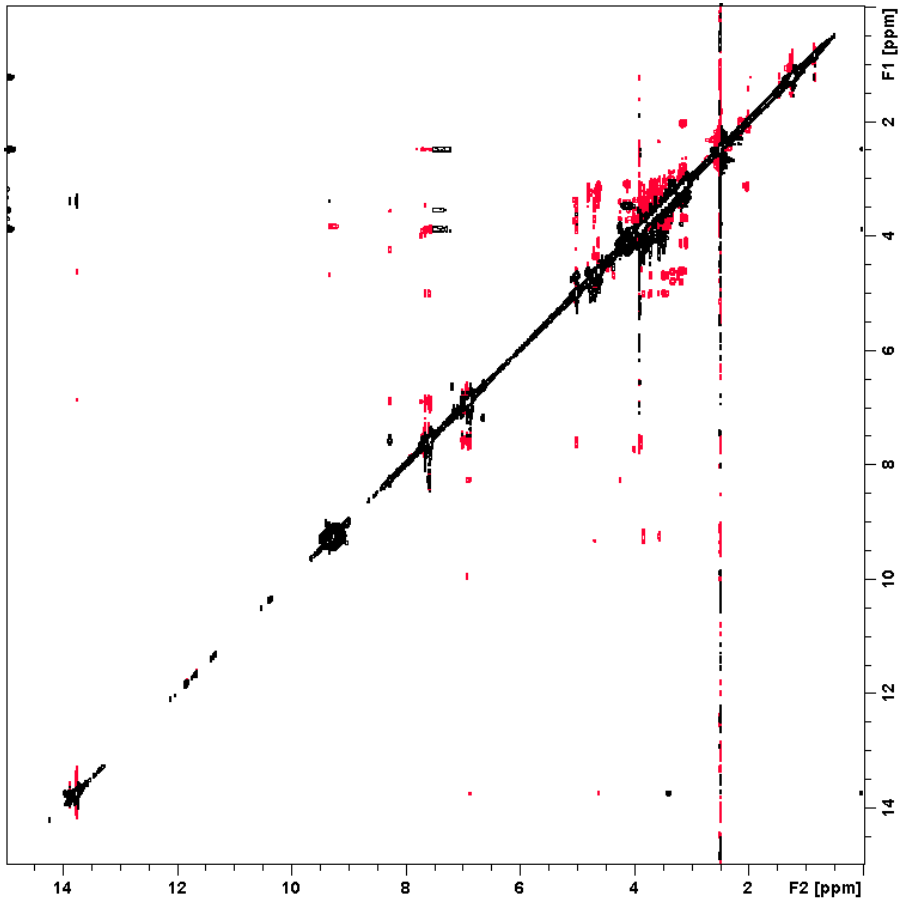

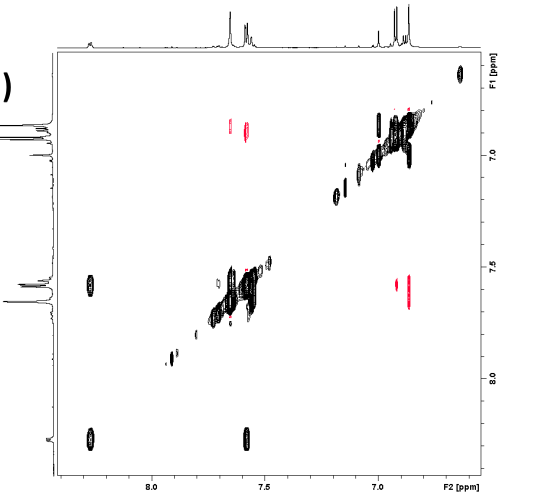

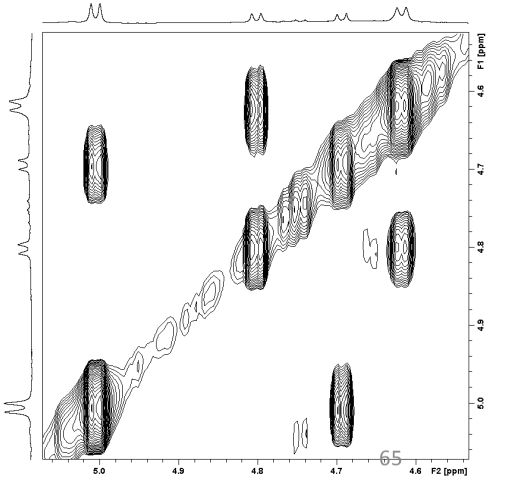

Figure S64. 1D ^{1}H NMR spectrum of Chrysoeriol 6,8-di-C-β-D-glucopyranoside (10)

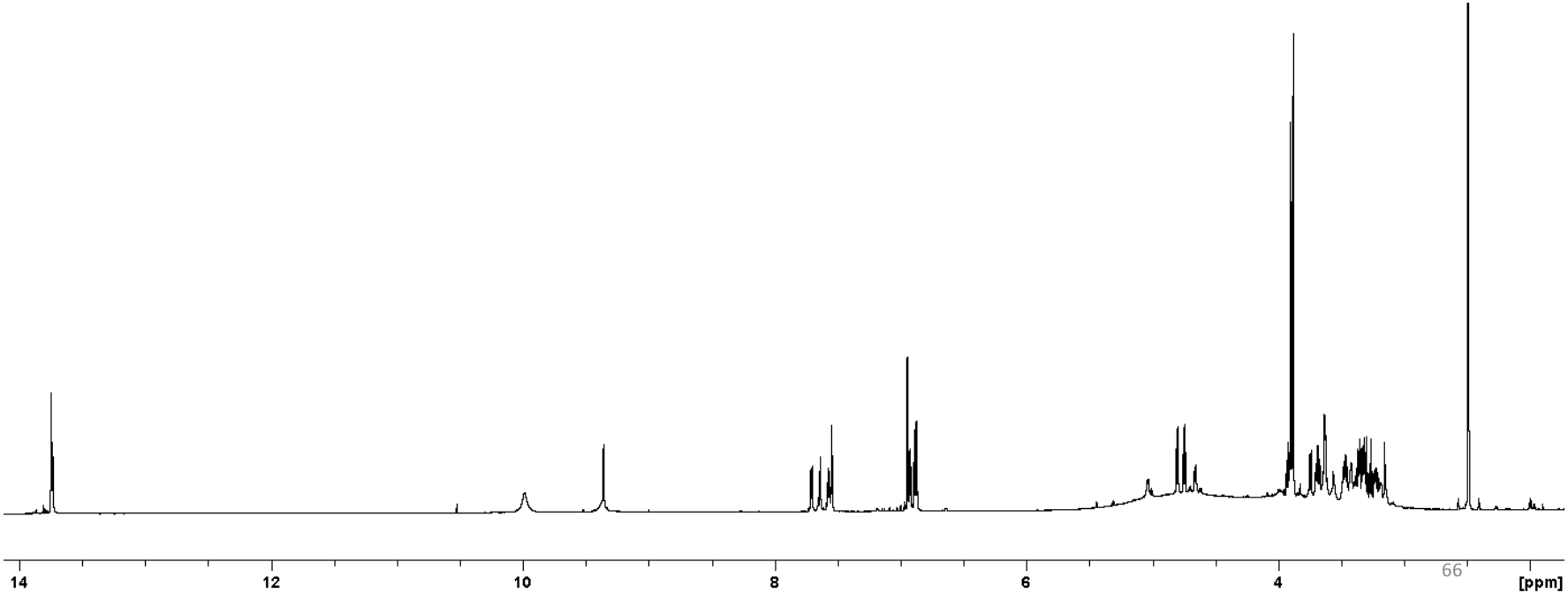

Figure S65. 2D ^{1}H-^{13}C HSQC spectrum of Chrysoeriol 6,8-di-C-β-D-glucopyranoside (10)

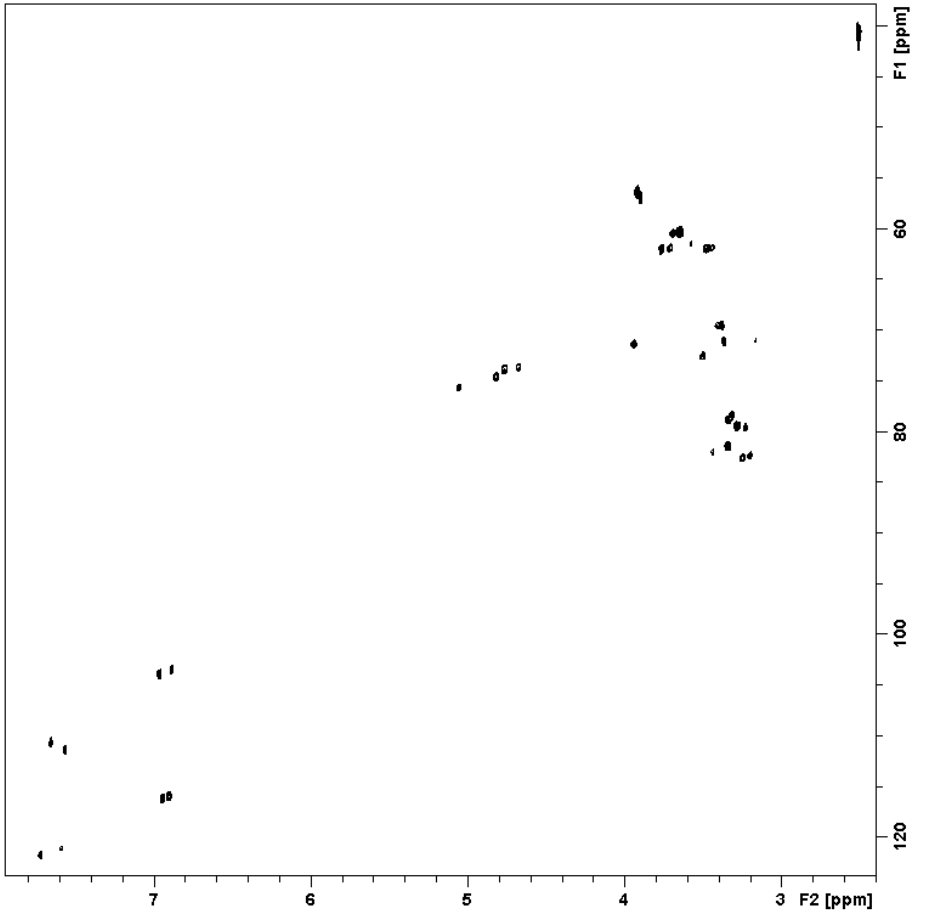

Figure S66. 2D ^{1}H-^{13}C HMBC spectrum of Chrysoeriol 6,8-di-C-β-D-glucopyranoside (10)

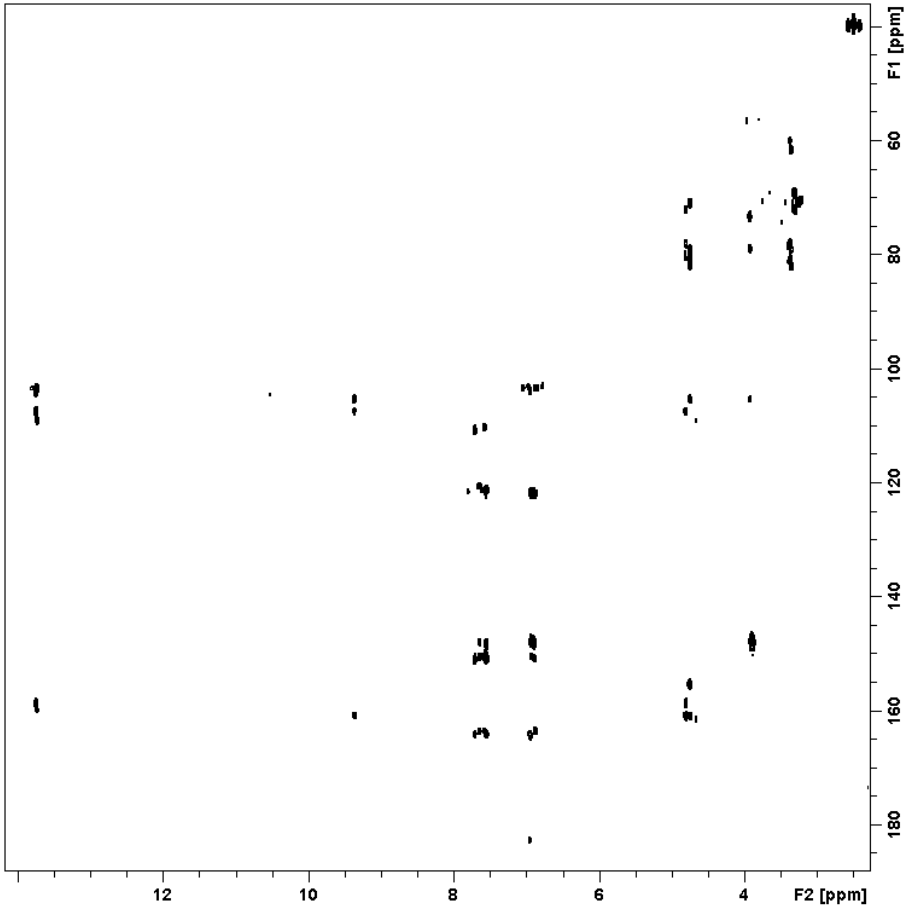

Figure S67. 2D ^{1}H-^{13}C HSQC-TOCSY spectrum of Chrysoeriol 6,8-di-C-β-D-glucopyranoside (10)

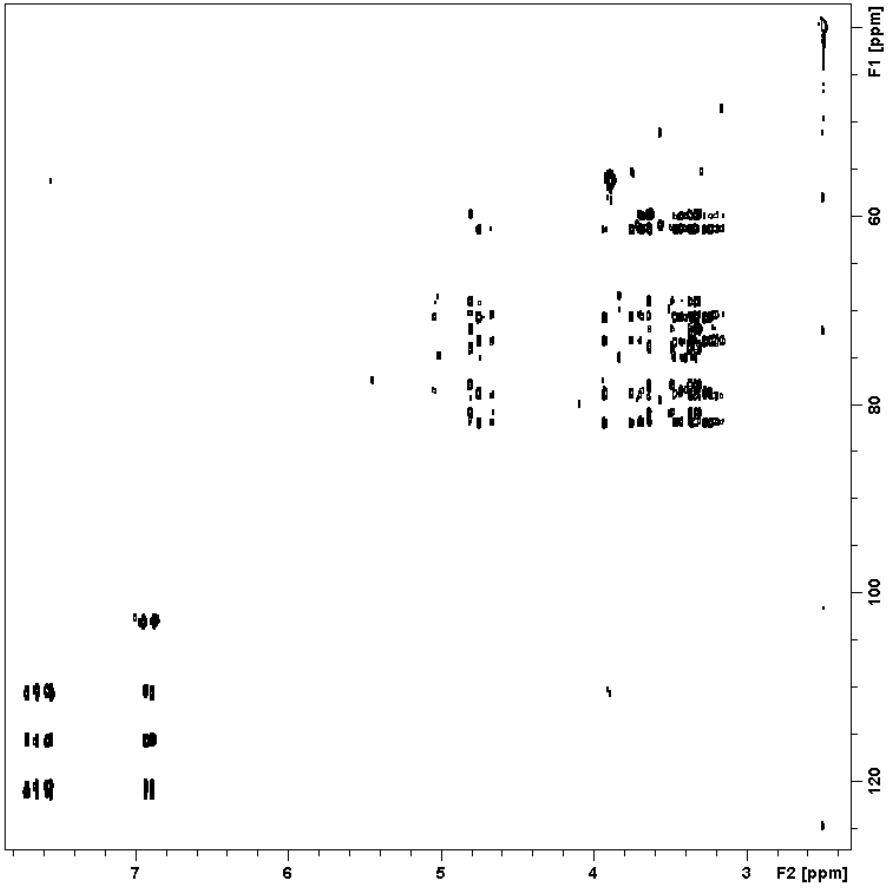

Figure S68. 2D ^{1}H-^{1}H COSY spectrum of Chrysoeriol 6,8-di-C-β-D-glucopyranoside (10)

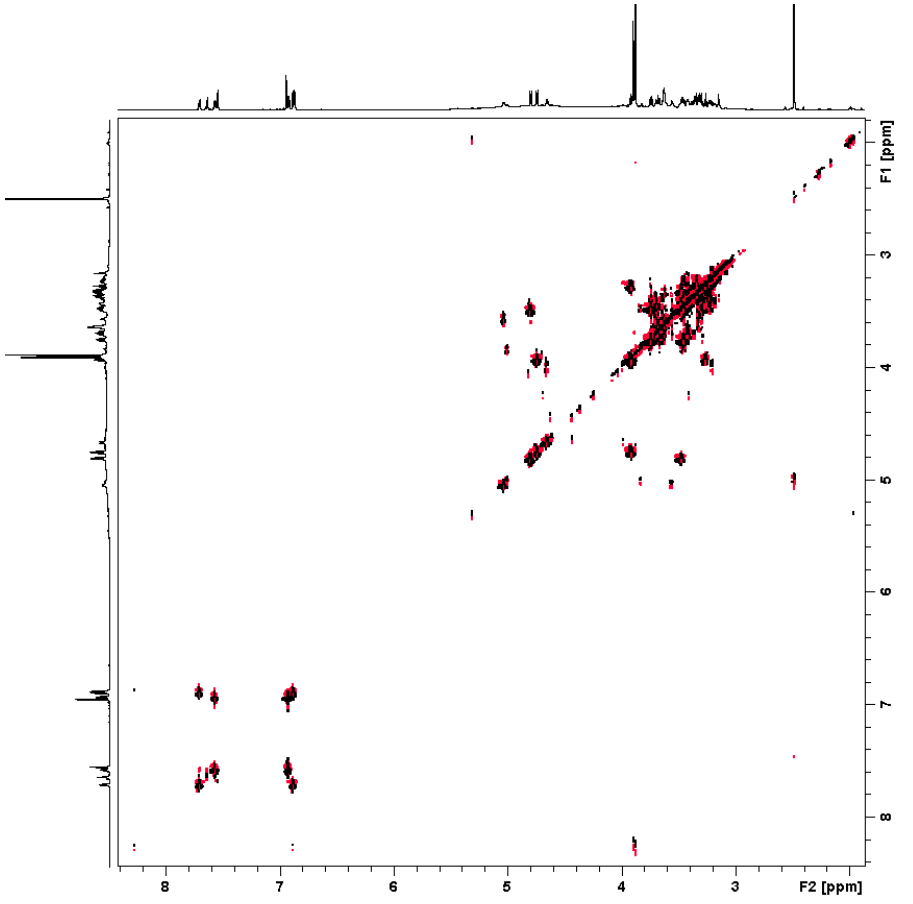

Figure S69. 2D ^{1}H-^{1}H ROESY spectrum of Chrysoeriol 6,8-di-C-β-D-glucopyranoside (10)

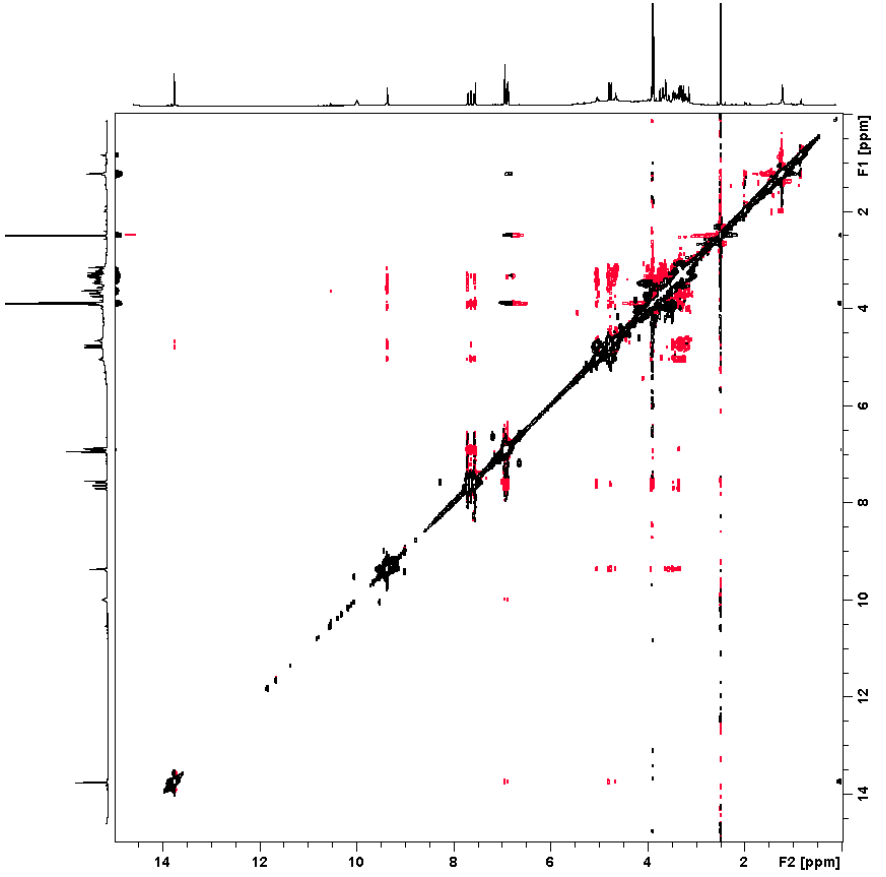

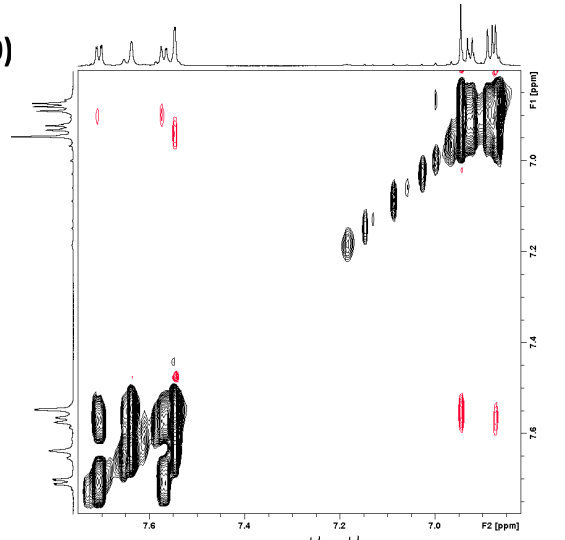

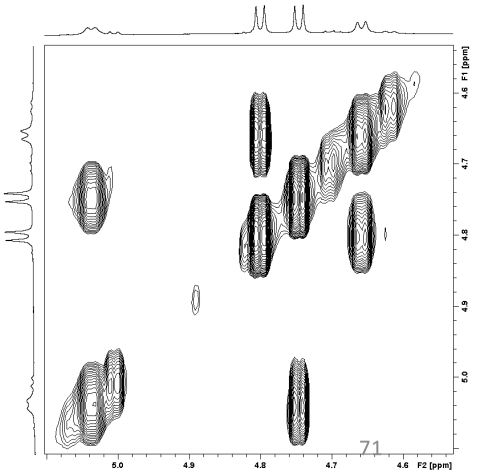

Figure S70. High resolution mass spectrum of sarsasapogenin 3-galactopyranoside (2)

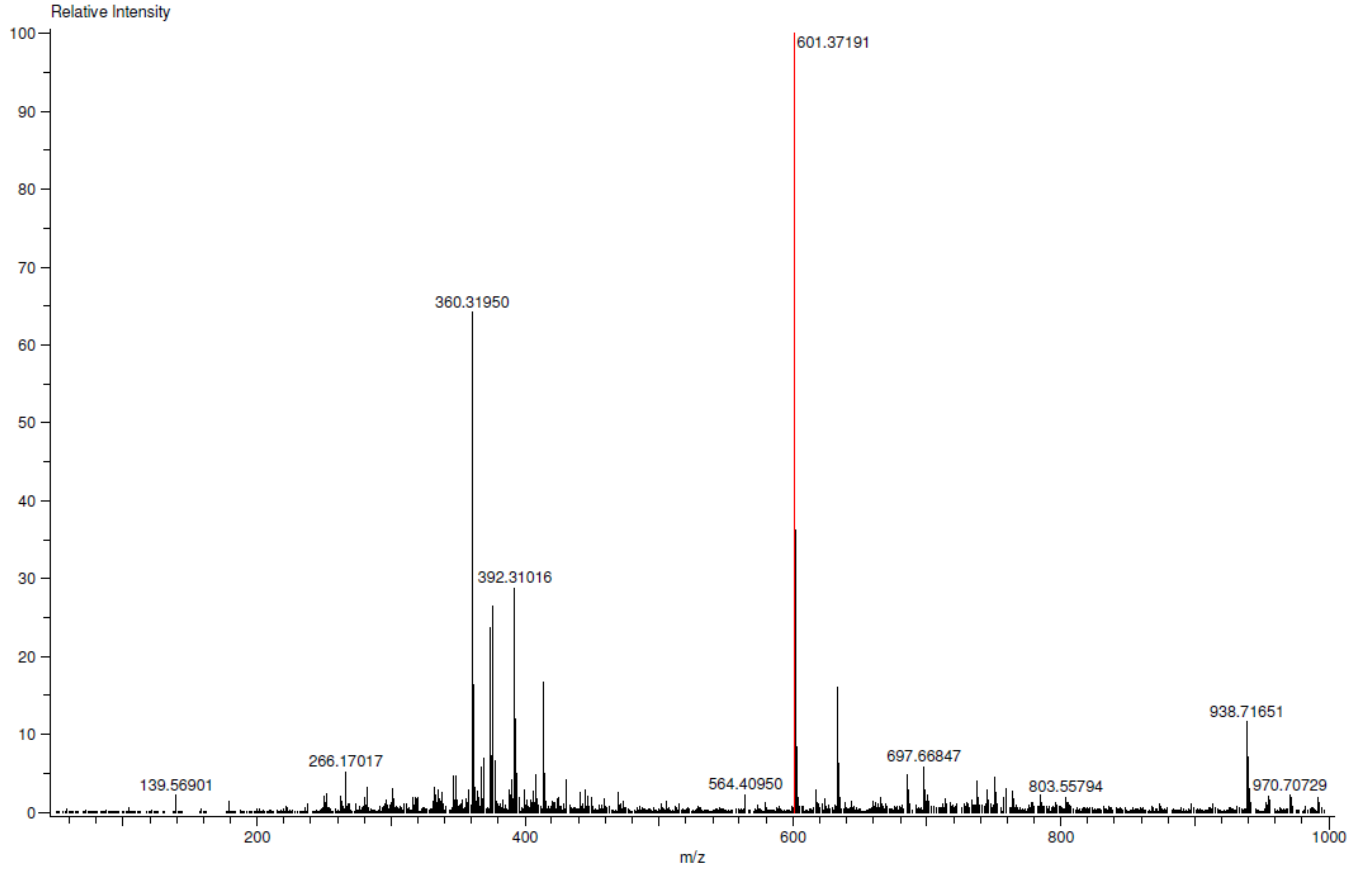

Figure S71. High resolution mass spectrum of sarsasapogenin-3-O-(2'-O-β-glucopyranosyl-β-galactopyranoside) (3)

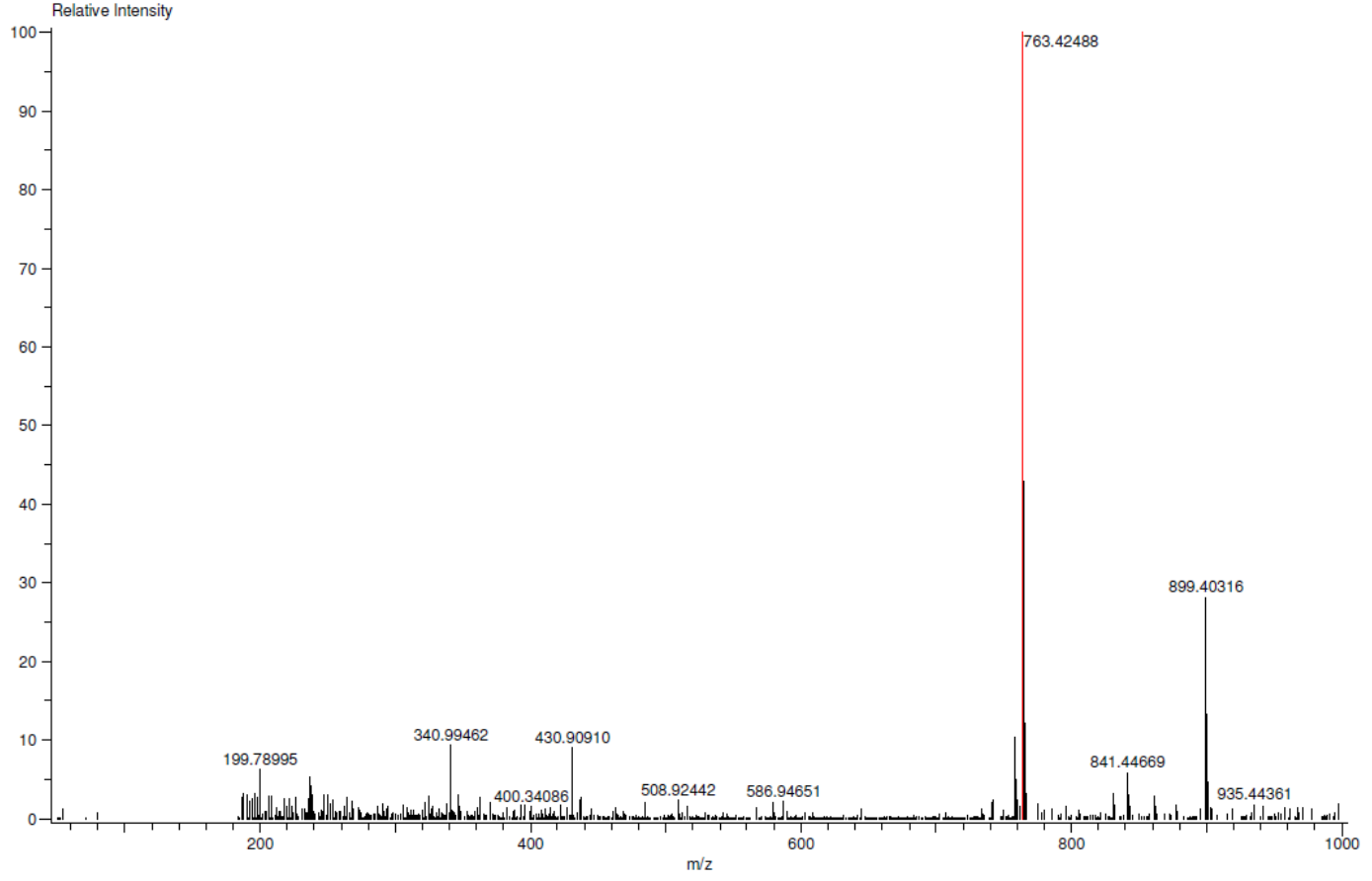

Figure S72. High resolution mass spectrum of sarsasapogenin-3-O-(2’-O-β-glucopyranosyl-3’-O-α-arabinopyranosyl-β-galactopyranoside) (**4**)

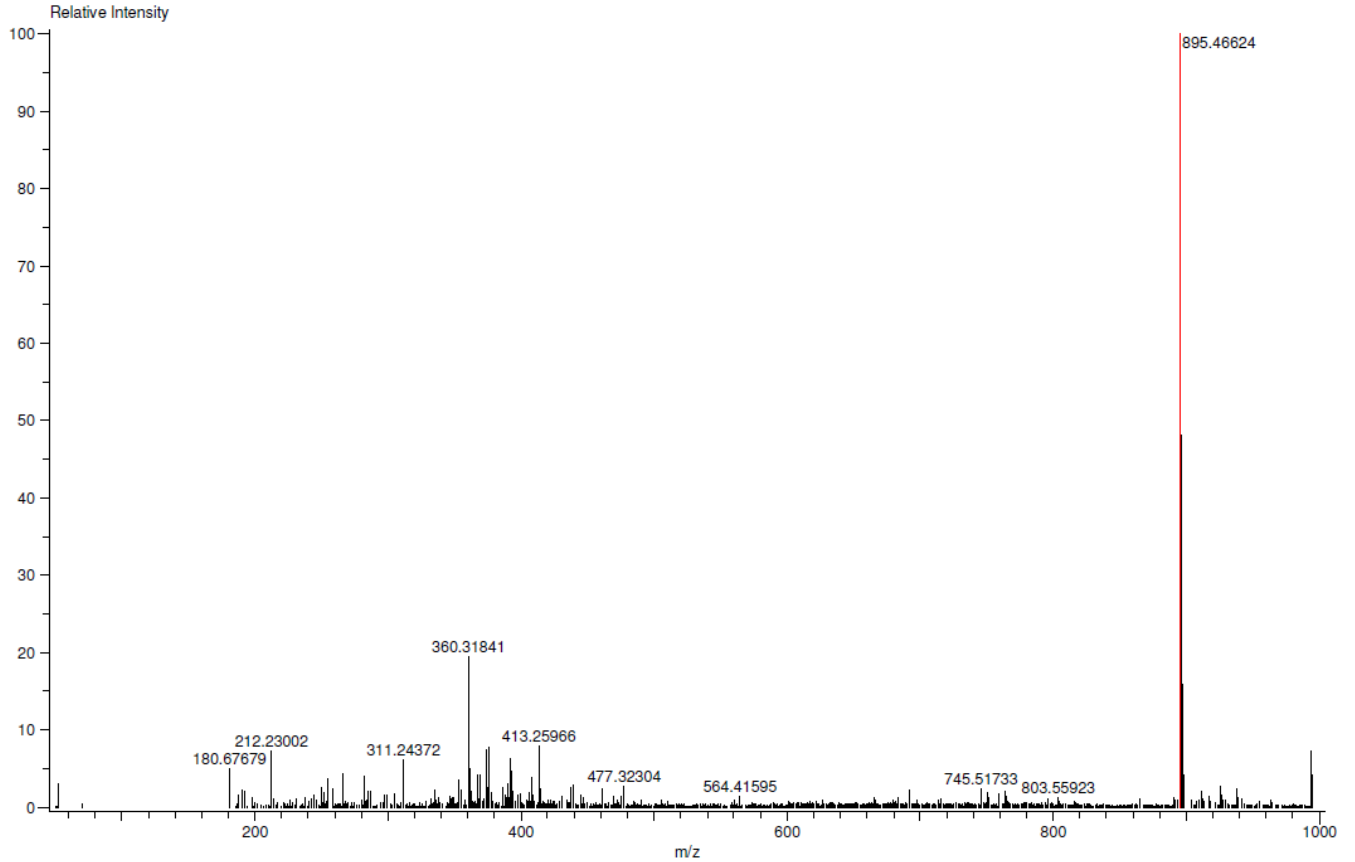

Figure S73. High resolution mass spectrum of chrysoeriol 6-C-β-arabinofuranosyl-8-C-β-glucopyranoside (5)

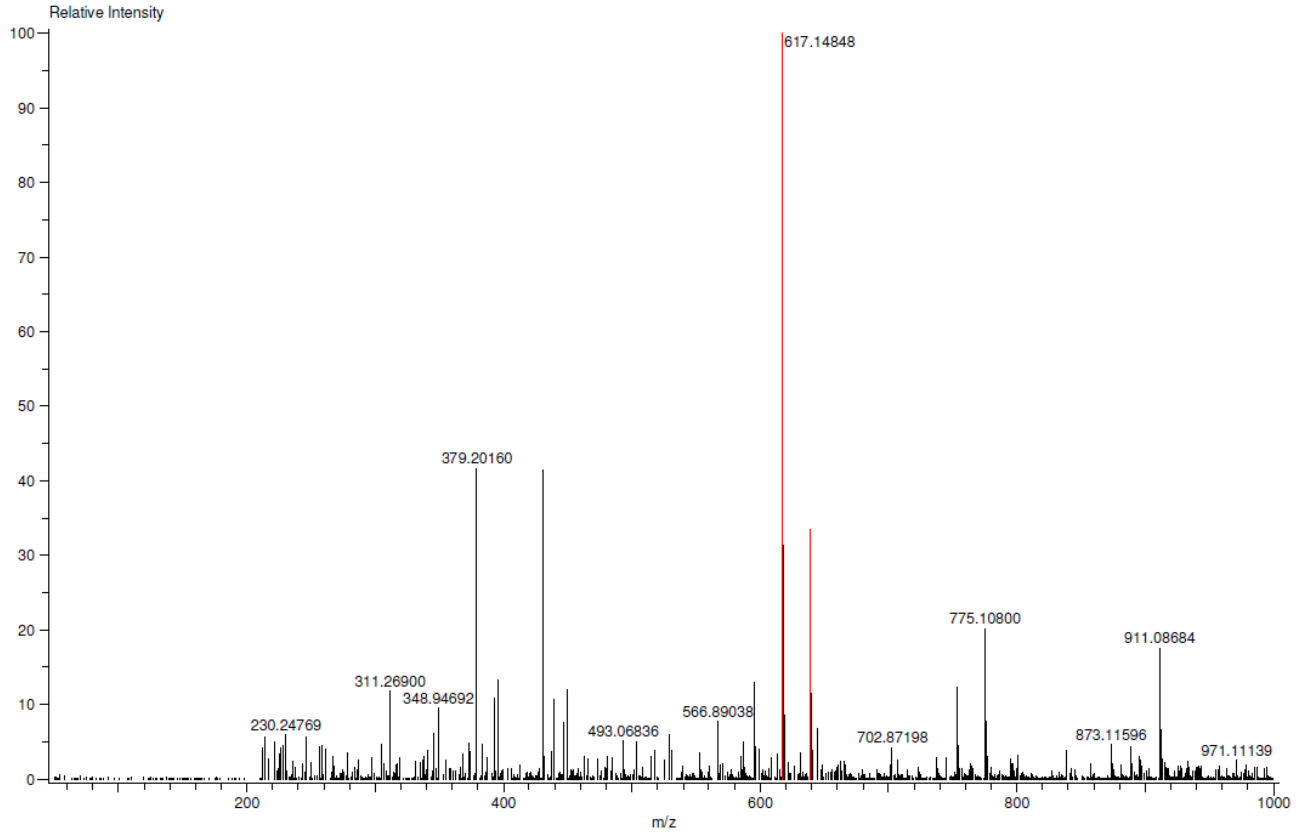

Figure S74. High resolution mass spectrum of chrysoeriol 6-C-β-arabinopyranosyl-8-C-β-glucopyranoside (6)

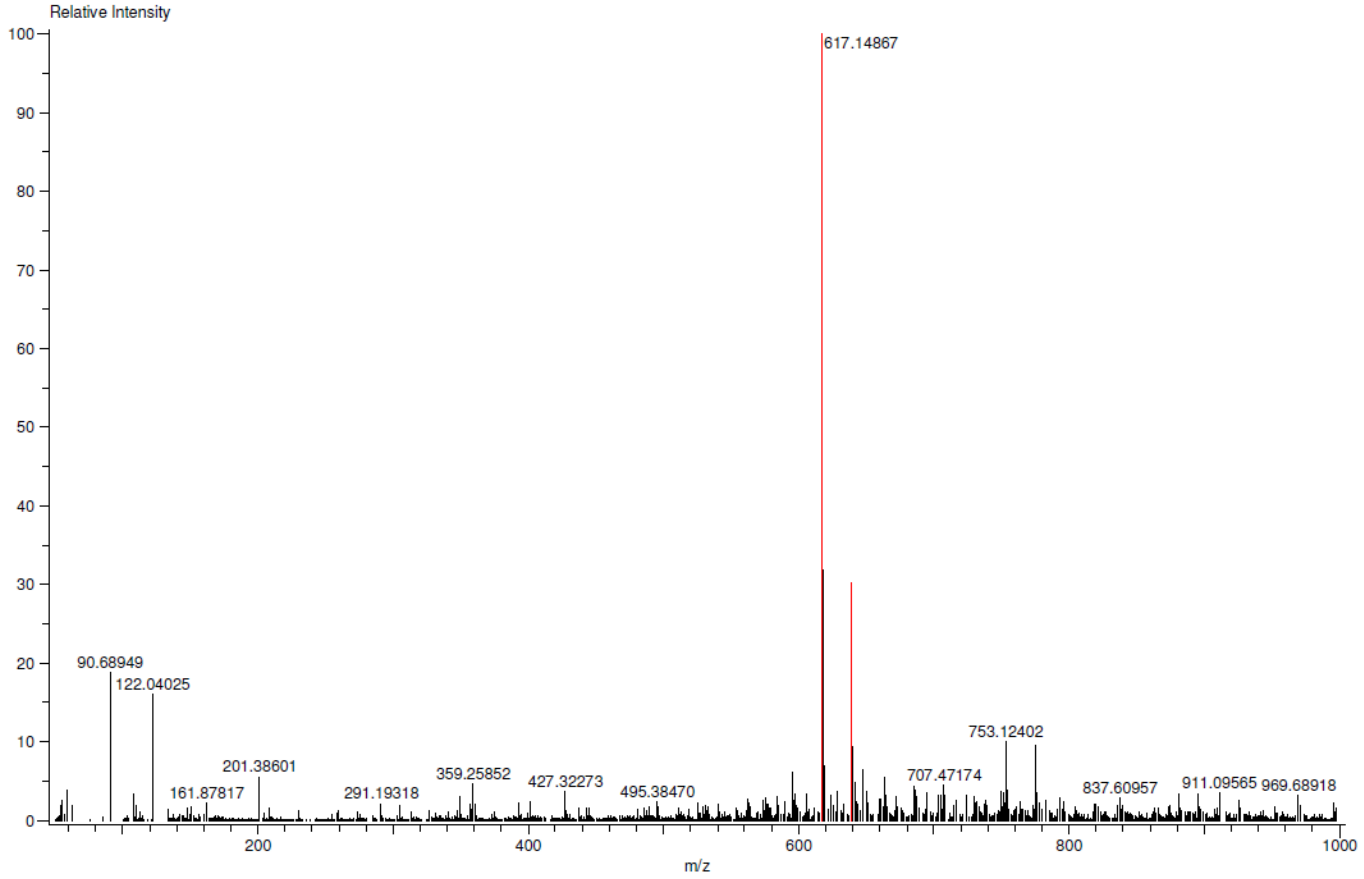

Figure S75. High resolution mass spectrum of chrysoeriol 6-C-β-xylopyranosyl-8-C-β-glucopyranoside (7)

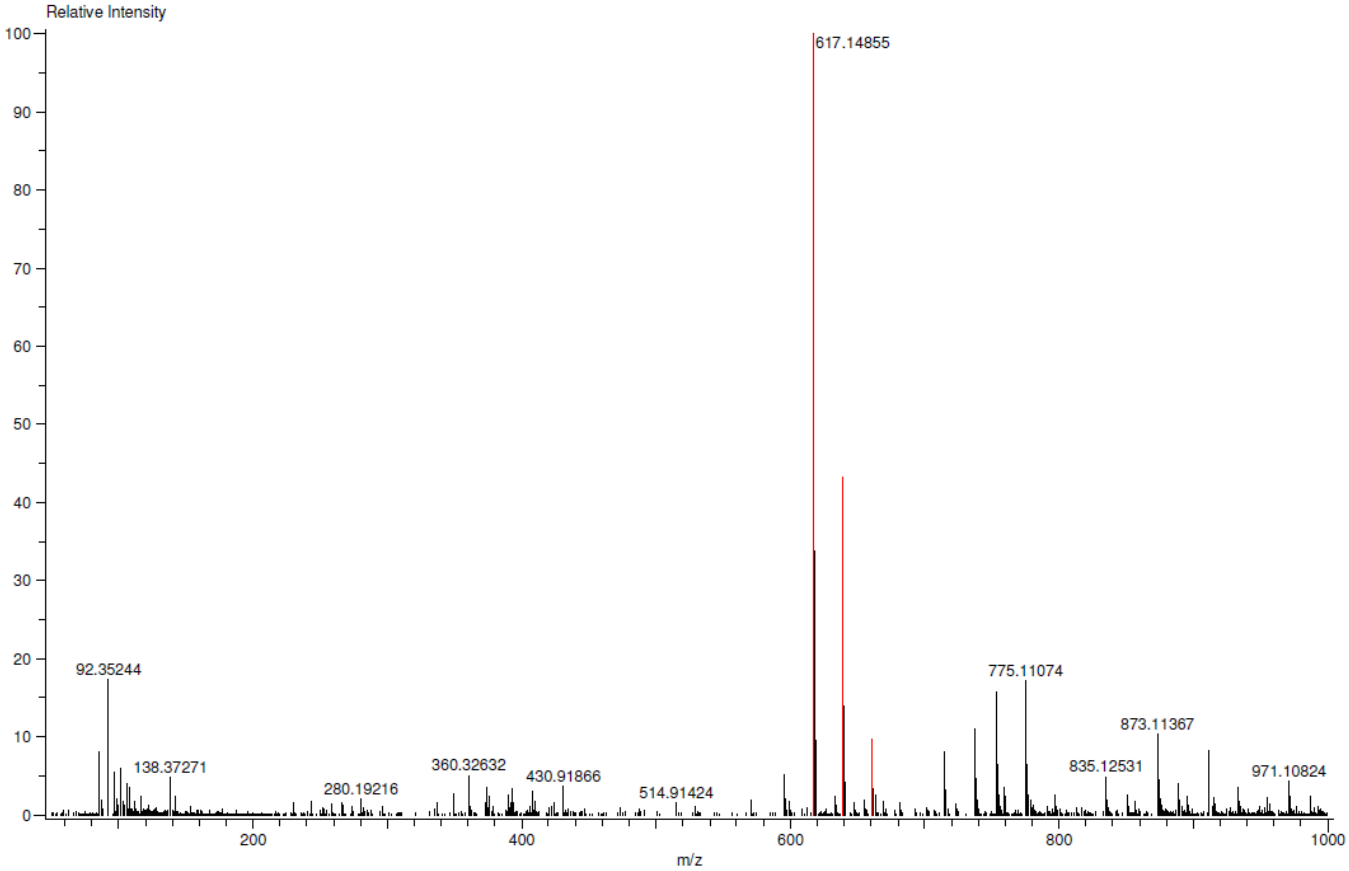

Figure S76. High resolution mass spectrum of chrysoeriol 6-C-β-galactopyranosyl-8-C-β-glucopyranoside (8)

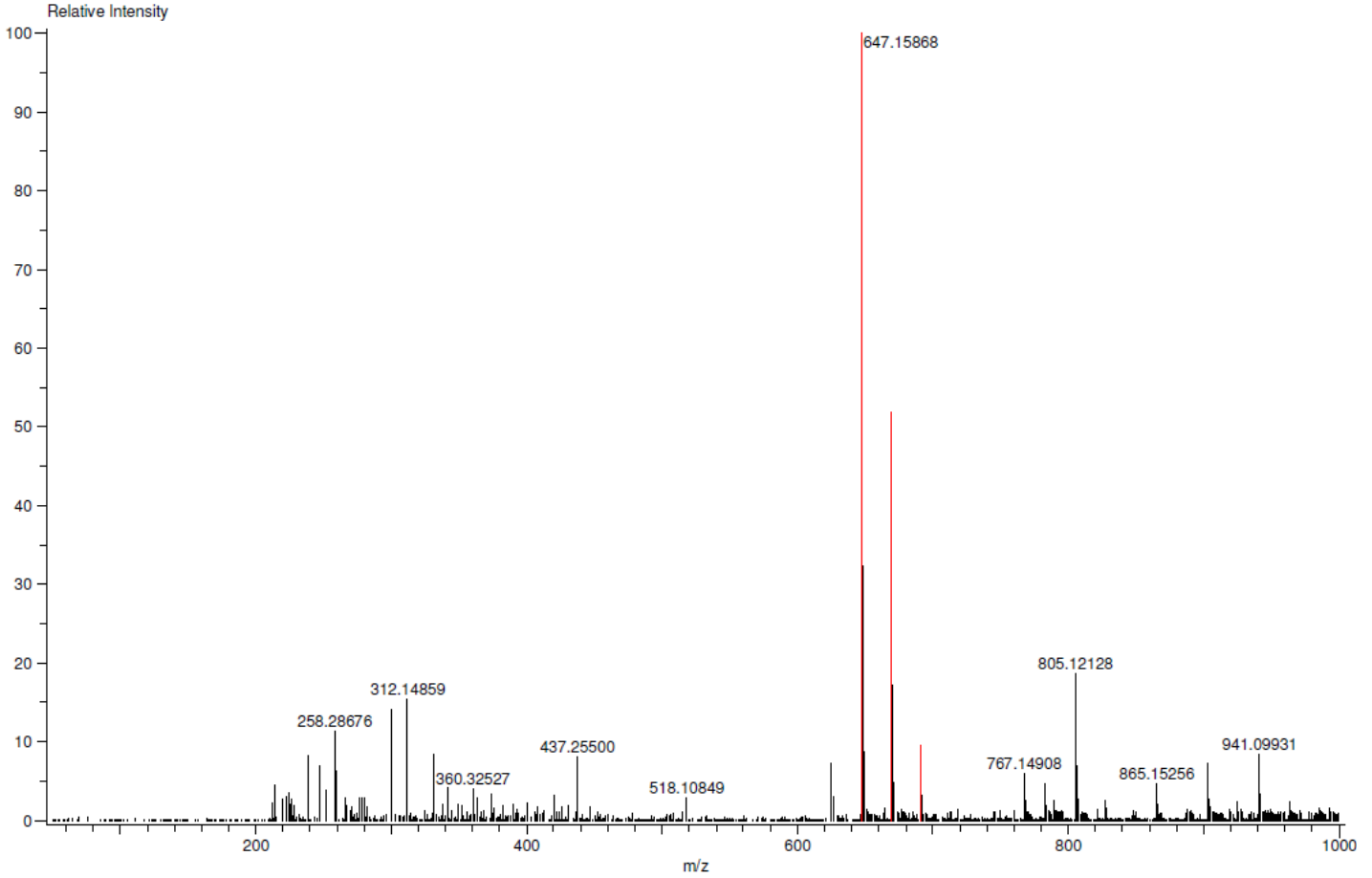

Figure S77. High resolution mass spectrum of chrysoeriol 6-C-β-glucopyranosyl-8-C-β-galactopyranoside (9)

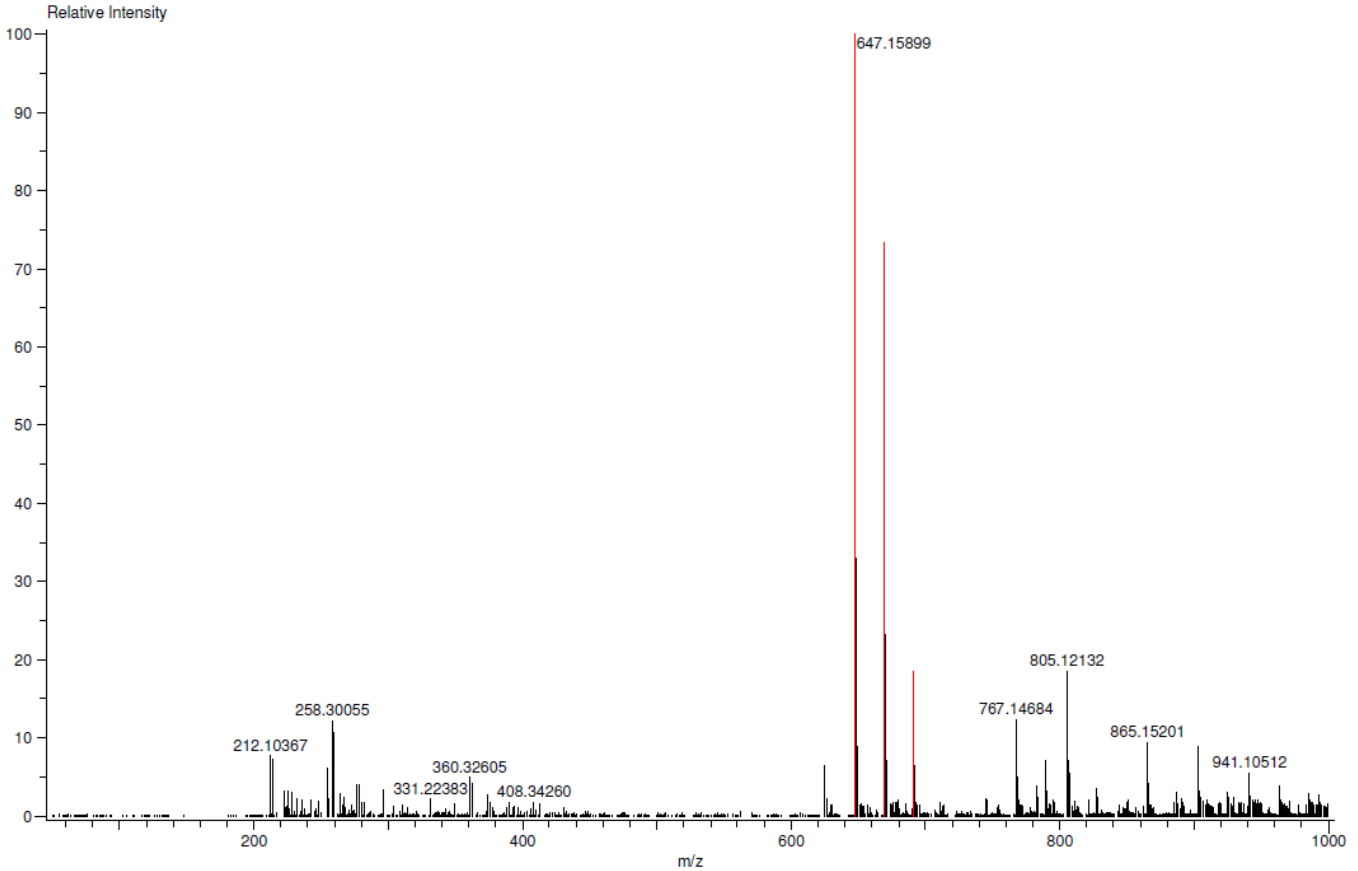

Figure S78. HPLC chromatogram of the aqueous phase of extract of *N. ossifragum* detected at 280 ± 10 nm

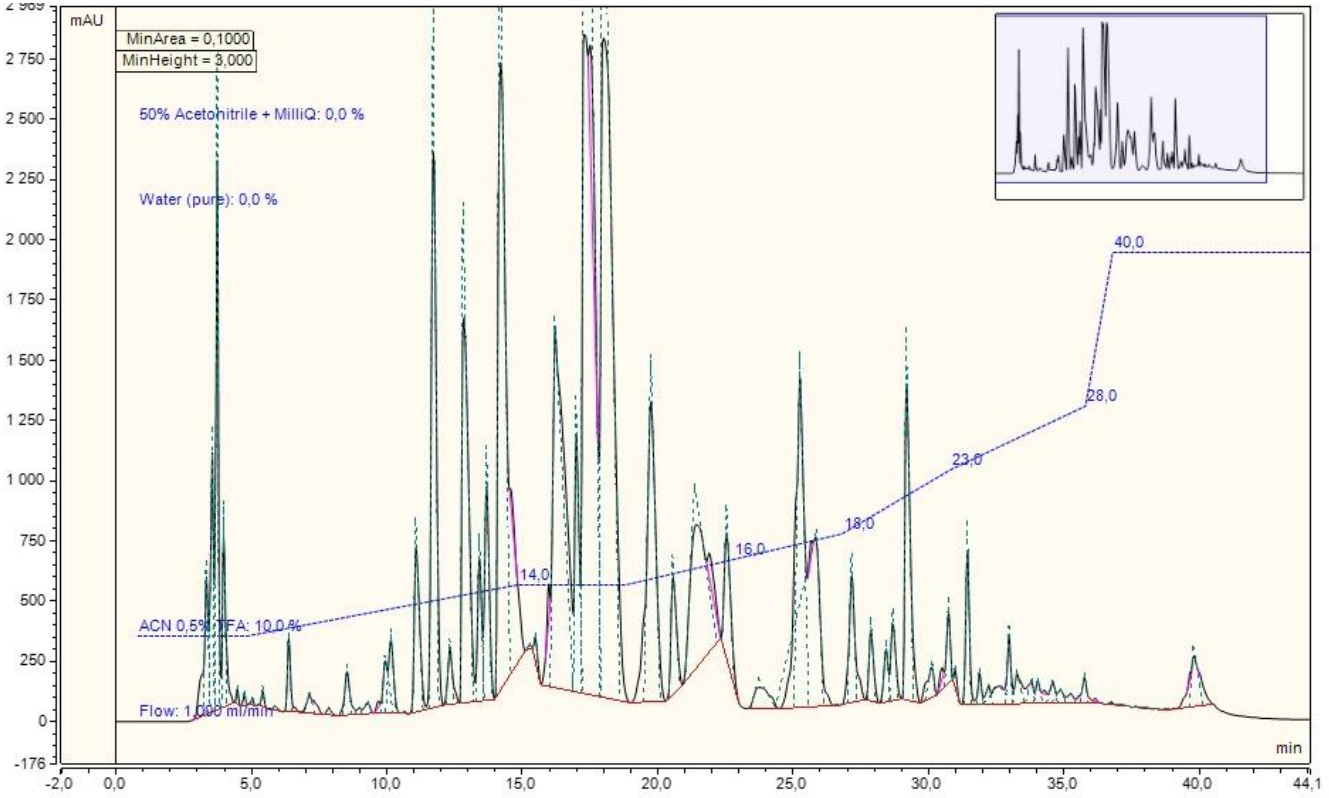

Figure S79. CD spectra of 5-10

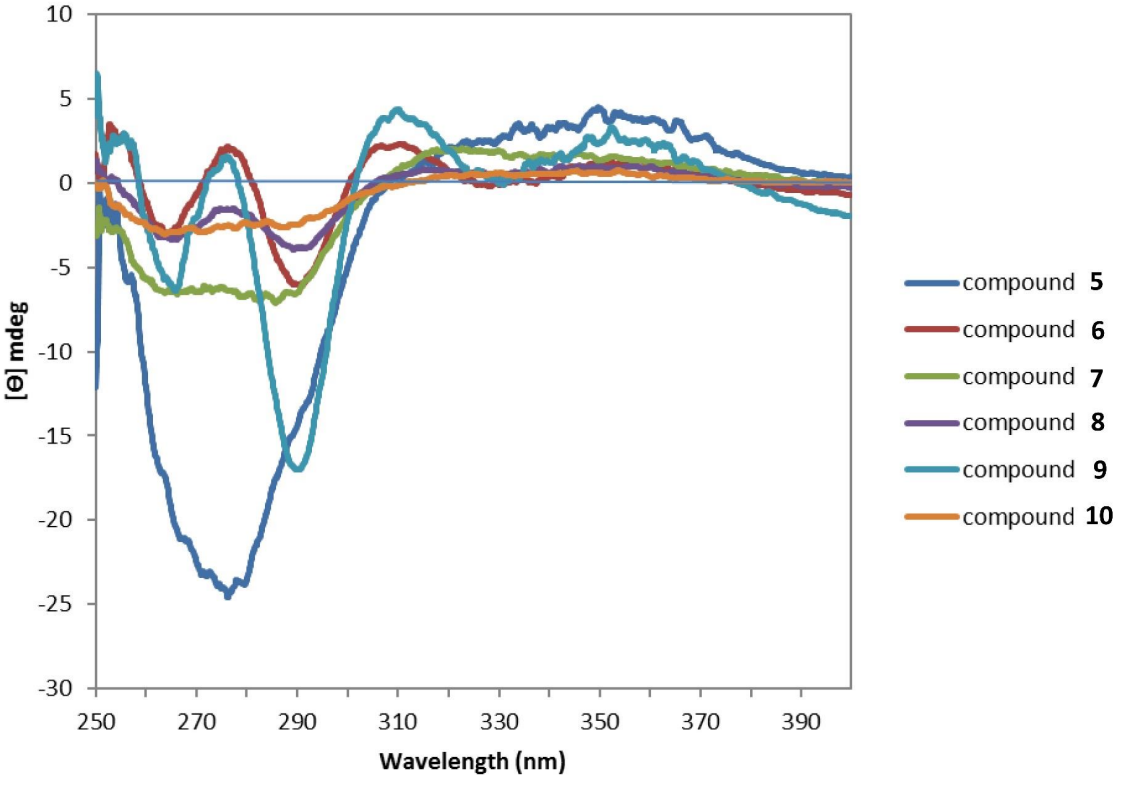

Paper II

Paper III

Paper IV

molecules

MDPI

Article

Cytotoxic Natural Products Isolated from *Cryptogramma crispa* (L.) R. Br.

Andrea Estefania Carpinteyro Diaz [1], Lars Herfindal [2], Heidi Lie Andersen [3] and Torgils Fossen [1,*]

[1] Department of Chemistry and Centre for Pharmacy, University of Bergen, N-5007 Bergen, Norway; andrea.diaz@uib.no
[2] Department of Clinical Science and Centre for Pharmacy, University of Bergen, N-5009 Bergen, Norway; lars.herfindal@uib.no
[3] University Gardens, University of Bergen, Allégt. 41, N-5007 Bergen, Norway; heidi.andersen@uib.no
* Correspondence: torgils.fossen@uib.no; Tel.: +47-55-583463; Fax: +47-55-589490

Abstract: Parsley fern, *Cryptogramma crispa*, is a common fern in arctic–alpine regions, and even though this species has been known since ancient times and has been presumed to cause the poisoning of horses, its natural products have not previously been investigated. Here, we characterise 15 natural products isolated from the aerial parts of *Cryptogramma crispa*, including the previously undescribed compound 3-malonyl pteroside D. The structure determinations were based on several advanced 1D and 2D NMR spectroscopic techniques, Circular Dichroism spectroscopy and high-resolution mass spectrometry. The pteroside derivatives exhibited selective moderate cytotoxic activity against the acute myeloid leukaemia MOLM13 cell line and no cytotoxicity against the normal heart and kidney cell lines, suggesting that their potential anticancer effect should be further investigated.

Keywords: *Cryptogramma crispa*; aerial parts; pterosin; pteroside; NMR; cytotoxicity

Citation: Diaz, A.E.C.; Herfindal, L.; Andersen, H.L.; Fossen, T. Cytotoxic Natural Products Isolated from *Cryptogramma crispa* (L.) R. Br. *Molecules* **2023**, *28*, 7723. https://doi.org/10.3390/molecules28237723

Academic Editors: Francesco Cacciola, Maurizio Battino, Milen I. Georgiev, Vincenzo De Feo, Maria Z. Tsimidou and Luca Rastrelli

Received: 31 October 2023
Revised: 20 November 2023
Accepted: 21 November 2023
Published: 23 November 2023

1. Introduction

The leptosporangiate fern genus *Cryptogramma* of the family Pteridaceae comprise nine species and is referred to as parsley fern, as its foliage resembles that of parsley [1]. *Cryptogramma crispa* (L.) R. Br. (Figure 1) is a small rupestral fern widely distributed from the montane to the subalpine zones of the temperate and boreal regions of Europe, with two main distribution centres: the northern area, including the highest mountains in the British Isles and west Scandinavia, and the southern area comprising the highest mountains in south Europe. Within its northern distribution area, *C. crispa* occurs over a broad altitudinal range, between 20 m and 2800 m above sea level [2,3].

C. crispa is a strongly calcifuge species that only grows on non-carbonaceous bedrocks, often forming patches. This species is quite hardy and can be covered by snow during the winter and receive lots of solar radiation during the summer [3,4].

According to observations within Norwegian traditional medicine, horses that excessively consume parsley ferns are susceptible to colic, thus explaining its Norwegian name hestespreng (which means "horse bloating"). Even though the traditional observation has not been unambiguously confirmed in modern studies [5], this species appears to be a potentially interesting source of bioactive natural products. While the existing literature regarding *C. crispa* is mainly limited to studies of the botanical characteristics of the plant, only a restricted number of studies have explored its phytochemical composition.

In the current literature, only relatively volatile compounds, including alkyl esters, fatty acids, primary alcohols, aldehydes, and alkanes, have hitherto been identified by GCMS from *C. crispa* [6]. Some carotenoid derivatives and shikimic acid derivatives have also been suggested to be present in this plant [7]. However, the structures of these compounds remain elusive. To the best of our knowledge, no studies exist in the current literature about the isolation and identification of pure compounds from this plant species.

Figure 1. Aerial parts of *Cryptogramma crispa*. Photo: Andrea Estefania Carpinteyro Diaz.

As part of our ongoing research on the description of new natural products with potential applications as lead compounds of future anticancer drugs, we report on the characterisation of 15 natural compounds from the aerial parts of *C. crispa*, which have been identified from this plant species for the first time, including a novel compound, as well as their cytotoxic activity towards leukaemia cells and normal kidney and heart cell lines.

2. Results and Discussion

The methanolic extract obtained from the aerial parts from *Cryptogramma crispa* was concentrated under reduced pressure and subjected to separation via liquid/liquid partition with petroleum ether followed by ethyl acetate. The components of the aqueous and ethyl acetate phases were further separated via adsorption chromatography, gel filtration chromatography, and preparative HPLC.

The fourteen known compounds isolated from *C. crispa* are: quercetin (**1**), quercetin 3-*O*-*β*-galactopyranoside (**2**), quercetin 3-*O*-*β*-glucopyranoside (**3**), quercetin 7-*O*-*β*-glucopyranoside (**4**), kaempferol 7-*O*-*β*-glucopyranoside (**5**), ferulic acid (**6**), ferulic acid 4-*O*-*β*-glucopyranoside (**7**), *p*-coumaric acid-4-*O*-*β*-glucopyranoside (**8**), caffeic acid (**9**), chlorogenic acid (**10**), chlorogenic acid methyl ester (**11**), pteroside D (**12**), pteroside X (**13**), and pterosin D (**15**) (Figure 2). These compounds were identified for the first time in parsley fern with using several 1D and 2D NMR spectroscopic techniques. Compound **13** was previously identified as pteroside X by Murakami et al. [8] from *Pteris fauriei* Hieron using 1D ^{1}H NMR. In this paper, complete ^{1}H and ^{13}C data for pteroside X are available for the first time.

The UV spectrum of compound **14** recorded online during HPLC analysis exhibited λ_{max} values at 260, 215, and 198 nm (Figure S10), which are consistent with a 1-indanone derivative. The 1D ^{1}H NMR spectrum and the 1D ^{13}C NMR spectrum of **14** (Figures S1 and S2) showed the presence of an extensively substituted 1-indanone derivative, with only one aromatic hydrogen observed at δ 7.28 s (H-4) (Table 1) and one aliphatic hydrogen (H-3) observed at δ 5.94 s directly attached to the 1-indanone ring system. The 1D ^{1}H NMR spectrum and the 1D ^{13}C NMR spectrum of **14** showed the presence of four methyl groups at δ 1.19 (H-10), δ 0.96 (H-11), δ 2.42 (H-12), and δ 2.61 (H-15), respectively. The cross-peaks at δ 1.19/49.8 (H-10/C-2) and δ 0.96/49.8 (H-10/C-2) confirmed that these methyl groups were connected in the C-2 position. The cross-peaks at δ 2.42/145.2 (H-12/C-5) and δ 2.61/137.2 (H-15/C-7) confirmed

that these methyl groups were connected to the C-5 and C-6 positions, respectively (Figure 2). Moreover, a C2 unit was identified at δ 3.00/29.14 (H-13/C-13), δ 3.75/66.79 (H-14A/C-14), and δ 3.56/66.79 (H-14B/C-14). The cross-peaks at δ 3.00/145.2 (H-13/C-5) and δ 3.00/137.2 (H-13/C-7) confirmed that this unit was attached to the C-6 position of the aromatic ring of compound **14** (Figure 2; Tables 1 and 2). Furthermore, the 1D ^{1}H NMR spectrum and the 1D ^{13}C NMR spectrum of **14** showed the presence of a glucosyl substituent and a malonyl substituent, respectively (Figures S1 and S3; Tables 1 and 2). All the ^{1}H and ^{13}C resonances belonging to the glucosyl substituent were assigned using the combined information gained from the 1D selective TOCSY spectrum (Figure S2), the 2D ^{1}H-^{13}C HSQC spectrum (Figure S5), the 2D ^{1}H-^{13}C H2BC spectrum (Figure S6), and the 2D ^{1}H-^{1}H COSY spectrum of **14** (Figure S7). The cross-peaks at δ 4.20/66.8 (H-1′/C-14), δ 3.75/102.9 (H-14A/C-1′), and δ 3.56/102.9 (H-14B/C-1′) observed in the 2D ^{1}H-^{13}C HMBC spectrum of **14** (Figure 3) confirmed that the glucosyl substituent was attached to C-14. The sugar unit was identified as glucose with a *β*-configuration because of the large coupling constant (δ 4.20 d 7.8 Hz; H-1′). The cross-peak at δ 5.94/167.2 (H-3/C-1″) observed in the HMBC spectrum (Figure 3) confirmed that the malonyl unit was attached to C-3 (Figure 2).

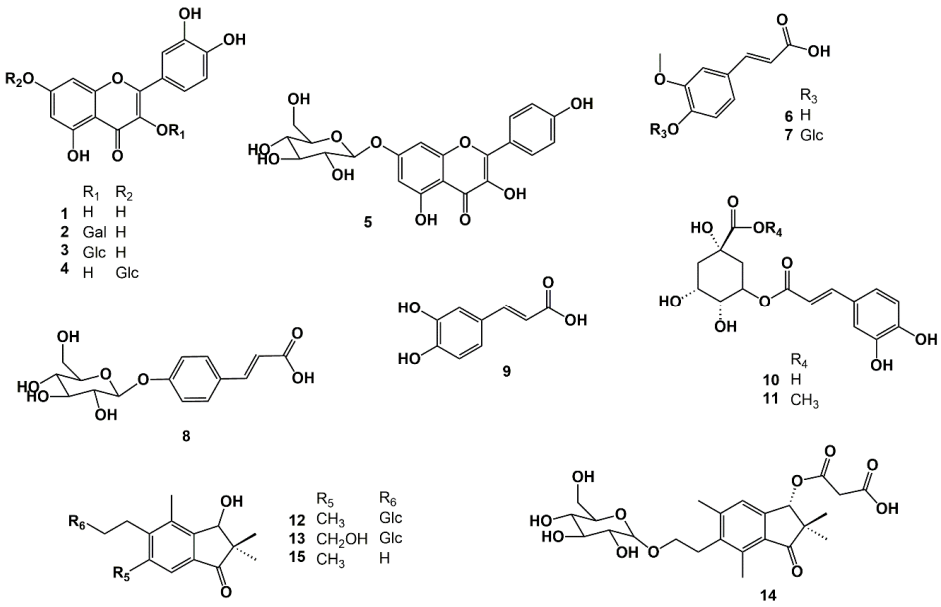

Figure 2. Molecular structures of compound **1–15** characterised from *Cryptogramma crispa* (L.) R. Br.

Table 1. ^{1}H chemical shift values (ppm) and coupling constants (Hz) of Pteroside D (**12**), Pteroside X (**13**), 3-malonyl-pteroside D (**14**), and Pterosin D (**15**) dissolved in DMSO-D_6 at 298K.

	Compound 12	**Compound 13**	**Compound 14**	**Compound 15**
	δ ^{1}H	δ ^{1}H	δ ^{1}H	δ ^{1}H
1				
2				
3	4.64	4.66	5.94 s	4.64
4	7.30 s	7.62 s	7.28 s	7.30 s
5				
6				
7				
8				
9				

Table 1. *Cont.*

	Compound 12	Compound 13	Compound 14	Compound 15
10	1.08 s	1.10 s	1.19 s	1.08 s
11	0.91 s	0.92	0.96 s	0.91 s
12	2.41 s	4.65 s	2.42 s	2.40 s
13	2.97 m	2.95 t 7.9	3.00 m	2.84 dd 8.5, 7.3
14A	3.75 m	3.75 m	3.75 m	3.45 dd 8.5, 7.3
14B	3.55 m	3.54 dt 10.1, 7.9	3.56 m	
15	2.57	2.58 s	2.61 s	2.56 s
14-*O*-*β*-glc				
1′	4.20 d 7.8	4.18 d 7.8	4.20 d 7.8	
2′	2.98 dd 2.8; 9.1	2.95 dd 9.0, 7.8	2.94 dd 9.0, 7.8	
3′	3.15 dd 8.5; 9.1	3.12 t 8.9	3.12 t 8.9	
4′	3.06 dd 8.5; 9.7	3.03 dd 9.7, 8.8	3.02 dd 9.8, 8.8	
5′	3.09 ddd 2.2; 5.8; 9.7	3.08 ddd 9.7, 6.0, 2.2	3.08 ddd 9.8, 6.0, 2.2	
6A′	3.66 dd 2.2; 11.8	3.64 dd 11.8, 2.2	3.64 dd 11.8, 2.2	
6B′	3.44 dd 5.8; 11.8	3.42 dd 11.8, 6.0	3.41 dd 11.8, 6.0	
3-*O*-malonyl				
1″				
2″			3.50 s	
3″				

Table 2. ^{13}C chemical shift values (ppm) of Pteroside D (**12**), Pteroside X (**13**), 3-malonyl-pteroside D (**14**), and Pterosin D (**15**) dissolved in DMSO-D_6 at 298K.

	Compound 12	Compound 13	Compound 14	Compound 15
	δ ^{13}C	δ ^{13}C	δ ^{13}C	δ ^{13}C
1	209.26	209.23	207.21	209.12
2	51.06	51.01	49.77	50.88
3	75.45	75.35	77.61	75.25
4	125.18	121.75	125.42	124.92
5	144.48	148.08	145.19	144.20
6	136.60	134.93	138.15	137.19
7	136.55	136.25	137.15	136.15
8	129.62	129.88	129.91	129.39
9	153.19	153.12	147.74	152.81
10	23.04	22.85	23.46	22.95
11	20.67	20.64	20.11	20.59
12	21.03	61.38	20.96	20.95
13	29.22	28.10	29.14	32.22
14A	67.13	67.43	66.79	59.81
14B				
15	13.58	13.22	13.4	13.50
14-*O*-*β*-glc				
1′	103.08	102.95	102.91	
2′	73.73	73.56	73.56	
3′	77.07	76.87	76.90	
4′	70.33	70.15	70.19	
5′	77.10	76.99	77.02	
6A′	61.31	61.14	61.16	
6B′				
3-*O*-malonyl				
1″			167.18	
2″			41.62	
3″			168.00	

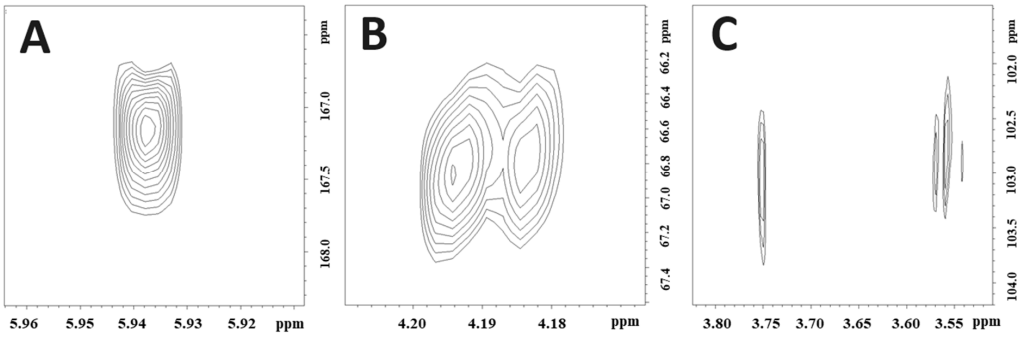

Figure 3. Important HMBC cross-peaks for structure determination of 3(R)-O-malonyl pteroside D (compound **14**). (**A**) The cross-peak at δ 5.94/167.2 (H-4/C-1″) confirms the malonyl substituent's connection to the 1-indanon core. (**B**) The cross-peak at δ 4.18/66.8 (H-1′/C-14) and (**C**) the cross-peaks detected at δ 3.75/102.9 (H-14A/C-1′) and δ 3.56/102.9 /H-14B/C-1′), confirming the connection of the glucosyl unit to the alkyl group at C-14.

The stereochemistry of the chiral carbons belonging to C-3 of the 1-indanone core structure was determined via Circular Dichroism (CD) spectroscopy (Figure S9). The CD spectrum of **14** showed a negative Cotton effect at 301 nm and a positive Cotton effect at 333 nm, which was in accordance with 3*R* configuration [9]. Therefore, compound **14** was identified as 3(*R*)-*O*-malonyl pteroside D (Figure 2). A negative molecular ion $[M - H]^-$ at m/z 495.1861 corresponding to $C_{24}H_{32}O_{11}$ (calculated: m/z 495.1872; $\Delta = -2.17$ ppm) observed in the high-resolution mass spectrum of compound **14** confirmed this identification (Figure 2 and Figure S8 (in the Supplementary Materials)).

Pterosins are sesquiterpenoids with a 1-indanone core structure; the glucoside version is called a pteroside. This name originates from the fern *Pteridium aquilinum* var. *latiusculum*, which is one of the oldest and most common plants in the world and the first plant source from which such compounds were isolated. At the end of the 19th century, reports of lethal intoxication in cattle were established after consuming *P. aquilinum* [10,11]. Pterosin D and Pteroside D were first isolated by Yoshihira et al. [12] from *P. aquilunum* and have later been found in other fern varieties, such as *P. aqullinum* subsp. *wightianum* (Wall) Shich, *H. punctata* (Thunb) Mett, *J. scammanae* Tryon, *M. speluncae* (L.) Moore, *M. strigosa* (Thunb) Presl, and *D. wilfordii* (Moore) Christ [13].

Flavonoids are important natural products of ferns. A multitude of these compounds has hitherto been reported from ferns belonging to Dryopteridaceae, Thelypteridaceae, Selaginellaceae, Equisetaceae, Helminthostachyaceae, Ophioglossaceae, Lygodiaceae, Athyriaceae, and Aspleniaceae species [13]. In the genus Pteridaceae, the flavonoids of the *Pteris* species have been extensively investigated. The main flavonoids of ferns in this compound class are flavones, flavonols, and flavanones [14,15]. All the flavonoids identified in *C. crispa* in this paper are flavonols, where the derivatives of quercetin predominate.

In our ongoing research that aims to identify new lead compounds for future anticancer therapy, the cytotoxic activity of four 1-indanone derivatives (compounds **12**, **13**, **14**, and **15**) were tested towards the acute myeloid leukaemia cell line MOLM-13. Table 3 presents the EC_{50} values after 72 h exposure, which in our previous work, have shown to reveal cytotxic effects at concentrations giving no cell death at 48 h [16].

Moderate and relatively similar cytotoxicity levels towards this cell line were observed for all the compounds, with EC_{50} values ranging from 182.88 ± 0.08 μM for compound **12** to 197.88 ± 0.18 μM for compound **14**. The cytotoxicity of pterosin D and pteroside D could be regarded with the sugar moiety; meanwhile, adding a substituent in the C-3 position and on C-5 decreases the cytotoxicity of these 1-indanone structures [12,17].

Table 3. Cytotoxicity of compounds **12**–**15** against three mammalian cell lines. The compounds were dissolved in DMSO. The cells were tested for metabolic activity after 72 h of incubation. The EC_{50} values were determined via non-linear regression from 3 independent experiments (MOLM13), as described in the methods section. The data from H9c2 and NRK cells originate from three experiments. "-" denotes that no data are available due to low or no observed toxicity above concentrations of 200 µM.

	MOLM13 (µM)	H9c2 (µM)	NRK (µM)
Compound **12**	182.88 ± 0.08	-	-
Compound **13**	191.66 ± 0.13	-	-
Compound **14**	197.88 ± 0.18	-	-
Compound **15**	189.96 ± 0.16	-	-

These compounds exhibited selective cytotoxic activity towards MOLM13, which is illustrated by the fact that none of these compounds were cytotoxic towards the normal cell lines NRK and heart cells, respectively (Table 3). Pterosides are 1-indanone derivatives that are structurally related to ptaquiloside derivatives, which are cancer-promoting agents [18]. However, the cancer-promoting effects are normally not observable within a short timescale of 24 to 72 h, which was applied in our experiments to determine the cytotoxicity of individual compounds. McMorris et al. [19], who studied the structure–activity relationship of the structurally related illudins isolated from *Omphalotus illudens* mushrooms, reported that illudins have a significant anticancer potential. Illudins are structurally related to ptaquiloside structures with fewer cytotoxic effects than ptaquiloside. Some of these compounds, for example, illudin M and illudin S, exhibit significant antibacterial activity [20]. The latter-mentioned compounds are more potent than the pterosides described in this paper, with cytotoxic effects against myeloid leukaemia HL 60 cells in the range of 6-100 nM [21]. According to Liston and Davis [22], EC_{50} concentrations of around 180 µM are within the upper range of biologically relevant anticancer drugs. However, our determinations of cytotoxic activity have been performed on cell cultures; henceforth, the predictions of which concentrations can be achieved in vivo remain elusive.

In comparing the cytotoxicity of the pterosides presented in this work with the other 1-indanone structure, we found that the mild and selective toxicity towards AML MOLM13 cells is a positive discovery worthy of further investigations.

3. Materials and Methods

3.1. Plant Material

Fresh plant material of *Cryptogramma crispa* was collected during the summers of 2021 and 2022 on the mountain of Fløyen, in Bergen, Norway, at 302 m above sea level (coordinates 60.397687 N and 005.337902 E). A voucher specimen of *C. crispa* was deposited at the herbarium BG, University of Bergen (accession number BG/S-168787). Before extraction, the fresh plant material was stored at −25 °C for preservation.

3.2. Extraction and Partition Purification with Organic Solvents

Aerial parts of *Cryptogramma crispa* (1.9 kg) were extracted with 22.5 L HPLC-grade methanol (Sigma-Aldrich, St. Louis, MO, USA) for 72 h maceration at room temperature without mixing. The extraction yield was 8.6% of the wet weight. Considering the water content was 94.1%, the dry weight extraction yield was 46.9%. The methanolic extract was percolated through glass wool and concentrated with rotary evaporators under reduced pressure. The resulting concentrated aqueous extract (700 mL) was purified via liquid–liquid partition three times with petroleum ether (Petroleum ether–ACS reagent, Sigma-Aldrich, Saint Louis, MO, USA) using a total volume of 4.0 L. The resulting water phase was further purified via liquid–liquid partition three times with ethyl acetate (Ethyl Acetate–ACS reagent ≥ 99.5%, Sigma-Aldrich, Saint Louis, MO, USA) using a total volume of 3.2 L.

The residual aqueous phase and the ethyl acetate phase were individually concentrated with a rotavapor to a volume of 200 mL each.

3.3. XAD-7 Absorption Chromatography

The concentrated residual aqueous extract (200 mL) was added to an Amberlite XAD-7 column (column dimensions 50 × 1000 mm, containing 500 g Amberlite® XAD-7, 20–60 mesh, Sigma-Aldrich, Saint Louis, MO, USA) to remove bulk substances, like sugars, polysaccharides, and free aliphatic amino acids, from the extract when distilled water was used as a mobile phase. Under these solvent conditions, fewer polar and aromatic compounds are absorbed by the XAD-7 column material. The latter compounds are readily eluted from the XAD-7 column when the mobile phase is changed to pure methanol (HPLC grade). The mobile phase gradient consisted of 5.0 L distilled water, followed by 8.0 L methanol. The flow rate was 5 mL/min. This chromatographic separation gave a total of 13 fractions with volumes of 1 L, which were analysed individually via analytical HPLC. The same procedure was conducted with the ethyl acetate phase, whereby 16 fractions were obtained and analysed individually via analytical HPLC.

3.4. Sephadex LH-20 Gel Filtration Chromatography

The combined fractions 4–7 and 10–11 from the XAD-7 purification of the water phase were individually concentrated to a volume of 20 mL and further separated individually via gel filtration chromatography with a Sephadex LH-20 column (column dimensions 50 × 1000 mm, containing 500 g of Sephadex® LH-20, Sigma-Aldrich, Saint Louis, MO, USA) using a gradient of super distilled water and methanol containing 0.1% TFA (Trifluoroacetic acid—for HPLC, ≥ 99.0%, Sigma-Aldrich, Saint Louis, MO, USA). The gradient consisted of 2.5 L Water–methanol–TFA 80:20:0.1 $v/v/v$, followed by 2.5 L Water–methanol–TFA 50:50:0.1 $v/v/v$, 2.5 L Water–methanol–TFA 30:70:0.1 $v/v/v$, and finally 2.5 L methanol–TFA 100:0.1 v/v. The flow rate was 5 mL/min. Each collected fraction had a volume of 90 mL and was analysed via analytical HPLC. From the Sephadex separation of the combined XAD-7 fractions 4–7, 80 fractions were collected. The combined fractions, 12–15, 31–34, 38–39, and 42–48, were afterwards individually separated via preparative HPLC. From the Sephadex separation of the combined XAD-7 fractions 10–11, 30 fractions were collected. The combined fractions 22–24 were thereafter separated via preparative HPLC. A similar procedure was followed for the Sephadex LH-20 separation of the combined XAD-7 fractions 7–10, resulting from the purification of the ethyl acetate partition of the extract. From the Sephadex separation of these combined XAD-7 fractions, 43 fractions were collected. Pure pteroside D (compound **12**) was isolated in fraction 11, while quercetin (compound **1**) and quercetin 3-O-β-galactopyranoside (compound **2**) were identified in fraction 29.

3.5. Preparative HPLC

Individual pure compounds of the fractions from Sephadex LH-20 column chromatography were isolated via preparative HPLC (Thermo Scientific preparative HPLC equipped with a Dionex Ultimate 3000 variable wavelength detector) equipped with a C_{18} Ascentis column (column dimensions 250 × 20 mm; 5 µm, spherical particles). A gradient of two solvents was used for elution, consisting of mobile phase A (super distilled water–TFA 99.9:0.1; v/v) and mobile phase B (acetonitrile–TFA 99.9:0.1; v/v) (acetonitrile was used for HPLC, gradient grade, ≥99.9%, Sigma-Aldrich, Saint Louis, USA). The elution profile consisted of isocratic elution with A-B (90:10 v/v) for 4 min, followed by a linear gradient from A-B (90:10 v/v) to A-B (80:20 v/v) for the next 10 min, isocratic elution with A-B (80:20 v/v) for the next 20 min, followed by a linear gradient from A-B (80:20 v/v) to A-B (70:30 v/v) for the next 10 min, followed by isocratic elution with A-B (70:30 v/v) for the next 20 min.

The flow rate was 15 mL/min. Portions of 750 µL were manually injected into the HPLC column and were manually collected based on the peaks that appeared in the online chromatogram recorded at 280 nm. Analytical HPLC was used to analyse the fractions from

preparative HPLC separation. Following this strategy, 42.6 mg compound **1**, 66.0 mg of compound **2**, 1.7 mg of compound **3**, 4.6 mg of compound **4**, 2.0 mg of compound **5**, 1.5 mg of compound **6**, 6.5 mg of compound **7**, 12.9 mg of compound **8**, 5.3 mg of compound **9**, 3.9 mg of compound **10**, 21.7 mg of compound **11**, 36.8 mg of compound **12**, 6.3 mg of compound **13**, 2.8 mg of compound **14**, and 18.4 mg of compound **15** were isolated.

3.6. Analytical HPLC

Individual samples were analysed using an Agilent Technologies 1260 Infinity II HPLC instrument equipped with a multidiode array detector, an autoinjector, and a 250 × 4.6 mm, 5 µm SUPELCO analytical Ascentis® C18 column. HPLC separation was performed according to the method previously published by Nguyen et al. [23]. Two solvents were used for elution: mobile phase A (super distilled water–TFA 99.9:0.1; v/v) and mobile phase B (acetonitrile–TFA 99.9:0.1; v/v), with a flow rate of 1 mL/min, and aliquots of 20 µL were injected. The elution profile began with initial conditions of 90% A and 10% B. Gradient elution followed this for 10 min at 14% B, and then isocratic elution from 10 to 14 min. The subsequent gradient conditions were as follows: 16% B at 18 min, 18% B at 22 min, 23% B at 26 min, 28% B at 31 min, and 40% B at 32 min. This was followed by isocratic elution from 32 to 40 min, gradient elution from 40 to 43 min at 10% B, and final isocratic elution from 43 to 46 min at 10% B [23].

3.7. Spectroscopy

High-resolution mass spectra were recorded using a JEOL AccuTOF™ JMS T100LC (JEOL Ltd., Tokyo, Japan) instrument fitted with an electrospray ion source operated in positive mode at a resolving power of approximately 6000 FWHM. Mass spectra were recorded over the mass range of 50–2000 m/z. The samples were analysed as methanolic solutions and introduced to the ESI spray chamber with weakly acidified (0.01% HCOOH) acetonitrile (Acetonitrile—for HPLC, gradient grade, ≥99.9%, Sigma-Aldrich, Saint Louis, MO, USA) used as a spray reagent.

UV-Vis absorption spectra were recorded online during analytical HPLC analysis over the 210-600 nm wavelength range in steps of 2 nm.

Circular Dichroism (CD) spectra were recorded at 20 °C with a nitrogen atmosphere using a Jasco J-810 spectropolarimeter (Jasco Products LLC, Oklahoma City, OK, USA) equipped with a Peltier temperature control unit. This instrument was used to analyse compound **14** (2.9 mM) dissolved in 100% methanol (methanol for HPLC, ≥99.9%, Sigma-Aldrich, Saint Louis, MO, USA). The spectrum obtained was the average of 6 scans and a buffer scan with 100% methanol, which was subtracted from the spectrum. The spectrum was scanned from 185 to 400 nm. A 1 mm path-length cell was used during analysis.

NMR samples were prepared by dissolving the isolated compound in deuterated dimethylsulfoxide (DMSO-D_6; 99.96 atom% D, Sigma-Aldrich, Saint Louis, MO, USA). The 1D ^{1}H, 1D ^{13}CAPT, 2D ^{1}H-^{13}C HMBC, 2D ^{1}H-^{13}C HSQC, ^{1}H-^{13}C HSQC-TOCSY, 2D ^{1}H-^{13}C H2BC, 2D ^{1}H-^{1}H COSY, and 2D ^{1}H-^{1}H ROESY NMR experiments were conducted at 850.1300 MHz and 213.7654 MHz for ^{1}H and ^{13}C, respectively, using Bruker BioSpin AVANCE III HD 850 MHz instrument (Bruker Biospin AG, Fällanden, Switzerland) equipped with a ^{1}H, ^{13}C, and ^{15}N triple-resonance cryogenic probe at 298 K. The 1D ^{1}H NMR experiment (pulse program: zg30) was performed with 32 scans. The sweep width was 16 ppm, and the acquisition time was 1 min 57 s. The 1D ^{1}H selective TOCSY NMR experiment (pulse program: seldigpzs) was performed with 16 to 128 scans, depending on the individual sample concentrations. The sweep width was 16 ppm, and the acquisition time was between 1 min 57 s (NS = 16) and 10 min 19 s (NS = 128). The 1D ^{13}CAPT NMR experiment (pulse program: jmod) was performed with 512 to 15 800 scans, depending on the individual sample concentrations. The sweep width was 240 ppm, and the acquisition time was between 23 min 7 s (NS = 512) and 11 h 48 min 18 s (NS = 15 800). The 2D ^{1}H-^{13}C HMBC NMR experiment (pulse program: hmbcgplpndqf) was performed with 2 to 24 scans, depending on the individual sample concentrations and 256 experiments in

F1. The sweep widths were 10 to 14 ppm for ^{1}H and 220 ppm for ^{13}C. The acquisition time was between 15 min 55 s (NS = 2) and 3 h 5 min 14 s (NS = 24). The 2D edited ^{1}H-^{13}C HSQC experiment (pulse program: hsqcedetgpsisp2.3) was performed with 2 to 8 scans, depending on the individual sample concentrations, and 256 experiments in F1. The sweep widths were 10 ppm for ^{1}H and 160 ppm for ^{13}C. The acquisition time was between 20 min 1 s (NS = 2) and 1 h 18 min 8 s (NS = 8). The 2D ^{1}H-^{13}C H2BC NMR experiment (pulse program: h2bcetgpl3) was performed with 2 to 16 scans, depending on the individual sample concentrations and 256 experiments in F1. The sweep widths were 10 ppm for ^{1}H and 160 ppm for ^{13}C. The acquisition time was between 15 min 57 s (NS = 2) and 2 h 4 min 13 s (NS = 16). The 2D ^{1}H-^{13}C HSQC-TOCSY NMR experiment (pulse program: hsqcdietgpsisp2) was performed with 2 to 16 scans, depending on the individual sample concentrations and 256 experiments in F1. The sweep widths were 10 ppm for ^{1}H and 160 ppm for ^{13}C. The acquisition time was between 21 min 11 s (NS = 2) and 2 h 44 min 42 s (NS = 16). The 2D ^{1}H-^{1}H ROESY NMR experiment (pulse program: roesyphpp2) was performed with 8 scans and 256 experiments in F1. The sweep width was 10 ppm. The acquisition time was 1 h 25 min 36 s. The 2D ^{1}H-^{1}H COSY NMR experiment (pulse program: cosygpppqf) was performed with 8 scans and 256 experiments in F1. The sweep width was 10 ppm. The acquisition time was 1 h 25 min 36 s.

3.8. Cytotoxicity

Stock solutions were prepared by dissolving pure compounds to a final concentration of 20 mM in DMSO. The normal rat kidney epithelial cells (NRK, ATCC no.: CRL-6509) and rat cardiomyoblasts (H9c2, ATCC no.: CRL-1446) were cultured in DMEM medium supplemented with 10% foetal bovine serum (FBS, Invitrogen, Carlsbad, CA, USA). When the cells reached 80% confluence, they were detached in a mild trypsin treatment (0.33 mg/mL trypsin for 5 min at 37 °C), centrifuged (160× *g*, 4 min), and reseeded in fresh medium to 25% confluence.

The AML cell line MOLM13 (DSMZ no.: ACC554 [24]) was cultured in RPMI-1640 medium enriched with 10% FBS 8mM L-glutamine (Sigma Life Science, London, UK). The cells were kept in suspension cultures at a density of between 150,000 and 700,000 cells/mL.

All media were supplemented with 1 IU/mL penicillin and 1 mg/mL streptomycin (both from Cambrex, Liège, Belgium) and incubated in a humidified atmosphere (37 °C, 5% CO_2).

For the cytotoxicity experiments, the NRK and H9c2 cells were seeded in 96-well tissue culture plates (4000 cells/well, 0.1 mL) and left overnight to attach before adding the compounds. The MOLM13 cells were seeded in 96-well tissue culture plates at 20,000 cells/well in 0.1 mL on the day of the experiment.

The compounds dissolved in DMSO were added to the cells, and the plates were kept overnight before adding the tetrazolium salt WST-1 according to the manufacturer's instructions (Roche Diagnostics GmbH, Mannheim, Germany). The plates were further incubated for two hours before the signal was recorded at 450 nm with a reference at 620 nm. For blank subtraction, only the medium-added WST-1 and plant compounds were used. This procedure was conducted after 24 and 72 h.

After the recording of WST-1, the cells were then fixed with 2% buffered formaldehyde (pH 7.4) with 0.01 mg/mL of the DNA-specific fluorescent dye, Hoechst 33342. The presence of dead (apoptotic or necrotic) cells was verified via differential interference contrast and fluorescence microscopy as previously described by Oftedal et al. and Myhren et al. [25,26].

EC_{50} values were determined using four-parameter regression analysis described by Viktorsson et al. [27] using SigmaPlot v14 software (Systat Software Inc., San Jose, CA, USA).

4. Conclusions

For the first time, 15 natural products, including the previously undescribed compound 3(*R*)-*O*-malonyl pteroside D, have been characterised from *Cryptogramma crispa* (L.) R. Br. The four isolated 1-indanone derivatives were tested for their cytotoxic activity towards the acute myeloid leukaemia cell line MOLM-13, and all these compounds

exhibited moderate and relatively similar cytotoxicity. This is particularly noteworthy considering that pterosides are 1-indanone derivatives of plants that are structurally related to ptaquiloside compounds, which are known their cancer-promoting agents.

The indane core, a common feature in these compounds, appears to be significant. Illudins, natural products with structures related to ptaquiloside, have been reported to have significant anticancer potential and fewer cytotoxic effects than ptaquiloside.

This study provides valuable insights into the potential of 1-indanone derivatives as lead compounds for future anticancer therapy. Their selective cytotoxic activity towards the MOLM13 cell line and lack of cytotoxicity towards normal cell lines highlight their potential for targeted cancer treatment. Moreover, future structure–activity relationship studies could reveal the modifications that improve the active compounds' potency and possibly selectivity. As such, we believe that our active compounds merit further investigations to reveal their potential as possible drug leads.

Supplementary Materials: The following supporting information can be downloaded at: https://www.mdpi.com/article/10.3390/molecules28237723/s1, Figure S1: 1D ^{1}H NMR spectrum of 3-manolyl pterosideD; Figure S2: 1D ^{1}H selective TOCSY NMR spectrum of 3 manolyl pteroside D; Figure S3: 1D ^{13}CAPT NMR spectrum of 3 manolyl pteroside D; Figure S4: 2D ^{1}H-^{13}C HMBC NMR spectrum of 3 manolyl pteroside D; Figure S5: 2D ^{1}H-^{13}C HSQC NMR spectrum of 3 manolyl pteroside D; Figure S6: 2D ^{1}H-^{13}C H2BC NMR spectrum of 3 manolyl pteroside D; Figure S7: 2D ^{1}H-^{1}H COSY NMR spectrum of 3 manolyl pteroside D; Figure S8: High Resolution Mass Spectrum of 3 manolyl pteroside D; Figure S9: Circular Dichroism (CD) spectrum of 3 manolyl pteroside D; Figure S10: UV spectrum of 3 manolyl pteroside D.

Author Contributions: Conceptualization, T.F., L.H. and H.L.A.; methodology, A.E.C.D., H.L.A., L.H. and T.F.; software, A.E.C.D., L.H. and T.F.; validation, A.E.C.D., L.H. and T.F.; formal analysis, A.E.C.D., L.H. and T.F.; investigation, A.E.C.D., L.H. and T.F.; resources, T.F., L.H. and H.L.A.; data curation, T.F., L.H. and H.L.A.; writing—original draft preparation, A.E.C.D., H.L.A., L.H. and T.F.; writing—review and editing, A.E.C.D., L.H. and T.F.; visualization, A.E.C.D., L.H. and T.F.; supervision, T.F. and L.H.; project administration, T.F. and L.H.; funding acquisition, L.H. and T.F. All authors have read and agreed to the published version of the manuscript.

Funding: The study was partly supported financially by the Norwegian Society for Children's Cancer (Grant nos. 180007 and 190004). The Research Council of Norway partly supported this work through the Norwegian NMR Platform, NNP (226244/F50).

Institutional Review Board Statement: Not applicable.

Informed Consent Statement: Not applicable.

Data Availability Statement: Data are contained within the article and Supplementary Materials.

Acknowledgments: The authors acknowledge Bjarte Holmelid for recording the HRMS and Reidun Aesoy for assistance with cell maintenance. Special thanks is given to Knut J. Børve for kindly sharing his knowledge about the fern *Cryptogramma crispa* and encouraging this project.

Conflicts of Interest: The authors declare no conflict of interest.

References

1. Metzgar, J.S.; Alverson, E.R.; Chen, S.; Vaganov, A.V.; Ickert-Bond, S.M. Diversification and reticulation in the circumboreal fern genus *Cryptogramma*. *Mol. Phylogenetics Evol.* **2013**, *67*, 589–599. [CrossRef] [PubMed]
2. Veit, M.; Bilger, W.; Mühlbauer, T.; Brummet, W.; Winter, K. Diurnal Changes in Flavonoids. *J. Plant Physiol.* **1996**, *148*, 478–482. [CrossRef]
3. Tomaselli, M.; Petraglia, A.; Rossi, G.; Adorni, M. Contribution to the environmental ecology of *Cryptogramma crispa* (L.) R. Br. ex Hooker in the Alps. *Flora* **2005**, *200*, 175–186. [CrossRef]
4. Pajaro´n, S.; Pangua, E.; Garci´a-A´lvarez, L. Sexual expression and genetic diversity in populations of *Cryptogramma crispa* (Pteridaceae). *Am. J. Bot.* **1999**, *86*, 964–973. [CrossRef]
5. Fægri, K. *Norges Planter: Blomster og Trær i Naturen: Med et Utvalg fra Våre Nabolands Flora: 2*, 2nd ed.; Cappelen: Oslo, Norway, 1970; Volume 2.

6. Guo, Y.; Li, J.J.; Busta, L.; Jetter, R. Coverage and composition of cuticular waxes on the fronds of the temperate ferns *Pteridium aquilinum*, *Cryptogramma crispa*, *Polypodium glycyrrhiza*, *Polystichum munitum* and *Gymnocarpium dryopteris*. *Ann. Bot.* **2018**, *122*, 555–568. [CrossRef]
7. Fons, F.; Froissard, D.; Morel, S.; Bessière, J.-M.; Buatois, B.; Sol, V.; Fruchier, A.; Rapior, S. *Pteridaceae* Fragrant Resource and Bioactive Potential: A Mini-review of Aroma Compounds. *Nat. Prod. Commun.* **2018**, *13*, 651–655. [CrossRef]
8. Murakami, T.; Taguchi, S.; Nomura, Y.; Tanaka, N.; Satake, T.; Saiki, Y.; Chen, C. Weitere Indan-1-on-Derivate der Gattung Pteris. *Chem. Pharm. Bull.* **1976**, *24*, 1961–1964. [CrossRef]
9. Kuroyanagi, M.; Fukuoka, M.; Yoshihira, K.; Natori, S. The Absolute Configurations of Pterosins, 1-Indanone Derivatives from Bracken, *Pteridium aquilinum* var. *Latiusculum*. *Chem. Pharm. Bull.* **1974**, *22*, 723–726. [CrossRef]
10. Penberthy, J. Vegetable poisoning (?) simulating anthrax in cattle. *J. Comp. Pathol. Ther.* **1893**, *6*, 266–275. [CrossRef]
11. Storrar, D. Cases of vegetable poisoning in cattle. *J. Comp. Pathol. Ther.* **1893**, *6*, 276–279. [CrossRef]
12. Yoshihira, K.; Fukuoka, M.; Kuroyanagi, M.; Natori, S.; Umeda, M.; Morohoshi, T.; Enomoto, M.; Saito, M. Chemical and toxicological studies on bracken fern, *Pteridium aquilinum* var. *latiusculum*. I. Introduction, extraction and fractionation of constituents, and toxicological studies including carcinogenicity tests. *Chem. Pharm. Bull.* **1978**, *26*, 2346–2364. [CrossRef] [PubMed]
13. Cao, H.; Chai, T.-T.; Wang, X.; Morais-Braga, M.F.B.; Yang, J.-H.; Wong, F.-C.; Wang, R.; Yao, H.; Cao, J.; Cornara, L.; et al. Phytochemicals from fern species: Potential for medicine applications. *Phytochem. Rev.* **2017**, *16*, 379–440. [CrossRef] [PubMed]
14. Harada, T.; Saiki, Y. Pharmaceutical Studies on Ferns. VIII. Distribution of Flavonoids in Ferns. (2). *Pharm. Bull.* **1955**, *3*, 469–472. [CrossRef]
15. Wollenweber, E. Exudate flavonoids in ferns and their chemosystematic implication. *Biochem. Syst. Ecol.* **1989**, *17*, 141–144. [CrossRef]
16. Giraud, F.; Bourhis, M.; Ebrahimi, E.; Herfindal, L.; Choudhury, R.R.; Bjørnstad, R.; Døskeland, S.O.; Anizon, F.; Moreau, P. Synthesis and activities of new indolopyrrolobenzodiazepine derivatives toward acute myeloid leukemia cells. *Bioorg. Med. Chem.* **2015**, *23*, 7313–7323. [CrossRef]
17. Saito, M.; Umeda, M.; Enomoto, M.; Hatanaka, Y.; Natori, S.; Yoshihira, K.; Fukuoka, M.; Kuroyanagi, M. Cytotoxicity and carcinogenicity of pterosins and pterosides, 1-indanone derivatives from bracken (*Pteridium aquilinum*). *Cell. Mol. Life Sci.* **1975**, *31*, 829–831. [CrossRef]
18. Hikino, H.; Miyase, T.; Takemoto, T. Biosynthesis of pteroside B in *Pteridium aquilinum* var. *Latiusculum*, proof of the sesquiterpenoid origin of the pterosides. *Phytochemistry* **1976**, *15*, 121–123. [CrossRef]
19. McMorris, T.C.; Kelner, M.J.; Wang, W.; Estes, L.A.; Montoya, M.A.; Taetle, R. Structure-activity relationships of illudins: Analogs with improved therapeutic index. *J. Org. Chem.* **1992**, *57*, 6876–6883. [CrossRef]
20. Anchel, M.; Hervey, A.; Robbins, W.J. Antibiotic Substances from Basidiomycetes. *Proc. Natl. Acad. Sci. USA* **1950**, *36*, 300–305. [CrossRef]
21. Kelner, M.J.; McMorris, T.C.; Beck, W.T.; Zamora, J.M.; Taetle, R. Preclinical evaluation of illudins as anticancer agents. *Cancer Res.* **1987**, *47*, 3186–3189.
22. Liston, D.R.; Davis, M. Clinically Relevant Concentrations of Anticancer Drugs: A Guide for Nonclinical Studies. *Clin. Cancer Res.* **2017**, *23*, 3489–3498. [CrossRef] [PubMed]
23. Nguyen, X.H.T.; Juvik, O.J.; Øvstedal, D.O.; Fossen, T. 6-Carboxydihydroresveratrol 3-O-β-glucopyranoside—A novel natural product from the Cretaceous relict *Metasequoia glyptostroboides*. *Fitoterapia* **2014**, *95*, 109–114. [CrossRef]
24. Matsuo, Y.; MacLeod, R.; Uphoff, C.; Drexler, H.; Nishizaki, C.; Katayama, Y.; Kimura, G.; Fujii, N.; Omoto, E.; Harada, M.; et al. Two acute monocytic leukemia (AML-M5a) cell lines (MOLM-13 and MOLM-14) with interclonal phenotypic heterogeneity showing MLL-AF9 fusion resulting from an occult chromosome insertion, ins(11;9)(q23;p22p23). *Leukemia* **1997**, *11*, 1469–1477. [CrossRef] [PubMed]
25. Oftedal, L.; Selheim, F.; Wahlsten, M.; Sivonen, K.; Døskeland, S.O.; Herfindal, L. Marine Benthic Cyanobacteria Contain Apoptosis-Inducing Activity Synergizing with Daunorubicin to Kill Leukemia Cells, but not Cardiomyocytes. *Mar. Drugs* **2010**, *8*, 2659–2672. [CrossRef]
26. Myhren, L.; Nilssen, I.M.; Nicolas, V.; Døskeland, S.O.; Barratt, G.; Herfindal, L. Efficacy of multi-functional liposomes containing daunorubicin and emetine for treatment of acute myeloid leukaemia. *Eur. J. Pharm. Biopharm.* **2014**, *88*, 186–193. [CrossRef]
27. Viktorsson, E.; Grøthe, B.M.; Aesoy, R.; Sabir, M.; Snellingen, S.; Prandina, A.; Åstrand, O.A.H.; Bonge-Hansen, T.; Døskeland, S.O.; Herfindal, L.; et al. Total synthesis and antileukemic evaluations of the phenazine 5,10-dioxide natural products iodinin, myxin and their derivatives. *Bioorganic Med. Chem.* **2017**, *25*, 2285–2293. [CrossRef] [PubMed]

Cytotoxic Natural Products Isolated from *Cryptogramma crispa* (L.) R. Br.

Supplementary Data

NMR spectra

Mass spectrum

CD spectrum

UV spectrum

Figure S1. 1D ^{1}H NMR spectrum of 3-manolyl pteroside D

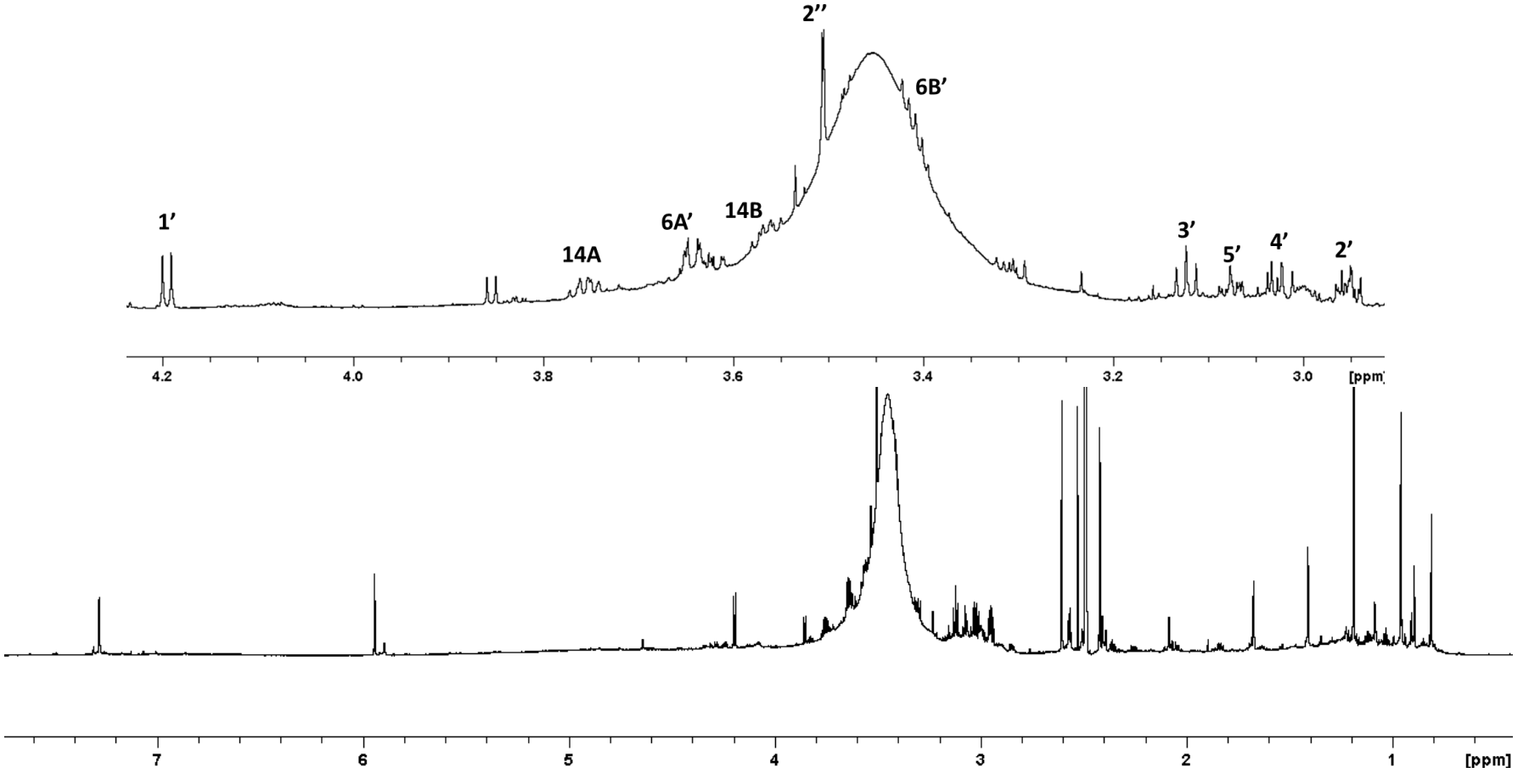

Figure S2. 1D ^{1}H selective TOCSY NMR spectrum of 3-manolyl pteroside D

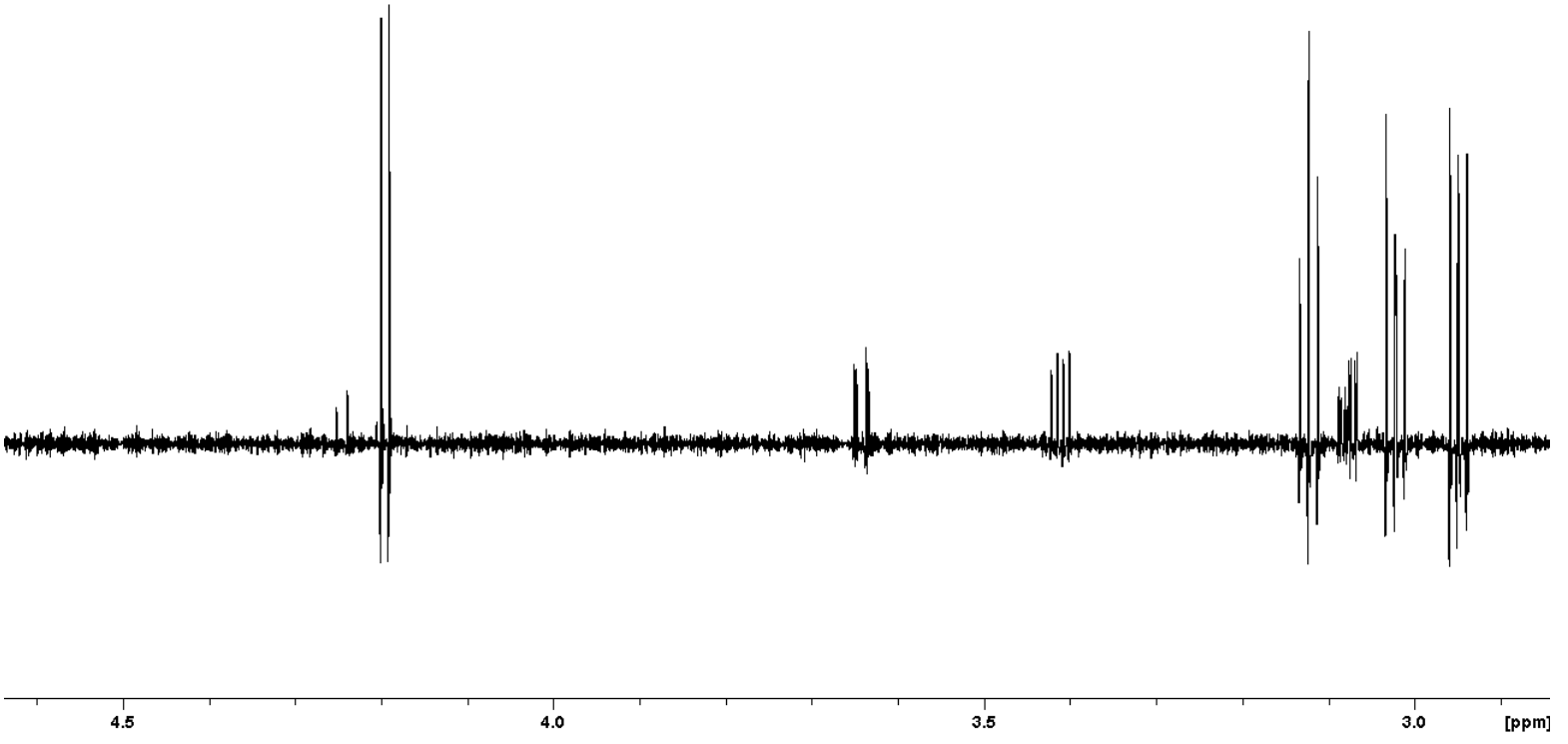

Figure S3. 1D ^{13}CAPT NMR spectrum of 3-manolyl pteroside D

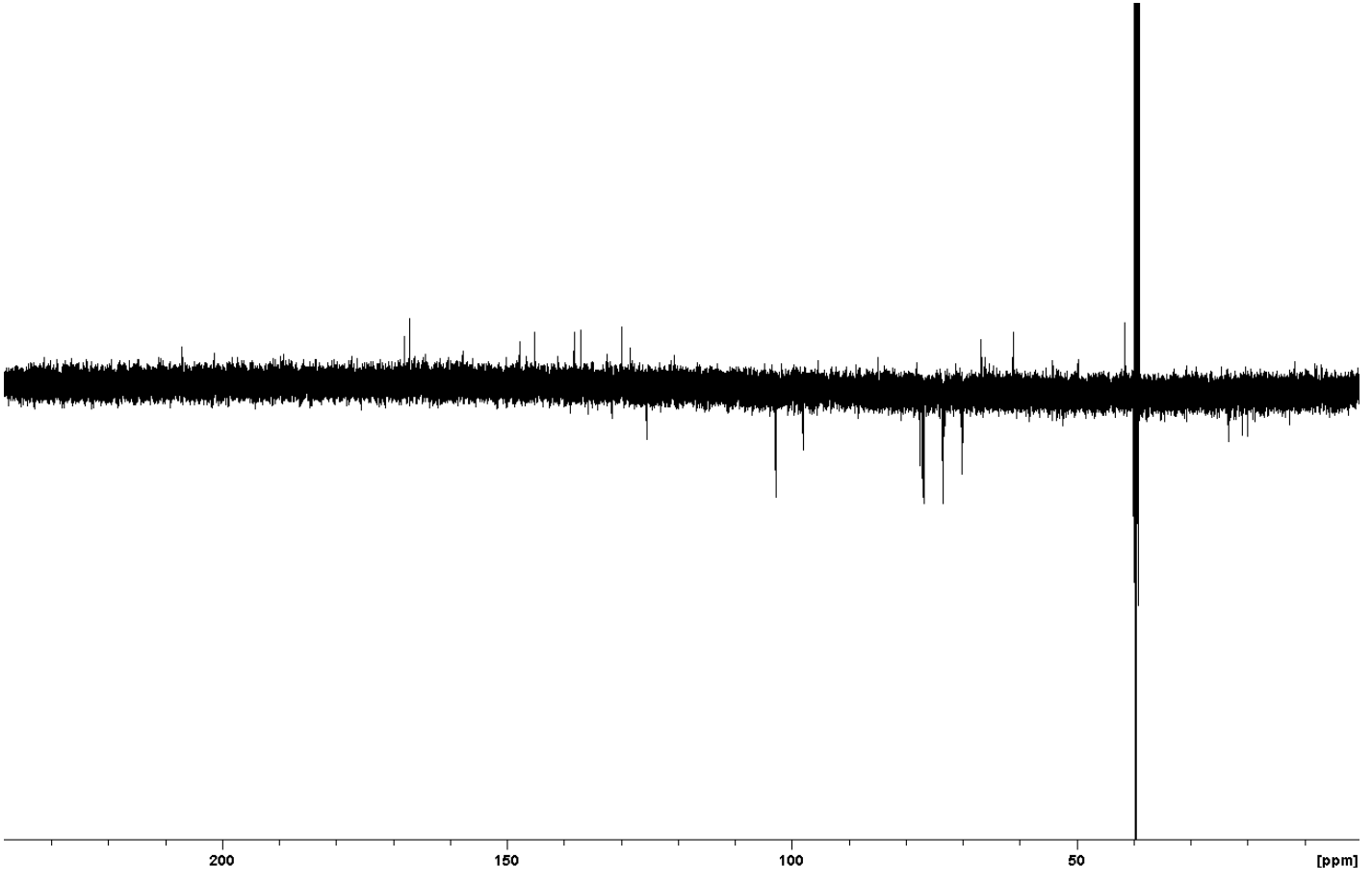

Figure S4. 2D ^{1}H-^{13}C HMBC NMR spectrum of 3-manolyl pteroside D

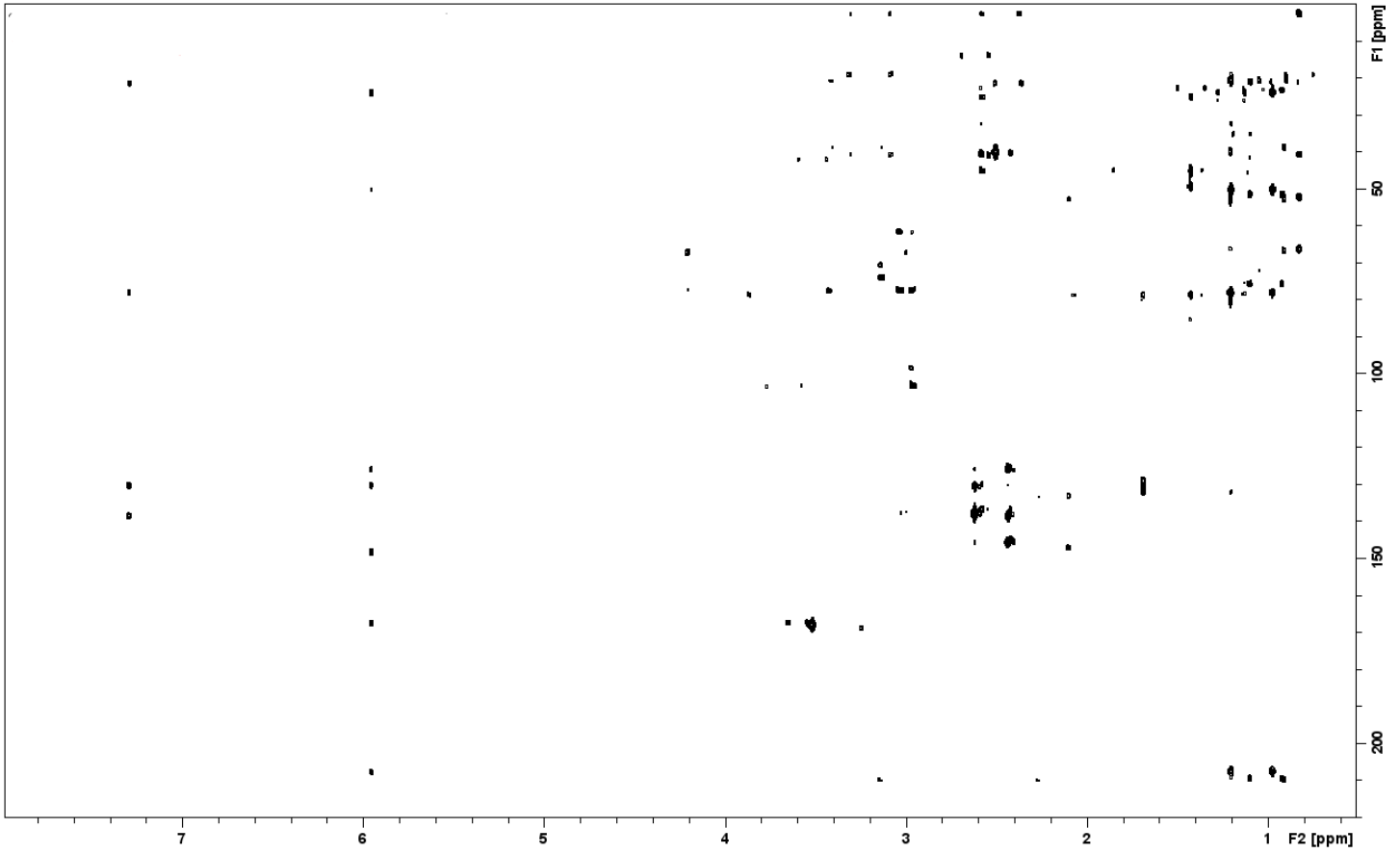

Figure S5. 2D ^{1}H-^{13}C HSQC NMR spectrum of 3-manolyl pteroside D.

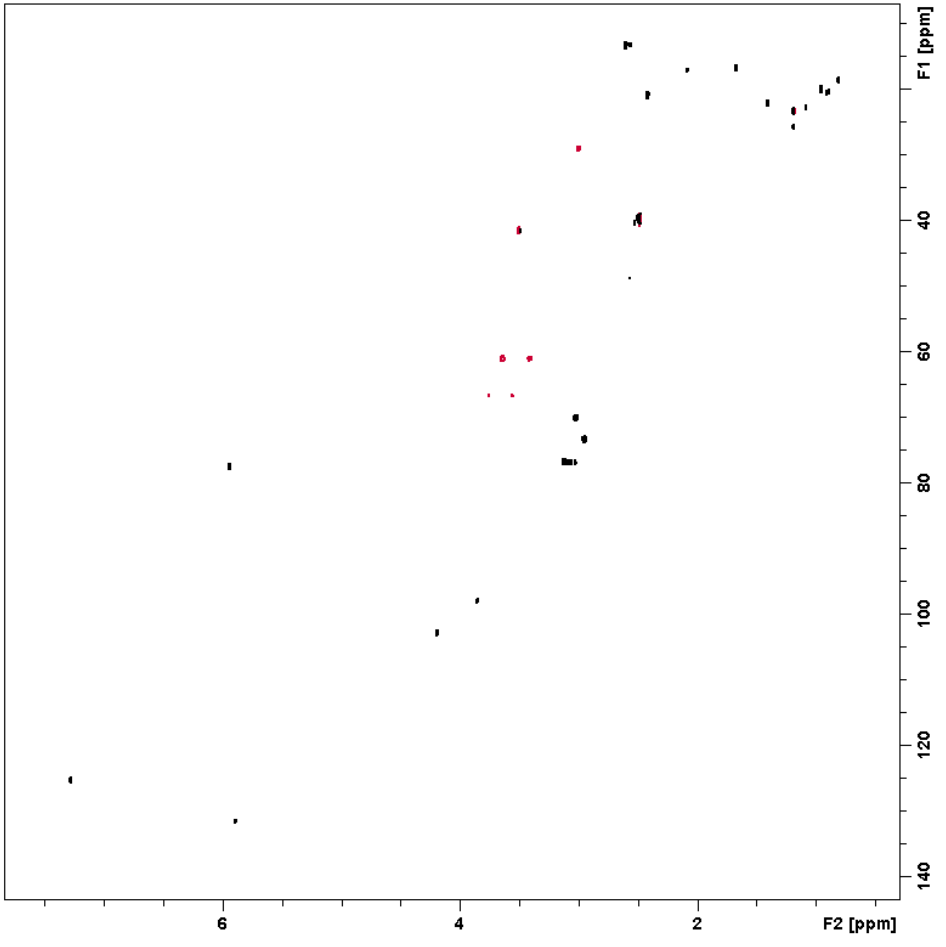

Figure S6. 2D ^{1}H-^{13}C H2BC NMR spectrum of 3-manolyl pteroside D.

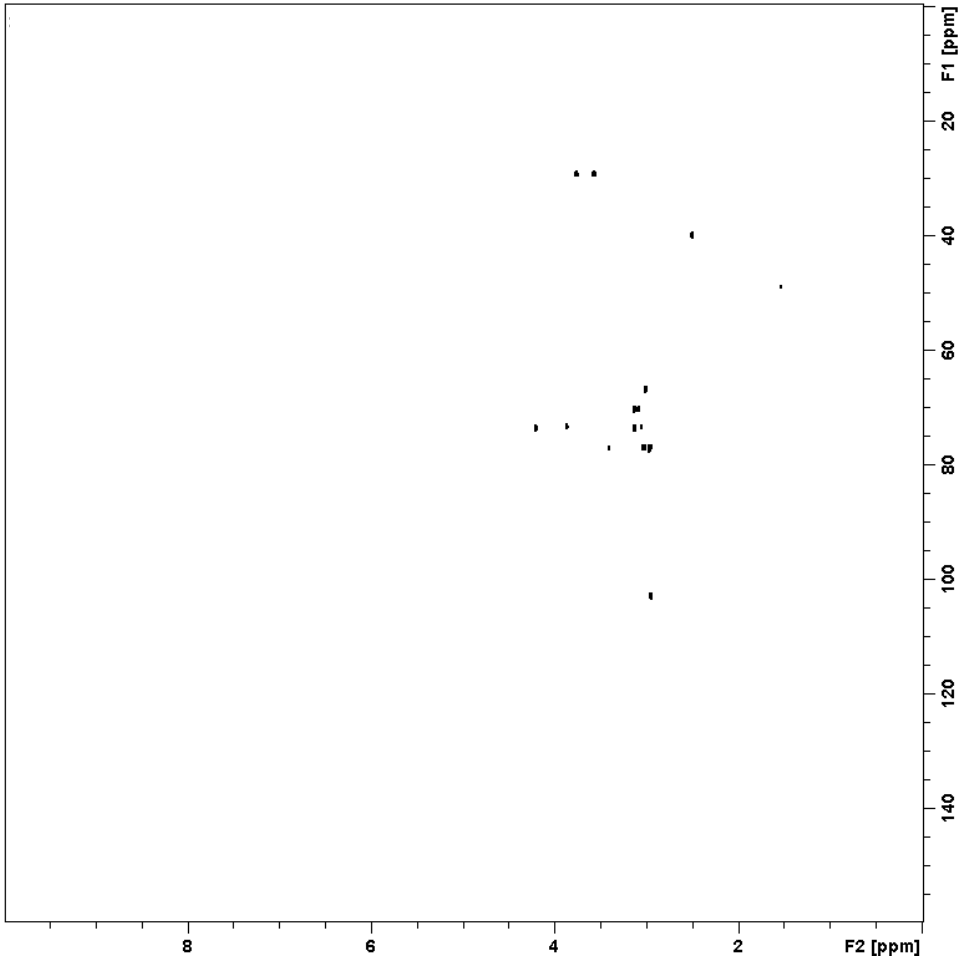

Figure S7. 2D ^{1}H-^{1}H COSY NMR spectrum of 3-manolyl pteroside D.

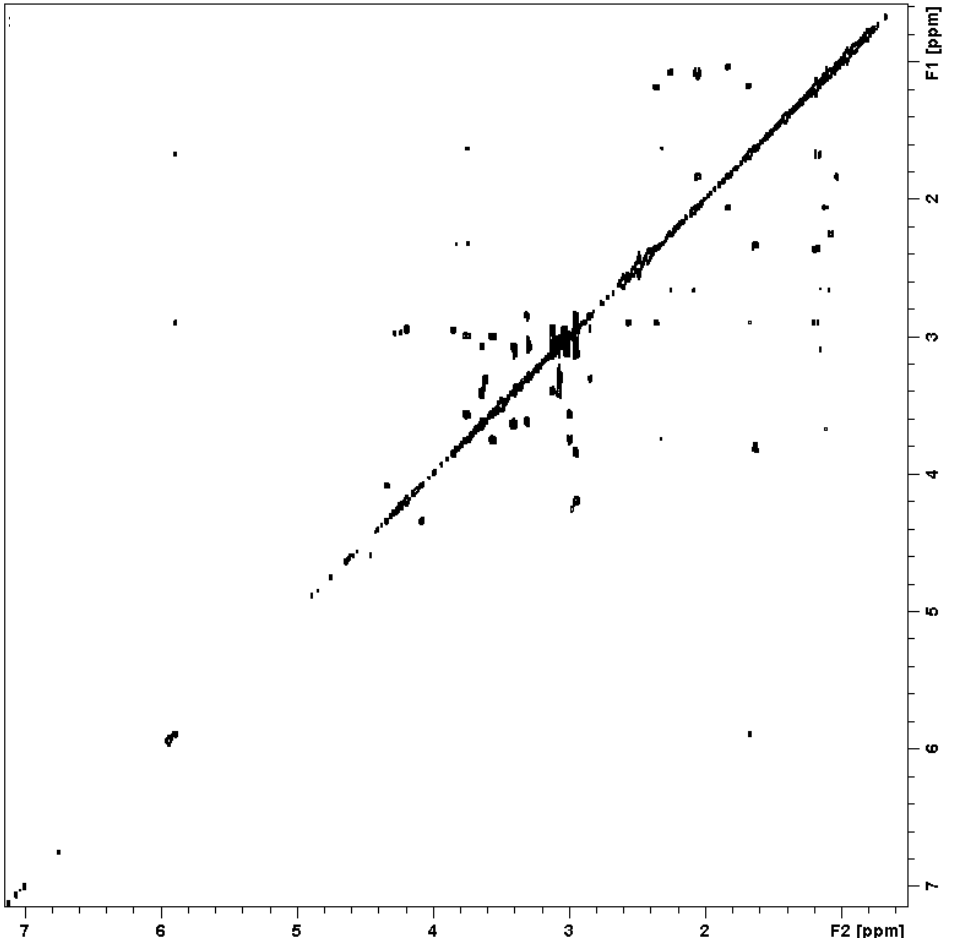

Figure S8. High Resolution Mass Spectrum of 3-manolyl pteroside D.

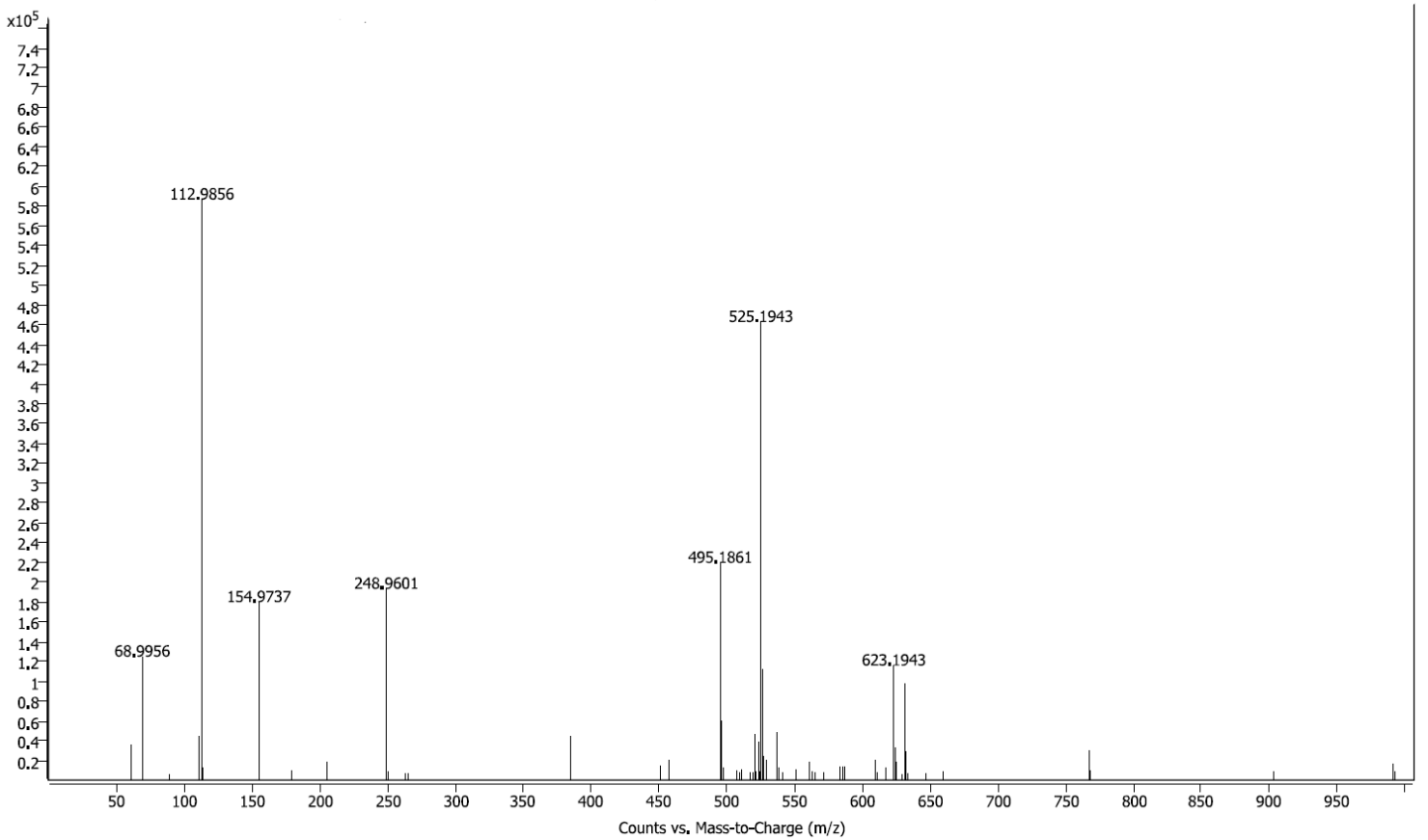

Figure S9. Circular Dichroism (CD) spectrum of 3-manolyl pteroside D.

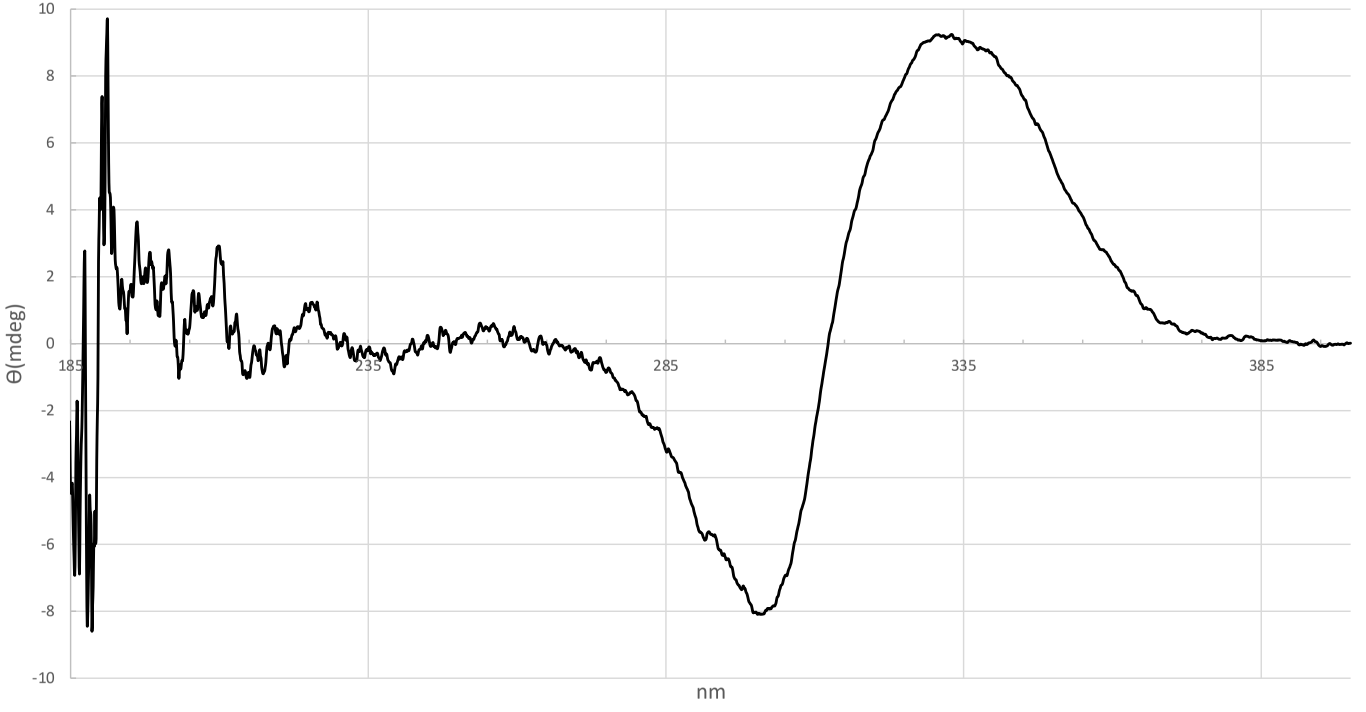

Figure S10. UV spectrum of 3-manolyl pteroside D.

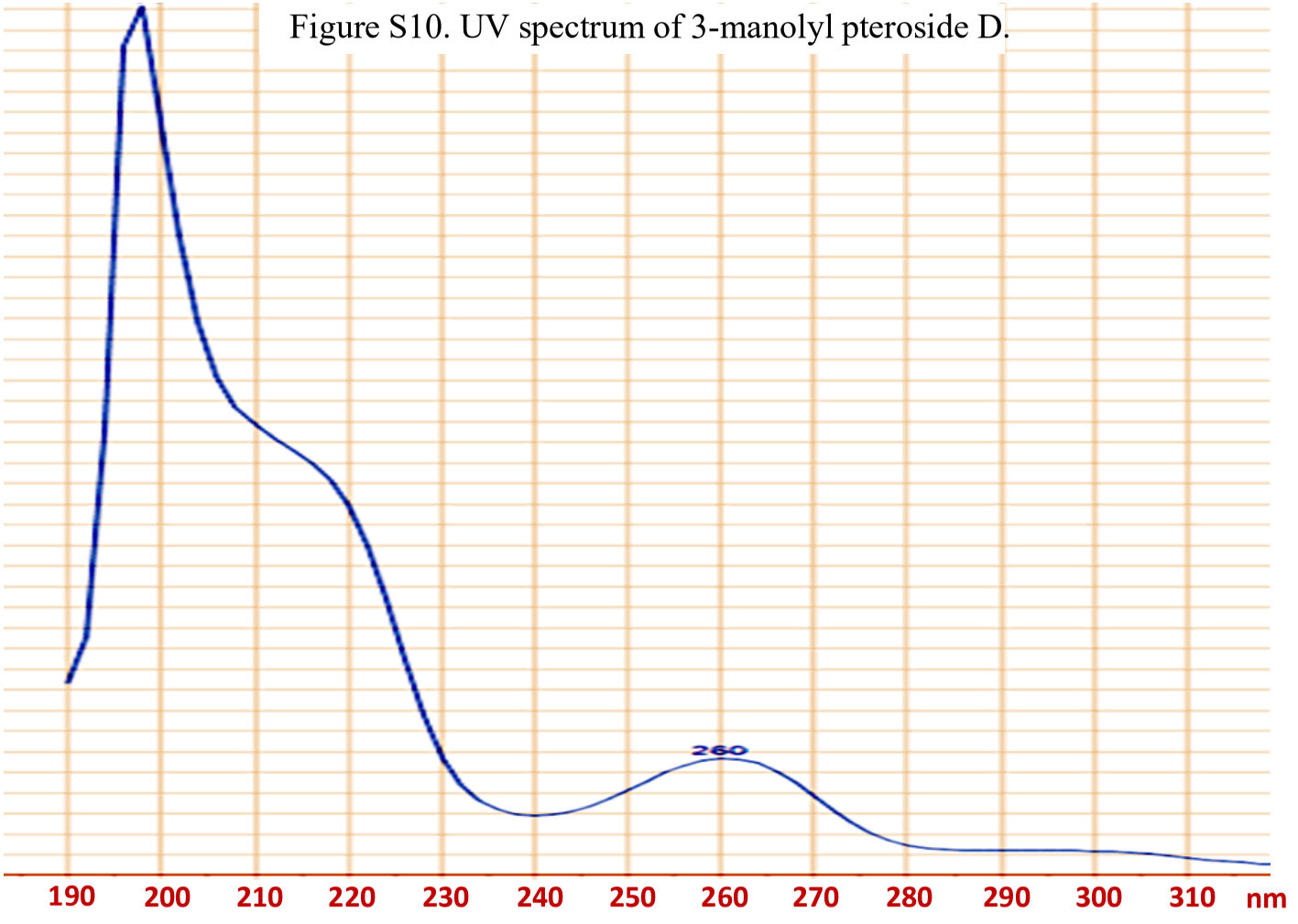

Paper V

scientific reports

Check for updates

OPEN

A novel bicyclic lactone and other polyphenols from the commercially important vegetable *Anthriscus cerefolium*

Rune Slimestad[1], Bendik Auran Rathe[2], Reidun Aesoy[2], Andrea Estefania Carpinteyro Diaz[3], Lars Herfindal[2] & Torgils Fossen[3]✉

Garden chervil, *Anthriscus cerefolium* (L.) Hoffm. is an important herb commonly applied in Norwegian large-scale commercial kitchens. This species is a highly enriched source of phenolics, containing 1260 mg gallic acid equivalents (GAE) 100^{-1} g DM, however, the individual phenolic compounds have been scarcely characterized. Here we report on the qualitative and quantitative content of phenolics in garden chervil. The structure of the main phenolic compound was elucidated to be the previously undescribed compound 1,3-dicaffeoyl-5-malonyl-δ-quinide (1) by means of 1D- and 2D NMR and high-resolution mass spectrometry. The known flavones apigenin 7-*O*-β-(2″-apiofuranosylglucopyranoside) (= apiin) (2), apigenin 7-(2″-apiosyl-6″-malonylglucoside) (3) and luteolin 7-glucoside (4) were also identified. Compound 3 is reported for the first time from this plant species. The main phenolic compound, 1,3-dicaffeoyl-5-malonyl-δ-quinide, exhibited moderate cytotoxicity towards acute monocytic leukaemia cells (MOLM-13) and rat kidney epithelial cells (NRK) with EC_{50} between 400 and 600 μM.

Garden chervil or French parsley (*Anthriscus cerefolium* (L.) Hoffm.) is an annual umbelliferous plant with delicate 2- to 3-pinnate leaves and dentated to pinnatisect leaflets. The plant has been utilized as medicinal plant by humankind for millennia and is mentioned in the encyclopedi *Historia naturalis* by Pliny the elder (23–79 AD) as an ingredient in vinegar recommended against hiccup[1]. This species is also mentioned by the seventeenth century Danish pioneer scientist Simon Paulli (1648) who report on its' use against gallstones[2]. The leaves contain about 0.4% (v/w DM) essential oil, where estragole (= methylchavicol) and 1-allyl-2,4-dimethoxybenzen are the main constituents[3]. The herb has been suggested as a good source for phytosterols and new aroma constituents, which may be useful in human nutrition[4]. The use of Garden chervil as a food in private households seems to be limited as this species is only to a limited extent made available for customers by retailers and supermarkets. However, this species is established as one of the major herbs applied within Norwegian large-scale commercial kitchens[5], where Garden chervil is used as a cheaper alternative to parsley to give a mild taste of anise, parsley, black pepper and caraway. The knowledge about the phytochemistry and potential health impact of Garden chervil has been studied in current literature and several phenolic constituents of Garden chervil have been characterized. In current literature, several flavones and flavonols have been identified in chervil. The previously reported flavones are all derivatives of apigenin and luteolin, including apiin (apigenin 7-apiosylglucoside)[6,7], luteolin 7-glucoside, luteolin 7-apiosylglucoside[8], whereas the identified flavonols are kaempferol, quercetin and isorhamnetin derivatives[7,9]. Several derivatives of quinic acid, in addition to the phenylpropanoids, where the latter compounds occur in the essential oils, have also been reported as phenolic constituents from this species[7,9,10]. These identifications were mainly based on hyphenated mass spectrometry and comparisons with available standards[7]. The observed antimicrobial activity of extracts of chervil may be assigned to the content of relatively volatile compounds including the known antibiotic compound carvacrol[7,11]. Studies of biological activity of pure compounds isolated from chervil are, however, lacking in current literature.

The major objective of this paper is to determine the qualitative and quantitative content of the phenolics of garden chervil by state-of-the-art multidimensional NMR spectroscopic and hyphenated chromatographic

[1]PlantChem AS, Eikenveien 334, 4596 Eiken, Norway. [2]Department of Clinical Science and Centre for Pharmacy, University of Bergen, Jonas Lies vei 87, 5009 Bergen, Norway. [3]Department of Chemistry and Centre for Pharmacy, University of Bergen, Allègaten 41, 5007 Bergen, Norway. ✉email: Torgils.Fossen@uib.no

methods and to determine the therapeutic potential of the main phenolic constituent towards acute monocytic leukaemia cells.

Materials and methods

Reagents and materials. Fresh cut chervil was received from Frøvoll Farm, Randaberg, located in Southwestern Norway (59°0′56.3″ North, 5°37′25.8″ East). Experimental research and field studies on the plants, including the collection of plant material complied with relevant institutional, national, and international guidelines and legislation. Ferric chloride hexahydrate (Fluka), potassium hexacyanoferrate, 2,2-azino-bis (3-ethylbenzothiazoline-6-sulfonic acid) (ABTS), potassium peroxodisulfate, gum Arabic, hydrochloric acid, 85% phosphoric acid, gallic acid, Trolox, potassium phosphate, sodium chloride, chlorogenic acid and formic acid were provided from Merck, Norway. Methanol (Rathburn) and acetonitrile (Rathburn) were provided from Teknolab AS, Norway.

Sample preparation and analysis. Sample preparations were performed as described by Slimestad et al.[14]. Fresh garden chervil, including leaves and stems, were lyophilized for 72 h using a freeze-dryer (CoolSafe 4 ScanVac, ScanLaf AS, Denmark). Dry matter contents were determined based on the sample weights prior to and after lyophilization. Dried plant material was minced in a bowl chopper and grinded (Bosch KM13, Slovenia). For determination of total phenolic content, radical scavenging capacity and UHPLC analysis, 200 mg of the sample was extracted with 10 mL methanol in a 20 mL test tube at ambient temperature for 48 h in the darkness. Samples were filtered through 0.4 µm syringe filters prior to analysis. Two parallel samples were analysed[14].

Fractionation and isolation. Fractionation and isolation of phenolics from garden chervil was based on extracts obtained from 500 g fresh plant material (160 g dry weight). The plant material was minced (about 20 mm), and extraction was performed two times for 24 h in the darkness by using 2 × 500 mL portions of methanol. The extract was filtered (folded filter quality 315, VWR Norway), concentrated to a volume of 100 mL on a rotavapor (Büchi, Switzerland), and partitioned against equal volumes of dichloromethane, in order to remove chlorophylls and lipophilic content. The water phase was further concentrated to a total volume of 50 mL, and the concentrated aqueous extract was applied to a bed of 0.5 kg Amberlite XAD-7 HP (Sigma) in a 5 × 60 cm open-top glass column, rinsed with 2 L distilled water and eluted by use of 2 L MeOH as mobile phase. The XAD-7 purified extract was finally concentrated to a volume of 50 mL.

Further purification was performed by size-exclusion chromatography by using a 5 × 100 cm open-top column filled with 500 g Sephadex LH20 (GE Healthcare, Norway). A step-gradient elution was used with increasing concentrations of methanol in the mobile phase (0, 20, 40, 60 and 80%; 0.1% TFA)[14]. Pure compounds were isolated by preparative HPLC. The HPLC instrument was equipped with a 250 × 20 mm, C18 Ascentis column. Two solvents were used for elution; mobile phase A (water-TFA 99.9:0.1 v/v) and mobile phase B (methanol-TFA 99.9:0.1 v/v). Portions of 200 µL were manually injected into the HPLC column and the collected fractions were transferred to HPLC vials for purity control using analytical HPLC[14].

Total phenolic content. Total phenolic content was determined in accordance with the method of Price and Butler with stabilization of the Prussian Blue complex as described by Graham[12,13] and Slimestad et al.[14]. 100 µL of sample was diluted with 3 mL deionized water and mixed with 1 mL of a 0.1 M ferric chloride in 0.1 M hydrochloric acid solution together with 1 mL of 8 mM potassium ferricyanide solution. The reaction was allowed to run for fifteen minutes at ambient temperature. 5 mL of an acidic gum Arabic solution was added (1 g gum Arabic dissolved in 100 mL hot water. 10 mL of this solution was mixed with 10 mL 85% phosphoric acid and 30 mL water). Absorption at 700 nm was measured by use of an Agilent 8453 spectrophotometer (Agilent Technologies, Matriks, Norway). Samples were measured against a standard curve of gallic acid, and outputs are given as gallic acid equivalents, mg GAE g^{-1}[14].

Radical scavenging. The TEAC assay (Trolox Equivalent Antiradical Capacity) was carried out following the procedures previously described by Slimestad et al.[14] and Re et al.[15]. 2,2-azino-bis (3-ethylbenzothiazoline-6-sulfonic acid) (ABTS) was dissolved in water to a 7 mM solution with potassium persulfate to a concentration of 2.45 mM. The solution was kept at ambient temperature for about 16 h. The $ABTS^{\cdot+}$ solution was diluted with PBS (phosphate buffered saline: 100 mM KH_2PO_4-buffer, pH 7.4 and 150 mM NaCl), to an absorbance of 0.70 (± 0.02) at 734 nm. Samples were diluted so that, after the introduction of a 10 µL aliquot of each extract into the assay, they produced between 20 and 80% inhibition of the blank absorbance. After addition of 1.0 mL of diluted $ABTS^{\cdot+}$ solution to 10 µL of extracts or trolox standards (final concentration 0–15 µM) in PBS, the absorbance reading was taken at 6 min. Appropriate PBS blanks were run in each assay. The final TEAC decolorization assay values were calculated against a standard curve of 0–10 mg Trolox in 100 mL methanol, and the percentage of inhibition of absorbance at 734 nm were expressed as mg TEAC 100 g^{-1} DW[14,15].

U(H)PLC-MS. The qualitative and relative quantitative contents of individual flavonoids and other phenolic compounds was determined by using an Agilent 1290 Infinity II instrument equipped with a 6120 quadrupole mass detector[14]. Separation was achieved with a Zorbax Eclipse XDB-C8 column (2.1 × 100 mm, 1.8 µm, Agilent Technologies). Water with 0.02% HCOOH (solvent A) and acetonitrile (solvent B) were used for gradient elution with the following time program (% B in A): from 0 to 10 (in 1 min), from 10 to 25 (in 25 min), from 25 to 95 (2 min), from 95 to 0 (1 min), and finally isocratic recondition for 1 min. Flow was set to 0.300 mL/min (max back pressure 540 bar), and injections of 5 µL was used. UV-detection was performed at 280, 320 and 360 nm

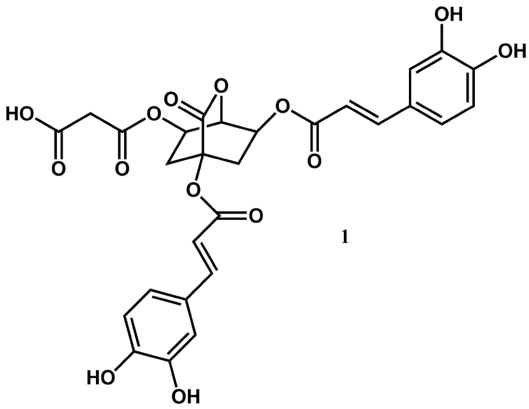

Figure 1. Structure of the previously undescribed compound 1,3-dicaffeoyl-5-malonyl-δ-quinide (**1**) isolated from *Anthriscus cerefolium*. Structure was drawn in ChemDraw Professional 18.0. https://www.alfasoft.com/no/produkter/lab/chemdraw.html.

at 4 nm band width. Masses in the range 250–800 Da was detected using a scan time of 500 ms, a fragmentor at 70 V, and detection was in both positive and negative mode[14]. Gas source temperature was set to 350 °C with flow at 10 L min^{-1}, nebulizer pressure was 35 psi, whereas capillary voltage was 4 kV[14].

High-resolution mass spectrometry (LC-HRMS) was used for exact mass determination of isolated compounds. An iClass UPLC (Waters) equipped with a C18 BEH column (1.7 um, 2.1 × 50 mm, Waters) was used for introducing the samples to the mass spectrometer. A gradient of A) 0.2% formic acid and B) acetonitrile was used as follows (% B in A): 1 (isocratic for 0.5 min), from 1 to 90 (in 2 min). The mass spectrometer (timsTOF, Bruker) was used in ESI+-mode with an ionization at 2 kV, and with full scan 100–2000 Da with resolution R = 50,000 (FWHM) at 1000 Da. Exactness at RMS < 1 ppm[14].

NMR. NMR samples were prepared by dissolving the isolated compounds in deuterated dimethylsulfoxide (DMSO-D_6; 99.96 atom % D, Sigma-Aldrich). The 1D ^{1}H and the 2D ^{1}H–^{13}C HMBC, the 2D ^{1}H–^{13}C HSQC, the 2D ^{1}H–^{13}C HSQC-TOCSY, the 2D ^{1}H–^{13}C H2BC, 2D ^{1}H–^{13}C 1,1 Adequate, the 2D ^{1}H–^{1}H COSY and 2D ^{1}H–^{1}H ROESY NMR experiments were obtained at 850 MHz at 298 K on a Bruker 850 MHz instrument equipped with a ^{1}H, ^{13}C, ^{15}N triple resonance cryogenic probe[14].

Cytotoxicity assays. The cell lines used to study cytotoxicity were: Molm-13[16], MV4-11 human monocytic leukemia cells (ATCC, CRL-9591), human acute myeloid leukemia cell line OCI-AML3 (ATCC, ACC-582), NRK rat kidney epithelial cells (ATCC, CRL-6509), and H9c2 cardiomyoblasts (ATCC, CRL-1446). See Bjørnstad et al. 2019 for a description of culture conditions and media for the different cell lines[17]. The cytotoxicity measurements were performed as described earlier[18]. In brief, the compound was dissolved in DMSO, and further diluted in DMSO. Using a pipette robot (Mosquito High Volume, SPT Labtech), 1 L was transferred to 96-well plates to create identical plates for testing on different cells. Cell suspension was then added, and the cells incubated for 72 h before assessment of viability using the WST-1 cell proliferation assay (Roce Applied Sciences). Some experiments were also performed with dilution series performed in culture medium to exclude the effect of DMSO on cell viability. After recording the WST-1 signal, the cells were fixed, DNA stained using Hoechst 33342, and cell death confirmed by microscopic evaluation of nuclear and surface morphology[18].

Results and discussion

The dry matter content of chervil, *Anthriscus cerefolium,* was found to be 32.3% which is higher compared to the dry matter content of parsley, *Petroselinum crispum*, at 24.7% provided by the same grower[14]. The total phenolic content was found to be 1260 mg gallic acid equivalents (GAE) 100 g^{-1}, quite similar to that of parsley (1270 mg GAE 100 g^{-1})[14]. The antiradical potential was found to be 50 ± 5 mg TEAC 100 g^{-1}, similar to the level detected in parsley, 54 mg TEAC 100 g^{-1}[14] and comparable to previous studies of chervil[11].

From a methanol extract of fresh garden chervil (*Anthriscus cerefolium* L.) four phenolic compounds were detected by means of UHPLC-DAD-MS analysis (Fig. 1, Table 1). Preparative isolation of the phenolics was achieved by repetitive size-exclusion chromatography (Sephadex LH-20) and preparative HPLC. In total five compounds were isolated. Compounds **2**, **3** and **4** were identified as apigenin 7-*O*-β-(2″-apiofuranosylglucopyranoside) (**2**, apiin), luteolin 7-*O*-β-glucopyranoside (**3**), and apigenin 7-*O*-β-(2″-apiofuranosyl-6″-malonylglucopyranoside) (**4**) by a combination of several 1D and 2D NMR experiments (Tables S1, S2) and high-resolution mass spectrometry (Table 1). Apiin and luteolin 7-*O*-β-glucopyranoside have previously been identified in chervil[6,7], while apigenin 7-*O*-β-(2″-apiofuranosyl-6″-malonylglucopyranoside) is identified in garden chervil for the first time.

t_R (min)	λ_{max} (nm)	Pos./neg. ions	HRMS $[M+H]^+$	Calc. formula	Compounds
7.82	266, 336	565, 271 /563	565.1547	$C_{26}H_{29}O_{14}$	Apigenin 7-apiosylglucoside (apiin) (**2**)
8.31	300sh, 330	585, 423 /601	585.1234	$C_{28}H_{25}O_{14}$	1,3-Dicaffeoyl-5-malonyl-δ-quinide (**1**)
ND	ND	ND	449.1076	$C_2{}^1H_{21}O_{11}$	Luteolin 7-glucoside (**4**)
9.42	266, 336	651, 271 /649	651.1544	$C_{29}H_{31}O_{17}$	Apigenin 7-malonylapiosylglucoside (**3**)

Table 1. UHPLC-MS and HRMS data of main phenolics in methanolic extracts of chervil, *Anthriscus cerefolium*. Characteristic ions (*m/z*) from mass detection is listed with the pseudomolecular ions ($[M+H]^+$ or $[M-H]^-$) followed by fragments ions included those of the aglycone moieties. *Nd* not determined.

The central bicyclic δ-quinide ring system of **1** was assigned by the $^1H/^{13}C$ crosspeaks at δ 2.44/69.9 (H2A/C3), δ 1.96/69.9 (H2B/C3), δ 5.20/35.7 (H3/C2), δ 5.20/68.8 (H3/C4), δ 3.87/69.9 (H4/C3), δ 3.87/72.0 (H4/C5), δ 5.32/68.8 (H5/C4), δ 5.32/31.8 (H5/C6) and δ 2.41/72.0 (H6/C5) observed in the 2D $^1H-^{13}C$ H2BC spectrum, the $^1H/^1H$ crosspeaks at δ 2.44/5.20 (H2A/H3), δ 1.96/5.20 (H2B/H3), δ 2.44/1.96 (H2A/H2B), δ 5.20/3.87 (H3/H4), δ 3.87/5.32 (H4/H5) and δ 5.32/2.41 (H5/H6) observed in the 2D $^1H-^1H$ COSY spectrum. The substituents of the central bicyclic δ-quinide ring system of **1** were identified as two caffeoyl units and a malonyl unit (Table 2). The $^1H/^{13}C$ crosspeaks at δ 6.28/78.8 (H8′/C1), δ 6.23/69.9 (H8″/C3) and δ 5.20/166.2 (H3/C9″) confirmed that the caffeoyl units were attached to the δ-quinide ring system at position 1 and 3, respectively. A crosspeak at δ 5.32/166.7 (H5/C1‴) confirmed the linkage between the malonyl substituent and the δ-quinide ring system at position 5. Thus, **1** was identified as the previously undescribed natural product 1,3-dicaffeoyl-5-malonyl-δ-quinide. A molecular ion at *m/z* 585.1234 corresponding to $C_{28}H_{25}O_{14}$ (calculated 585.1245, δ = − 1.9 ppm) observed in the high-resolution mass spectrum of **1** confirmed this identity.

A related compound with similar central bicyclic δ-quinide ring system to that of **1**, namely 3,5-O-dicaffeoyl-epi-δ-quinide, has previously been reported to occur in processed coffee beans, where the identification was solely based on mass spectrometry[19]. Recently, Stojkovic et al. reported the presence of several derivatives of quinic acid acylated with caffeoyl and malonyl moieties, which were identified by hyphenated high resolution mass spectrometry (UHPLC-MS)[7], however, none of these compounds were lactones.

Previously, extracts of chervil have exhibited weak to moderate cytotoxic activity towards cancer cell lines including gliblastoma cells, where EC_{50} of 765 µg/mL was observed[7,20], however, the cytotoxicity of pure compounds isolated from chervil has not been reported in current literature. The cytotoxicity of the main phenolic compound 1,3-dicaffeoyl-5-malonyl-δ-quinide (**1**) towards MOLM13, OCI-AML3 and MV4-11 acute leukaemia cells and towards normal cell lines (NRK cells and H9C2) (Fig. 2 shows results on MOLM13 and NRK cells after 24 and 72 h incubation). 1,3-dicaffeoyl-5-malonyl-δ-quinide (**1**) exhibited moderate toxicity towards all cell lines tested with EC_{50} values above 1000 µM at 24 h incubation, and between 400 and 600 µM at 72 h incubation (Fig. 2 and data not shown). The compound did not show selective cytotoxicity towards any of the leukemia cell lines compared to the non-cancerous cell lines.

Conclusions

Chervil (*Anthriscus cerefolium* (L.) Hoffm) is a very rich source of phenolic compounds, 1260 mg GAE 100^{-1} g DM, and its methanolic extract has a high antiradical capacity. Interestingly, though the two species contain the same main flavones (apiin and apigenin 7-(2″-apiosyl-6″-malonylglucoside)), the major phenolic constituent of chervil is a bicyclic lactone; 1,3-dicaffeoyl-5-malonyl-δ-quinide (**1**). This compound is reported for the first time. 1,3-dicaffeoyl-5-malonyl-δ-quinide exhibited moderate cytotoxic activity towards human leukaemia and normal cell lines.

	δ ^{1}H	δ ^{13}C
1		78.82
2A	2.44 dd 4.4, 14.0	35.7
2B	1.96 m	
3	5.20 dt 4.4, 9.0	69.86
4	3.87 dd 3.7, 8.8	68.8
5	5.32 dd, 4.4, 8.1	71.98
6	2.41 m	31.83
7		172.08
1-*O*-*Z*-caffeoyl		
1′		125.59
2′	7.08 d 2.1	115.25
3′		145.80
4′		148.83
5′	6.78 d 8.2	116.02
6′	7.02 dd 2.1, 8.2	121.67
7′	7.49 d 15.7	146.26
8′	6.28 d 15.7	113.89
9′		165.43
3′-OH	9.19 s	
4′-OH	9.67 s	
3-*O*-*Z*-caffeoyl		
1″		125.70
2″	7.06 d 2.1	114.98
3″		145.80
4″		148.69
5″	6.77 d 8.2	115.99
6″	6.99 dd 2.1, 8.2	121.67
7″	7.49 d 15.7	145.66
8″	6.23 d 15.7	114.13
9″		166.17
3″-OH	9.21 s	
4″-OH	9.63 s	
5-*O*-malonyl		
1‴		166.65
2A‴	3.31 d 15.9	41.74
2B‴	3.22 d 15.9	
3‴		167.94
3‴-OH	12.5 s (br) (very broad)	

Table 2. ^{1}H and ^{13}C NMR chemical shift values (ppm) and coupling constants (Hz) of 1,3-dicaffeoyl-5-malonyl-δ-quinide (**1**) isolated from *Anthriscus cerefolium* recorded in DMSO-D_6 at 298 K.

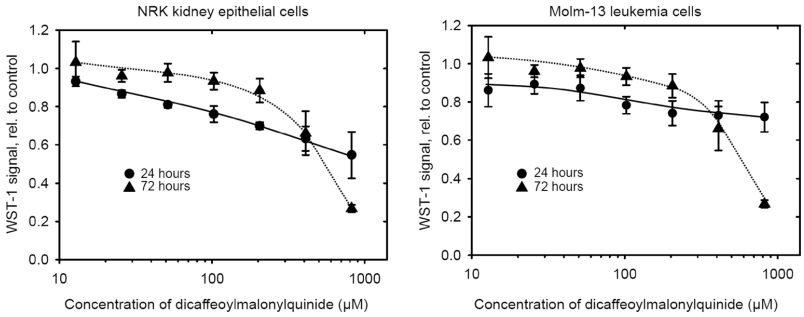

Figure 2. Cytotoxicity of 1,3-dicaffeoyl-5-malonyl-δ-quinide (**1**) towards NRK kidney epithelial cells and Molm-13 leukemia cells. The figure was created with SigmaPlot 14 (Systat Software, Inc., San Jose, CA, USA). https://systatsoftware.com/sigmaplot/.

Received: 13 November 2021; Accepted: 26 April 2022
Published online: 12 May 2022

References

1. Plinius Maior, G. *Naturalis Historia* (77).
2. Paulli, S. *Flora Danica* (1648).
3. Chizzola, R. Composition of the essential oils from *Anthriscus cerefolium* var. trichocarpa and *A. caucalis* growing wild in the urban area of Vienna (Austria). *Nat. Product Commun.* **6**, 1147–1150 (2011).
4. Milovanović, M., Banjac, N. & VucelićRadović, B. Functional food: Rare herbs, seeds and vegetable oils as sources of flavors and phytosterols. *J. Agric. Sci.* **54**, 80–93 (2009).
5. Slimestad, R., Hansen, J. S. & Verheul, M. Intake of vegetables and vegetable pigments during a lunch meal in Norwegian canteens with salad bars. *J. Food Agric. Environ.* **16**, 14–21 (2018).
6. Kurihara, T. & Kikuchi, M. Studies on the constituents of Anthriscus sylvestris Hoffm. II. On the components of flowers and leaves. *Yakugaku Zasshi J. Pharm. Soc. Jpn.* **99**, 602–606 (1979).
7. Stojkovic, D. *et al.* Extract of *Herba Anthrisci cerefolii*: Chemical profiling and insights into its anti-glioblastoma and antimicrobial mechanism of actions. *Pharmaceuticals* **14**, 55 (2021).
8. Fejes, S. *et al.* Antioxidant activity of different compounds from *Anthriscus cerefolium* L. (Hoffm). *Acta Horticult.* **597**, 191–198 (2003).
9. Abdulmanea, K. *et al.* Immunochemical and HPLC identification of isoflavonoids in the Apiaceae family. *Biochem. Syst. Ecol.* **45**, 237–243 (2012).
10. Zwaving, J. H., Smith, D. & Bos, R. The essential oil of chervil *Anthriscus cerefolium* (L.) Hoffm. *Pharm. Weekblad* **106**, 182–189 (1971).
11. Ortan, A. *et al.* Innovative phytosynthesized silver nanoarchitectures with enhanced antifungal and antioxidant properties. *Appl. Surf. Sci.* **358**, 540–548 (2015).
12. Price, M. L. & Butler, L. G. Rapid visual estimation and spectrophotometric determination of tannin content of sorghum grain. *J. Agric. Food Chem.* **25**, 1268–1273 (1977).
13. Graham, H. D. Stabilization of the Prussian blue color in the determination of polyphenols. *J. Agric. Food Chem.* **40**, 801–805 (1992).
14. Slimestad, R., Fossen, T. & Brede, C. Flavonoids and other phenolics in herbs commonly used in Norwegian commercial kitchens. *Food Chem.* **309**, 125678 (2020).
15. Re, R. *et al.* Antioxidant activity applying an improved ABTS radical cation decolorization assay. *Free Radic. Biol. Med.* **26**, 1231–1237 (1999).
16. Matsuo, Y. *et al.* Two acute monocytic leukemia (AML-M5a) cell lines (MOLM-13 and MOLM-14) with interclonal phenotypic heterogeneity showing MLL-AF9 fusion resulting from an occult chromosome insertion, ins(11;9)(q23;p22p23). *Leukemia* **11**, 1469–1477 (1997).
17. Bjørnstad, R. *et al.* A kinase inhibitor with anti-Pim kinase activity is a potent and selective cytotoxic agent toward acute myeloid leukemia. *Mol. Cancer Ther.* **18**, 567–578 (2019).
18. Vu, M. *et al.* Toxic aromatic compounds from fruits of *Narthecium ossifragum* L. *Phytochemistry* **132**, 76–85 (2016).
19. Blumberg, S., Frank, O. & Hofmann, T. Quantitative studies on the influence of the bean roasting parameters and hot water percolation on the concentrations of bitter compounds in coffee brew. *J. Agric. Food Chem.* **58**, 3720–3728 (2010).
20. Mazzio, E. A. & Soliman, K. F. A. In vitro screening for the tumoricidal properties of international medicinal herbs. *Phytother. Res.* **23**, 385–398 (2009).

Acknowledgements

The present study is in part supported by the Bionær program of the Research Council of Norway ('Biofresh' Project No. 255613/E50), the NordForsk Nordic Center of Excellence "NordAqua" (No. 82845), the Western Norway Health Authorities, and the Norwegian Society for Children's Cancer. This work was partly supported by the Research Council of Norway through the Norwegian NMR Platform, NNP (226244/F50). Cato Brede is acknowledged for HRMS analysis.

Author contributions

R.S., T.F., and L.H. planned and designed the research project. R.S. and A.E.C.D. isolated the compounds. T.F. determined the structures of the isolated compounds. B.A.R., R.A. and L.H. performed the tests of cytotoxic

activity of the novel compound towards normal and cancer cell lines. T.F., R.S., L.H. and A.E.C.D. wrote the manuscript.

Competing interests
The authors declare no competing interests.

Additional information
Supplementary Information The online version contains supplementary material available at https://doi.org/10.1038/s41598-022-11923-0.

Correspondence and requests for materials should be addressed to T.F.

Reprints and permissions information is available at www.nature.com/reprints.

Publisher's note Springer Nature remains neutral with regard to jurisdictional claims in published maps and institutional affiliations.

Supplementary material

A novel bicyclic lactone and other polyphenols from *Anthriscus cerefolium* (L.) Hoffm., an important vegetable in Norwegian large-scale commercial kitchens

Rune Slimestad, Bendik Auran Rathe, Reidun Æsøy, Andrea Estefania Carpinteyro Diaz, Lars Herfindal and Torgils Fossen

Table S1. ^{1}H NMR chemical shift values (δ ^{1}H, ppm) and coupling constants (Hz) of apigenin 7-(2''-apiosylglucoside) (**2**, apiin), apigenin 7-(2''-apiosyl-6''-malonylglucoside) (**3**) and luteolin 7-*O*-β-glucopyranoside (**4**) isolated from *Anthriscus cerefolium* recorded in DMSO-D_6 at 298K.

	2	**3**	**4**
3	6.83 s	6.86 s	6.74 s
6	6.42 d 2.2	6.41 d 2.2	6.43 d 2.2
8	6.80 d 2.2	6.77 d 2.2	6.78 d 2.2
2'	7.93 'd' 8.7	7.95 'd' 8.9	7.42 d 2.4
3'	6.93 'd' 8.7	6.93 'd' 8.9	
5'	6.93 'd' 8.7	6.93 'd' 8.9	6.90 d 8.3
6'	7.93 'd' 8.7	7.95 'd' 8.9	7.44 dd 2.4, 8.3
5-OH	12.95 s		
5-OH		12.97 s	
4'-OH	10.39	10.42 s	
7-*O*-*β*-glucopyranoside			
1'''	5.16 d 7.7	5.20 d 7.8	5.07 d 7.7
2'''	3.53 dd, 7.7, 9.1	3.54 m	3.25 dd 7.7, 9.0
3'''	3.49 t 9.1	3.49 m	3.29 t 9.0
4'''	3.20 t 8.9	3.21 m	3.17 dd 9.0, 9.5
5'''	3.48 m	3.78 ddd 2.1, 7.0, 9.6	3.43 ddd 9.5, 5.8, 2.1
6A'''	3.72	4.39 dd 2.1, 12.0	3.70 dd 2.1, 11.9
6B'''	3.48 m	4.11 dd 7.0, 12.0	3.47 dd 5.8, 11.9

2’’-*O*-apiofuranosyl		
1’’’	5.35 d 1.2	5.34 d 1.4
2’’’	3.76 d 1.2	3.74 d 1.4
4A’’’	3.92 d 9.4	3.91 d 9.5
4B’’’	3.66 d 9.4	3.66 d 9.5
5A’’’	3.33 d 11.2	3.31 m
5B’’’	3.30 d 11.2	3.28 m
6’’-*O*-malonyl		
2A’’’		3.40 d 15.7
2B’’’		3.36 d 15.1

Table S2. ^{13}C NMR chemical shift values (δ ^{13}C, ppm) of apigenin 7-(2’’-apiosylglucoside) (**2**, apiin) apigenin 7-(2’’-apiosyl-6’’-malonylglucoside) (**3**) and luteolin 7-*O*-β-glucopyranoside (**4**) isolated from *Anthriscus cerefolium* recorded in DMSO-D_6 at 298K.

	2	**3**	**4**
2	164.41	164.43	164.8
3	103.23	103.18	103.4
4	182.13	182.10	182.1
5	161.29	161.21	161.7
6	99.48	99.45	99.7
7	162.83	162.49	163.2
8	94.94	94.76	94.9
9	157.06	157.02	157.2
10	105.52	105.56	105.5
1’	121.17	121.08	121.6
2’	128.75	128.68	113.8
3’	116.14	116.08	146.0
4’	161.50	161.45	150.1
5’	116.14	116.08	116.8
6’	128.75	128.68	119.4
7-*O*-*β*-glucopyranoside			
1’’’	98.27	97.90	100.1
2’’’	75.89	75.56	73.3
3’’’	76.94	76.53	76.6
4’’’	69.94	69.90	69.8
5’’’	77.17	73.72	77.4
6’’’	60.67	64.06	60.8
2’’-*O*-apiofuranosyl			
1’’’	108.88	108.83	
2’’’	76.22	76.15	
3’’’	79.44	79.38	
4A’’’	74.14	74.07	

5A’’’	64.36	64.36
6’’-*O*-malonyl		
1’’’		166.87
2’’’		41.41
3’’’		167.85

Graphic design: Communication Division, UiB / Print: Skipnes Kommunikasjon AS

uib.no

ISBN: 9788230867945 (print)
9788230846384 (PDF)